# ARCH-E Design Report

## Autonomous Reconfigurable Crew/Cargo Hauler for Exploration

### Group 21


| | | | |
|---|---|---|---|
| Oisín FitzGerald | 5550874 | Justin Hu | 5501180 |
| Daria Ispas | 5457599 | Jakob Joos | 5550602 |
| Adriana Medina Vega | 5502217 | Bora Menekse | 5454395 |
| Nick Portheine | 5077842 | Jeremy Smith | 5478022 |
| Nathaniel Steenhuis | 4880293 | Swastik Swain | 5550025 |
| Alexis Van den Heede | 5506611 | | |

Tutor: Dr. Angelo Cervone
Client: Andrew Clark, Airbus Defence and Space UK
Coaches: Direnc Atmaca MSc, Hauke Felix Maathuis MSc
Institution: Delft University of Technology
Place: Faculty of Aerospace Engineering, Delft



TU Delft
Delft University of Technology

[This page is intentionally left blank.]

# Nomenclature

**4BMS** 4-Bed Molecular Sieve
**ADCS** Attitude Determination and Control System
**AG** Approach Gate
**AP** Approach Phase
**ARCH-E** Autonomous Reconfigurable Crew/Cargo Hauler for Exploration
**BER** Bit Error Rate
**BOL** Beginning of Life
**BPF** Band-Pass Filter
**BPSK** Binary Phase-Shift Keying
**CAMRAS** Carbon dioxide And Moisture Removal Amine Swingbed
**CBM** Common Berthing Mechanism
**CC** Convolutional Code
**CDH** Command and Data Handling
**CECE** Common Extensible Cryogenic Engine
**CER** Cost Estimation Relationship
**CFC** Central Flight Computer
**CHX** Condensing Heat Exchanger
**$CO_2$** Carbon Dioxide
**COTS** Commercial Off-The-Shelf
**CSM** Command and Service Module
**DC** Direct Current
**DOD** Depth of Discharge
**DOT** Design Option Tree
**DPDT** Double Pole Double Throw
**DSN** Deep Space Network
**DTE** Direct-to-Earth
**ECLSS** Environmental Control and Life Support System
**EIRP** Equivalent Isotropic Radiated Power
**EOL** End of Life
**EPS** Electrical Power System
**ESA** European Space Agency
**EVA** Extravehicular Activity
**FOV** Field of View
**FY** Fiscal Year
**G/T** Gain-to-System Noise Temperature Ratio
**GEO** Geostationary Orbit
**GNC** Guidance, Navigation, and Control
**GPS** Global Positioning System
**GRACE** Gravity Recovery and Climate Experiment
**H/W** Hardware
**HLS** Human Landing System
**HPBW** Half Power Beamwidth
**HRS** Humidity Reclamation System
**ICSIS** International Communication System Interoperability Standards
**IGM** Iterative Guidance Mode
**IMU** Inertial Measurement Unit
**IOV** In-Orbit Vehicle
**IR** Infrared
**ISRO** Indian Space Research Organisation
**ISRU** In-Situ Resource Utilisation
**ISS** International Space Station
**ITU** International Telecommunication Union
**KSAT** Kongsberg Satellite Services
**KSC** Kennedy Space Center
**$LCH_4$** Liquid Methane
**LCO** Liquid Carbon Monoxide
**LDPC** Low-Density Parity-Check
**LEGS** Lunar Exploration Ground Sites
**LEO** Low Earth Orbit
**$LH_2$** Liquid Hydrogen
**LiOH** Lithium Hydroxide
**LLO** Low Lunar Orbit
**LNA** Low Noise Amplifier
**LOI** Lunar Orbit Insertion
**LOX** Liquid Oxygen
**LV** Launch Vehicle
**LWST** Launch Window Sidereal Time
**MBP** Main Braking Phase
**MCC** Mid-course Correction
**MIPS** Million Instructions Per Second
**MMOD** Micrometeoroids and Orbital Debris
**MMOI** Mass Moment of Inertia
**NAC** Narrow Angle Camera
**NASA** National Aeronautics and Space Administration
**NGLV** Next Generation Launch Vehicle
**NRHO** Near-Rectilinear Halo Orbit
**NSN** Near Space Network
**OAO** One Array Out
**OTV** Orbital Transfer Vehicle
**PCEC** Project Cost Estimating Capacity
**PCU** Power Conditioning Unit
**PDI** Powered Descent Initiation
**PEG** Powered Explicit Guidance
**PMD** Power Management and Distribution
**$ppCO_2$** Partial Pressure of Carbon Dioxide

**PPT** Peak Power Tracker
**PROP** Propulsion
**PSR** Permanently Shadowed Region
**QPSK** Quadrature Phase-Shift Keying
**RAAN** Right Ascension of Ascending Node
**RAMS** Reliability, Availability, Maintainability, and Safety
**RP-1** Rocket Propellant-1
**RS** Reed-Solomon
**RX** Receiving Signal
**S/C** Spacecraft
**S/W** Software
**SADM** Solar Array Drive Mechanism
**SAM** Spacecraft Atmosphere Monitor
**SANSA** South African National Space Agency
**SAWD** Solid Amine Water Desorption
**$SiO_2$** Silicon Dioxide
**SLOC** Source Lines Of Code
**SLS** Space Launch System
**SNR** Signal-to-Noise ratio
**SOCP** Second-Order Cone Programming
**SOI** Sphere of Influence
**SPDT** Single Pole Double Throw
**SRP** Solar Radiation Pressure
**STR&MECH** Structures and Mechanisms
**SZM** Shielded Zone of the Moon
**TBC** To Be Confirmed
**TBD** To Be Determined
**TCCS** Trace Contaminant Control System
**TCS** Thermal Control System
**TDRSS** Tracking and Data Relay Satellite System
**TEG** Throttled Explicit Guidance
**TEI** Trans-Earth Injection
**TG** Terminal Gate
**THMS** Thermal & Humidity Management System
**TLI** Trans-Lunar Injection
**TP** Terminal Phase
**TRL** Technology Readiness Level
**TT&C** Telemetry, Tracking, and Command
**TWR** Thrust to Weight Ratio
**TWTA** Traveling-Wave Tube Amplifier
**TX** Transmitting Signal
**ULA** United Launch Alliance
**UPFG** Unified Powered Flight Guidance
**UTC** Coordinated Universal Time
**UWMS** Universal Waste Management System
**WAC** Wide Angle Camera
**WBS** Work Breakdown Structure
**WFD** Work Flow Diagram
**ZEM/ZEV** Zero-Effort-Miss/Zero-Effort-Velocity

$\alpha$ Primary strut horizontal angle (°), load fraction (−), geocentric right ascension (°)
$\alpha_{1/2}$ Half power beam angle (°)
$\beta$ Secondary strut horizontal angle (°)
$\boldsymbol{F_T}$ Thrust vector (N)
$\boldsymbol{F}$ Force vector (N)
$\boldsymbol{r}$ Position vector (m)
$\boldsymbol{V}$ Velocity vector (m/s)
$\Delta V$ Change in velocity (km/s)
$\delta$ Solar cell decay rate (%/year), secondary strut axial angle (°), geocentric declination (°)
$\epsilon$ Inclination of ecliptic plane (°)
$\eta$ Efficiency (−)
$\gamma_R$ Specific attenuation (dB/km)
$\hat{b}$ Binormal (−)
$\lambda$ Planet half-angle (°), wavelength (m), solar ecliptic longitude (°)
$\mathcal{F}_C$ Moon-Centered Moon-Fixed reference frame
$\mathcal{F}_I$ Moon-Centered Inertial reference frame
$\mathcal{F}_L$ Landing reference frame
$\mu$ Gravitational parameter ($m^3/s^2$)
$\Omega$ Right ascension of ascending node (°)
$\omega$ Argument of periapsis (°), Natural Frequency (rad/s)
$\Phi$ Solar constant ($W/m^2$)
$\phi$ Angle of incidence (°), tip-over angle (°), latitude (°)
$\rho$ Density ($kg/m^3$)
$\rho_s$ Effective slenderness ratio (−)
$\sigma$ Stefan-Boltzmann Constant ($W/m^2K^4$), stress (Pa)
$\tau$ Polarisation angle (°)
$\theta$ Solar incidence angle (°), horizontal angle of center of gravity (°), elevation angle (°), true anomaly (°)
$\xi$ Slosh mode factor (−)
$\zeta$ Damping ratio (−)
$A$ Area ($m^2$), strut cross-sectional area ($m^2$), azimuth (°)
$a$ Semi-major axis (km), acceleration ($m/s^2$), albedo (−)
$A_a$ Absorbing area ($m^2$)
$A_f$ Frontal area ($m^2$)
$A_r$ Ram area ($m^2$)

| | |
|---|---|
| $A_s$ | Sunlit area ($m^2$) |
| $B$ | Magnetic field strength (B), primary strut reaction force (m) |
| $b$ | Landing leg base (m) |
| $C$ | Electrical capacity (Ah) |
| $c$ | Damping constant (N s/m) |
| $C_d$ | Drag coefficient |
| $c_m$ | Center of mass (m) |
| $c_p$ | Center of pressure (m) |
| $C_R$ | Radiation pressure coefficient (−) |
| $C_{20}$ | Moon's second zonal harmonic (−) |
| $C_{22}$ | Moon's sectoral harmonic (−) |
| $D$ | Diameter (m), residual dipole moment ($A\,m^2$) |
| $d$ | Tank diameter (m) |
| $DOF$ | Degree of freedom (−) |
| $E$ | Elastic modulus (GPa) |
| $e$ | Eccentricity (−), Coefficient of Restitution (−) |
| $e_t$ | Pointing offset angle (°) |
| $F$ | Force (N) |
| $f$ | Frequency (Hz) |
| $f_e$ | Eigenfrequency (Hz) |
| $F_T$ | Thrust force (N) |
| $G$ | Gain (−) |
| $g_0$ | Standard gravity ($m/s^2$) |
| $h$ | Height (m), liquid height (m) |
| $h_R$ | Rain height (km) |
| $h_{cg}$ | Centre of gravity height above ground (m) |
| $I$ | Second moment of area ($m^4$) |
| $i$ | Inclination (°) |
| $I_d$ | Inherent degradation (-) |
| $I_{sp}$ | Specific impulse (s) |
| $I_{xx}$ | Mass moment of inertia about x-axis ($kg\,m^2$) |
| $I_{yy}$ | Mass moment of inertia about y-axis ($kg\,m^2$) |
| $I_{zz}$ | Mass moment of inertia about y-axis ($kg\,m^2$) |
| $J_2$ | Earth's second zonal harmonic (−) |
| $J_s$ | Solar intensity ($W/m^2K$) |
| $K$ | Buckling design factor (−) |
| $k$ | Spring constant (N/m) |
| $L$ | Loss (−), length (m) |
| $L_1$ | Slosh pendulum length (m) |
| $L_d$ | Life degradation (-) |
| $M$ | Moment (N m), magnetic constant ($T\,m^3$) |
| $m$ | Mass (kg) |
| $MF$ | Margin factor |
| $MS$ | Margin of safety (−) |
| $OC$ | Operating cost ($/h) |
| $OF$ | Oxidiser/fuel ratio (−) |
| $P$ | Power (W), pressure (Pa) |
| $q$ | Heat flux ($W/m^2$), reflectance factor (-) |
| $R$ | Radius (km), secondary strut reaction force (m), critical effective slenderness ratio (−), rain rate (mm/h |
| $r$ | Tank cylindrical radius (m), structure ring radius (m), strut radius (m) |
| $r_m$ | Tank ellipsoidal height (m) |
| $S$ | Distance (m) |
| $T$ | Period (s) |
| $t$ | Time (s), tank thickness (mm) |
| $T_a$ | Aerodynamic torque (N m) |
| $T_D$ | Magnetic torque (N m) |
| $T_g$ | Gravity gradient torque (N m) |
| $T_m$ | Magnetic torque (N m) |
| $T_s$ | Solar radiation pressure torque (N m) |
| $T_{IR}$ | Effective radiating temperature (K) |
| $ttt$ | Predicted time to perilune (s) |
| $V$ | Voltage (V), volume ($m^3$) |
| $v$ | Velocity (km/s) |
| $v_{rel}$ | Spacecraft velocity relative to rotating atmosphere (km/s) |
| $x$ | Length along strut (m), displacement (m) |

# Executive Overview

ARCH-E is a Design Synthesis Exercise of eleven TU Delft Aerospace Engineering BSc students. ARCH-E stands for Autonomous Reconfigurable Crew/Cargo Hauler for Exploration. It is focused on designing a reusable and reconfigurable lunar lander. This report offers a comprehensive overview of the vehicle's architecture, astrodynamics, subsystems, risks, operations, and the mission's sustainability strategy. Additionally, this report details the verification and validation methods, as well as the project's future plans. It builds on the Project Plan, Baseline Report, and Midterm Report, which detailed the project's organisational structure and initial technical functions. This report will present a complete and detailed overview of the design choices and their outcomes.

## Project Objectives

In recent years, the race to the Moon has been reignited by NASA's commitment to returning to the lunar surface and establishing a permanent presence on and around the Moon. The concurrent rapid growth of commercial launch services has turned this shot for the Moon into a competition as NASA resolves to outsource more and more operations. This aligns with the mission need statement:

**Mission Need Statement**

To enable the future colonisation of the Moon, humanity must tackle and overcome its associated challenges.

The Human Landing System (HLS) contracts awarded to SpaceX and Blue Origin have highlighted the need for innovative solutions in the field of lunar landers. In particular, the Appendix P Broad Agency Announcement[1], under which the Blue Moon concept was selected, emphasises the need for a sustainable presence on the Moon. Reusability is to be built into the design, with flexible crewed/cargo operations and the capability to transfer between lunar orbit and the surface once a year for 10 years. This leads to the project objectives, which are as follows:

**Project Objective Statement**

To design a reconfigurable lunar landing vehicle able to carry from Earth to the lunar surface either a usable cargo mass of 5000 kg or a human crew of up to four.

## Market Analysis

Space exploration technologies have a significant interest in current society, driving economic growth, new career paths, and technological advancements. The renewed interest in lunar exploration, fuelled by reduced launch costs and potential lunar resources, has led to a $26 billion global investment in the sector in 2023 [1]. ARCH-E's mission, a collaboration between Delft University of Technology and Airbus Defense and Space UK, aims to address this interest with a versatile, reusable lunar lander capable of carrying cargo or crew. The lander's modular design, focus on sustainability, and operational efficiency position it to meet the increasing demand for lunar missions. Key stakeholders include space agencies, commercial entities, and regulatory bodies. Competitors like SpaceX, Blue Origin, and Dynetics also drive market growth with innovative lander designs, highlighting the intense competition in the lunar exploration sector.

## Functional Analysis & Requirements Overview

A functional analysis of the system was developed into a Functional Breakdown Structure and Functional Flow Diagram. From these, ten mission phases were identified: 1. Launch from Earth's surface, 2. Low Earth parking orbit, 3. Lunar Transfer, 4. Lunar landing, 5. Surface operations, 6. Lunar

[1] https://www.nasa.gov/humans-in-space/nextstep-appendix-p-human-landing-system-sustaining-lunar-development/ [cited 17 June 2024]

launch, 7. Low lunar parking orbit, 8. Earth transfer, 9. Reconfiguration, 10. End-of-life operations. Combining customer needs with the detailed analysis, approximately 250 requirements were identified that span across the mission, subsystems, and sustainability aspects. From this comprehensive list, we have highlighted the following key requirements that are paramount for the design phase:

Key Requirements:

**HOPE-STK-ADS-010** The vehicle shall be a reconfigurable lunar lander able to carry from Earth to the lunar surface either a usable cargo mass of 5000 kg or a crew of up to four humans.

**HOPE-STK-ADS-070** The option shall be considered of (partially) refuelling the lander vehicle on the lunar surface or Moon orbit, using in-situ produced propellants.

**HOPE-STK-ADS-080** The option shall be considered of refuelling the lander vehicle in Earth orbit in preparation for the next trip to the Moon, thus not requiring Earth re-entry or landing.

**HOPE-STK-HLS-002** The initial HLS will provide a habitable environment for 8 Earth days without predeployed assets.

**HOPE-STK-HLS-004** The HLS will provide automated rendezvous and docking.

**HOPE-STK-HLS-007a** The HLS will survive eclipse periods with preplaced surface infrastructure.

**HOPE-STK-HLS-008** The HLS will provide the capability to perform automated transfers between the lunar orbit and the lunar surface, and from the lunar surface to the lunar orbit.

## Vehicle Architecture and Trajectory

The vehicle will be composed of a lander and an Orbital Transfer Vehicle (OTV), both launched on SpaceX's Starship. The lander can be reconfigured by removing unnecessary components, therefore the environmental control and life support system (ECLSS), displays, and seats will be removed from the module to change from a crew to a cargo configuration. The removed parts will be placed in another existing or new module and will remain in Earth's orbit or be returned to Earth. The OTV will perform the trans-lunar injection for the lander and then return to Earth orbit on a free-return trajectory. The lander performs lunar descent and ascent and returns to Earth orbit by itself. Both modules are refuelled and reconfigured in Earth orbit. The trajectory of ARCH-E in this architecture can be visualised in Figure 1. To further investigate the mission's characteristics, a simulation of the lunar ascent, descent, and trans-lunar orbit was performed to obtain precise values for sizing the vehicle.

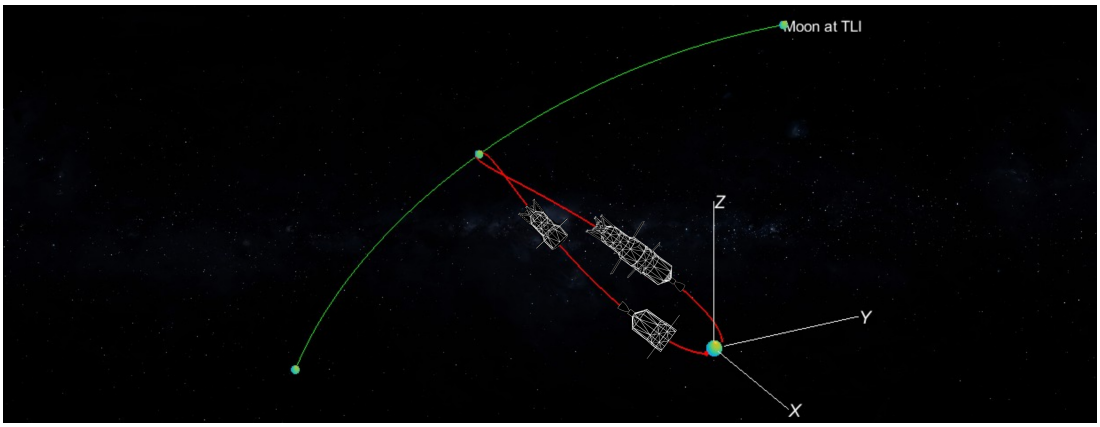


**Figure 1:** Final Mission Architecture

## Design Overview

The final mass, power, and cost budgets estimated for the vehicle can be seen in Table 1. The mass budget is refined for the design choices taken. The values include both the 5 t of payload and the estimated mass of the lander and OTV combined.

**Table 1:** Summary of Technical Parameters

| ARCH-E | | |
|---|---|---|
| **Main Parameters** | Mass | Dry Mass: 22 t |
| | | Propellant Mass: 344.8 t |
| | | Payload Mass: 5 t |
| | Dimensions | 33.5 m Length 7.2 m Diameter |
| | Power | Crew: 3360 W |
| | | Cargo: 2360 W |
| | Total Program Cost | US$ 35.27 billion (FY2024) |
| | Recurring Cost | US$ 45730/kg (FY2024) |
| | $\Delta V$ | OTV: 8.12 km/s |
| | | Lander: 12.48 km/s (including ascent & descent) |
| **Trajectory** | Orbits | LEO to LLO, OTV on Free Return Trajectory |
| **Propulsion** | Engines | OTV: 1 x Raptor 2 Vacuum |
| | | Lander: 5 x BE-7 |
| | Tanks | Material: 301 Full Hard Stainless Steel |
| | | Lander: 200 $m^3$ $LH_2$ and 74.5 $m^3$ LOX |
| | | OTV: 92.7 $m^3$ $CH_4$ and 192.1 $m^3$ LOX |
| **Power** | Solar Panels | Azur Space TJ GaAs 3G30-Adv Cells |
| | | OTV: 4 x Arrays with 24.5 $m^2$ Total Area |
| | | Lander: 4 x Arrays with 42.8 $m^2$ Total Area |
| | Batteries | OTV: 18 x Saft VES16 8s4p Li-Ion |
| | | Lander: 30 x Saft VES16 8s4p Li-Ion |
| | Bus | 28 V DC |
| **ADCS** | Sensors | 3 x AA-STR Star Tracker |
| | | 6 x ISS-T5 Sun Sensor |
| | | 2 x Miniature Inertial Measurement Unit |
| | Actuators | 18 x $LCH_4$/LOX RCS 20 lbf Thrusters |
| | | 18 x $GH_2$/LOX Thrusters |
| **TT&C** | Antennas | 1 x Parabolic Antenna |
| | | 4 x Phased-Array Antenna |
| | | 4 x Low-Gain Antenna |
| | | 2 x Omni-Directional Antennas |
| | Link Budget Margins | 3 dB-8.9 dB |
| **CDH** | Processors | 5 x BAE RAD5545 with 4 GB RAM |
| | Data Storage | 2 x CORECI 2 4 TB |
| **GNC** | Sensors | 4 x Inertial Measurement Unit |
| | | 2 x Optical Navigation System + Docking Camera |
| | | 2 x LIDAR |
| **Thermal** | Cooling | Cryocooler 690 W |
| | Insulation | Mylar Foil with Aluminium Backing |
| **Structures** | Materials | Aluminium Truss Structure & Titanium Landing Legs |
| | Tip-Over Angle | 14° |

## Subsystems and Components

The mission will use chemical propulsion, specifically $LH_2$/LOX propellant for the lander and $LCH_4$/LOX propellant for the orbital transfer vehicle. For thermal management, a thermal coating with specific emissivity and absorptivity values is required. The thermal control system will use radiators to dissipate heat from the electrical components into space and cryocoolers to circulate low-temperature fluid between the tanks and radiators to prevent boil-off. ARCH-E will be powered by solar panels, with batteries storing energy to ensure functionality during eclipse periods. Additionally, the vehicle will carry twenty-two attitude determination sensors to monitor its orientation throughout the mission. These sensors will be complemented by 18 attitude control thrusters to maintain three-axis control of the vehicle's orientation. For communication, ARCH-E will incorporate three main antennas in the lander and two in the orbital transfer vehicle, which will operate in the S-band during nominal operations, and are capable of communicating with both the Deep Space Network and the Near Space Network. Five flight computers will power each vehicle. Guidance inputs are obtained with Inertial Measurement Units, an Optical Navigation System, and LIDAR, depending on the mission phase. An

aluminium truss structure and titanium landing legs ensure adequate support during launch, propulsive manoeuvres, and landing. The environmental control and life support system provides the crew with the requirements for a safe and comfortable working environment, while its modularity enables tailoring it to specific missions. The integration of the vehicle and the final layout of ARCH-E can be visualised in Figure 2.

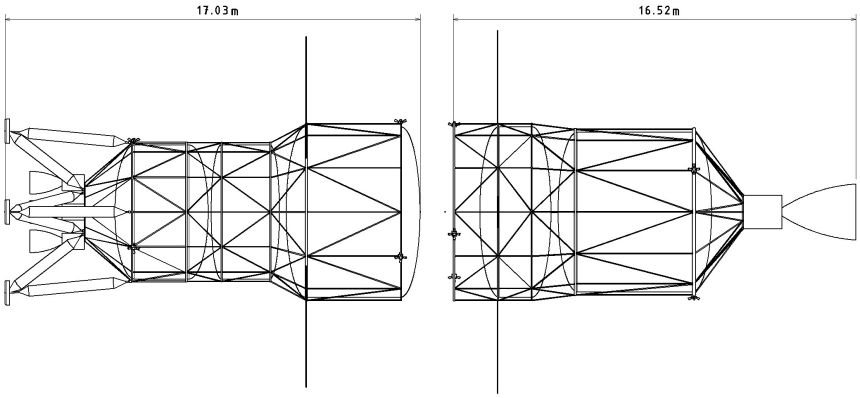


**Figure 2:** ARCH-E Layout, Lander on the Left, OTV on the Right

## Mission Risks

An in-depth analysis of mission risks has been performed, detailing each risk with an associated ID, related requirements, and mitigation and contingency strategies. This analysis has identified risks for every subsystem as well as general mission risks. The chosen architecture involves a modular vehicle, necessitating docking procedures that introduce several new risks for the mission, including the potential for docking failures. Additionally, the use of solar arrays increases the number of failure points, requiring contingency strategies for power management. The decision to use chemical propulsion, specifically cryogenic propellants, also introduces new potential risks, such as propellant handling and storage issues. Therefore, all these risks need to be carefully managed to ensure mission success.

## Operations

The mission can be divided into four key operational phases: 1. Refuelling operations include returning both the OTV and the lander to Low-Earth Orbit, docking with the designated tanker, and finally re-docking the OTV and lander. 2. Extra-vehicular operations enable the crew to safely exit and re-enter the vehicle, ensuring they can always return to a pressurised and stable environment. 3. After a successful mission, all necessary configuration changes are performed to transit from a crew to a cargo module or vice versa, ensuring it is ready for the next mission. 4. The final phase involves end-of-life operations. After completing its mission, ARCH-E will transition to serve as an international payload bay on the lunar surface, supporting future missions. Each of these phases is critical for the mission’s success, requiring correct execution and coordination.

## Sustainability

The design and production of the ARCH-E lunar lander prioritise sustainability through strategic choices in propulsion, material selection, and manufacturing processes. Sustainable materials are selected based on their performance, durability, embodied energy, and recyclability. The vehicle’s design addresses the space debris challenge with several systems being designed for hazard avoidance, precise tracking, and robust construction to prevent in-orbit breakups. Lean manufacturing strategies also reduce waste and prioritise eco-friendly materials and energy-efficient practices during the production phase of the project. During operations, real-time tracking and debris detection minimises environmental impact and ensures compliance with international agreements. Finally, end-of-life plans include repurposing the payload bay and docking port for future missions.

# Contents

# 1 | Introduction

In the renewed race to the Moon, there will be a high demand for transportation services to and from the lunar surface. As evident from NASA's Human Landing System (HLS) requirements, sustained presence capabilities for landers are desired. Multiple lander systems are currently in various stages of development, such as SpaceX's Starship HLS, Blue Origin's Blue Moon, and Dynetics' ALPACA. In addition to the capabilities of these concepts, value could be gained from a single architecture capable of supporting the initial stages of exploration, as well as servicing a potential lunar colony with supplies and astronauts. For such a system, a large number of reuses will also be key, driving down recurring costs. A low recurring cost, identified as a key requirement, increases the viability of ventures on the lunar surface, such as helium-3 extraction or manufacturing. A lander with high levels of flexibility, reusability, reliability, and cost-effectiveness would support the developing lunar economy and allow for sustained growth of human presence on the Moon and utilisation of its resources.

A reconfigurable spacecraft provides a novel solution to this challenge. In response to this need, ARCH-E is being developed for Airbus Defence and Space UK as a reusable, crew/cargo-capable lander architecture. It will provide both a short-term option for exploration, as well as a robust and efficient foundation for supporting future lunar infrastructure. With its high level of modularity, it will allow the program to expand in response in tandem with the demands of the market. To achieve full reusability, a mission architecture without expendable elements is developed, and the same vehicle is reconfigured for both crew and cargo operations. These factors drive the design of all other subsystems and present unique challenges, such as orbital refuelling and removing/reconfiguring elements of the spacecraft in orbit.

This report presents the Phase 0 design work done for the ARCH-E project. First, the market conditions are analysed to gain insights into the real-world context in which this design work is performed. The market analysis, containing a value proposition, stakeholders, competitors, and SWOT analysis is presented in Chapter 2. Next, a functional analysis is performed in Chapter 3 to set up the project. Based on the functions identified for the spacecraft a Functional Breakdown Structure and Functional Flow Diagram are developed and discussed. The stakeholder, mission, and system-level requirements are discussed in Chapter 4. A summary of the trade-offs performed in the previous reports is given in Chapter 5. This chapter highlights the major design decisions made as part of the preliminary design phase and the logic that resulted in the general mission architecture. At this point, an overview of the system as designed is given in Chapter 6, including top-level parameters and the chosen configuration.

Building on the trajectory analysis performed in the previous report, Chapter 7 describes in detail the full mission profile of ARCH-E. Trajectory simulations are employed to arrive at more accurate $\Delta V$ estimates for each of the propulsive manoeuvres over an Earth-Moon return trip. Possible landing sites and perturbations during flight are also examined. Chapter 8 details the development of lunar ascent & descent simulation, implementing a guidance algorithm to arrive at a $\Delta V$ requirement and an accurate description of this crucial phase of the mission. With the propulsive needs of the mission known, the Propulsion System is designed in Chapter 9, encompassing propellants, engines, pressurisation, and tanks. Continuing the detailed subsystem design, the Thermal Control System is discussed in Chapter 10. The spacecraft environment is first examined to arrive at heating and cooling needs for different mission phases. Critical subsystems for thermal control are identified and the subsystem is subsequently sized. Next, the Environmental Control and Life Support System accommodating the crew and cargo is designed and is described in Chapter 11, with a focus on the selection of the subsystem components and the packaging architecture. The Electrical Power System providing ARCH-E with the power to function is sized in Chapter 12. Based on the power requirements of the other subsystems, power generation and storage methods are selected, and calculations are performed to determine their required dimensions and mass. Communications with the ground station are described in Chapter 13, which describes the design of the Tracking, Telemetry, and Command subsystem, including the link budget and operations. Chapter 14 concerns the combined development of the Guidance, Navigation, and Control and the Command and Data Handling subsystems, since

the two, determining the position and calculating the guidance solution, are highly interconnected. In Chapter 15 the control modes of the spacecraft are defined and the disturbance torques it will face are described and quantified. This is combined with the selection of attitude determination and attitude control hardware to complete the Attitude Determination and Control System. The structure to support all of these functions is analysed in Chapter 16 using a combination of finite element methods and analytical techniques.

Technical risks are described on a subsystem level in each chapter. However, the most important mission risks are discussed in more detail in Chapter 17 along with the accompanying risk maps. The full operational flow and logistics of an ARCH-E mission are developed in Chapter 18 along with RAMS and end-of-life (EOL) procedures. The Sustainable Development Strategy of the project, encompassing design & production considerations, sustainable operations and EOL are covered in Chapter 19 Compliance with the requirements and their verification and validation procedures are presented in Chapter 20. In Chapter 21 a roadmap is laid out for future project activities. It picks up at the conclusion of the DSE and describes the project's development and operational life until EOL, including manufacturing, integration, assembly, and testing considerations. Finally, in Chapter 22 the conclusions of the report are presented, along with recommendations for future work.

# 2 | Market Analysis

This market analysis discusses the reasons behind entering the lunar exploration market, identifies its specific demands, and explores how the ARCH-E mission will add value to this sector. It also highlights key stakeholders through an interest-influence map, delves into market segments, and addresses investments, revenue projections, and competitors. The positioning of ARCH-E within the market is analysed through SWOT analysis, alongside potential changes to increase its value proposition.

**Motivation:** Technologies developed for space exploration have significant terrestrial applications, boosting the economy, creating new industries, and advancing everyday technologies[1]. Advances required for lunar exploration benefit various sectors, including medicine, driving economic growth. The pursuit of lunar resources and associated geopolitical advantages fuels market expansion. Governments' strategic interests led to a global investment increase to $26 billion in 2023 [1]. Space exploration fosters STEM careers in sectors like IT, medicine, and aviation. Historical lunar exploration efforts have inspired innovations such as personal computers, the internet, and medical advancements, enhancing economic prospects. The Moon holds valuable resources like helium-3, crucial for medical and potential fusion applications[2] [2]. Recent cost reductions in space mission launches have revitalised lunar exploration interest [3].

**Market Need:** The transportation of humans and resources between Earth and the Moon drives demand for lunar orbit and surface projects. Key requirements include mining, manufacturing, exports, and infrastructure development. Market players seek diverse vehicle types from lunar landers for surface descent to exploration rovers tailored to specific tasks [4]. Establishing a sustainable commercial lunar economy is crucial amid financial constraints in space exploration. Following anticipated crewed Artemis mission success, future missions aim for infrastructure and resource utilisation, driven by resource availability and extraction interest. Public-private partnerships, like Commercial Lunar Payload Services (CLPS), Human Landing System (HLS), and Lunar Cargo Transportation and Landing by Soft Touchdown (LCNS), are pivotal. NASA emphasises financial prudence, technical excellence, and regulatory adaptability to ensure mission viability, risk management, safety, and economic growth [5]. Reusable, reconfigurable lunar landers are essential for efficient crew and cargo transport. "As-a-service" models, cost-effective and scalable, meet government and commercial demands, reducing infrastructure management burdens. This approach supports recurring services, crew transfers, increased capacity, and efficient lunar surface transport, therefore driving market competition for innovative solutions[3,4].

**Value Proposition:** The ARCH-E mission represents a collaborative effort between academic institutions such as Delft University of Technology and commercial entities like Airbus Defense and Space UK. It offers a versatile lunar lander designed to carry up to 5000 kg of cargo or transport a crew of four with minimal modifications. By maximising shared elements and subsystems between cargo and crew versions, ARCH-E enhances cost-efficiency and simplifies maintenance. This dual-purpose capability reduces the need for separate vehicles or missions, lowering mission costs significantly. After deployment into Earth orbit, ARCH-E autonomously travels to the Moon and returns, minimising ground segment costs and labour. This advancement in autonomous operations contributes to the field of space autonomy. With a planned 10 year mission lifetime requiring minimal in-space maintenance, the lander's modular design ensures simple component replacement, enhancing operational efficiency and longevity. Refuelling in low Earth orbit (LEO) post-mission reduces re-entry costs and additional launch needs. The lander employs non-toxic, non-corrosive propellants ($LCH_4$/LOX for the OTV and $LH_2$/LOX for the lander), prioritising safety and sustainability in lunar and terrestrial environments. Strategic placement of DEBIE-1 sensors on the vehicles aims to refine models of the meteoroid and space debris environment, crucial for future lunar missions [6–8].

[1] URL https://www.nasa.gov/humans-in-space/why-go-to-space/ [cited 13 June 2024]

[2] URL https://www.esa.int/Enabling_Support/Preparing_for_the_Future/Space_for_Earth/Energy/Helium-3_mining_on_the_lunar_surface [cited 24 April 2024]

[3] URL https://www.nasa.gov/commercial-lunar-payload-services/ [cited 14 June 2024]

[4] URL https://www.nasa.gov/reference/human-landing-systems/ [cited 14 June 2024]

**Stakeholders:** The development of ARCH-E involves several shareholders with distinct roles and interests. Airbus Defense & Space is the main client for the ”Moon 2030” project. Astronauts who will fly aboard the lander are critical end-users, alongside potential commercial customers interested in utilising the lander's capabilities. Delft University of Technology oversees the project, utilising it as an educational opportunity for students to gain practical aerospace engineering design experience. Governments benefit because the project stimulates economic activity and encourages technological development, also contributing through funding and regulatory support [4]. ESA and NASA are particularly interested in the project as it aligns with their objectives of expanding human presence in space and advancing reliable transportation methods. NASA's Artemis program, which contracts commercial companies for lunar transport systems, highlights their keen interest in this area and the potential advantages they can gain from the project's success. Additionally, these agencies serve as potential scientific clients and collaborators, thereby broadening the project's influence and capabilities through technical cooperation. The high-level requirements of NASA's Human Landing System (HLS) were found to be similar to those provided by Airbus for this mission, in Chapter 4 [9]. As a result, the high-level system requirements can be adjusted slightly such that the vehicle can satisfy the needs of both Airbus and NASA. It is of particular interest because this opens up the possibility for additional funding beyond Airbus. Since 2019 NASA has been in the process of developing its lunar human landing capabilities by awarding commercial contracts to aerospace companies such as Blue Origin and SpaceX. Although the HLS contracts have already been awarded, it is possible that there could be future opportunities to obtain more funding from NASA [10, 11]. Regulatory entities ensure compliance with space laws and safety standards. The launch company provides the launch vehicle, crucial for deploying the lander into space. Commercial customers like private or public companies can benefit from the project, since it gives them access to lunar resources, such as helium-3 and rare Earth elements. It enables the transport of equipment for lunar commercial activities such as propellant production. Figure 2.1 shows the influence-interest map of the stakeholders.

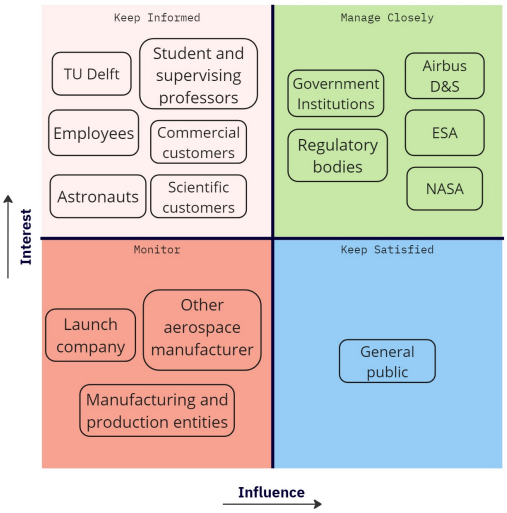


**Figure 2.1:** Stakeholder Map

**Market segments:** The space industry involves designing, manufacturing, and delivering components for outer space. Its annual revenue is estimated at $690 billion in 2023 by the World Economic Forum and is expected to reach $1.8 billion by 2035 as space-enabled technologies advance, assuming an average growth rate of 9% per annum, a figure significantly above the growth rate of global GDP [12]. The Bank of America Institute estimated this market at $469 billion in 2021, up over 60 % from estimates a decade prior, and expects it to grow at around $1.1 trillion by 2030, assuming an average annual growth rate of 11 % [13]. Lunar exploration has been the driving force behind unprecedented growth in the space exploration sector, leading to a remarkable increase in global government investment, which reached $26 billion in 2023, according to a report by Euroconsult. Ambitious lunar missions are projected to boost investment to nearly $33 billion by 2032, highlighting lunar exploration's pivotal role in shaping the future of space exploration. This market expansion is anticipated to continue fueling global investment, with Moon exploration expected to achieve a remarkable 5 % compound annual growth rate over the next decade, ultimately reaching nearly $17 billion by 2032 [1]. Various actors are targeting the Moon for research, exploration, and establishing a sustainable presence, as well as for gathering data to support experiments and commercial activities. These include space agencies and private entities utilising vehicles like orbital payloads, landers, and rovers. Collaboration between space agencies and commercial providers is growing, illustrated by NASA's procurement of Moon landers and crewed vehicles, and ESA's contracting for mission-enabling services for its ISRU demonstrator mission.

**Competitors:** Several companies are currently developing lunar landers, with the main competitors

being SpaceX and Blue Origin, both of which have been awarded contracts by NASA to develop landers for the Artemis missions. These contracts are worth $2.9B billion and $3.4 billion, respectively[5,6]. Each crewed mission will transport a team of two astronauts to the lunar surface for approximately 7 days, utilising the Lunar Gateway space station[7]. NASA has also tasked SpaceX and Blue Origin with developing landers for later cargo missions, which will transport 12 - 15 tons of cargo to the lunar surface[8]. Another competitor segment is those under CLPS and NASA funding, these aim to commercialise payload transportation to the moon. Firefly's lunar lander, Blue Ghost, features a box-shaped structural framework with four landing legs. It includes two decks for mounting equipment and has a payload capacity of 155 kg. Designed to deliver payloads to any location on the lunar surface starting in 2024, Blue Ghost aims to execute ten missions[9]. Astrobotic's Peregrine lunar lander can transport a payload capacity of 120 kg[10]. Intuitive Machines placed their NOVA-C lander, named Odysseus, near the Moon's south pole. This lander provided launch and landing services, capable of delivering approximately 100 kg of payload to the lunar surface[11].

**Position in market:** The ARCH-E lunar lander aims to compete with its dual-purpose design capable of carrying both cargo (up to 5000 kg) and crew (up to four people) with minimal modifications, thereby enhancing versatility and reducing development costs. The ARCH-E vehicle's reconfiguration capabilities are anticipated to raise the cost per unit mass delivered to the lunar surface, owing to the increased complexity and associated overall costs. Competitors' exact recurring costs per unit mass delivered to the Moon are not precisely known, but they are anticipated to slightly outperform the ARCH-E vehicle due to their specialised design focus. Figure 2.2 shows the strengths, weaknesses, opportunities, and threats of ARCH-E through a SWOT analysis. ARCH-E's primary strength lies in its reconfigurability, which offers unparalleled mission flexibility compared to competitors. This adaptability supports diverse lunar missions and facilitates a long-term lunar presence. However, launching such a large vehicle by 2030 entails significant financial and environmental costs, putting ARCH-E at a disadvantage against earlier-developed competitors. Despite these challenges, ARCH-E capitalises on humanity's renewed lunar interest and aligns well with the growing lunar market. Its substantial cargo capacity is crucial for developing lunar infrastructure, though it necessitates expensive launch solutions. Supported by Airbus Defence and Space UK's extensive space engineering expertise, ARCH-E aims to establish itself as a competitive lunar lander.

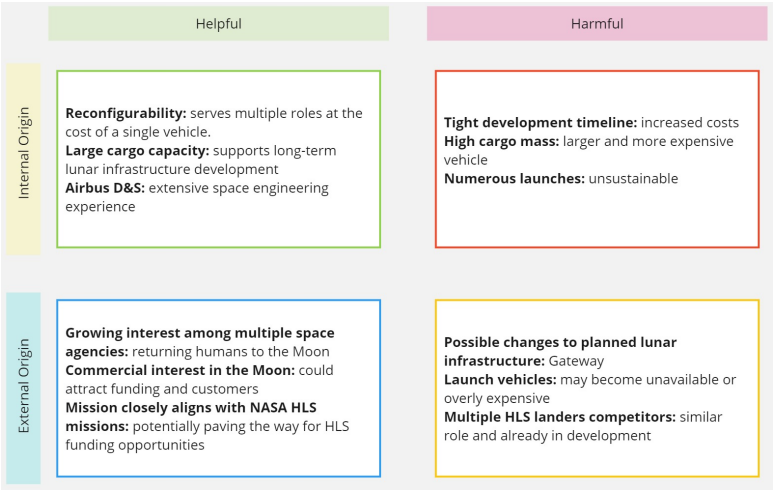


**Figure 2.2:** SWOT Analysis

**Forecast:** To enhance ARCH-E's competitiveness and value, optimising its reconfiguration capabilities to reduce costs per unit mass delivered to the lunar surface is crucial. This would make ARCH-E more appealing in a competitive market focused on cost efficiency. Strengthening partnerships with international space agencies and industry leaders could also accelerate technological advancements and expand ARCH-E's market presence significantly.

[5] URL https://www.nasa.gov/humans-in-space/nasa-awards-spacex-second-contract-option-for-artemis-moon-landing/ [cited 3 May 2024]
[6] URL https://www.nasa.gov/news-release/nasa-selects-blue-origin-as-second-artemis-lunar-lander-provider/ [cited 3 May 2024]
[7] URL https://www.nasa.gov/image-article/nasa-spacex-test-starship-lunar-lander-docking-system/ [cited 30 April 2024]
[8] URL https://www.nasa.gov/directorates/esdmd/artemis-campaign-development-division/human-landing-system-program/work-underway-on-large-cargo-landers-for-nasas-artemis-moon-missions/ [cited 3 May 2024]
[9] URL https://fireflyspace.com/blue-ghost/ [cited 15 June 2024]
[10] URL https://www.astrobotic.com/lunar-delivery/landers/ [cited 15 June 2024]
[11] URL https://www.intuitivemachines.com/im-1 [cited 15 June 2024]

# 3 | System Functional Analysis

In this chapter, a Functional Breakdown Structure (FBS) and a Functional Flow Diagram (FFD) are developed. Before generating additional requirements, the functions to be performed by the system have to be identified. Both the FBS and the FFD represent the same functions in different ways, with separate visualisations supporting the identification of additional requirements.

In Section 3.1, the methodology for creating the FBS is introduced. Section 3.2 deals with the development of the FFD. Finally, Section 3.3 discusses the results obtained from the functional analysis.

## 3.1. Functional Breakdown Structure

The Functional Breakdown Structure, shown in Figure 3.1, is a method for visualising all the functions a system will have to perform over its operational life. These functions are grouped by function level, where a given function is the sum of all lower-level functions under it. The FBS is not chronological; instead, its purpose is to organise the various functions of the system at different levels depending on the level of detail. This means some functions will be repeated throughout the mission, shown by the upper right red box, however, they are only included once in a functional breakdown structure. This means that some functions are only broken down into one function and a repeated one which is not shown.

## 3.2. Functional Flow Diagram

Next, the Functional Flow Diagram is developed. This is shown in Figure 3.2. Compared to the Functional Breakdown Structure, the same functions are present but the arrows follow the chronological and logical order of the functions the system has to perform throughout its lifetime. The operations evolve chronologically from top to bottom and left to right. Logical connections are made with OR and AND blocks, and diverging paths for decisions made based on specified conditions are indicated with text showing the conditions. The hierarchy of functions is also shown from left to right, starting with Level 1 functions (blue), followed by Level 2 (green) and Level 3 (white) functions. Continuous functions are indicated with the yellow block.

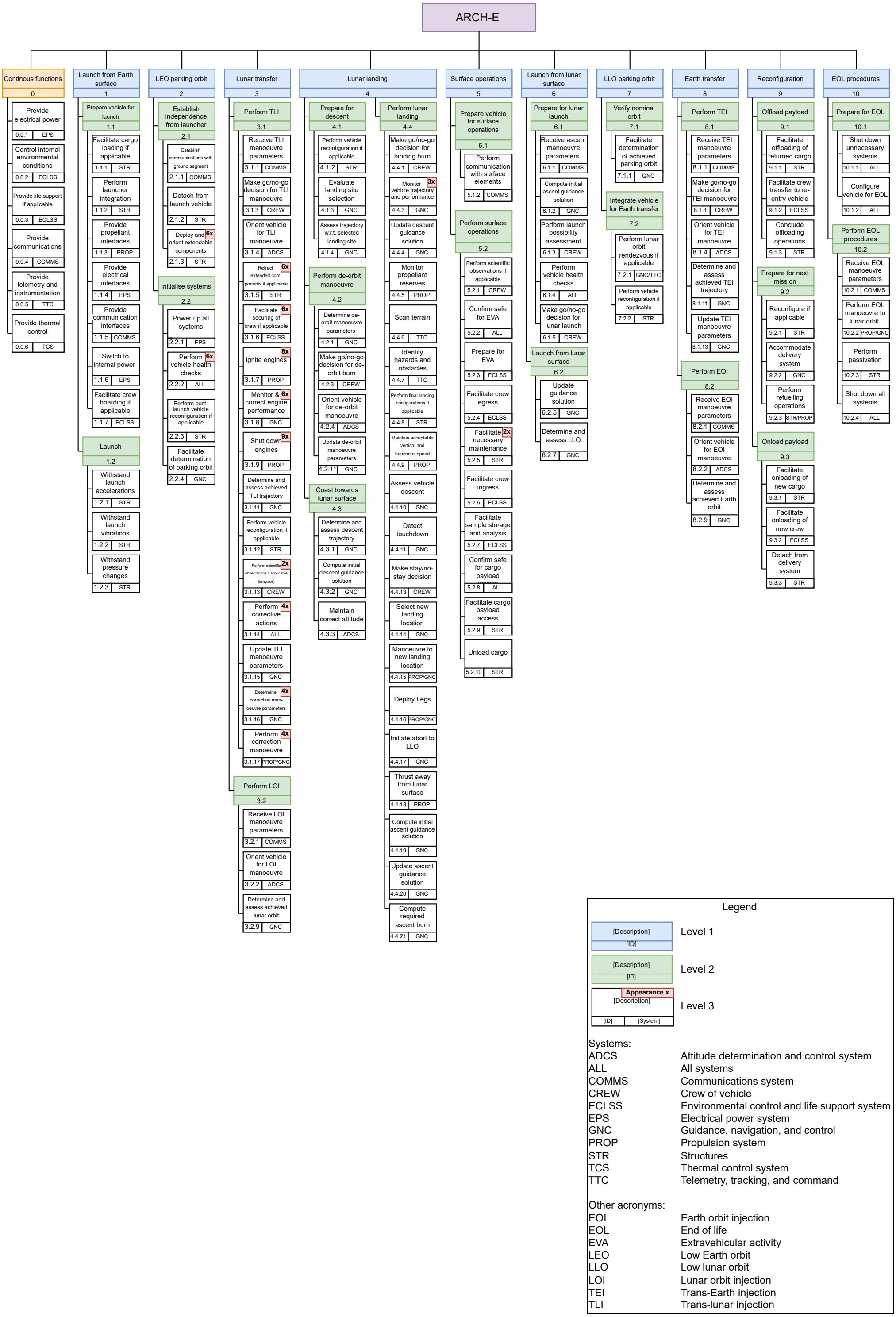


**Figure 3.1:** Functional Breakdown

Launch from Earth surface 1
Prepare vehicle for launch 1.1
Facilitate cargo loading if applicable 1.1.1 STR
Perform launcher integration 1.1.2 STR
AND
Provide propellant interfaces 1.1.3 PROP
Provide electrical interfaces 1.1.4 EPS
Provide communication interfaces 1.1.5 COMMS
Switch to internal power 1.1.6 EPS
AND
Facilitate crew boarding if applicable 1.1.7 ECLSS
Launch 1.2
AND
Withstand launch accelerations 1.2.1 STR
Withstand launch vibrations 1.2.2 STR
Withstand pressure changes 1.2.3 STR
Provide electrical power 0.0.1 EPS
Control internal environmental conditions 0.0.2 ECLSS
Provide life support if applicable 0.0.3 ECLSS
Provide communications 0.0.4 COMMS
Provide telemetry and instrumentation 0.0.5 TTC
Provide thermal control 0.0.6 TCS
Continuous functions
LEO parking orbit 2
Establish independence from launcher 2.1
Establish independent communications with ground segment 2.1.1 COMMS
Detach from launch vehicle 2.1.2 STR
Deploy and orient extendable components 2.1.3 STR
Initialise systems 2.2
Power up all systems 2.2.1 EPS
Perform vehicle health checks 2.2.2 ALL
Perform post-launch vehicle reconfiguration if applicable 2.2.3 STR
Facilitate determination of parking orbit 2.2.4 GNC
Lunar transfer 3
Perform TLI 3.1
Receive TLI manoeuvre parameters 3.1.1 COMMS
Perform vehicle health checks 2.2.2 ALL
Make go/no-go decision for TLI manoeuvre 3.1.3 CREW
Go
Orient vehicle for TLI manoeuvre 3.1.4 ADCS
Retract extended components if applicable 3.1.5 STR
Facilitate securing of crew if applicable 3.1.6 ECLSS
Ignite engines 3.1.7 PROP
Monitor and correct engine performance 3.1.8 GNC
Shut down engines 3.1.9 PROP
Deploy and orient extendable components 2.1.3 STR
Determine and assess achieved TLI trajectory 3.1.11 GNC
Within accuracy margin
Perform vehicle reconfiguration if applicable 3.1.12 STR
Perform scientific observations if applicable 3.1.13 CREW
Outside accuracy margin
Determine correction manoeuvre parameters 3.1.16 GNC
Perform correction manoeuvre 3.1.17 PROP/GNC
No-go
Update TLI manoeuvre parameters 3.1.15 GNC
Perform corrective actions 3.1.14 ALL
Perform LOI 3.2
Receive LOI manoeuvre parameters 3.2.1 COMMS
Orient vehicle for LOI manoeuvre 3.2.2 ADCS
Retract extended components if applicable 3.1.5 STR
Facilitate securing of crew if applicable 3.1.6 ECLSS
Ignite engines 3.1.7 PROP
Monitor and correct engine performance 3.1.8 GNC
Shut down engines 3.1.9 PROP
Deploy and orient extendable components 2.1.3 STR
Determine and assess achieved lunar orbit 3.2.9 GNC
Lunar landing 4
Prepare for descent 4.1
Perform scientific observations if applicable 3.1.13 CREW
Perform vehicle reconfiguration if applicable 4.1.2 STR
Evaluate landing site selection 4.1.3 GNC
Assess trajectory w.r.t. selected landing site 4.1.4 GNC
Orbital changes not required
Orbital changes required
Determine correction manoeuvre parameters 3.1.16 GNC
Perform correction manoeuvre 3.1.17 PROP/GNC
Perform de-orbit manoeuvre 4.2
Determine de-orbit manoeuvre parameters 4.2.1 GNC
Perform vehicle health checks 2.2.2 ALL
Make go/no-go decision for de-orbit burn 4.2.3 CREW
Go
Orient vehicle for de-orbit manoeuvre 4.2.4 ADCS
Retract extended components if applicable 3.1.5 STR
Faciliate securing of crew if applicable 3.1.6 ECLSS
Ignite engines 3.1.7 PROP
Monitor and correct engine performance 3.1.8 GNC
Shut down engines 3.1.9 PROP
No-go
Update de-orbit manoeuvre parameters 4.2.11 GNC
Perform corrective actions 3.1.14 ALL
Coast towards lunar surface 4.3
Determine and assess descent trajectory 4.3.1 GNC
Compute initial descent guidance solution 4.3.2 GNC
Maintain correct attitude 4.3.3 ADCS
Compute required ascent burn 4.4.22 GNC
Ignite engines 3.1.7 PROP
Monitor and correct engine performance 3.1.8 GNC
Shut down engines 3.1.9 PROP
No-go
Perform lunar landing 4.4
Make go/no-go decision for landing burn 4.4.1 CREW
Go
Ignite engines 3.1.7 PROP
Monitor vehicle trajectory and performance 4.4.3 GNC
Acceptable
Monitor propellant reserves 4.4.5 PROP
Sufficient propellant reserves
Scan terrain 4.4.6 TTC
Identify hazards and obstacles 4.4.7 TTC
Current landing site is suitable
Perform final landing configurations if applicable 4.4.8 STR
AND
Maintain acceptable vertical and horizontal speed 4.4.9 PROP
Deploy Legs 4.4.16 GNC
Detect touchdown 4.4.11 GNC
Shut down engines 3.1.9 PROP
Make stay/no-stay decision 4.4.13 CREW
No-stay
Stay
Update descent guidance solution 4.4.4 GNC
Not acceptable
Insufficient propellant reserves
Manoeuvre to new landing location 4.4.15 PROP/GNC
Select new landing location 4.4.14 GNC
Current landing site is unsuitable
Assess vehicle descent 4.4.10 GNC
Acceptable
Not acceptable
Update ascent guidance solution 4.4.21 GNC
Initiate abort to LLO 4.4.17 GNC
AND
Thrust away from lunar surface 4.4.18 PROP
Monitor vehicle trajectory and performance 4.4.3 GNC
Shut down engines 3.1.9 PROP
Compute initial ascent guidance solution 4.4.19 GNC
Surface operations 5
Prepare vehicle for surface operations 5.1
Deploy and orient extendable components 5.1.1 STR
Perform communication with surface elements 5.1.2 COMMS
Perform surface operations 5.2
Perform scientific observations if applicable 5.2.1 CREW
OR
Confirm safe for EVA 5.2.2 ALL
Prepare for EVA 5.2.3 ECLSS
Facilitate crew egress 5.2.4 ECLSS
Facilitate necessary maintenance 5.2.5 STR
Facilitate crew ingress 5.2.6 ECLSS
Facilitate sample storage and analysis 5.2.7 ECLSS
Another EVA planned
Last EVA performed
Confirm safe for cargo payload 5.2.8 ALL
Facilitate cargo payload access 5.2.9 STR
Unload cargo 5.2.10 STR

**Figure 3.2:** Functional Flow Diagram

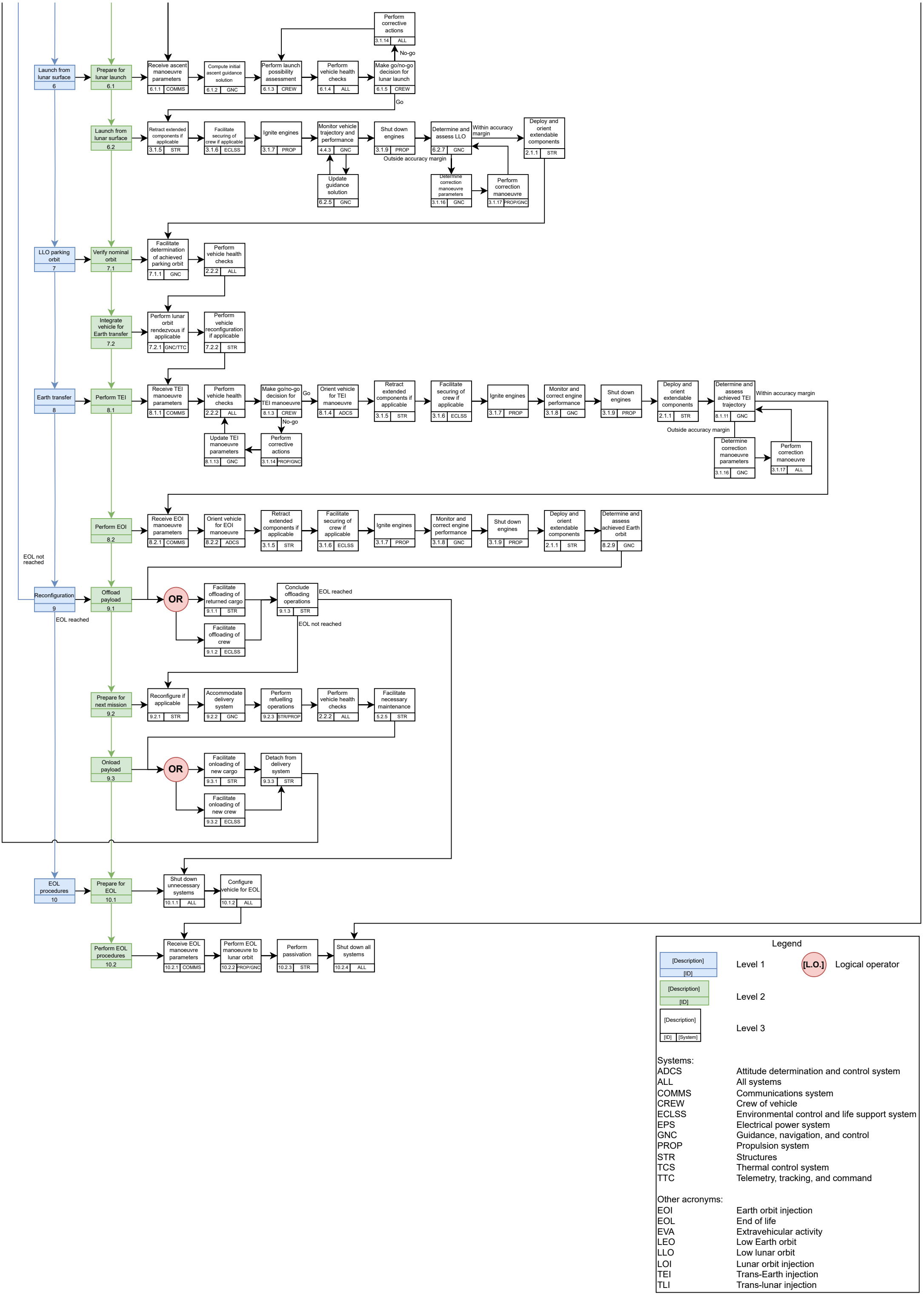


**Figure 3.2:** Functional Flow Diagram

## 3.3. Discussion of Functional Analysis

The Functional Analyses (FBD and FFD) are segmented into major mission phases and continuous functions performed throughout the vehicle's lifetime. The initial phase involves launching from the Earth's surface, which includes pre-launch activities like vehicle integration, loading, and interface provision, indicated by an AND block. For crewed missions, the crew boards before launch, initialising continuous functions that remain active until the vehicle's end of life (EOL). In cargo configurations, cargo loading occurs prior to launcher integration. The vehicle must endure launch loads, vibrations, and pressure changes, indicated by an AND block.

In the second phase, the vehicle reaches low Earth orbit (LEO), establishing independence from the launch vehicle by initialising power generation and communication systems before separating and becoming fully operational. Reconfiguration may be required if the vehicle's launch configuration differs from its mission configuration.

The third phase, lunar transfer, starts with the trans-lunar injection (TLI) maneuver. It involves receiving parameters from ground command, checking vehicle health, and making a go/no-go decision. If no-go, corrective actions are performed, and parameters are updated for another health check. If go, the TLI maneuver is executed with performance monitored and adjusted. Post-maneuver, trajectory accuracy is assessed, and correction maneuvers are performed if needed. Lunar orbit injection (LOI) follows, with similar functions to TLI.

The fourth phase is the lunar landing, beginning with descent preparations. The landing site, pre-selected by mission planners, is evaluated and corrected if necessary while in low lunar orbit (LLO). Upon compatibility, the de-orbit maneuver is initiated, with a go/no-go decision similar to TLI. Post de-orbit, the vehicle coasts towards the lunar surface, determining trajectory and computing initial guidance solutions while maintaining the correct landing attitude.

During the landing burn, a go/no-go decision is again made. If no-go, the vehicle ascends back to LLO; if go, the descent guidance solution is updated continuously. If trajectory or performance deviates, an abort to LLO is executed. The vehicle monitors propellant reserves and scans the terrain for hazards. If unsuitable, it maneuvers to a new location. Upon a suitable landing site, final configurations like deploying landing legs are performed, followed by final descent while maintaining acceptable speeds and assessing descent. Touchdown triggers a stay/no-stay decision; if no stay, the ascent maneuvers begin. If stay, surface operations commence.

Surface operations, the fifth phase, involve preparation and execution. Cargo missions focus on deployment, while crewed missions involve multiple EVAs for extended stays.

The sixth phase, lunar ascent, begins after surface operations. The vehicle readies and performs ascent, recalculating guidance solutions and including contingency actions for possible no-go decisions or off-nominal orbits.

In the seventh phase, back in lunar orbit, the vehicle's parking orbit and health are checked. Optional rendezvous and reconfiguration functions are included if mission architecture requires it.

The eighth phase involves transfer back to Earth, similar to the lunar transfer phase, with trans-Earth injection (TEI) and Earth orbit injection (EOI). After receiving burn data and performing guidance calculations, the spacecraft and crew prepare for the burn, followed by its execution.

The ninth phase concludes with the spacecraft in LEO parking orbit, readying for the next mission. Logic flow depends on the previous and next mission configurations, involving unloading and receiving crew or cargo and refuelling.

End-of-life procedures, the tenth phase, are outside the main loop and are initiated based on specific system criteria (HOPE-SYS-340 and HOPE-SYS-350), detailed in Chapter 18.

# 4 | Requirements

This chapter covers all the high-level requirements for the design study. First, the stakeholder requirements from Airbus Defence and Space UK and NASA are given. This is followed by system and mission requirements for the ARCHE-E mission.

## 4.1. Stakeholder Requirements

The design team has been given a set of stakeholder requirements by Airbus Defence and Space UK. These have been combined with the project objectives from NASA's Human Landing System programme. The resulting set of stakeholder requirements is shown in Table 4.1.

**Table 4.1:** Stakeholder Requirements

| ID | Requirement | Rationale |
|---|---|---|
| HOPE-STK-ADS-010 | The vehicle shall be a reconfigurable lunar landing vehicle able to carry from Earth to the lunar surface either a useable cargo mass of 5000 kg or a crew of up to four humans. | This is a project objective statement given by Airbus Defence and Space UK. |
| HOPE-STK-ADS-020 | The selected launch vehicle shall be compatible with the mission timeline. | To ensure the project will be able to commence according to HOPE-STK-ADS-050. |
| HOPE-STK-ADS-031 | The lander vehicle shall not contaminate the lunar surface with any significant debris. | The lander will not leave any element behind on the Lunar surface (except payload). Propellant exhaust and micro debris due to landing/sandblasting will not be considered significant but should be minimised. |
| HOPE-STK-ADS-040 | Cargo and crew versions of the lunar lander shall be characterised by as many common elements and sub-systems as possible. | The vehicle cost must be kept to a minimum as much as possible. |
| HOPE-STK-ADS-050 | The lander vehicle shall be launched no later than 2030. | This is a project objective statement given by Airbus Defence and Space UK. |
| HOPE-STK-ADS-070 | The option shall be considered of (partially) refuelling the lander vehicle on the lunar surface or Moon orbit, using in-situ produced propellants. | This is derived from ADS' customer requirement HOPE-SUST-03. |
| HOPE-STK-ADS-080 | The option shall be considered of refuelling the lander vehicle in Earth orbit in preparation for the next trip to the Moon, thus not requiring Earth re-entry or landing. | This is derived from ADS' customer requirement HOPE-SUST-04. |
| HOPE-STK-HLS-001a | The HLS will support a minimum of four crew as a sortie mission. | This is a project objective statement from NASA's Human Landing System. |
| HOPE-STK-HLS-002 | The initial HLS will provide a habitable environment for 8 Earth days without pre-deployed assets. | This is a project objective statement from NASA's Human Landing System. |
| HOPE-STK-HLS-003 | The HLS will accommodate the transfer of crew and cargo between the HLS and a crewed staging vehicle for lunar surface missions. | This is a project objective statement from NASA's Human Landing System. |
| HOPE-STK-HLS-004 | The HLS will provide automated rendezvous and docking. | This is a project objective statement from NASA's Human Landing System. |
| HOPE-STK-HLS-006a | The HLS will provide global lunar surface access for round-trip crew and cargo transfers from the Lunar Gateway. | This is a project objective statement from NASA's Human Landing System. |
| HOPE-STK-HLS-007a | The HLS will survive eclipse periods with pre-emplaced surface infrastructure. | This is a project objective statement from NASA's Human Landing System. |
| HOPE-STK-HLS-008 | The HLS will provide the capability to perform automated transfers between the lunar orbit and the lunar surface, and from the lunar surface to lunar orbit. | This is a project objective statement from NASA's Human Landing System. |
| HOPE-STK-HLS-009 | The HLS will accommodate at least 100 kg of science experiments and technology demonstrations, including at least 20 kg of return mass to lunar orbit. | This is a project objective statement from NASA's Human Landing System. |
| HOPE-STK-HLS-010 | The HLS will provide the capability for EVA on the lunar surface. | This is a project objective statement from NASA's Human Landing System. |
| HOPE-STK-HLS-011 | The HLS will provide vehicle design and capabilities to enable effective and efficient crew performance throughout the mission. | This is a project objective statement from NASA's Human Landing System. |

## 4.2. Mission Requirements

The stakeholder requirements from the previous section have been translated into mission requirements. The resulting requirements set is shown in Table 4.2.

## 4.3. System Requirements

The stakeholder and mission requirements from the previous section have been translated into system requirements. The resulting set of system requirements is shown in Table 4.3.

**Table 4.2:** Mission Requirements

| ID | Requirement | Rationale |
|---|---|---|
| HOPE-MISS-010 | The mass of materials transported to the lunar surface by the cargo version of the lander vehicle shall not be less than 5000 kg per launch. | The cargo mass is specified by Airbus Defense and Space UK and needs to be sufficiently large. |
| HOPE-MISS-020 | The volume of material transported to the lunar surface by the cargo version of the lander vehicle shall not be less than 50 $m^3$ per launch. | The volume of cargo is specified by Airbus Defense and Space UK. |
| HOPE-MISS-030 | The vehicle shall be capable of transporting a human crew of no less than $4$ to the lunar surface and back on each manned trip of the lander vehicle. | The number of crew is specified by Airbus Defense and Space UK. |
| HOPE-MISS-040 | Once released from the launcher in an Earth parking orbit, the vehicle shall be able to autonomously transfer from the parking orbit to Moon orbit, Moon surface, and back to Earth. | The cargo version will not have any crew to pilot the vehicle. |
| HOPE-MISS-060a | All materials and propellants used by the lander vehicle shall be non-toxic and not hazardous for the crew and the lunar and terrestrial environment. | This is specified by Airbus Defense and Space UK. |
| HOPE-MISS-070 | The lander vehicle shall have a reliability of $95\%$ or higher. | The vehicle's reliability is specified by Airbus Defense and Space UK. |
| HOPE-MISS-080 | The lander vehicle shall be fully re-usable in both the cargo or human configuration for a minimum of $10$ Earth-Moon return trips. | This is specified by the stakeholder Airbus Defence and Space UK. |
| HOPE-MISS-090 | The lander vehicle shall require no in-space maintenance for a minimum design lifetime of $10$ years. | To decrease maintenance requirements so that the mission is less dependent on maintenance schedules decreasing costs. |
| HOPE-MISS-120 | The launch cost shall be lower than 25 k€/kg of payload delivered to the Moon (calculated taking into account only recurring costs, not including any development or qualification costs). | The cost per kg of payload is specified by the stakeholder Airbus Defence and Space UK. |
| HOPE-MISS-150 | The crew version of the lander vehicle shall sustain all crew at all times. | The crew must survive the mission. |
| HOPE-MISS-161 | The vehicle shall be able to handle single-engine out and partial sensor failure scenarios during lunar ascent and descent and reach a safe and stable state. | The crew must survive dangerous events and return to Earth safely. The ability to abort ascent and descent is vital for crew safety in case of certain TBD failures, such as GNC system failure. |
| HOPE-MISS-180 | The crew version of the lander shall provide a habitable environment for the crew. | The crew should function optimally without psychological issues stemming from a poor habitat. |
| HOPE-MISS-190 | The mission shall facilitate a habitat on the lunar surface for a minimum of $4$ crew members for a minimum of $6.5$ days. | The crew must survive on the lunar surface, for a duration driven by initial NRHO for HLS' sustained architecture. |
| HOPE-MISS-200 | The mission shall accommodate the transfer of crew to a crewed staging vehicle. | This is specified by the stakeholder Airbus Defence and Space UK. |
| HOPE-MISS-210 | The mission shall facilitate global access to the lunar surface. | This allows for the entire lunar surface to be within reach of the lander, increasing the variety of missions possible. |
| HOPE-MISS-220 | The mission shall provide the capability to transport cargo to and from a staging vehicle. | This is required by the HLS specifications. |
| HOPE-MISS-230 | The mission shall provide the capability to transfer propellant from a staging vehicle. | This is required by the HLS specifications. |
| HOPE-MISS-241 | The mission shall be able to transport a minimum of 100 kg of cargo from the lunar surface to LEO in cargo configurations and 100 kg for crew configuration. | Crew upmass minimum driven by HLS requirements, and cargo upmass is driven by the lander payload up mass in crew configuration. |
| HOPE-MISS-270 | The selected Earth parking orbit shall facilitate return of lunar samples to Earth's surface. | The Earth's parking orbit should be compatible with a vehicle that can return lunar samples to the Earth's surface. |
| HOPE-MISS-271 | The selected Earth parking orbit shall facilitate return of the human crew to Earth's surface. | The Earth's parking orbit should be compatible with a vehicle that can return the human to the Earth's surface. |
| HOPE-MISS-272 | The selected Earth parking orbit shall facilitate refuelling of both versions of the vehicle. | The Earth parking orbit should be compatible with a vehicle that can refuel ARCH-E's vehicle. |
| HOPE-MISS-272 | The selected Earth parking orbit shall facilitate re-configuring of both versions of the vehicle. | The Earth parking orbit should be compatible with reconfigurable operations of the ARCH-E vehicle. |
| HOPE-MISS-274 | The selected Earth parking orbit shall facilitate reloading of both versions of the vehicle. | The Earth parking orbit should be compatible with reloading operations of the ARCH-E vehicle. |
| HOPE-MISS-275 | The selected transfer orbits to and from Earth parking orbit for the crewed vehicle shall take no more than $23$ Earth days (TBC). | This prevents excessive transfer times for crew that would increase life support requirements. |
| HOPE-MISS-276 | The selected transfer orbits to and from Earth parking orbit for the cargo vehicle shall take no more than $176$ Earth days (TBC). | This is based on a total mission time (Earth to Moon and back once) of $1$ year. |
| HOPE-MISS-277 | The selected lunar parking orbit shall facilitate the landing of crew on the lunar surface. | The lunar parking orbit should overfly the landing site as this simplifies landing operations. |
| HOPE-MISS-278 | The selected lunar parking orbit shall facilitate the lunar sample return from the lunar surface. | The lunar parking orbit should overfly the ascent site as this simplifies ascent, rendezvous, and docking operations. |
| HOPE-MISS-279 | The selected lunar parking orbit shall facilitate the landing of cargo on the lunar surface. | The lunar parking orbit should overfly the landing site as this simplifies landing operations. |
| HOPE-MISS-290 | The mission launch azimuth shall be between 35 deg and 120 deg degrees. | Follows from the selected launch site, the Kennedy Space Center |
| HOPE-MISS-LEG-010 | The mission shall comply with the Outer Space Treaty of 1967. | To comply with the relevant space legislation. |
| HOPE-MISS-LEG-020 | The mission shall comply with all launch policies provided by Airbus Defence and Space UK. | To comply with the standards set by the stakeholder, Airbus Defence and Space UK. |
| HOPE-MISS-LEG-030 | The mission shall comply with European Code of Conduct for Space Debris Mitigation guidelines. | This ensures that the mission will not contribute to the problem of space debris. |
| HOPE-MISS-LEG-040 | The mission shall comply with all signed treaties of UN COPUOS. | To comply with the relevant space legislation. |
| HOPE-MISS-LEG-050 | The mission shall comply with all legal rules applicable to the selected launch company. | To comply with the relevant legislation. |
| HOPE-MISS-LEG-060 | The mission shall comply with all relevant laws of the country of the launch site. | This is necessary to ensure that the launch vehicle can be used to launch the vehicle. |
| HOPE-MISS-LEG-070 | The mission shall comply with the planetary protection standard ECSS-U-ST-20C. | To comply with the relevant space legislation. |

**Table 4.3:** System Requirements

| ID | Requirement | Rationale |
|---|---|---|
| HOPE-SYS-010 | The system shall be able to be placed in LEO with a selected launch vehicle. | The vehicle must be launched using existing or in development launch vehicles. |
| HOPE-SYS-020 | The system shall withstand all launch loads with no damage. | The safety of the crew is of paramount importance. |
| HOPE-SYS-060 | The vehicle shall be able to passivation all sources of onboard stored chemical energy. | The system should not pose a potential threat to future missions. |
| HOPE-SYS-070 | The vehicle shall not release any uncontrollable mission-related objects during any phase of the mission. | The system should not pose a potential threat to future missions. |
| HOPE-SYS-081 | The system shall not expose the crew to more than 4.0 G sustained in the +Gx direction. | Limits the accelerations that the crew experience to ensure their safety. |
| HOPE-SYS-082 | The system shall not expose the crew to more than 4.0 G sustained in the -Gx direction. | Limits the accelerations that the crew experience to ensure their safety. |
| HOPE-SYS-083 | The system shall not expose the crew to more than 1.0 G sustained in the +Gy direction. | Limits the accelerations that the crew experience to ensure their safety. |
| HOPE-SYS-084 | The system shall not expose the crew to more than 1.0 G sustained in the -Gy direction. | Limits the accelerations that the crew experiences to ensure their safety. |
| HOPE-SYS-085 | The system shall not expose the crew to more than 0.5 G sustained in the -Gz direction. | Limits the accelerations that the crew experience to ensure their safety. |
| HOPE-SYS-086 | The system shall not expose the crew to more than 0.5 G sustained in the -Gz direction. | Limits the accelerations that the crew experiences to ensure their safety. |
| HOPE-SYS-100 | The vehicle shall have a probability of no penetration (PNP) greater than or equal to $0.76$ for items with the potential to create a catastrophic hazard if impacted or punctured by MMOD (micro-meteoroid and orbital debris). | This is derived from the International Space Station MMOD shielding requirements. |
| HOPE-SYS-110 | The vehicle shall provide the capability for the crewed configuration to autonomously abort the mission and execute all operations required to safely return to Earth. | The safety of the crew is of paramount importance. |
| HOPE-SYS-120 | The system shall be reusable at least $10$ times in the cargo or crew configuration. | This follows from HOPE-MISS-080. |
| HOPE-SYS-130 | The system shall be able to communicate with the Earth, other vehicle(s), and infrastructure on the Moon. | The vehicle must be able to communicate to ensure that the mission can be monitored by ground control and that the vehicle can safely rendezvous and dock. |
| HOPE-SYS-140 | The system shall be docking compatible with HLS crew staging vehicles. | The vehicle should be able to dock with other vehicles that are part of the HLS programme. |
| HOPE-SYS-200 | The system shall deliver the cargo to the lunar surface in an undamaged state. | The system should support any cargo to be used on the lunar surface. |
| HOPE-SYS-260 | During nominal operations, no component of the vehicle shall be left on the lunar surface at the end of the mission. | To limit any contamination of the lunar surface. |
| HOPE-SYS-280 | The vehicle shall allow the crew to move between the HLS and crewed staging vehicle without requiring EVA. | The crew should be able to move to and from the lander with relative ease. |
| HOPE-SYS-300 | The vehicle shall allow the crew to move cargo between the HLS and crewed staging vehicle without requiring EVA. | It is vastly simpler to move cargo between vehicles internally rather than externally. |
| HOPE-SYS-310 | The vehicle shall be able to receive propellants from a staging vehicle. | The vehicle must be refueled to be reusable. |
| HOPE-SYS-330 | The vehicle shall be capable of $156$ hours of uninterrupted surface operations in continuous darkness. | This is sized for the nominal lunar stay of $6.5$ days. |
| HOPE-SYS-360 | The system shall not have a single point of failure preventing the safe return of crew. | Crew safety is vital, and the system should have sufficient redundancy for crew return as far as feasible. |
| HOPE-SYS-370 | The vehicle shall remain in Earth orbit during lunar eclipse. | During lunar eclipse, the power requirements of the vehicle in the lunar orbit are excessive. |

# 5 | Trade-Off Summary

A number of trade-offs have been made throughout the design phase to make informed design decisions. This was done at the system level to select the best mission architecture, followed by several subsystem-level trade-offs to prepare for the detailed design phase.

### Mission Architecture Trade-Off

Several overall mission architectures were considered in the Midterm report [14]. Seven initial architectures were generated from a design option tree. These varied in the number of lander stages, the number of orbital transfer vehicles (OTV) used, and the refuelling strategy. Both single-stage and two-stage lander options were considered, as was the use of two, one, or zero OTVs. The refuelling strategy was a central part of the architectures; refuelling is necessary and could be done in orbit or on the surface, either on the Moon or on Earth. In-situ resource Utilisation (ISRU) was also included in the refuelling strategy. Due to the large number of options, a qualitative trade-off was first used to remove the least feasible options. Four options remained and were evaluated in more detail and quantitatively. These are illustrated in Figure 5.1. The quantitative architecture trade-off used several criteria. The most important was total mass at 30 % since mass drives the design more than any other factor and affects whether the vehicle can be launched. Reliability was weighted at 20 %, which included the complexity of the operations involved such as docking and undocking. Cost (15 %) focused on the recurring costs per mission since there is a maximum recurring cost requirement **HOPE-MISS-120**. Development risk (15 %) considered the Technology Readiness Level (TRL) involved with the architecture. Sustainability (10 %) and Future Expandability (10 %) were included to keep in mind the risk of contaminating the lunar environment, and the ability of the architecture to be adapted to future developments in lunar activities respectively.

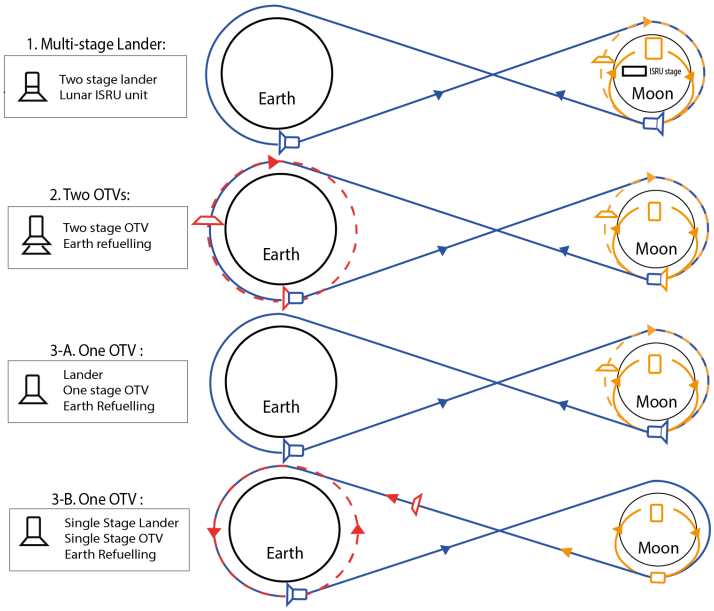


**Figure 5.1:** Sketch of Final Architectures

The four remaining architectures were evaluated on each criterion. The multi-stage lander involves a lander descent stage which remains on the lunar surface and generates propellant via ISRU, while the lander ascent stage returns to lunar orbit and is returned to Earth by an OTV. The descent stage returns to lunar orbit when its ISRU activity is complete, and waits to dock with the ascent stage when it is returned to the Moon by the OTV. This concept was ultimately rejected due to the high complexity involved, as well as the dependence on lunar ISRU which has a low TRL. The remaining options use Earth-orbit refuelling for all vehicles. The two-OTV option uses one OTV to bring the lander from Earth to lunar orbit, and a second to return it to Earth. The main drawbacks of this option were the high recurring cost of refuelling two OTVs and the lander, and the complexity of an additional vehicle which leaves more opportunity for failures. This led to this option being rejected as well.

The options with one OTV have a key difference; either the OTV remains in lunar orbit and returns the lander to Earth (as in 3-A), or the OTV performs the transfer to the Moon only and returns to Earth on a free-return trajectory, while the lander returns by itself (as in 3-B). The additional manoeuvres in option 3-A increased the OTV mass, and also the recurring cost. As a result. option 3-B was selected

as the best mission architecture. A sensitivity analysis confirmed this trade-off result.

### Subsystem Trade-offs

In addition to the overall mission architecture, several subsystem trade-offs were carried out to determine key aspects of the vehicle design[14]. The transfer trajectory, propellant, launch vehicle, reconfigurability strategy, and power system configuration were selected using trade-offs. In each case, a sensitivity analysis was used with varied criterion weights to confirm the results.

The transfer trajectory selection was the result of a trajectory analysis, design option tree, and comparison of five options. The resulting choice was a free-return trajectory with insertion into Low Lunar Orbit on arrival. This was based on a cost function considering the $\Delta V$ and the transfer time.

The propellant choice involved a trade-off between five liquid propellant combinations. The availability of deep-throttling engines using these propellants and the TRL were used as a criterion here. Also considered were the storability of propellants, the specific impulse, and the propellant density. The compatibility of ISRU was also a factor. Ultimately $LH_2$/LOX was selected, with $LCH_4$/LOX in second place. $LH_2$/LOX has a superior specific impulse and high TRL, is compatible with ISRU and there are deep-throttling engines in development. The propellant for the OTV only was later changed to $LCH_4$/LOX, which will be discussed in Chapter 9.

The launch vehicle (LV) trade-off considered ten launchers that are expected to be available in 2030. They were evaluated on their total launch costs, the failure risk, and the maturity of design. Reusability was also considered in the interests of sustainability. The trade-off concluded that either SpaceX's Starship (reusable) or Falcon Heavy (partially reusable) are the best options available; due to volume constraints with the vehicle, Starship was selected as it has a much larger fairing volume.

The lander's reconfigurability is a central part of the design. There are many options for switching between the cargo and crew configuration, so another trade-off was made to decide this. Five options were evaluated on five criteria: mass, cost, reliability, TRL, and complexity. Three options are single-element concepts where the crew and cargo are placed in the same pressurised volume. In the two two-element concepts, there are separate vehicles for crew and cargo. The trade-off was not fully conclusive; two of the single-element options were selected for further design since they scored very closely. These are built upon the same architecture but vary in how much reconfiguration is done. In the Major Reconfiguration option, hardware such as ECLSS, seats, and controls are removed from the lander to switch to the cargo configuration. In the Minor Reconfiguration option, this hardware is simply folded away to make room for cargo and avoid damage. The ECLSS architecture trade-off is continued in Chapter 11.

The last trade-off was for the EPS configuration. Five options for the power system design were considered using a number of criteria. The winning option was the use of solar arrays for power generation and secondary batteries for power storage. This configuration has extensive flight heritage and is suitable for a long vehicle lifetime.

# 6 | System Overview

This chapter aims to show an overview of the vehicle. This chapter shows the results of the detailed design of the subsystems explained in subsequent chapters, but provides context to their design, as many design elements are informed from the vehicle as a whole. It starts with giving the layout of the vehicle and the mass and power budgets. It ends with the cost breakdown of the entire program.

## 6.1. Layout

The shape of the vehicles shown in Figure 6.1 was mainly driven by the launch vehicle fairing dimensions. The lander's layout was driven by the center of mass for the landing. Having a high center of mass will increase the leg size to prevent tipping over. For this reason, the LOX tank, the most massive element, is put as low as possible. The payload hold is put next to provide easier access to the lunar surface than putting it on top of the LH2 tank, which does not affect the center of mass in a significant way. This does not affect crew safety as tank failure will likely cause mission failure regardless of payload position. To ensure crew safety they will be launched independently from the lander vehicle to LEO. The solar panels and antennas are mounted high up on the lander to limit damage due to lunar dust. The solar panels of the lander are also rotated from the docking port to maximise the docking capability of the lander. Other subsystems can be put between the tanks and attached to the main structure.

The OTV does not have the same center of mass limitations, the current design assumes that LOX is closest to the engine but if Starships's payload center of mass requires a different range the LCH4 tank and the LOX tank can switch places, with proper redesign of the ADCS and structure. Currently, the center of mass range required for Starship is not defined, hence an assumption is made on the layout to continue the design process.

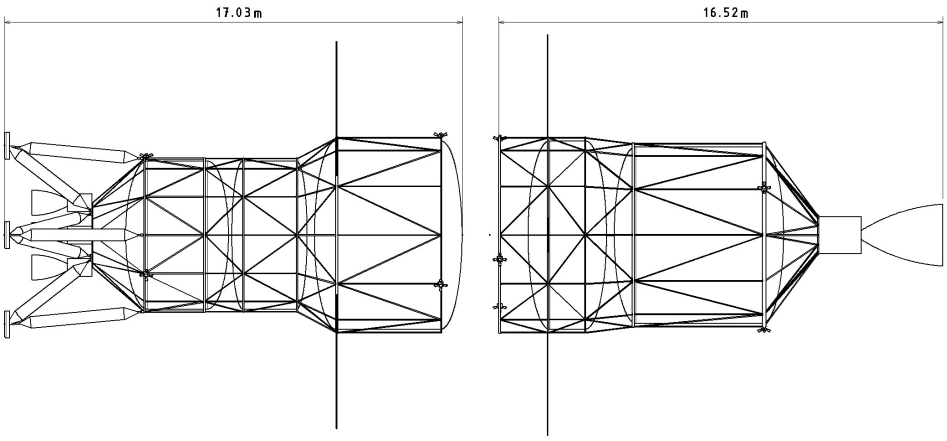


**Figure 6.1:** ARCH-E Layout, Lander on the Left, OTV on the Right

## 6.2. Mass Budgets

A dry mass overview of the various subsystems of each vehicle is shown in Table 6.1, the masses shown include their respective margin. The mass sizing of the respective subsystems are discussed in their chapter. The payload hold includes the mass of the pressure vessel required for the crew and cargo, as well as the ECLSS in the cargo configuration as this is always part of the vehicle. The part of the ECLSS that is put in when the crew is onboard is counted as the payload mass in the crew configuration, together with the crew mass and all their provisions as seen in Table 6.2.

Propulsion mass includes the propellant tank mass, engine mass, and piping mass. Structural mass between the two vehicles are similar, this is due to the lander's structural mass including both the main structure's mass and the landing leg mass, whereas the OTV does not have legs. EPS dry mass contributions mainly come from the solar panels and batteries for both vehicles.

TCS is heavier in the lander than the OTV, despite the OTV having more propellant, due to the different propellants being used in the vehicles. GNC is also heavier on the lander than the OTV due to requiring more sensors for the ascent and descent stages. The other mass element included in Table 6.1 is for various aspects of the vehicle that were not designed in detail during this phase of the design but still accounted for at this design stage. The margin used at this design stage is 20 % as per the margin philosophy laid out by ESA [15]. At this design stage, most subsystems are still in ECSS category D, as they components need modifications for integration prior to launch [16]. Some components, like the batteries, are COTS and flight proven. These will have a lower margin than 20% at the component level, however, all subsystems still have some components that require modifications so 20% is listed in Table 6.1.

**Table 6.1:** Subsystem Dry Mass Budget

| Element | OTV | | Lander | |
|---|---|---|---|---|
| | Mass [kg] | Margin % | Mass [kg] | Margin % |
| Payload hold | 0 | 0 | 1024 | 20 |
| Propulsion | 4394 | 20 | 1728 | 20 |
| Structure | 2281 | 20 | 2280 | 20 |
| EPS | 198 | 20 | 396 | 20 |
| TCS | 1500 | 20 | 600 | 20 |
| TTC | 73 | 20 | 99 | 20 |
| CDH | 150 | 20 | 150 | 20 |
| GNC | 55 | 20 | 103 | 20 |
| ADCS | 3500 | 20 | 700 | 20 |
| Other | 2050 | 20 | 800 | 20 |
| Total dry | 14201 | 20 | 7880 | 20 |

**Table 6.2:** Payload Masses

| Configuration | Down Payload [kg] | Up Payload [kg] |
|---|---|---|
| Crew | 2750 | 2750 |
| Cargo | 5000 | 2750 |

Table 6.2 shows the payload that the lander carries depending on the configuration and where the vehicle is headed. The down payload refers to what the vehicle is capable of bringing from LEO down to the lunar surface, and the up mass is the mass the vehicle is capable of returning from the lunar surface. The crew mass is driven by the ECLSS sizing done in Chapter 11. The up and down payload for the crew configuration is the same as it is required by **HOPE-STK-ADS-031** to leave no significant debris on the lunar surface. The down payload mass for the cargo configuration is determined by **HOPE-STK-ADS-010**, the up payload was chosen to be the same as the up payload in the crew configuration. This causes the cargo configuration to be the most massive hence the propellant sizing will be done for that load case.

**Table 6.3:** Mass Breakdown

| Element | Mass [tons] | |
|---|---|---|
| | Average | Margin % |
| **Lander** | | |
| Payload | 5.00 | 0 |
| Dry | 7.78 | 20 |
| Propellant | 90.17 | 20 |
| Gross | 103.05 | 20 |
| **OTV** | | |
| Dry | 14.20 | 20 |
| Propellant | 254.62 | 20 |
| Gross | 268.82 | 20 |
| Total Stack Mass | 371.87 | 20 |

Knowing the dry mass of both vehicles as well as the payload during the various mission stages, the amount of propellant was calculated using the rocket equation, results of which are found in Table 6.3. The $\Delta V$ values for the orbital manoeuvres are calculated in Chapter 7 and for ascent and descent initially taken from literature and then iterated with an ascent and descent guidance software in Chapter 8. The payload here is the cargo down payload which has 0 margin as it is known exactly how much payload capacity the vehicle is required to have. The propellant calculations had multiple margins applied as per ESA's margin philosophy [15]. The calculated $\Delta V$ had a margin of 5 %, and the $I_{sp}$ of the engine were scaled by 5 % to account for potential changes in the engine's performance over the course of their development. This resulted in an entire stack mass of 371.87 tons.

## 6.3. Power Budgets

The power budgets of the crew lander and the OTV are shown in Table 6.4 and Table 6.5 respectively. The cargo lander is the same as the crew lander but with a reduced ECLSS power, so a separate budget is not needed. These budgets are used in Chapter 12 to size the EPS. The ECLSS is the largest draw of power for the lander, with a high constant power demand. The TCS is also a significant portion of the power in both the lander and OTV as there is a high continuous power needed to cool the cryogenic propellant. The variations in power between phases are largely due to the activation of the ADCS and propulsion systems during manoeuvres. It should be noted that the duration of these phases are different, and some phases do not have power generation as indicated in tables 6.4 and 6.5. This is taken into account during the EPS sizing in Section 12.2. Peak power demands are also discussed in Section 12.4.

**Table 6.4:** Crew Lander Power Demand per Phase [W]

| System | Burn* | Coast | Descent/Ascent* | Orbit | Orbit (Eclipse)* | Surface Ops | Slew | Safe |
|---|---|---|---|---|---|---|---|---|
| ADCS | 360 | 65 | 360 | 360 | 65 | 65 | 655 | 65 |
| TCS | 768 | 768 | 768 | 768 | 797 | 768 | 768 | 768 |
| TTC | 284 | 284 | 284 | 284 | 284 | 284 | 284 | 284 |
| GNC | 241 | 241 | 559 | 241 | 24 | 24 | 559 | 24 |
| PROP | 709 | 355 | 709 | 355 | 355 | 355 | 355 | 355 |
| STRUC | 0 | 0 | 0 | 0 | 0 | 0 | 0 | 0 |
| EPS | 55 | 55 | 55 | 55 | 55 | 55 | 55 | 55 |
| ECLSS | 1200 | 1200 | 1200 | 1200 | 1200 | 1200 | 1200 | 1200 |
| CDH | 96 | 96 | 96 | 96 | 96 | 96 | 96 | 96 |
| Total | 3713 | 3064 | 4031 | 3359 | 2876 | 2847 | 3971 | 2847 |

*No power generation

**Table 6.5:** OTV Power Demand per Phase [W]

| System | Burn* | Coast | Descent/Ascent* | Orbit | Orbit (Eclipse)* | Surface Ops | Slew | Safe |
|---|---|---|---|---|---|---|---|---|
| ADCS | 360 | 65 | 0 | 360 | 65 | 0 | 655 | 65 |
| TCS | 670 | 670 | 0 | 670 | 833 | 0 | 670 | 670 |
| TTC | 229 | 229 | 0 | 229 | 229 | 0 | 229 | 229 |
| GNC | 241 | 148 | 0 | 148 | 24 | 0 | 148 | 24 |
| PROP | 709 | 355 | 0 | 355 | 355 | 0 | 355 | 355 |
| STRUC | 0 | 0 | 0 | 0 | 0 | 0 | 0 | 0 |
| EPS | 55 | 55 | 0 | 55 | 55 | 0 | 55 | 55 |
| ECLSS | 0 | 0 | 0 | 0 | 0 | 0 | 0 | 0 |
| CDH | 96 | 96 | 0 | 96 | 96 | 0 | 96 | 96 |
| Total | 2360 | 1617 | 0 | 1912 | 1656 | 0 | 2206 | 1494 |

*No power generation

## 6.4. Program Cost Breakdown

For the cost breakdown of the ARCH-E program, NASA's Project Cost Estimating Capacity (PCEC V2.3) tool was used to calculate the cost of the OTV and lander during all phases of the mission from development until and including production and testing costs (see Table 6.6). PCEC provides parametric cost estimation relationships (CER) based on the mass of each vehicle element, based on similar mission types [17]. For this analysis, the standard template for a crewed spacecraft was used, where the lander payload was assumed to be the 5000 kg of payload, whereas for the OTV, the payload was assumed to be the lander wet mass. Furthermore, it was assumed that the production quantity was 1, and the total number of flights, and the flight rate per year, was equal to 1. The components required for reconfiguration are included into the recurring costs. Finally, the costs associated with the

development of the software code were only included in the cost estimation for the lander, as the OTV would use the same code for its computers. Operations costs were calculated separately. For this calculation, the re-occurring cost for propellant and (re)fuelling of the vehicle (including launch vehicle cost), as well as ground station operations, was taken into account. The cost for the 2 Starships required to launch the OTV and lander were taken into the non-recurring costs.

For the propellant, a cost of 23.50 $/kg for $LH_2$ [18], 0.30 $/kg for LOX [18], and 8.80 $/kg[1] for $LCH_4$ (FY24), was assumed. Based on the propellant mass calculations in Chapter 9, this resulted in a cost estimate of 341 768 $ for the lander and 572 402 $ for the OTV. This would require 3 to 5 Starship launches for the propellant (dependent on a 100 ton vs 200 ton payload capacity) and an additional 2 to launch to OTV and lander. 1 Falcon 9 launch would be required for the launch of the crew/cargo for every mission (assuming Dragon stays in orbit and waits for ARCH-E to return back to Earth). Moreover, the cost of a Starship launch is currently 100 M$, but SpaceX is expected to reduce this cost to 10 M$. It was assumed that the cost would be 30 M$, as the 10 M$ does not include any profits, and to include any other uncertainties in this cost. This would cost a maximum of 570 M$ per mission if 4 100 M$ Starship launches and 10 Falcon 9 launches, and a minimum of 160 M$ per mission if 2 100 M$ Starship launches and 10 Falcon 9 launches are required. Finally, the ground stations would cost a total of 2.9 M$ per mission. Based on these assumptions, a total recurring cost for the 10 missions would be 1.64 - 5.74 B$. This implies 32.71 - 114.71 k$/kg (FY24) for recurring costs.

**Table 6.6:** Cost Breakdown in M$ (FY15)

| | OTV | | | Lander | | |
|---|---|---|---|---|---|---|
| **Description** | **Design & Development** | **System Testing** | **Prod-uction** | **Design & Development** | **System Testing** | **Prod-uction** |
| Project management | 285.9 | - | 37.3 | 221.5 | - | 22.4 |
| Systems engineering | 1183.1 | - | 56.0 | 725.1 | - | 32.1 |
| Product assurance | - | - | - | - | - | - |
| Structures | 452.2 | 110.9 | 85.2 | 399.2 | 88.8 | 68.2 |
| Mechanisms | 211.9 | 37.2 | 28.6 | 204.4 | 34.1 | 26.2 |
| Thermal protection | 37.3 | 7.1 | 5.5 | 18.2 | 2.8 | 2.1 |
| Propulsion system | 4310.1 | 142.5 | 109.6 | 1155.8 | 18.4 | 14.2 |
| Attitude control | 639.6 | 258.7 | 199.0 | 119.6 | 38.6 | 29.7 |
| Guidance, navigation & control | 50.0 | 18.5 | 14.2 | 66.0 | 31.9 | 24.5 |
| Telemetry & tracking | 15.0 | 7.9 | 6.0 | 17.1 | 10.2 | 7.9 |
| Command and data handling | 78.1 | 44.4 | 34.1 | 78.1 | 44.4 | 34.1 |
| Range Safety | 12.3 | 1.0 | 0.8 | 12.3 | 1.0 | 0.8 |
| Electric Power | 53.7 | 3.6 | 2.8 | 93.1 | 7.2 | 5.6 |
| Crew Systems | - | - | - | 23.1 | 20.6 | 15.9 |
| Software | - | - | - | 1427.5 | - | - |
| Integration & assembly | 119.3 | - | 66.9 | 81.9 | - | 38.6 |
| System test operations | 2047.6 | - | - | 1095.0 | - | - |
| Ground segment | 1789.4 | - | - | 1167.1 | - | - |

As can be seen from Table 6.6, the cost estimation is based on the assumption that every component will be developed by ARCH-E (i.e. nothing is commercial-off-the-shelf (COTS). Based on the PCEC analysis, a total development, testing, and manufacturing cost of 14.91 B$ for the OTV, and 8.93 B$ for the lander (FY24), was calculated. These costs cannot be compared separately however, based on the assumption that the payload of the OTV is the lander, as discussed previously. Adding a total operational cost over the 10 missions, and the 2 launches for the OTV and lander, a total program cost of 25.67 - 29.77 B$ was calculated. An additional 35% reserve needs to be included to account for project delays and other cost overruns [19]. This brings to total program cost, including reserves, up to 34.65 - 40.18 B$ (FY24). Which implies an overall cost per kilogram between 684.5 - 764.4 k$/kg. Investigating other cost estimations are recommended for further design stages.

[1] URL https://spaceimpulse.com/2023/06/13/how-much-does-rocket-fuel-cost/ [cited 19 June 2024]

# 7 | Mission Analysis

Mission analysis is the analysis of satellite orbits to determine how best to achieve the objectives of a space mission [20]. This is necessary to ensure the safety and success of the mission. Section 7.1 discusses the lunar landing site selection based on sunlight, resources, and terrain. Section 7.2 examines the perturbations the spacecraft encounters during its trajectory. Section 7.3 designs the Low Lunar Orbit that will allow for optimal access to the launch site. Section 7.4 patches together the Low Earth Orbit and Low Lunar Orbit through means of a free-return trajectory. Section 7.5 outlines the design of the Low Earth Orbit that set the spacecraft up for the free-return trajectory. Lastly, Section 7.6 gives a comprehensive overview of the $\Delta V$ budgets for both the lander and OTV.

## 7.1. Landing Site Analysis and Selection

Selecting an appropriate landing site is a crucial part of any mission bound for the lunar surface, as it plays a significant role in determining scientific outcomes. Although not explicitly part of the ARCH-E mission, this section outlines a high-level analysis used to determine an array of possible landing sites. The decision is largely driven by factors including sunlight availability, potential resources such as water ice, and challenges imposed by the terrain. Overall, ARCH-E aims to demonstrate exceptional landing capabilities on rough terrain, while possibly trying to maximise the scientific return.

Most of the Apollo missions focused on equatorial landing sites that are defined by their relatively smooth terrain. In contrast, this mission will demonstrate landing capabilities on ragged, uneven challenging terrain characterised by numerous boulders and craters. By targeting the vicinity of the lunar poles, ARCH-E intends to prove the effectiveness and reliability of its landing systems. Besides the demonstrative aspect, this approach also allows access to regions with high scientific interest and valuable resources. For instance, the potential presence of water ice in permanently shadowed regions (PSR)[1] is a driving factor. While ARCH-E currently does not involve ISRU techniques, water ice may still prove invaluable for scientific research. However, over the mission lifetime, the TRL of ISRU will increase, and it may become feasible to provide drinking water and produce hydrogen.

Furthermore, the lunar poles provide major advantages in terms of time spent in daylight. ”Peaks of eternal light”, i.e. areas with near continuous sunlight exist in this region. This is crucial for the spacecraft as it is solar powered, and thus provided with an almost constant energy source. Another benefit is that extreme temperature fluctuations, which the lunar surface is characterised by, are moderated this way[2].

The decision to land on the poles imposes restrictions on the lunar orbit, meaning it must be polar. Polar orbits provide relatively good flexibility in terms of landing sites, as they cut through the equator. This means it is possible to land on certain equatorial sites as well.

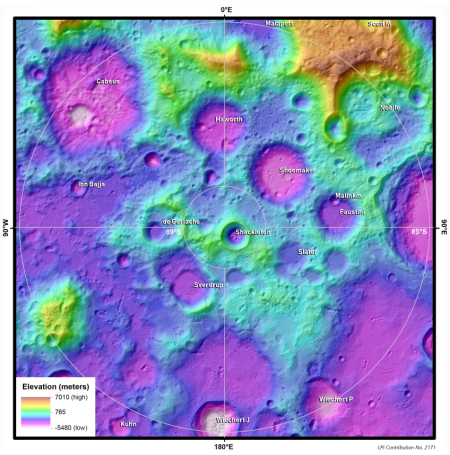


**Figure 7.1:** Landing Sites on the Lunar South Pole

There are numerous options to consider in terms of landing sites on both the lunar south pole and north pole. Figure 7.1 shows well-known possible landing sites on the south pole including Shackleton crater, de Gerlache crater, and Spudis crater. North pole landing sites include the Whipple crater and the Hinshelwood crate. For the purpose of this section and Chapter 8 on ascent/descent guidance, one specific landing site will be selected to demonstrate the guidance algorithm. In reality, however, an array of landing sites may be considered and the lander shall be able to descend to all of the aforementioned sites and more.

[1] URL https://www.lpi.usra.edu/lunar/lunar-south-pole-atlas/ [cited 19 June 2024]
[2] URL https://www.lpi.usra.edu/lunar/lunar-south-pole-atlas/ [cited 19 June 2024]

Although the terrains are harsher, the region of the south pole with latitude between 88° and 90°S is considered to be the best descent option due to the higher availability of sunlight and potential water ice. Specifically, the region between Shackleton and de-Gerlache crater is selected as the landing site for demonstration purposes due to its near-continuous sunlight and potential water ice in its PSR. Within this region, four smaller landing sites may be identified which have been shortlisted by Artemis missions. These sites are presented and ranked in Table 7.1. Site C1 (89.4°S, 136.2°W) is selected based on the performed technical assessment in [21].

**Table 7.1:** Summary and Ranking of Each Landing Site on the Basis of Technical Assessment and Expected Scientific Outcomes [21]

| Site | Avg. Elevation [m] | Avg. Slope [°] | Max. Avg. Illumination at 2 m level [°] | Avg. Earth Visibility [°] | Avg. Temp. [K] | No. of PSR | Rank |
|---|---|---|---|---|---|---|---|
| S | 1500 | 20 | 87 | 29 | 130 | 2 | 4 |
| C1 | 1807 | 11.5 | 88 | 30 | 132 | 1 | 1 |
| C2 | 1594 | 10.6 | 78.1 | 31 | 153 | 2 | 2 |
| D | 1105 | 14 | 80 | 44 | 167 | 3 | 3 |

## 7.2. Perturbation Analysis

To proceed with an accurate orbit design, it is important to know which perturbations the spacecraft will encounter along its path around and between the central bodies. Typically, the most prominent of these perturbations are those of a non-spherical central body and atmospheric drag. There are also other minor perturbations to be considered such as those from solar radiation pressure and gravitational interactions with celestial objects like the moon (or Earth in case of lunar orbit) and the sun.

The Earth and Moon are oblate spheroids and this lack of symmetry means that the force of gravity on spacecraft is not directed toward the center of the body. Oblateness also causes a variation with latitude which is called a zonal variation. For Earth, $J_2$ is the second zonal harmonic and it is a dimensionless parameter that quantifies the major effects of oblateness on the spacecraft's orbit. The Moon's counterpart is called $C_{20}$. The value of $J_2$ for Earth is $1.082\,63 \times 10^{-3}$ and $C_{20}$ for the Moon is $202.7 \times 10^{-6}$. Since the Moon's geometry is much more uneven, its gravitational field also varies heavily with longitude. Unlike for Earth, the lunar sectorial harmonic $C_{22}$ is of the same magnitude as $C_{20}$, thus it is considered. For prograde orbits, the most notable effects on the orbit are on $\Omega$ called nodal regression (clockwise rotation of the line of nodes) and on $\omega$ called periapsis precession (counterclockwise rotation of the apse line). The perturbing gravitational acceleration $\mathbf{p}$ due to $J_2$ in the ECIEq frame is presented in Equation 7.1 [22]. $R$ is the radius of the central body, $r$ is the norm of the spacecraft position with respect to the center of the central body, $\mu$ is the gravitational parameter of the central body and $x, y\&z$ are the components of $r$. The Moon's coefficients are the same. The formulas for accelerations due to $J_3$ up to $J_7$ may be found in [23]. For indices larger than 7 the zonal harmonics all remain more than three orders of magnitude smaller than J2, so $J_2$ up and until $J_7$ will be used for the simulations.

$$\mathbf{p_{J_2}} = \frac{3}{2}\frac{J_2 \mu R^2}{r^4}\left[\frac{x}{r}(5\frac{z^2}{r^2}-1)\hat{\mathbf{i}} + \frac{y}{r}(5\frac{z^2}{r^2}-1)\hat{\mathbf{j}} + \frac{z}{r}(5\frac{z^2}{r^2}-3)\hat{\mathbf{k}}\right]. \tag{7.1}$$

In LEO at altitudes of 200 km, there is sufficient air density to exert drag and cause aerodynamic heating which could deorbit the spacecraft. Its main effects are thus to decrease $h$ or $a$ and $e$. Along with $J_2$, this is one of the main perturbations for the LEO orbit. For the LLO, while drag is a factor, its effect is much smaller due to the low air density. The perturbing acceleration $\mathbf{p}$ due to atmospheric drag is presented in Equation 7.2 [22]. $\rho$ is the atmospheric density, $v_{rel}$ is the norm of the velocity

vector $\mathbf{v_{rel}}$ of the spacecraft relative to the rotation of the atmosphere, $C_D$ is the drag coefficient, $A_f$ is the frontal area of the spacecraft and $m$ is its mass. The model uses the US Standard Atmosphere 1976 model to define atmospheric density variation with altitude. Drag in lunar orbit is considered to be negligible due to its sparse exosphere (one 25-trillionth the density of Earth's atmosphere)[3], hence this term reduces to zero for lunar orbit.

$$\mathbf{p_d} = -\frac{1}{2}\rho v_{rel}\left(\frac{C_D A_f}{m}\right)\mathbf{v_{rel}} \quad (7.2) \qquad \mathbf{p_{srp}} = -\nu\frac{S}{c}\frac{C_R A_a}{m}[\cos\lambda\hat{\mathbf{i}} + \cos\epsilon\sin\lambda\hat{\mathbf{j}} + \sin\epsilon\sin\lambda\hat{\mathbf{k}}]. \quad (7.3)$$

Perturbations from solar radiation pressure (SRP) also affect the spacecraft's motion. While the effect of SRP is relatively small in LEO and LLO, it is a larger factor during the coasting arc. It is characterised by collisions between the spacecraft and photons carrying energy and momentum. The solar radiation perturbation in the Earth Centered Inertial Equatorial (ECIEq) reference frame may be quantified as shown in Equation 7.3 [22]. $S$ is the solar energy flux, $c$ is the speed of light, $\nu$ is the shadow function (1 for sunlight conditions, 0 otherwise), $C_R$ is the spacecraft's radiation pressure coefficient, $A_a$ is the absorbing area, $\lambda$ is the solar ecliptic longitude and $\epsilon$ is the inclination of the ecliptic plane with respect to the central body's equatorial plane.

Lastly, N-body perturbations are also an influence on the spacecraft's motion which is characterised by the N-body problem (NBP). In this system, the Earth, Moon, and Sun are primary bodies in orbit around the system's barycenter, while the spacecraft has negligible mass and does not affect the primaries. In this sense, the spacecraft's motion will be perturbed by all primary bodies at any point in its orbit. Lunar and solar (and Earth's) gravity should thus be considered and can be modelled with Equation 7.4 [22]. $\mu_{nb}$ is the gravitational parameter of the $n$th body, $r_{nb/s}$ is the norm of the position vector $\mathbf{r_{nb/s}}$ of the third body relative to the spacecraft and $r_{nb}$ is the norm of the position vector $\mathbf{r_{nb}}$ of the third body relative to the central body. While the computed solar position is based on a model that incorporates mean anomaly, solar longitude, and the obliquity of the ecliptic, the lunar position is computed based on detailed ephemeris data and models that account for the Moon's orbital elements.

$$\mathbf{p_{nb}} = \mu_{nb}\left(\frac{\mathbf{r_{nb/s}}}{r_{nb/s}^3} - \frac{\mathbf{r_{nb}}}{r_{nb}^3}\right) \quad (7.4) \qquad \ddot{\mathbf{r}} = -\mu\frac{\mathbf{r}}{r^3} + \mathbf{p_{J_2}} + \mathbf{p_d} + \mathbf{p_{srp}} + \mathbf{p_{3b}} \quad (7.5)$$

Overall the model considers both secular and periodic variations in orbital elements due to the aforementioned perturbations. To account for and model these perturbations, they are integrated directly into the equation of motion resulting in Equation 7.5 which is implemented in MATLAB. The codes for the individual perturbations are taken directly from [22]. To account for a general model, these are then merged into one single code. This code is then verified by comparing the contributions of the individual perturbations in the general code, to their respective outputs in their individual code assuming the same conditions.

## 7.3. Low Lunar Orbit Design

The LLO selection directly impacts the descent and surface operations of the mission. Given the specific requirements of demonstrative site C1, the chosen LLO must ensure frequent passes, stable communication, and appropriate illumination. Key parameters of the LLO are its Keplerian elements including the semi-major axis $a$, eccentricity $e$, inclination $i$, right ascension of the ascending node $\Omega$ and argument of perilune $\omega$. Furthermore, $\theta$ is the true anomaly. Along the process, there will be orbit design for the specific landing site C1 and for the general case.

To define the orbit, a reference frame must first be defined. The Moon Centered Inertial Equatorial Reference Frame (MCIEq) is used as it is simple and stable, meaning it is not influenced by the rotation of the Moon. The system has its origin at the Moon's center of mass. The x-axis points towards the vernal equinox (the direction of the ascending node of the Moon's orbit about Earth on the ecliptic plane). The z-axis points towards the Moon's rotational north pole, perpendicular to its equatorial plane. The y-axis points 90° east of the x-axis, lying in the equatorial plane to complete the

[3]URL https://www.nasa.gov/general/what-is-ladee-the-lunar-atmosphere-and-dust-environment-explorer/ [cited 19 June 2024]

right-handed coordinate system. The frame along with the orbital elements are shown in Figure 7.2. The angular momentum vector is $h$ normal to the orbital plane and is used instead of the semi-major axis for visualisation purposes.

The selection of LLO will influence descent requirements, therefore a strategy must be defined to set up the descent process. After the lunar transfer arc, the lander will arrive at the targeted perilune of the lunar fly-by where it inserts into an initial circular LLO at 100km altitude. This altitude is targeted as it provides reasonable access to the lunar surface, while still being safe from targeting errors that would cause impact. Most of the Apollo missions also orbited around this altitude [24] (Apollo 11 at exactly 100 km). This altitude provides a stable platform ensuring operational safety and effective communication with Earth, allowing for thorough system checks. From this altitude, the lander will perform a Hohmann transfer to a circular pre-descent orbit of 10 km which allows for detailed scouting of the lunar surface and descent preparations. This approach ensures a safe and controlled descent, ensuring efficient fuel use and increasing landing accuracy.

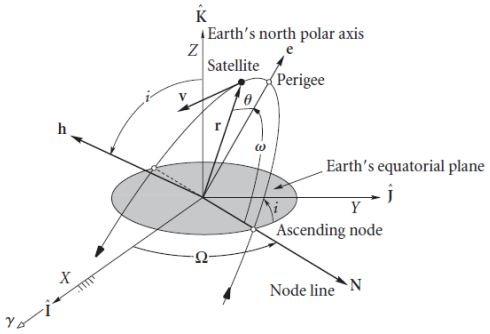


**Figure 7.2:** Inertial Equatorial Reference Frame and the orbital elements [22]

Section 7.1 defined that from the selected orbit, the region with latitude between 88°-90°S should be reachable, and specifically site C1. The inclination of the orbit should thus be equal to the latitude of site C1 so that the orbit will pass directly over it. For free-return trajectories, the RAAN for the LLO will lie within 5° of the Moon's antipode (line connecting the center of Moon and Earth, hence it may be assumed that the spacecraft arrives at a RAAN of 180° [24]. The argument of perilune is undefined in the case of a circular orbit. The convention is then to define the eccentricity vector along the line of nodes $\hat{N}$ defined in Figure 7.2, i.e. to set the argument of perigee to zero.

**Table 7.2:** Orbital Parameters of the LLO Orbits

| Orbital Parameter | Initial | Pre-Descent |
|---|---|---|
| $a$ [km] | 1837 | 1757 |
| $e$ [-] | 0 | 0 |
| $i$ [°] | 89.4 | 89.4 |
| $\Omega$ [°] | 180 | 180 |
| $\omega$ [°] | 0 | 0 |
| T [s] | 7065 s | 6609 s |

**Table 7.3:** Secular Variation of Orbital Parameters in LLO

| Parameter | Secular Variation over 3 Orbits at 100 km | Secular Variation over 1 Orbit at 10 km |
|---|---|---|
| $\bar{\dot{h}}$ $[km^2/s^2]$ | $-3.09 \times 10^{-2}$ | $-1.68 \times 10^{-1}$ |
| $\bar{\dot{e}}$ [-] | $2.78 \times 10^{-5}$ | $6.28 \times 10^{-4}$ |
| $\bar{\dot{i}}$ [°] | $-4.57 \times 10^{-7}$ | $-1.75 \times 10^{-5}$ |
| $\bar{\dot{\Omega}}$ [°] | $-3.09 \times 10^{-3}$ | $-9.08 \times 10^{-2}$ |

The spacecraft's lunar orbit will of course be perturbed and this perturbation should be quantified and consequently rectified. The lander should stay in orbit for at least one orbit to perform proper mapping and system check and maximally three orbits to avoid much orbit maintenance. Another orbital correction manoeuvre must be performed in 10 km orbit as the lander will complete at least one revolution before initiating descent to be able to perform enough system checks and make a decision on whether to descend. The analysis showed that orbital elements show secular and short-period behaviour, as expected. The secular variation is considered for orbit maintenance purposes and is presented below in Table 7.3.

A manoeuvre combining a shape and plane change must be implemented in both orbits to ensure the spacecraft may reach its desired position. The formulas used to calculate the $\Delta V$ of all of the station-keeping manoeuvres to go from the perturbed orbit 2 back to original orbit 1 are presented below

in Equation 7.6 and Equation 7.7 [22], assuming that the manoeuvre is performed at the periapsis of the perturbed slightly elliptical orbit.

$$\cos\delta = \cos i_1 \cos i_2 + \sin i_1 \sin i_2 cos\Delta\Omega \quad (7.6)$$

$$\Delta V = \sqrt{V_1^2 + V_2^2 - 2V_1V_2\cos\delta} \quad (7.7)$$

The magnitude of this manoeuvre in the 100 km orbit is 0.1 m/s whereas for the manoeuvre in the 10 km orbit would be 2.85 m/s. The Hohmann transfer from 100 km to 10 km can be trivially calculated to be 83.32 m/s. The lander thus spends a total of86.27 m/s while in LLO.

## 7.4. Free-Return Trajectory Design

The purpose of the transfer phase is to patch together the LLO and LEO which ensures that the spacecraft will depart and arrive safely and accurately from and to its desired destination. This part of the mission includes trans-lunar injection (TLI), the coasting phase & mid-course corrections (MCC), and lunar orbit insertion (LOI). The objective is then also to obtain the $\Delta V$ requirements for these manoeuvres, and the total time of flight.

A MATLAB implementation for a numerical lunar transfer simulation is used, written by Curtis [22]. One key assumption made in the code is that manoeuvres are considered to be impulsive, meaning $\Delta V$'s are applied instantaneously (**AS-MA-01**). This is an idealisation through which the rocket thrust may be omitted in the equations of motion. This assumption is satisfactory for manoeuvres where the spacecraft position changes only slightly during the time that the manoeuvring rockets fire. This is valid for high-thrust rockets with burn times that are short compared with the coasting time of the vehicle [22]. The longest burn in this mission takes only about 0.1 % of the coasting time and hence this assumption may hold. The error in the $\Delta V$ caused by this assumption is estimated to be lower than 10 %, according to Larbi and Stoll [25]. This means burn time is not included in the simulation.

Keeping in mind the aforementioned assumptions, the implementation of the code is presented in Figure 7.3. The code assumes an initial state of the spacecraft in TLI. The user must then specify the geocentric right ascension $\alpha_0$, declination $\delta_0$, flight path angle $\gamma_0$, altitude $h_0$ and velocity $v_0$ at TLI. Furthermore, the predicted time to perilune $ttt$ and the desired date & time of arrival at the lunar sphere of influence (SOI) in UTC must be stated. The code then uses MATLAB's ode45 function to integrate the trajectory.

To understand the concept of SOI, consider that at some point along the Earth to Moon coasting arc, the Moon's gravitational pull on the spacecraft will exceed that of Earth. Typically in patched conic techniques, this sphere of influence may be seen as a mere speck relative to the vast interplanetary distances. However, the Moon's sphere of influence lies about 66 200 km from its center [22], which extends out to over one-sixth of the distance to Earth so it can hardly be considered a speck. Another complication is that the Earth and Moon are somewhat comparable in mass, so their barycenter lies almost three-quarters of an Earth radius from the Earth's center. The Moon's motion can thus not be accurately described as rotating around the center of Earth.

The code outputs data for both the Moon and spacecraft at various mission phases. For the spacecraft, the outputs at TLI are the required $\Delta V_{TLI}$ for TLI and the inclination of the translunar orbit $i_{TLI}$. When the spacecraft reaches perilune, the outputs are the altitude of perilune $h_{peri}$, its velocity relative to the Moon $v_{rel}$, the inclination of its osculating plane $i_{peri}$, the time elapsed since TLI $t_{peri}$ and the $\Delta V_{LOI}$ required for lunar orbit insertion. Upon the spacecraft's return to Earth, the outputs are the elapsed time since TLI $t_f$, the altitude of perigee $h_f$, final geocentric right ascension $\alpha_f$ and declination $\delta_f$ and the $\Delta V_{EOI}$ required for Earth orbit insertion. For the Moon, its geocentric right ascension $\alpha_m$ & declination $\delta_m$ and distance to Earth $r_m$ are the outputs at various times. Furthermore, $err$, the distance between Moon's actual position at perilune arrival and its position after the predicted flight time $ttt$ is also an output. The code performs numerical integration of Equation 7.5 using MATLAB's `ode45` implementation.

To touch upon the concept of the osculating plane, since the orbit is not Keplerian as it results from the

gravitational force of at least two bodies, it does not lie in a single plane. Each point of the trajectory has its osculating plane defined by its velocity and acceleration vectors. The unit normal $\hat{b}$ to the osculating plane is called the binormal which is found through Equation 7.8, and the inclination is found by Equation 7.9.

$$\widehat{\mathbf{b}} = \frac{\mathbf{v} \times \mathbf{a}}{\|\mathbf{v} \times \mathbf{a}\|} \tag{7.8}$$

$$i = \arccos(\hat{b_z}) \tag{7.9}$$

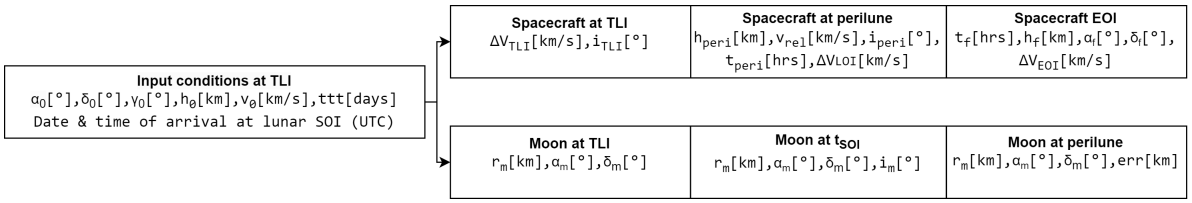


**Figure 7.3:** MATLAB Code Inputs & Outputs for Lunar Transfer Simulation

The objective is then to find a suitable combination of the input parameters that allow for reaching $h_{peri}$ of 100 km with the lowest $\Delta V$, with an inclination of the osculating plane as close as possible to the target 89.4°. There are constraints on the input parameters. Parameters $\alpha_0$, declination $\delta_0$ are constrained by the inclination of the LEO but are variable, whereas $h_0$ is fixed by the LEO orbit. The RAAN of the LEO may thus be determined as a result of the selected $\alpha_0$ and $\delta_0$. A constraint for $v_0$ is that it must be lower than the escape velocity for the selected altitude.

Furthermore, the date and time should also be altered. The mission will launch in 2029, to allow the lander as much time as possible to be developed. The Moon completes an orbit around Earth in one Sidereal month (27.32 days), hence one specific month is considered for launch. A summer launch is preferred, as it generally features more stable weather and longer daylight hours which provides more flexibility for daily launch windows. This also gives several months of buffer time before the start of 2031, acting as a cushion in the event of a failure to launch.

To optimise the combination of parameters, a for loop should be implemented to run through an array of values for each of the inputs with set steps resulting in around $10^{11}$ simulations required to find an optimum value. This computational power is out of reach for the technologies available during the project, hence some variables must be constrained arbitrarily. The date and time for lunar SOI entry, and thus the Moon's position is chosen to be constrained, as it proved easier to run through the initial conditions of the spacecraft in this way. The chosen date and time for this is 1st of July 2030, 15:00:00 UTC, which also complies with the requirement that the spacecraft shall remain in LEO during the lunar eclipse occurring on 15th of June 2030 [26]. Furthermore, the initial altitude is set to 200 km as is explained in Section 7.5. The right ascension, declination, and flight path angle are iterated in steps of 5°. The initial velocity is chosen to be optimised separately after defining viable aforementioned conditions, while the predicted time to perilune is set to three days. The results of the mission analysis for this phase are as follows. A representation of the trajectory directly from the MATLAB code is shown in Figure 7.4.

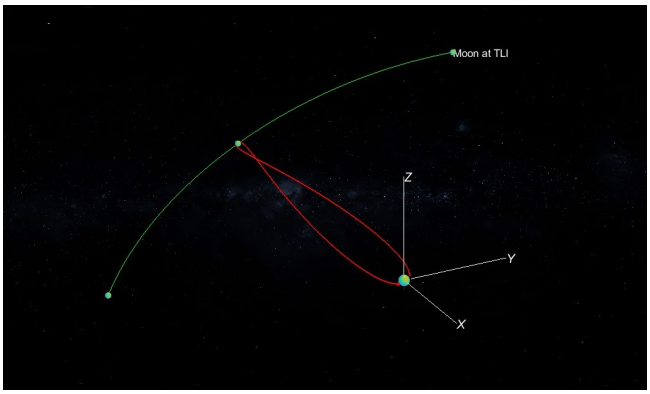


**Figure 7.4:** Free-Return Trajectory Showing the Moon's Orbit (Green) and the Spacecraft's Orbit (Red) in Geocentric Equatorial Reference Frame

The OTV shall provide the TLI burn on the 28th of June at 08:15:50 UTC with a magnitude of 3.1112 km/s when the spacecraft is at an altitude of 200 km at a right ascension of 90°, declination of 15° with a flight path angle of 40°. After a 2.888 day flight, the spacecraft reaches perilune on the 2nd of July

at 05:34:36 UTC at 102.6 km altitude. The OTV and lander will then detach and the lander performs LOI into a circular orbit with a plane change manoeuvre of 65.4° costing 3.2801 km/s. A complication that arises when targeting a perilune of 100 km is that for the OTV, the perigee upon return to Earth is around 20 000 km making EOI too expensive. Thus, an in-track MCC must be employed costing 0.5653 km/s, just after exiting the lunar SOI on the 2nd of July at 20:09:13 UTC. The MCC (and TEI for the lander) is modelled by pulling the state vector of the spacecraft, manually adding a $\Delta V$ to its components and integrating it back into the code. Thus, the OTV arrives at a perigee of 200.2 km on the 5th of July at 05:15:42 UTC where it must perform EOI with a magnitude of 3.1234 km/s. After completing its mission and inserting back into LLO, the lander must perform TEI when it is at the far side of the Moon [24] to target a 200 km perigee with an inclination 120.4° since the lander will also arrive in the orbit, which cost 1.2491 km/s. It must then also perform EOI after a 2.68 day flight, adding another 3.1194 km/s to the lander's budget. The OTV and lander have both reached LEO at this point and may begin their phasing manoeuvre and refuelling operations described in Section 7.5.

## 7.5. Low Earth Orbit Design and Launch Considerations

The success of the mission highly depends on the selected launch windows. These are periods where the spacecraft must launch to achieve its objectives efficiently. The various opportunities for launching both into LEO and into TLI are discussed in this section. Variables including launch azimuth, monthly launch windows and daily launch windows will be defined.

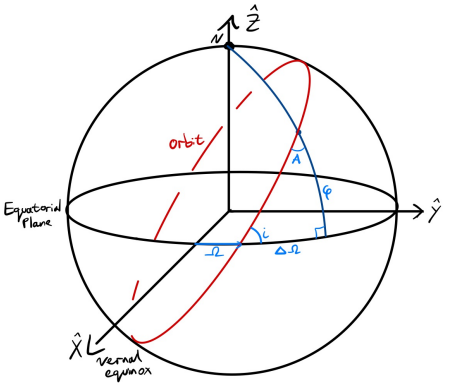


**Figure 7.5:** Spherical Launch Triangle in ECIEq Reference Frame

A launch vehicle analysis is performed in [14] where the selected launch site is Kennedy Space Center (KSC) (28.5°N, 80.6°W). This imposes restrictions on the reachable parking orbits. To understand what this means, it is useful to draw the LEO orbit in the Earth Centered Inertial Equatorial reference frame shown in Figure 7.5. The local meridian is drawn from north direction to the equator. This represents the longitude of the launch site. This line will intersect the orbit at some point from which the latitude $\phi$ can be determined. The azimuth angle $A$ is measured clockwise from north direction towards the plane of the orbit. The launch window location angle is denoted as $\Delta\Omega$, which will lead to determining the launch window sidereal time (LWST) in Equation 7.11. Furthermore, the large circle is the celestial sphere which has no physical meaning but is useful for defining geometries. A spherical triangle is obtained through this process, and its solution is Equation 7.10

Thus, for a given latitude of the launch site, a range of possible of possible inclinations may be achieved, however the minimum achievable inclination is equal to the latitude of the launch site as shown in Figure 7.6. This corresponds to a launch azimuth of 90°E, i.e. launching due east into a prograde orbit, which takes full advantage of the earth's rotational velocity of about 0.404 km/s (at 28.5°N) [22].

$$\cos i = \cos\phi \sin A. \tag{7.10}$$

$$LWST = \Omega + \Delta\Omega. \tag{7.11}$$

To obtain a realistic launch window, a range of acceptable launch azimuth is set from 80°E to 100°E which translates to an inclination of between 28.5° and 30.1°. This range also complies with **HOPE-MISS-290**, and it is chosen to keep the space vehicle on the Eastern Test Range following any abort during launch [24]. Figure 7.5 implies that for an orbit with inclination higher than the latitude of the launch site, the planet rotates the launch site through the orbit twice per day, which is the only time when the spacecraft can be launched into LEO. The options are thus near the descending and ascending node. Applying spherical trigonometry to Figure 7.5, this is allows for a daily launch window of 2 h 42 m 15 s. To know the precise launch times, it is necessary to know the RAAN of the LEO. It may be obtained from the geocentric right ascension $\alpha$, declination $\delta$ and altitude conditions at TLI. The computation involves first converting the aforementioned parameters into a state vector and then into Keplerian elements. This process is executed using a MATLAB implementation from [22]. The

parameters of the orbit are given in Table 7.4.

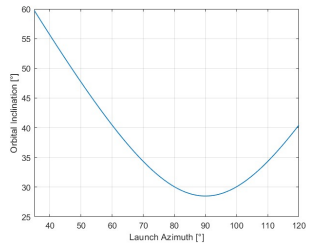


**Figure 7.6:** Achievable Inclinations for Various Launch Azimuths at $\phi = 28.5°$

**Table 7.4:** Orbital Parameters of the LEO Orbit

| Orbital Parameter | Value |
|---|---|
| $a$ [km] | 6578 |
| $e$ [-] | 0 |
| $i$ [°] | 28.5 |
| $\Omega$ [°] | 60.0 |
| $\omega$ [°] | 0 |
| T [s] | 5309 |

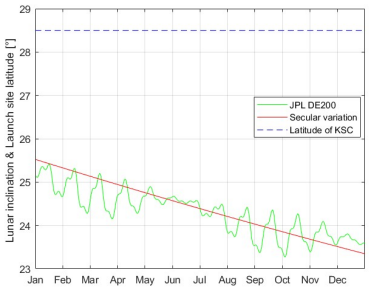


**Figure 7.7:** Variation of Lunar Inclination from January 1, J2029 to January 1, J2030

The motivation for the selection of the orbital parameters is similar to that of the LLO. A circular orbit is preferred as it is more straightforward to perform orbit control. Drag perturbations would be enough to de-orbit the spacecraft if not corrected, moreover it would circularise the orbit [22]. Hence an elliptical orbit would be disadvantageous. Additionally, circular orbits are more predictable in terms of ground track which simplifies communication. Lastly, the spacecraft experiences a more uniform solar heating. An altitude of 200 km is selected, based on previous missions such as Apollo 8[4] and Apollo 11[5] which achieved an altitude of 190 km and 185 km respectively prior to TLI. While this altitude is characterised by moderately high drag, the spacecraft would not be greatly affected as it will not stay in orbit for a long time period. This altitude also provides benefits such as lower radiation exposure and it requires less energy to reach for the launch vehicle, maximising payload capacity.

Launching into LEO at 28.5° inclination is the ideal case as this is the nearest achievable value with respect to the Moon's orbital inclination around Earth. The inclination of the Moon's orbit around Earth oscillates over time, and Figure 7.7 shows this phenomenon in the geocentric equatorial frame for the relevant period of consideration. It is calculated in [22] using JPL's DE200 model. A secular variation is added to allow for an easier comparison to the latitude of KSC. Thus, the chosen inclination brings the spacecraft as close as possible to a coplanar trajectory, minimising the $\Delta V$ for the required plane change manoeuvre. Additionally, it is evidently more beneficial to launch as early as possible, as the Moon's inclination is closer to the minimum achievable orbit inclination from KSC. The ideal case would be to launch into 28.5° inclination at 90°E azimuth. Using the calculated RAAN, assuming the spacecraft performs TLI after one orbit and providing approximately one half hour extra for launch sequence, launch may be assumed to happen on the 28th of June at 06:00:00 UTC.

Once the spacecraft is inserted into LEO by the launcher, it orbit for 1.5 hours to 4.5 hours as set by Apollo 11 guidelines [24]. The minimum time is mainly determined by the time required to perform system checks. The maximum duration is limited by the extra $\Delta V$ required to perform TLI. Based on the maximum LEO duration of 4.5 hours, a perturbation analysis is in place. The analysis showed that orbital elements show a secular and short-period behaviour, as expected. The secular variation is considered for orbit maintenance purposes and is presented below in Table 7.5. The worst case is considered, spending 4.5 hours in LEO. A combined shape and plane change must be implemented in both orbits to ensure the spacecraft may reach its desired position in preparation for TLI. The magnitude of this manoeuvre is 0.966 m/s.

**Table 7.5:** Secular Variation of Orbital Parameters in LEO

| Parameter | Secular Variation over 4.5 hours at 200 km |
|---|---|
| $\bar{\dot{h}}$ $[km^2/s^2]$ | −1.12 |
| $\bar{\dot{e}}$ [-] | $2.48 \times 10^{-4}$ |
| $\bar{\dot{i}}$ [°] | $-1.46 \times 10^{-1}$ |
| $\bar{\dot{\Omega}}$ [°] | $-2.28 \times 10^{-3}$ |

[4] URL https://www.nasa.gov/missions/apollo/apollo-8-mission-details/ [cited 19 June 2024]
[5] URL https://www.nasa.gov/history/apollo-11-mission-overview/ [cited 19 June 2024]

### $\Delta V$ for Operations

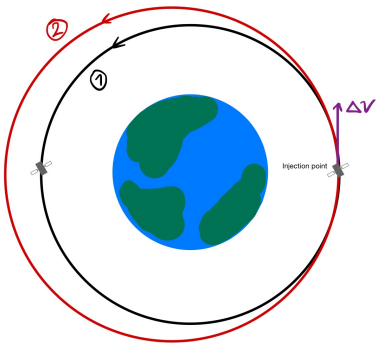


**Figure 7.8:** Example Phasing Manoeuvre for $\Delta\theta = 180°$

When the OTV returns to LEO it must reach a refuelling vehicle. This likely requires a phasing manoeuvre as shown in Figure 7.8, as the two spacecraft will most probably not meet directly. The OTV would insert into a slightly elliptical orbit 2 at its perigee with a higher period to end up at the same spot as the refuelling vehicle some time later and then insert into the original orbit 1 again. The worst possible case is that the OTV arrives in LEO with a difference in true anomaly of 180° with respect to the refuelling vehicle. The $\Delta V$ requirement is designed for this. To relax this requirement slightly, it is possible to extend the duration of the phasing manoeuvre, i.e. the number of orbits that may be completed before the spacecraft are phased. For this phasing procedure, the OTV may take 6.5 days (about 105 orbits) to perform the manoeuvre, as there is no crew on-board. The $\Delta V$ required for this manoeuvre is 49.6 m/s.

About 6.5 days pass as the lander should complete its mission on the lunar surface. When it returns to Earth, the OTV must phase with it. Again, the most expensive manoeuvre is considered. Following the calculations from the OTV's LEO perturbation analysis, the $\Delta V$ required for orbital maintenance across the period the lander is not in LEO is 33.48 m/s. Once the lander and OTV are back in LEO, the two spacecraft must merge back together. The maximum number of orbits is limited to 10.5 for the lander due to crew comfortability and safety considerations, making the manoeuvre around 15 hours long. The $\Delta V$ expenditure by the OTV is then 0.497 km/s. The lander however must perform orbit maintenance for at least 15 hours requiring about 3.22 m/s to stay in the correct orbit.

## 7.6. $\Delta V$ Budgets

Table 7.6 gives a comprehensive overview of the results concerning the $\Delta V$ requirements for both the OTV and the lander based on the mission analysis performed in this chapter. For each phase of the mission, the $\Delta V$ is shown and subsequently added to arrive at a final value for both vehicles. The final value includes a 10 % margin that is applied due to assumption **AS-MA-01**. This margin can be considered to include $\Delta V$ for MCCs required due to discrepancies between the ideal assumptions used to derive the model and reality. Furthermore, the total $\Delta V$ for the lander may be seen as an approximate upper bound as the drastic plane change manoeuvre at perilune may not be required for missions that accept the arrival inclination saving more than 1.5 km/s. Lastly, an approximate upper bound for the mission duration may be around 13 days, consisting of 3 days to perilune, 6.5 days on the lunar surface, 3 days to perigee and 0.5 days for LEO operations.

**Table 7.6:** $\Delta V$ Requirements per Mission for the Lander and OTV excl. Lunar Ascent/Descent

| **Manoeuvre** | **Lander** $\Delta V$ **[m/s]** | **OTV** $\Delta V$ **[m/s]** |
|---|---|---|
| Trans-Lunar Injection (TLI) | N/A[1] | 3111.2 |
| Lunar Orbit Insertion (LOI) | 3280.1 | N/A |
| LLO Hohmann transfer | 86.3 | N/A |
| Trans-Earth Injection (TEI) | 1249.1 | N/A |
| Mid-Course Correction (MCC) | N/A | 565.3 |
| Earth Orbit Insertion (EOI) | 3119.4 | 3123.4 |
| LLO station-keeping | 5.9 | N/A |
| LEO station-keeping | 3.2 | 34.5 |
| LEO phasing manoeuvres | N/A | 546.6 |
| Total $\Delta V$ (incl. 10 % margin) | 8518.4 | 8119.1 |

[1] N/A = Not Applicable

# 8 | Lunar Ascent and Descent

This chapter will cover the lunar ascent and descent analysis. Section 8.1 describes the simulation environment used for the analysis. Section 8.2 discusses descent to the lunar surface, while Section 8.3 discusses the subsequent return to orbit. This is followed by the verification and validation of the simulation tool in Section 8.4.

## 8.1. Simulation

To analyse the ascent and descent guidance software a program was developed that simulates the lander's motion in the lunar environment. This section will first describe the underlying principles upon which the simulation program is based. Then, the relevant assumptions made during the development will be discussed, and finally, an overview of the code structure will be given.

The simulation operates by numerically solving the translational equations of motion. These equations, applied to a generic body, describe the body's motion under the influence of gravity from a central body as well as external forces $\boldsymbol{F}$. For a spacecraft, this force vector is typically the thrust force $\boldsymbol{F_T}$ applied by the propulsion system as well as other perturbing forces; for this analysis, as will be discussed further below, these perturbing forces are not included, and thus $\boldsymbol{F} = \boldsymbol{F_T}$. These are shown in Equation 8.1 for the three position components $\boldsymbol{r}$, Equation 8.2 for the three velocity components $\boldsymbol{V}$, and Equation 8.3 for the mass $m$, for a total of seven scalar equations. In these equations, $\mu = 4902.800 \times 10^9\ \mathrm{m^3/s^2}$ is the gravitational parameter of the Moon, $I_{sp}$ is the specific impulse of the engines, and $g_0 = 9.806\,65\ \mathrm{m/s^2}$ is the standard gravitational acceleration.

$$\dot{\boldsymbol{r}} = \boldsymbol{V} \tag{8.1}$$

$$\dot{\boldsymbol{V}} = \frac{-\mu \boldsymbol{r}}{|\boldsymbol{r}|^3} + \frac{\boldsymbol{F_T}}{m} \tag{8.2}$$

$$\dot{m} = \frac{|\boldsymbol{F_T}|}{I_{sp} g_0} \tag{8.3}$$

Multiple reference frames are used in the simulation. The Moon-Centered Inertial frame $\mathcal{F}_I$ is an inertial frame with the origin at the center of the Moon, with the $\hat{\boldsymbol{i}}_{\boldsymbol{x}}$ axis oriented towards the intersection of the prime meridian and the equator at $t = 0$, the $\hat{\boldsymbol{i}}_{\boldsymbol{z}}$ axis pointing along the axis of rotation of the Moon, and $\hat{\boldsymbol{i}}_{\boldsymbol{y}}$ completing the right-handed system. This frame is used for the general equations of motion. The Moon-Centered Moon-Fixed frame $\mathcal{F}_C$ is a surface-fixed frame that rotates with the Moon, and is used to express a landing site in terms of a latitude, longitude, and altitude. Finally, the landing site frame $\mathcal{F}_L$ is an inertial frame located at the point of touchdown. The $\hat{\boldsymbol{i}}_{\boldsymbol{x}}$ axis is tangent to the local horizontal and points downrange in the direction of the lander's motion, the $\hat{\boldsymbol{i}}_{\boldsymbol{z}}$ axis is the local vertical, and the $\hat{\boldsymbol{i}}_{\boldsymbol{y}}$ axis is the crossrange direction used to complete the right-handed system. The landing site frame is inertial, but is defined with the origin at the landing site, which is expressed in $\mathcal{F}_C$; therefore, the landing site and the origin of $\mathcal{F}_L$ only coincide at the moment at touchdown. However, because the time of the MBP and AP are predetermined, the location of $\mathcal{F}_L$ is known and is constant throughout the descent.

Several assumptions were made during the development of the program, which are as follows:

- A1: The vehicle was assumed to be a point mass such that the equations of motion could be derived using Newtonian mechanics. The error that results from this assumption is proportional to the difference in the radial distance $R$ and the vehicle height. For the intended application, the error will be greatest at the lunar surface. To understand the magnitude of the error, a cylinder on the lunar surface with a mass of 50 800 kg, a height of 12 m, and a radius of 3.5 m, will have an error in the computed gravity force of only 0.016 %.
- A2: Vehicle attitude dynamics were neglected and assumed to be an output of the guidance system to simplify the simulation such that a usable program could be developed in the time available that would still allow for the testing of the basic functionality of the guidance system. However, this does have consequences on the reliability of the simulation results. This assump-

tion will likely result in underestimating the required $\Delta V$ for the lunar ascent and descent. Future iterations of the simulation should model attitude kinematics to improve the reliability of the model.

- A3: The radius of the Moon was assumed to be constant to simplify the initial analysis of the guidance software such that its basic functionality can be tested in a simple environment. However, it should be noted that this assumption is only valid for the initial analysis and should be improved upon in the future. In future iterations, irregularities in the lunar surface should modeled accurately, especially close to the desired landing site where variations in the terrain will likely have an effect on the response of the guidance system. For clarity, the Moon has a topographic range of 13 km[1], which is equivalent to a variation of $\pm 0.375$ % in lunar elevation with respect to the Moon's mean volumetric radius.
- A4: The center of the Moon was assumed to be an inertial frame of reference to derive the equations of motion using the Vehicle-Carried Normal Moon Reference Frame. This approach is commonly employed in trajectory analysis near planetary bodies. However, it is important to remember that this assumption only holds while the lander remains relatively close to the Moon. Given that our study focuses on analysing ascent and descent trajectories, this assumption is appropriate. Moreover, the brief duration of our simulation runs, typically just tens of minutes, further supports its validity
- A5: Orbital perturbations resulting from the Earth, Sun, Jupiter, and solar radiation pressure have been neglected in the simulation. The error that results from this assumption can be quantified by comparing the magnitudes of the induced accelerations. The gravitational acceleration relative to the Moon experienced by the vehicle in low lunar orbit due to the Moon is roughly 2.7 m/s$^2$, while the relative acceleration resulting from the Earth is on the order of 0.005 m/s$^2$, only 0.19 % of that caused by the Moon. Furthermore, the perturbations resulting from the Sun and Jupiter are even smaller in magnitude, while the acceleration induced by the Solar Radiation is of the magnitude $10^{-7}$ m/s$^2$ [22]. These accelerations are relatively small in magnitude, and since the ascent and descent phases will have a duration ranging in the tens of minutes, are safe to be neglected. It should be noted that these effects are not neglected in the orbital trajectory simulation discussed in Chapter 7.

The program consists of three phases: program setup, simulation, and post-simulation activities. Each of these is responsible for a distinct set of tasks as shown in Figure 8.8. The program setup is responsible for setting up the simulation environment and importing all required information to run the program. Part two has two tasks: firstly, simulating the vehicle motion by solving the equations of motion using either the Runge-Kutta 4 or the Runge-Kutta-Fehlberg method, and secondly, ensuring that ascent and descent guidance software is implemented accordingly. Finally, the third part of the program is responsible for all closing activities, such as saving and showing the simulation results.

## 8.2. Lunar Descent

After capturing around the Moon, the vehicle must then descent to the lunar surface and softly touch down. This must not only be done in an efficient manner, so that the minimum amount of propellant is expended, but also must be done in a safe and controlled way which is resilient to failure scenarios. The latter point is especially relevant to the ARCH-E mission, given the human crew onboard and the requirement for autonomous operations (**HOPE-MISS-040**).

The descent is controlled by a guidance algorithm, which commands the vehicle according to specific control laws. These control laws use the vehicle's current state to generate a desired thrust magnitude and direction as a function of time in order to drive the vehicle from the current state to a desired terminal state.

During the midterm phase, several descent guidance algorithms were identified for further investigation.

[1] URL https://nssdc.gsfc.nasa.gov/planetary/factsheet/moonfact.html [cited 18 June 2024]

Selection of the specific guidance algorithm is a significant choice, as a wide range of algorithms and techniques are available. Several factors important for consideration are the efficiency and optimality of the guidance solution in terms of propellant usage, as well as the algorithm's accuracy in achieving the desired landing position. The selected algorithm must also be robust, meaning that it can reliably converge to a solution under a variety of operational and input conditions.

Several descent guidance algorithms were identified from a literature study. These include Apollo's polynomial descent guidance and E-guidance, zero-effort-miss/zero-effort-velocity guidance, potential field methods, pseudospectral methods, convex guidance, and throttled explicit guidance [27–31]. Among these, convex guidance stood out as a strong option; a comparison between these methods found it to be the most optimal in terms of propellant usage [27]. Convex guidance involves rewriting the descent optimisation problem objective and constraints into the form of a second-order cone programming (SOCP) problem [28]. This is particularly attractive as it guarantees that the problem has only one global minimum propellant solution without additional local minima, which can be found quickly and efficiently through specialised solvers; these solver are also guaranteed to converge to the solution to a prescribed level of accuracy in a finite number of iterations [29]. Convex guidance is often used in studies with precise landing requirements, and is used by SpaceX for precision landing of their reusable rocket boosters [32].

The descent is split into three main phases, as shown in Figure 8.1. These phases are chosen to match those commonly found in powered descent studies, and also roughly correspond to the previously demonstrated Apollo descent strategy [33]. As described in Chapter 7, the lander is initially in a 100 by 100 km LLO parking orbit. It then performs a Hohmann transfer down to a 100 by 10 km orbit. At perilune, the descent begins with Powered Descent Initiation (PDI), which is 640 km downrange from the landing site. At PDI, the lander ignites its engines and enters the main braking phase (MBP), which lasts 620 s. During the MBP, the lander covers all but a couple of kilometers of the distance to the landing site and uses the majority of the propellant as it reduces the majority of its orbital velocity.

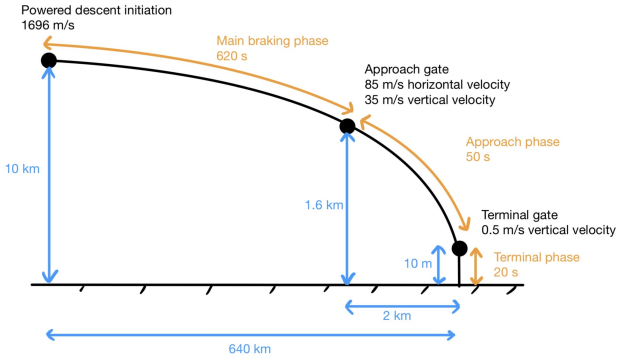


**Figure 8.1:** Descent Phases

The desired terminal conditions for the MBP are the Approach Gate (AG), at which point the lander transitions to the Approach Phase (AP). At the AG, the lander is 2 km downrange and 1.6 km above the landing site, travelling at 85 m/s downrange and descending at 35 m/s. During the AP, various sensors on the lander become active to scan the landing site for hazards and obtain accurate estimates of the lander's position and velocity relative to the terrain. It is during this phase that the lander can correct for errors introduced during the MBP, or target a new landing site if necessary. The end of the AP is reached at the Terminal Gate (TG), where the lander is directly above the landing site at an altitude of 10 m. The final phase of the descent, the Terminal Phase (TP), is a smooth vertical descent at a constant rate of 0.5 m/s. Any remaining horizontal velocity is nulled until the lander softly touches down on the lunar surface and the engines are shut down.

The process of converting the guidance problem to the convex form, known as convexification, is omitted here for brevity; an in-depth explanation can be found in [28–30]. During the MBP, constraints are applied for the initial conditions at PDI and the terminal conditions at the AG. A constraint is also applied to ensure that the thrust magnitude at all times lies bounded between the minimum and maximum thrust levels of the engines. The equations of motion (Equation 8.1 through Equation 8.3) are convexified through a change of variables, and the resulting equations are 'stacked' for all timesteps between PDI and the AG. The resulting solution is a zero-order hold of the thrust magnitude and direction at each timestep, meaning that these control inputs are held at constant values between

the discrete timestep nodes. A timestep of 5 s was chosen for the MBP, as this was shown by [30] to provide an acceptable balance between computational effort and accuracy. This choice introduces errors on the order of meters at the AG, which will be shown below to be negligible in terms of propellant usage.

Due to the significant downrange distance covered during the MBP, the Moon's curvature is non-negligible and must be taken into account. Similarly, an inverse-square gravity model that follows the curvature of the Moon must be used. This is achieved through formulating the dynamics as a linear time-varying system, and performing several solution iterations. At each iteration, the previous solution is used to compute the gravitational direction for the next solution, until the change in cost (i.e. propellant usage) between successive solutions falls below a certain tolerance.

During the AP, the initial conditions and terminal constraints are the AG and TG respectively. The timestep is decreased to 1 s, as the time-to-go and therefore the problem size for this phase is significantly smaller. In addition to the thrust constraint, a minimum glideslope constraint is applied, to ensure that the solution does not reach too low an altitude at too great a distance from the landing site. Expressing the problem in the $\mathcal{F}_L$ coordinate system is necessary for the glideslope constraint, but also necessitates a flat inverse-square gravity field; this is again implemented through iteration, but as a control input instead of the system dynamics directly. [30] shows that the errors introduced by this are on the order of millimeters and are thus negligible.

During the AP, a constraint can also be applied to the vehicle's attitude, which may be necessary to keep the landing site within the field of view (FOV) of the landing sensors, or to prevent excessive off-vertical attitudes. As will be discussed further in Chapter 14, although a preliminary configuration of the landing sensors has been identified, the precise constraints the lander's attitude in terms of the FOV of the sensors is not known at this design stage. However, [29] shows that applying a constraint as strict as keeping the thrust vector direction within 5° of the landing site direction relative to the vehicle for the entire AP until an altitude of 150 m causes only a 0.4 % increase in propellant used during the AP. Thus, the attitude constraint is not implemented for this analysis.

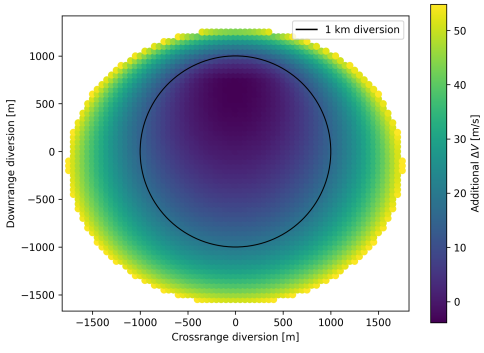


**Figure 8.2:** Extra $\Delta V$ for Landing Site Diversion

The AP is also the point at which landing site retargeting can be performed. If the lander's sensors detect that the terrain at the selected landing site is unsafe, the lander can select a new landing site. As the position of the AG is given relative to the landing site frame $\mathcal{F}_L$, this diversion is investigated by varying the downrange and crossrange position of the AG. The extra $\Delta V$ required for this diversion is shown in Figure 8.2. It should be noted that the lowest additional $\Delta V$ values in Figure 8.2 are negative, meaning that these AG parameters are more propellant-efficient than the selected design point . The reason for this is to allow for equal diversion capabilities along the downrange direction. If the design point was placed at the minimum location, there would be a very slight decrease in the nominal case. However, this would be at the expense of significant diversion capability should the lander wish to target a site further downrange. Given that the downrange and crossrange directions for different landing sites and orbits will be different for each landing, an equal priority for downrannge and crossrange diversion capability was selected. A distance of 1 km was selected to provide a balance between diversion capability and $\Delta V$ required; this is illustrated in Figure 8.2. The extra $\Delta V$ required for this diversion is 19.74 m/s.

The general procedure described in [29] was used to find the optimal parameters for the PDI downrange distange, MBP time to go, AG position and velocity, and AP time to go. An initial Monte Carlo search was performed over a range of parameters, and from there a refined range of parameters were selected. A MBP duration of 750 s was selected, with PDI beginning 740 km downrange from the landing site. The AG was placed at 2 km downrange and 1.6 km altitude, and the optimal velocity at the AG was

found to be 85 m/s horizontally and −35 m/s vertically. The AP time to go was set at 50 s for the nominal case, and 54 s for engine-out scenarios; ideally, the parameters would be identical for both cases, but it was found that imposing this constraint would significantly increase the $\Delta V$ for one of the two cases.

The resulting trajectory is shown in Figure 8.3, and a view of the AP specifically is shown in Figure 8.4. $\Delta V$ values are shown in Table 8.1. In line with the ESA $\Delta V$ margin philosophy, a 5 % margin is applied to the directly simulated manoeuvres. An extra contingency item for 20 s of hover time is also added for any non-nominal scenarios.

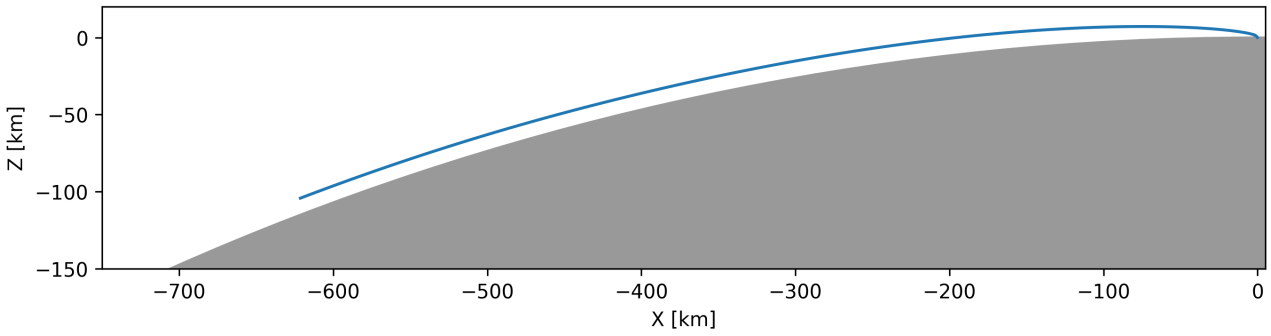


**Figure 8.3:** Full Descent Trajectory

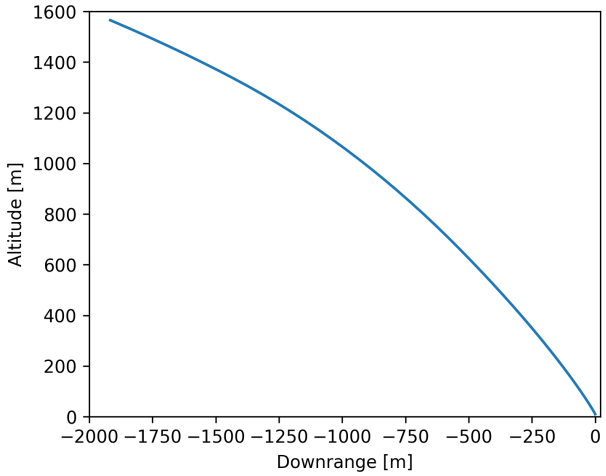


**Figure 8.4:** Approach Phase Trajectory

## 8.3. Lunar Ascent

After surface operations conclude and the lander is ready to return to lunar orbit, a separate ascent guidance algorithm is needed. Unlike descent, where the target terminal state is a specified position and velocity subject to glideslope, attitude, and time-to-go constraints, the target terminal state is a desired orbit comprising a collection of feasible position and velocity constraints. Additionally, the time-to-go is no longer fixed, as the precise orbital insertion time and point are not important due to the lack of orbital rendezvous around the Moon.

mA literature study of ascent guidance algorithms identified several possible options, including the Iterative Guidance Mode (IGM) developed for the Saturn launch vehicles [34], Powered Explicit Guidance (PEG) developed for the Space Shuttle and integrated into the Shuttle's Unified Powered Flight Guidance (UPFG) software [35], OPGUID [36], SWITCH [37], and various other implementations based on optimal control theory.

PEG was selected for the ascent guidance algorithm. It has extensive space heritage, having been developed for the Space Shuttle and integrated into the ascent guidance modes for the Shuttle's UPFG software. PEG is still in use today on SLS, and is often selected for conceptual planetary

ascent vehicle designs [33]. Additionally, a significant factor was the large amount of readily available documentation of the algorithm in terms of software flow charts and equations [35, 38, 39]. This latter constraint was particularly relevant for this design work, as time constraints limited the amount of time and effort available for creating a working piece of software from abstract equations and theory. For this reason, possible future design work could investigate the use of more modern and potentially more propellant-efficient algorithms.

The ascent consists of three distinct phases, as used in literature. The first is an initial vertical ascent until the lander reaches a predetermined vertical velocity. Next, the lander begins pitching over at a constant rate until it is pointed in the direction desired by PEG. Finally, the lander follows the PEG solution all the way until orbit. This is visualised in Figure 8.5. PEG is an iterative predictor-corrector algorithm, and at each guidance call it uses the vehicle's current state to predict the state at burnout. This is then corrected to generate steering commands to achieve the desired final state. The selected target orbit is a 15 by 100 km orbit. As the ascent is a continuous burn from liftoff to insertion into lunar orbit, it was found that ascending to a lower orbit, and then transferring to the 100 by 100 km parking orbit before TEI, was more efficient in terms of $\Delta V$ expended. The extra $\Delta V$ for the transfer to the parking orbit is modelled as a Hohmann transfer with two impulsive burns; as the magnitude of these burns is only on the order of a couple of tens of meters per second, the error introduced by this assumption is negligible.

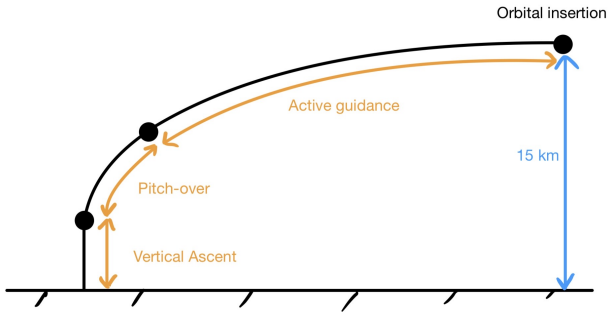


**Figure 8.5:** Ascent Phases

The trajectory is visualised in Figure 8.6, and data from the ascent is shown in Figure 8.7. For ease of visualisation, a launch from an equatorial launch site into a zero inclination orbit is shown. This does benefit from the rotation of the Moon, which gives the spacecraft an additional 4.62 m/s of initial velocity in the MCI frame. This velocity is doubled as the worst case is when the Moon rotates against the desired orbital velocity direction. As this has not been directly simulated, a 20 % margin is added to account for this. The transition from the vertical ascent phase to the pitch-over phase is set at a vertical velocity of 10 m/s, and the turn rate during the pitch-over phase is set at 3 °/s. Both the nominal and engine-out cases are shown. As can be seen, the engine-out scenario does not significantly alter the trajectory, and primarily manifests as a longer downrange distance covered before orbital insertion is reached. With perfect knowledge of the vehicle's state, PEG is able to achieve apolunes of 99.825 and 99.914 km and perilunes of 14.956 and 14.966 km for the nominal and engine-out cases respectively. Per the ECSS $\Delta V$ margin philosophy [15], a 5 % margin is applied to the $\Delta V$ values for directly simulated values. Further investigation of any additional contingencies will be performed for the final draft.

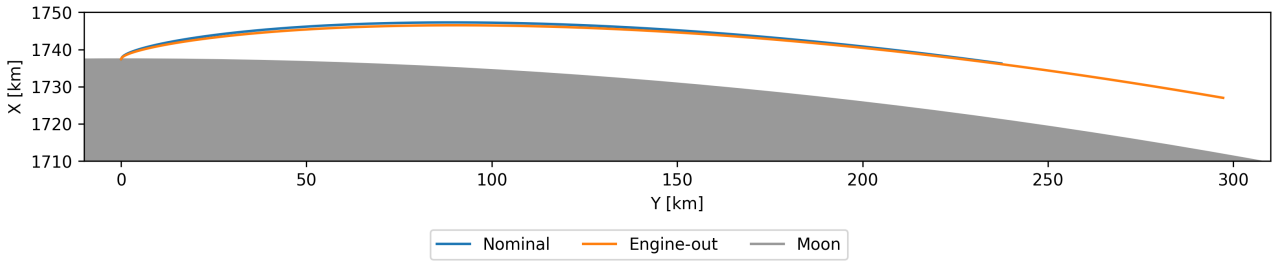


**Figure 8.6:** Ascent Trajectory for Nominal and Engine-out Scenarios in MCI coordinates

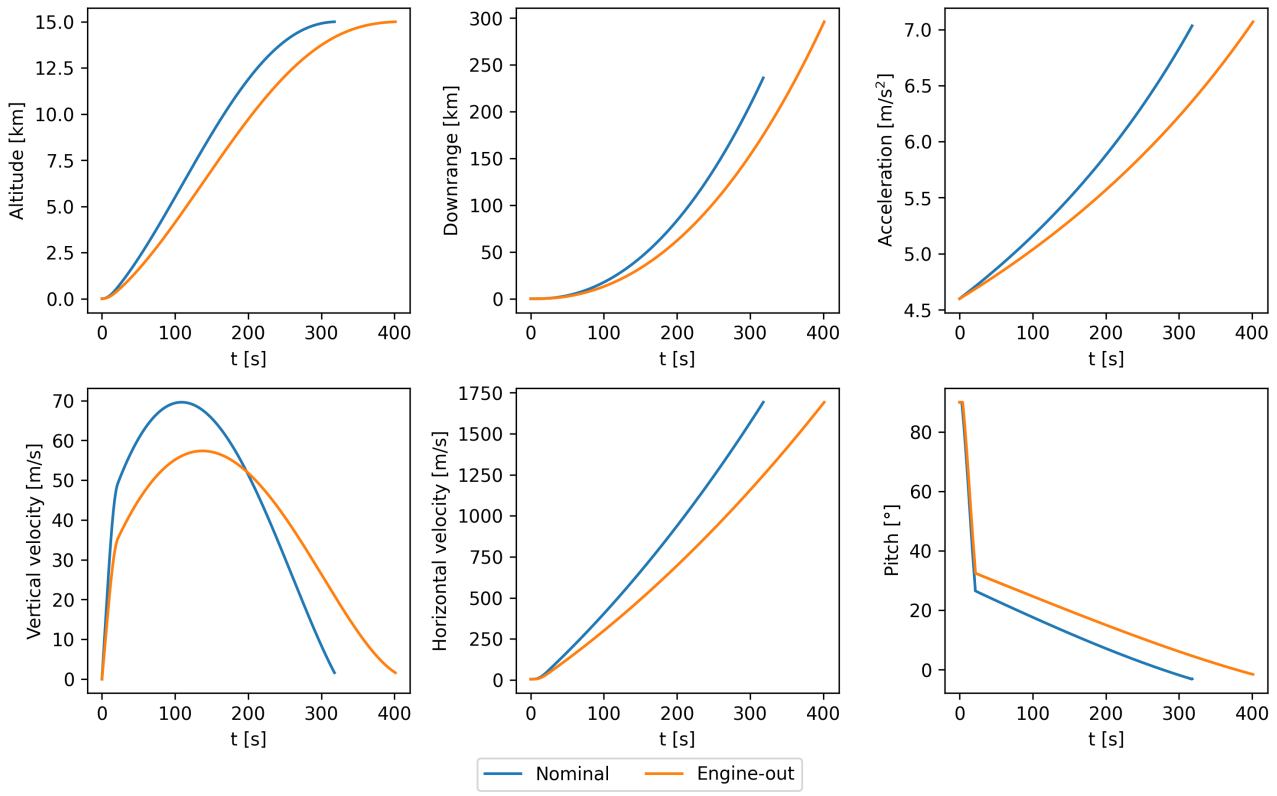


**Figure 8.7:** Ascent Data for Nominal and Engine-out Scenarios

**Table 8.1:** Ascent and Descent $\Delta V$ Budget

| **Item** | $\Delta V$ **[m/s]** | **Margin [%]** | $\Delta V$ **with margin [m/s]** |
|---|---|---|---|
| Descent MBP | 1698.60 | 5 | 1783.53 |
| Descent AP | 147.33 | 5 | 154.70 |
| Descent TP | 32.48 | 5 | 34.11 |
| Landing site retargeting | 19.74 | 5 | 20.73 |
| 20 s contingency hover | 32.48 | 5 | 34.11 |
| Correction for lunar rotation | 9.25 | 20 | 11.10 |
| Ascent to 100 by 15 km orbit | 1815.88 | 5 | 1906.68 |
| Transfer to 100 by 100 km parking orbit | 19.48 | 5 | 20.46 |
| **Total ascent and descent $\Delta V$, with margin:** | | | 3965.42 |

## 8.4. Verification and Validation

Verification and validation (V&V) was performed on the simulation environment to ensure that the model used is sufficiently representative, and that the results can be used with confidence.

First, the inputs for time limits and step size were examined. Both values of 0 and very high values were tried. The time limit showed acceptable behavior for an input of 0, as it immediately ended and indicated no computations were performed. For a high time limit, however, there was no indication of the expected running time, leading to confusion over the maximum running time that can performed in a reasonable time. Setting the step size to 0 resulted in an infinite loop, and as such the program was changed to exit and show a warning in this case. For high timesteps the plotting function failed due to a lack of data points.

Semi-major axis inputs of negative values and 0 were tested. This was found to cause errors, but as this is not realistic, a warning was added to ensure that a wrong error is not emitted without any

indication. Extremely high values for the SMA posed no problem, with values over 1 000 000 km still running smoothly.

Looking at eccentricity, for a value of 1 or above the code breaks down, which will be fixed in case the code needs to be used for parabolic or hyperbolic orbits. The code still ran for negative values, which was changed to give an error instead.

For inclination, RAAN, argument of periapsis and true anomaly, any angles outside the range (negative or >180 for inclination, negative or >360 for the others) were automatically converted by adding or subtracting 180 and 360 degrees, respectively, until within range. A warning was added to alert the user of this conversion.

All values of propellant mass were processed properly. A small graphic error was discovered when incorrect values for the landing site latitude were given, this was resolved by clipping the values to the −90 to 90° range. Setting the number of engines to 0 resulted in a division error, necessitating a warning to the user that this is an incorrect way of setting thrust levels to zero.

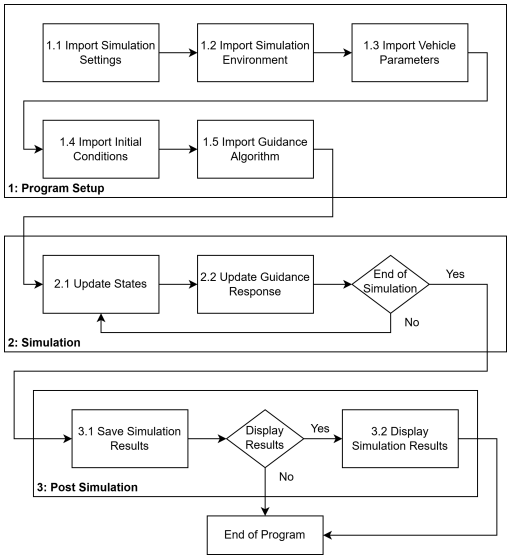


**Figure 8.8:** Code Flow Diagram

Several other bugs were discovered in this phase. If working with geographic coordinates, setting initial velocities to zero (such as at the start of ascent) the simulation would crash when applying thrust. Additionally, When flying directly over the poles, the simulation froze due to the singularity in geographic coordinates. These bugs were subsequently fixed.

Several comparisons to Keplerian orbits were performed to check the functionality of the orbital element conversions. For the given inputs, the nominal orbital times were calculated and the simulation was run for this amount of time at a timestep of 0.01 s. The position of the spacecraft was then assessed after this amount of time to determine the actual SMA after one orbit and the deviation in orbital period. The results are summarised in Table 8.2.

**Table 8.2:** Kepler Orbit Comparisons of the Ascent/Descent Simulation

| | **Orbital elements** | **Test 1** | **Test 2** | **Test 3** | **Test 4** |
|---|---|---|---|---|---|
| Inputs | SMA [km] | 2737.4 | 2737.4 | 2737.4 | 10000 |
| | Eccentricity [−] | 0 | 0.2 | 0 | 0 |
| | Inclination [°] | 0 | 35 | 0 | 0 |
| | RAAN [°] | 0 | 0 | 45 | 0 |
| | Argument of periapsis [°] | 0 | 0 | 45 | 0 |
| | True Anomaly [°] | 0 | 0 | 45 | 0 |
| Outputs | SMA error [m] | 14.675 | 5.988 | 14.675 | 693.962 |
| | Orbital period error [s] | 0.3391 | 0.3936 | 0.3391 | 32.1336 |

The level of error seen in these tests is acceptable and on the level expected from the RK4 integration. This means the code functions as expected and performs propagation successfully over one orbit.

Next, a convergence analysis was performed to investigate the effect of different timesteps. First, a 1000 km altitude circular orbit was simulated for one full orbit at timesteps of 100, 10, 1, 0.1 and 0.01 s. Next, the same analysis was performed for an orbit with an eccentricity of 0.7 and SMA of 6737.4 km. The errors in SMA, plotted on a logarithmic scale, can be seen in Figure 8.9 and Figure 8.10.

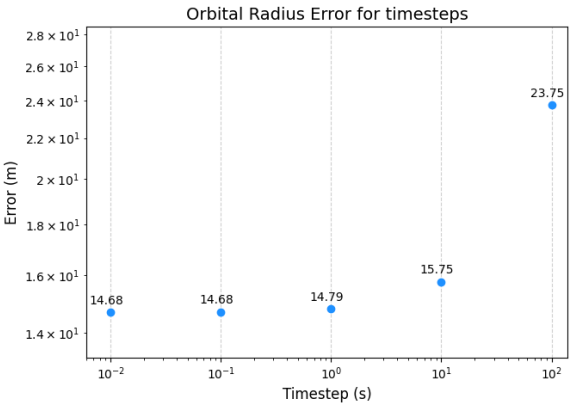


**Figure 8.9:** Error Convergence for Circular Orbit

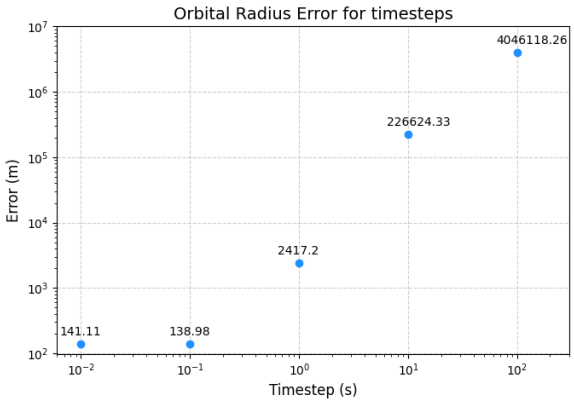


**Figure 8.10:** Error Convergence for Eccentric Orbit

Evidently, the initial error is much larger for the eccentric orbit. However, both decrease at a steady rate. In both cases the convergence hits a limit, again, most likely caused by the Runge-Kutta method. The error is on the order of 0.001%, which is acceptable for this use case.

In addition to the simulation tools, verification and validation were performed by comparing the results to other simulation results. For the descent, extensive test cases were documented in [28, 29]. Due to time constraints, the full range of tests documented in [29] could not be fully implemented, and instead a small range of tests were selected to verify the convex guidance implementation. One such test was the results for the main braking phase; for PDI occurring at a downrange distance of 630 km, and with the MBP lasting 660 s to target an AG at 1265 m downrange and 1625 m in altitude. The velocity at this AG is 67 m/s downrange and −60 m/s vertically. With these values, [29] finds the propellant usage during the MBP to be 760 kg for the reference vehicle studied. The simulation found a propellant usage of 766.0 kg, an error of 0.79 %. The cause for this discrepancy is unknown, but could possibly be due to slightly different SOCP solvers with different error tolerances; nevertheless, the simulation result is quite close to the literature results, and errors on this order of magnitude are encompassed within the margins applied in Table 8.1. Errors on the similar order of magnitude or were found for other tests.

For ascent, simulation data proved to be difficult to obtain, and the input data reported was not sufficiently comprehensive for fully reproducing the results. Nevertheless, some values from literature could be obtained to perform at least an initial check on the correctness of the simulation. One such source is [40], which investigates the ascent and rendezvous for the Altair lunar lander using PEG. Unfortunately, the primary focus of that analysis is the orbital rendezvous after lander reaches orbit, and the vehicle parameters used for the ascent are only discussed briefly. The target orbit is a 15.24 by 75 km orbit, and the vehicle's TWR is given as 'approximately equal to 0.35 Earth T/W'. The exact engine $I_{sp}$ is not known, but a NASA request for proposals of the ascent engine design[2] required an $I_{sp}$ of greater than 355 s. [40] reports that the nominal ascent burn duration is 420.4 s, and that a $\Delta V$ of 1833 m/s is used. The simulation tool yielded results of an ascent time of 413.5 s and a $\Delta V$ of 1824.1 m/s, which is an error of 0.48 % in the simulated $\Delta V$. The cause of this discrepancy is unknown, but considering the lack of precision in the vehicle parameters, the difference is sufficiently small to instill confidence in the software, at least during this stage of the design.

[2]URL https://www.flightglobal.com/nasa-initiates-lunar-lander-ascent-main-engine-development/76712.article [cited 24 June 2024]

# 9 | Propulsion System

This section concerns the design of the propulsion system of the lander and the OTV. Firstly, the propulsion system requirements and their verification methods are presented in Section 9.1, followed by a discussion of the propellant and engine choice in Section 9.2. Next, the propulsion feed system is explained in Section 9.3, including the tank pressurisation architecture and ADCS thruster interfacing. Tank design is presented in Section 9.4.1, and a propellant slosh analysis is given in Section 9.5. The relevant risks are detailed in Section 9.6. Finally, a sensitivity analysis is performed in Section 9.7.

## 9.1. Propulsion System Requirements

The propulsion system requirements are given in Table 9.1 and Table 9.2, along with their verification method and (non-)compliance. Some requirements with special considerations are mentioned here. **HOPE-PROP-160** and **HOPE-PROP-360** are not expected to be complied with since the tanks are single-point-of-failure components. They are accordingly designed with a safe-life philosophy. **HOPE-PROP-020** and **HOPE-PROP-210** are expected to be complied with since although the exact volume is not known at this stage, the propulsion systems fit in the Starship fairing. **HOPE-PROP-040** can be complied with by choosing high reliability components and conducting a reliability analysis. **HOPE-PROP-103** is expected to be complied with since the Raptor 2 Vacuum engine will perform similar length burns when sending Starship to the Moon or Mars. **HOPE-PROP-120** and **HOPE-PROP-330** can be complied with if inspection and potential maintenance is done, as the Raptor 2 Vacuum and BE-7 engines are reusable. **HOPE-PROP-170** and **HOPE-PROP-350** are expected to be complied with due to the presence of emergency vent valves. **HOPE-PROP-230** can be complied with if shielding is applied to the landing legs to prevent damage from kicked up lunar regolith. **HOPE-PROP-280** is expected to be complied with as the BE-7 will have to complete similar burns as the ARCH-E lander in the Blue Moon lander.

## 9.2. Propellant and Engine Selection

In the midterm report [14], $LH_2$ and LOX were selected as the propellants for the lander and OTV. However, trajectory calculations revealed that more thrust would be required than initially expected for the OTV TLI burn. $LH_2$/LOX engines with the required thrust, such as the BE-3U with 712 kN of thrust[1], have relatively low $I_{sp}$ values, meaning that the increased propellant required rendered the OTV too large to fit inside the payload fairing. Therefore, the OTV propellant was changed to $LCH_4$/LOX to drastically reduce its volume. $LCH_4$/LOX was chosen as it performed well in the original propellant type trade-off and provides a relatively high $I_{sp}$. Approximately 75 t of extra propellant is required, which does not impact the number of Starship launches required to launch and fuel the vehicle. The higher temperature of $LCH_4$ eases TCS and therefore EPS requirements. The lander still uses $LH_2$/LOX.

To comply with the tight development timeline, the vehicles will use engines that are already operational or currently in development, rather than using a new engine design that would have to be built, tested, and certified. For the lander, Blue Origin's BE-7 engine was chosen due to its advanced development level with more than 4000 s of cumulative firing time as of March 2023[2], high $I_{sp}$ of 453 s[3], and 20% deep-throttling capability[4]. Its planned use as a lunar landing engine also makes it suitable, as it needs to burn for at least 6 minutes continuously for the Blue Moon lander [5], which is similar to the ARCH-E lander. For the OTV, SpaceX's Raptor 2 Vacuum engine was chosen for its high thrust of 2530 kN[6], a high $I_{sp}$ of 380 s, and the fact that it is already operational. Key information about both engines can be found in Table 9.3.

[1] URL https://www.blueorigin.com/engines/be-3 [cited 16 June 2024]
[2] URL https://www.youtube.com/watch?v=soFwbAYlVXM [cited 23 June 2024]
[3] URL https://youtu.be/GQ98hGUe6FM?t=2474 [cited 16 June 2024]
[4] URL https://www.blueorigin.com/news/be7-engine-testing [cited 16 June 2024]
[5] URL https://youtu.be/GQ98hGUe6FM?t=2541 [cited 23 June 2024]
[6] URL https://www.spacex.com/vehicles/starship/ [cited 16 June 2024]

**Table 9.1:** Propulsion System Requirements

| ID | Requirement | Rationale | Verification Method | Check | Value |
|---|---|---|---|---|---|
| HOPE-PROP-010 | The OTV propulsion subsystem shall have a maximum wet mass of 260 000 kg. | Needs to comply with the overall mass budget. | Analysis, inspection, and/or demonstration of fully-fuelled tanks | ✓ | 259 009.71 kg |
| HOPE-PROP-011 | The OTV propulsion subsystem shall have a maximum dry mass of 4500 kg. | Needs to comply with the overall mass budget. | Analysis and inspection | ✓ | 4394.37 kg |
| HOPE-PROP-020 | The OTV propulsion subsystem shall have a maximum total volume of 344 $m^3$. | Needs to fit within launch vehicle fairing, should not be excessively large. | Analysis | Compliance Expected | |
| HOPE-PROP-040 | The propulsion subsystem shall have a minimum reliability of 0.994 (TBC) over the vehicle's mission lifetime. | Needs to be compatible with HOPE-MISS-070 and the overall reliability budget. | Analysis | Compliance Expected | |
| HOPE-PROP-060 | The OTV propulsion subsystem shall not diminish the performance of any other subsystem to the extent that it prevents them from meeting their respective requirements. | Exhaust and plumbing should not infringe on e.g. solar arrays, or any other subsystems. | Analysis | ✓ | No interference. |
| HOPE-PROP-070 | The OTV propulsion subsystem shall use a maximum power of 355 W under nominal load. | Needs to be compatible with the overall power budget. | Analysis and demonstration; test stand and/or vacuum chamber | ✓ | 354.54 W |
| HOPE-PROP-071 | The OTV propulsion subsystem shall use a maximum power of 710 W under peak load. | Needs to be compatible with the overall power budget. | Analysis and demonstration; test stand and/or vacuum chamber | ✓ | 709.08 W |
| HOPE-PROP-091 | The OTV propulsion subsystem shall be able to provide a total $\Delta V$ of 8119.1 m/s. | Needs to provide sufficient $\Delta V$. | Analysis | ✓ | 8119.1 m/s |
| HOPE-PROP-101 | The OTV propulsion subsystem shall not exceed a sustained thrust of 3 808 634 N (TBC). | Needs to prevent excessively high G-loads on the vehicle and crew, the value is calculated using an acceleration of 4 G. | Demonstration; test stand and/or vacuum chamber | ✓ | 2 530 116 N |
| HOPE-PROP-102 | The OTV propulsion subsystem shall be able to provide a minimum sustained thrust force of at least 2 150 000 N. | Needs to have sufficiently high TWR to not waste too much $\Delta V$ during manoeuvres. | Demonstration; test stand and/or vacuum chamber | ✓ | 2 150 000 N |
| HOPE-PROP-103 | The OTV propulsion subsystem shall be able to provide thrust for at least 383 s continously. | Engines need to be rated for sufficient burn time to execute manoeuvres. | Demonstration; test stand and/or vacuum chamber | Compliance Expected | |
| HOPE-PROP-120 | The OTV propulsion subsystem shall be able to restart 160 times (TBC). | Engines must ignite a sufficient number of times to perform manoeuvres including TLI, mid-course corrections, separation, phasing, docking, merging, and transfer. | Analysis or demonstration | Compliance Expected | |
| HOPE-PROP-130 | The propulsion subsystem shall have the capability to be refuelled during the mission. | This is required for the architecture selected to do 10 missions. | Demonstration | ✓ | Refuelling ports are present. |
| HOPE-PROP-140 | The propulsion subsystem shall accept power supplied at 28 V (TBC). | Needs to be compatible with the electrical bus [41]. | Analysis and demonstration | ✓ | 28 V |
| HOPE-PROP-150 | The OTV propellant tanks shall have a maximum nominal operating pressure of no more than 6 bar (TBC). | Constrains propellant tank design [42]. | Analysis and demonstration | ✓ | 6 bar |
| HOPE-PROP-160 | The OTV propulsion subsystem shall not have a single point of failure preventing the safe return of the crew back to Earth. | Needs to have sufficient redundancy to be safe for the crew. | Analysis | *X* | Tanks are single-point-of-failure components. |
| HOPE-PROP-170 | The OTV propulsion subsystem shall be capable of venting 0.6 kg/s (TBC). | This is to prevent tank rupture [42]. | Demonstration | Compliance Expected | |
| HOPE-PROP-190 | The lander propulsion subsystem shall have a maximum wet mass of 92 000 kg. | Needs to comply with the overall mass budget. | Inspection | ✓ | 91 896.90 kg |
| HOPE-PROP-200 | The lander propulsion subsystem shall have a maximum dry mass of 1800 kg. | Needs to comply with the overall mass budget. | Inspection | ✓ | 1728.40 kg |
| HOPE-PROP-210 | The lander propulsion subsystem shall have a maximum total volume of 350 $m^3$. | Needs to comply with launch vehicle fairing and other space constraints. | Inspection | Compliance Expected | |
| HOPE-PROP-230 | The lander propulsion subsystem shall not diminish the performance of any other subsystem to the extent that it prevents them from meeting their respective requirements. | The exhaust should not impinge on solar panels and other components. | Analysis | Compliance Expected | |
| HOPE-PROP-240 | The lander propulsion subsystem shall use a maximum power of 355 W under nominal load. | Needs to be compatible with the overall power budget. | Analysis and demonstration; test stand and/or vacuum chamber | ✓ | 354.54 W |
| HOPE-PROP-250 | The lander propulsion subsystem shall use a maximum power of 710 W under peak load for TBD seconds. | Needs to be compatible with the overall power budget. | Analysis and demonstration; test stand and/or vacuum chamber | ✓ | 709.08 |
| HOPE-PROP-270 | The lander propulsion subsystem shall be able to provide a total $\Delta V$ of 12 483.8 m/s. | Needs to provide sufficient $\Delta V$. | Analysis | ✓ | 12 483.8 m/s |
| HOPE-PROP-280 | The lander propulsion subsystem shall be able to provide thrust for at least 1100 s continuously. | Engines need to be rated for sufficient burn time to execute manoeuvres. | Demonstration | Compliance Expected | |
| HOPE-PROP-290 | The lander propulsion subsystem shall not exceed a sustained thrust of 361 008 N (TBC). | Needs to prevent excessively high G-loads on the vehicle and crew, the value is calculated using an acceleration of 4 G. | Demonstration; test stand and/or vacuum chamber | ✓ | 222 411.10 N |

**Table 9.2:** Continued Propulsion System Requirements

| ID | Requirement | Rationale | Verification Method | Check | Value |
|---|---|---|---|---|---|
| HOPE-PROP-300 | The lander propulsion subsystem shall be able to provide a maximum thrust force of at least 44482.22 N. | Needs to be sufficiently high for lunar descent and ascent to not waste too much $\Delta V$. | Demonstration; test stand and/or vacuum chamber | ✓ | 44 482.22 N |
| HOPE-PROP-310 | The lander propulsion subsystem shall be able to provide a minimum thrust force of $\leq$82 266.77 N (TBC). | Needs to have $\leq 1$ TWR at the Moon for a soft, controlled touchdown in final landing phase. | Demonstration; test stand and/or vacuum chamber | ✓ | 44 482.22 N |
| HOPE-PROP-320 | The lander propulsion subsystem shall be able to provide a variable thrust force ranging between 44482.22 N and 222411.10 N. | Need throttle control for fine touchdown adjustments. | Demonstration; test stand and/or vacuum chamber | ✓ | 44482.22–222411.10 N |
| HOPE-PROP-330 | The lander propulsion subsystem shall be able to restart 200 times (TBC). | Engines must ignite a sufficient number of times to perform manoeuvres including separation, LOI, orbit changes, descent, ascent, TEI, mid-course corrections, phasing, and docking. | Analysis or demonstration | Compliance Expected | |
| HOPE-PROP-340 | The lander propellant tanks shall have a maximum nominal operating pressure of no more than 2 bar (TBC). | Constrains propellant tank design [42]. | Analysis and demonstration | ✓ | 2 bar |
| HOPE-PROP-350 | The lander propulsion subsystem shall be capable to vent 0.6 kg/s (TBC). | To prevent tank rupture [42], mitigation for R-PROP-10. | Demonstration | Compliance Expected | |
| HOPE-PROP-360 | The lander propulsion subsystem shall not have a single point of failure preventing the safe return of the crew back to Earth. | Needs to have sufficient redundancy to be safe for crew. | Analysis | *X* | Tanks are single-point-of-failure components. |

**Table 9.3:** Lander and OTV Engine Specifications

| Engine | Propellants | Cycle | Thrust (kN) | $I_{sp}$ (s) | Throttle (%) |
|---|---|---|---|---|---|
| BE-7 | $LH_2$/LOX | Dual expander | 44.5 | 453 | 20–100 |
| Raptor 2 Vacuum | $LCH_4$/LOX | Full flow staged combustion | 2530 | 380 | 40–100 |

The lander will have five BE-7 engines, allowing for engine-out capability. The lander's TWR is between 0.54 and 2.70 at touchdown, satisfying requirement **HOPE-PROP-310**. The OTV will have one Raptor 2 Vacuum engine, as this provides sufficient thrust for the TLI burn while limiting thrust loads. In case this engine fails, the lander will always be able to return itself to LEO under its own propulsion.

## 9.3. Propulsion Feed System

With the propellant type and engines chosen, the feed system was designed. This is shown for the lander and OTV in Figure 9.1 and Figure 9.2. The main aspects to consider are the tank pressurisation architecture and the ADCS thruster interfaces. These are detailed below. Also shown is the integration of the tank thermal control system, which is described in detail in Chapter 10.

### 9.3.1. Tank Pressurisation Architecture

The lander and OTV use balloon tanks that are pressurised to hold their shape, allowing for very thin tank walls. They will use autogenous pressurisation, where the gaseous form of the propellants are used to maintain pressure [43], removes the need for separate helium tanks, reducing mass. This is a well developed technology, being used in the Centaur upper stage, the Space Shuttle [43], SLS [44], and Starship. During engine burns, the propellant gas can be tapped off directly from the engine turbopumps and routed back to the tanks [45]. At other times, a small amount of liquid propellant is heated into a gas and sent to the tank via compressors. This technology is being developed by ULA [46]. As the propellants are kept very near their boiling points, heating them to a gas will not require a large amount of power. This power, along with the power required to drive the compressors, is an important next step in future, more detailed design work.

Emergency vent valves are present to ensure that the tanks are not over-pressurised. Inlets for

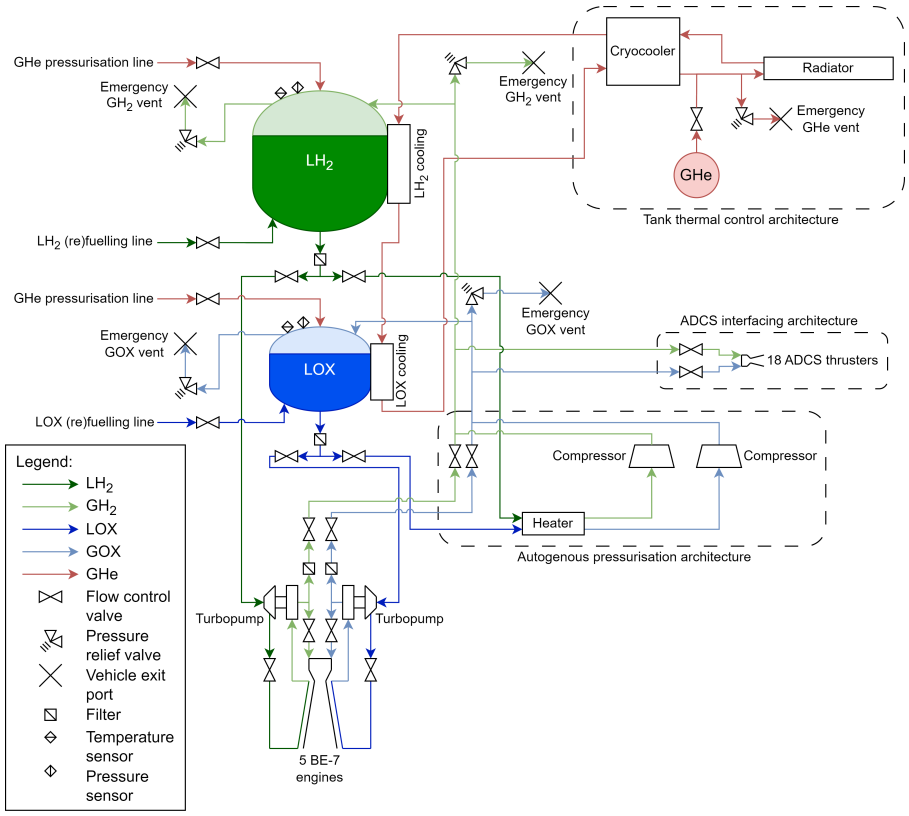


**Figure 9.1:** Lander Propulsion Feed System

gaseous helium (GHe) are also present to allow the vehicles to be pressurised with helium on the ground, during launch, and before they are fully fuelled. Refuelling will be done by lowering the tank pressure relative to the refuelling vehicle's tank pressure to allow the propellants to move through the refuelling lines, or applying a small thrust to to settle and move propellant through the transfer line.

The tank pressure is determined by the pressure required at the engine turbopump inlets and the tank material properties. A detailed tank structural analysis is presented in Section 9.4.2, but the selected pressures are presented here. Very little information about the BE-7 operating pressure is available, so information for the RL-10 engine has been used as a first estimate as they are very similar engines. They use the same propellants and engine cycle, and have similar thrust levels [47]. The lander will have a tank pressure of 2 bar based on Centaur flight data [48]. The OTV tank pressure will be 6 bar as this is used on Starship and the Raptor 2 Vacuum engine has been flight-proven in these conditions.

### 9.3.2. ADCS Thruster Interfacing

This section focuses on the integration of the ADCS thrusters with the overall propulsion and tank architecture. A detailed description of the entire ADCS system can be found in Chapter 15. To minimise mass, it is advantageous to use the same propellants for the main engines and the ADCS thrusters, since gaseous forms of the propellant are already present in the main propellant tanks. Additionally, the requirement **HOPE-MISS-06a** prohibits the use of toxic propellants such as hydrazine, which are commonly used for ADCS thrusters.

Gaseous hydrogen/oxygen and gaseous methane/oxygen ADCS thrusters have undergone a fair amount of research and development. The chosen thrusters are detailed in Chapter 15 and are fed by diverting gas from the tank pressurising lines to the thruster combustion chamber.

## 9.4. Propellant Tank Design

Tank sizing followed from the propellant masses calculated in the mass estimation. The largest constraining factor was the requirement to fit inside Starship's payload fairing, which drove the tank

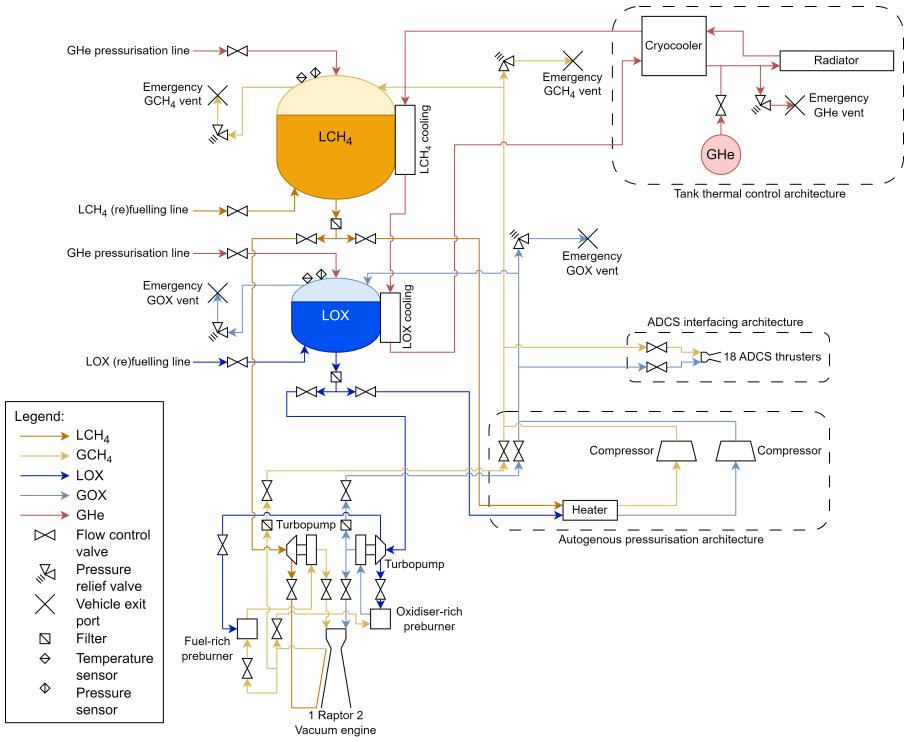


**Figure 9.2:** OTV Propulsion Feed System

shapes. The selected shape was a cylinder with ellipsoidal endcaps, which is relatively volume-efficient while still being resistant to internal pressure. The geometric sizing of the tanks is given below, followed by their structural analysis.

### 9.4.1. Geometric Sizing

The tank volumes were determined by calculating the fuel and oxidiser volumes using the engine fuel/oxidiser ratio and the propellant densities, and adding a 10 % margin to this [15]:

$$V_{tank_{fuel}} = 1.1 \frac{1}{1+OF} \frac{m_{prop}}{\rho_{fuel}} \quad (9.1) \qquad V_{tank_{oxidiser}} = 1.1 \frac{OF}{1+OF} \frac{m_{prop}}{\rho_{oxidiser}} \quad (9.2)$$

Where $V$ is the tank volume in m$^3$, $m$ is the propellant mass in kg, $\rho$ is the propellant density in kg/m$^3$, and $OF$ is the oxidiser/fuel ratio. The resulting tank volumes for the lander and OTV are shown in Table 9.4. The lander fuel and oxidiser tank dimensions are shown in Table 9.5. These dimensions were primarily driven by the need to fit the tanks into the Starship fairing.

**Table 9.4:** Lander and OTV Tank Volumes

| Vehicle | Fuel Tank Volume [m$^3$] | Oxidiser Tank Volume [m$^3$] |
|---|---|---|
| Lander | 200.00 | 74.51 |
| OTV | 92.67 | 192.10 |

**Table 9.5:** Lander and OTV Tank Dimensions

| Vehicle | Propellant | Radius [m] | Cylindrical Height [m] | Ellipsoidal Height [m] |
|---|---|---|---|---|
| Lander | $LH_2$ | 3.50 | 3.89 | 0.80 |
| | LOX | 2.75 | 2.22 | 0.80 |
| OTV | $LCH_4$ | 3.50 | 1.32 | 0.80 |
| | LOX | 3.28 | 4.70 | 0.80 |

### 9.4.2. Structural Analysis

The loads on the tanks can be calculated and used to find the tank thickness required to sustain them. The maximum allowable stress is minimum of the yield strength divided by a safety factor of 1.25 and the ultimate strength divided by a safety factor of 1.4 [49]. The material chosen is stainless steel 301 full hard, with a density of 8030 kg/m$^3$. This is because it has excellent material properties at cryogenic temperatures [50], shown in Table 9.6.

**Table 9.6:** Stainless Steel 301 Full Hard Material Properties [50]

| **Temperature [K]** | **Yield Strength [MPa]** | **Tensile Strength [MPa]** | **Maximum Allowable Stress [MPa]** |
|---|---|---|---|
| 20 ($LH_2$) | 1723.69 | 2344.22 | 1378.95 |
| 90 (LOX) | 1475.48 | 2027.06 | 1180.38 |
| 111.6 ($LCH_4$) | 1247.21 | 1944.32 | 1141.77 |
| 300 (atmosphere) | 1268.64 | 1406.53 | 1004.66 |

The main thrust loads are carried by the vehicle's truss structure, meaning that the tanks must carry internal pressure, the hydrostatic pressure of the propellant, and the force on the cylindrical tank cross-section due to the propellant mass under acceleration. For all of these equations, the stress could not exceed the allowable stress given in Table 9.6. The total pressure the tank must withstand is the sum of the internal pressure $P$ and the hydrostatic pressure $P_h$ (both in Pa), which is given by $P_h = \rho a h$ where $\rho$ is the propellant density in kg/m$^3$, $a$ is the vehicle acceleration in m/s$^2$, and $h$ is the height of the propellant in the tank. Two important assumptions are made here. Firstly, the ullage gas was assumed to have a negligible contribution to the hydrostatic pressure as it has a much lower density than the liquid propellants. Secondly, it was assumed that all the propellant is present in the tanks, with no residuals remaining in plumbing lines. This would be the worst-case scenario since the propellant height is maximum in this case. The height was calculated from the volume of propellant in the tanks, checking whether it would be within the cylindrical section of the tank or within the top ellipsoid endcap.

The hoop and longitudinal stresses for a doubly curved surface are [51]:

$$\sigma_{hoop} = \frac{(P + P_h)r}{2t}\left(2 - \frac{r}{r_m}\right) \tag{9.3}$$

$$\sigma_{long} = \frac{(P + P_h)r}{2t} \tag{9.4}$$

Where $r$ is the tank radius in m, $r_m$ is the height of the ellipsoidal endcap in m, and $t$ is the tank thickness in m. For the force on the cylindrical tank cross-section, the axial stress equation $\sigma_{ax} = F/(2\pi r t)$ was used, where $F$ is the propellant force in kg/m$^3$, $r$ is the tank radius in m, and $t$ is the tank thickness in m. The thin-walled assumption is being applied here, this is valid since the thickness is far smaller than the radius.

The process for selecting the tank thickness is as follows. First, the hydrostatic pressure was calculated and added to the selected tank pressure (2 bar for the lander and 6 bar for the OTV) to find the minimum thicknesses such that the maximum stresses are the values given in Table 9.6 (1378.95 MPa for $LH_2$, 1180.38 MPa for LOX, and 1141.77 MPa for $LCH_4$). Then, the load due to the propellant mass acting on the propellant endcaps was calculated using the critical load case, and the axial stress equation was used to find the minimum thickness to resist this load with the maximum allowable stresses. For the lander, the critical load case was the end of the TLI manoeuvre. For the OTV, the critical load case was the beginning of the TLI manoeuvre. This process was done separately for the cylindrical section and the top and bottom endcaps, allowing the thickness to vary between these sections, yielding a lightweight structure. This resulted in the tank thicknesses shown in Table 9.7. These represent very thin tank walls, meaning that internal pressure will always be required to prevent the tanks from buckling and collapsing under their weight, as is typical for balloon tanks. Sheets and strips of stainless steel 301 full hard are available commercially at these thicknesses, simplifying manufacturing.

**Table 9.7:** Lander and OTV Tank Thicknesses

| Vehicle | Propellant | Cylindrical thickness [mm] | Top endcap thickness [mm] | Bottom endcap thickness [mm] |
|---|---|---|---|---|
| Lander | $LH_2$ | 0.51 | 0.26 | 0.25 |
| | LOX | 0.51 | 0.26 | 0.24 |
| OTV | $LCH_4$ | 1.86 | 0.38 | 0.38 |
| | LOX | 1.77 | 0.37 | 0.39 |

**Table 9.8:** Lander and OTV Tank Masses

| Vehicle | Fuel Tank Mass [kg] | Oxidiser Tank Mass [kg] |
|---|---|---|
| Lander | 633.90 ($LH_2$) | 308.51 (LOX) |
| OTV | 860.09 ($LCH_4$) | 1934.28 (LOX) |

The tank mass is calculated by multiplying the thicknesses by the relevant section surface area and the material density of 8030 kg/m$^3$, and summing the results. A 20 % margin was applied to account for the pressurisation systems, plumbing lines, additional reinforcements, and fasteners [51]. The total tank masses, including the margin, are given in Table 9.8. Adding the engine masses yields a preliminary propulsion system mass. The mass of each BE-7 engine was estimated to be 157.2 kg based on the RL-10, as information on the BE-7 is not available. The lander propulsion system mass is then 1728.41 kg. The mass of one Raptor 2 Vacuum engine is 1600 kg, giving an OTV propulsion system mass of 4394.37 kg.

## 9.5. Propellant Slosh Analysis

It is important to quantify the impact of propellant slosh on vehicle motion. Lateral motion is particularly important as it can cause a long-lasting oscillation, imparting significant loads on the vehicle. Therefore, it is particularly important to analyse slosh during large lateral manoeuvres [52]. To that end, this analysis will focus on lander ascent and descent as these manoeuvres are likely to include significant lateral motion. The sloshing propellant is modelled using a mass-pendulum model shown in Figure 9.3. The propellant mass is replaced by a fixed mass representing propellant that does not slosh, and masses attached to pendulums representing sloshing propellant in various slosh modes [53]. It is assumed that only the first slosh mode (and thus one pendulum) is necessary to consider, as the following terms are negligible since they are only significant for very small accelerations [52]. The analysis will yield the natural frequency of the sloshing propellant, which should be avoided by the guidance system to prevent resonant oscillations [52].

To simplify the problem, cylindrical tanks were considered with the same volume as the vehicle propellant tank volumes. The liquid depth ratio $h/d$, pendulum length $L_1$, and mass of liquid $m_{liq}$ are given by [53]:

$$\frac{h}{d} = \frac{\frac{h}{h_{max}} h_{max}}{d} \quad (9.5) \qquad L_1 = \frac{d}{2\xi_1 \tanh\left(2\xi_1 \frac{h}{d}\right)} \quad (9.6) \qquad m_{liq_{prop}} = 1.1 m_{prop} \frac{h}{h_{max_{prop}}} \quad (9.7)$$

Where $h$ is the fill height of the propellant in m, $d$ is the cylindrical tank diameter in m, $h_{max}$ is the maximum height of the cylindrical tank in m, $\xi_1 = 1.841$ is the first slosh mode factor, and $m_{prop}$ is the total propellant mass in kg [53]. The factor of 1.1 in Equation 9.7 is present to account for the fact that the tank is sized 10% larger than the amount of propellant. The natural frequency of the sloshing propellant in Hz is given by [52]:

$$f = \frac{1}{2\pi} \sqrt{\frac{a_x}{L_1}} \quad (9.8)$$

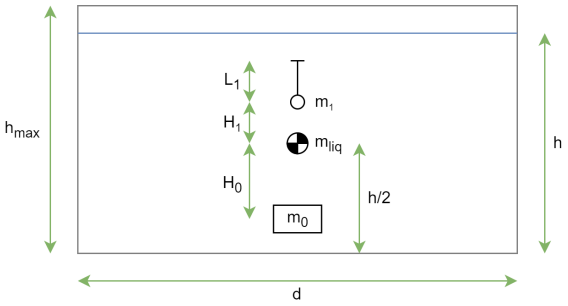


**Figure 9.3:** Propellant Slosh Model [53]

Where $a_x$ is the axial acceleration of the vehicle due to engine thrust in m/s$^2$ and $L_1$ is the pendulum length in m. The lander $LH_2$ mass is 12 881 kg and the $LH_2$ tank volume is 190.7 m$^3$. With a diameter $d$ of 7 m, $h_{max}$ for the $LH_2$ tank is 4.955 m. The lander LOX mass is 77 287 kg and the LOX tank volume is 78.15 m$^3$. With a diameter $d$ of 5.5 m, $h_{max}$ for the LOX tank is 3.289 m. The slosh frequency is found for fill levels $h/h_{max}$ of 0.200, 0.400, 0.600, 0.800, and 0.909, which is when all the propellant is present. The process is as follows. First, $h/d$, $m_{liq}$, and $L_1$ were found for the $LH_2$ and LOX tanks and for each fill level using Equation 9.5, Equation 9.7, and Equation 9.6. Then, the lander mass at each fill level was calculated by adding the dry mass, payload mass, $LH_2$ mass, and LOX mass. This mass, along with the minimum and maximum thrust of the lander (44 482 N and 222 411 N), were used to calculate the minimum and maximum acceleration acting on the lander at each fill level, using $a_x = F/m_{lander}$. From this, the slosh frequencies were calculated using Equation 9.8. These are presented for the $LH_2$ and LOX tanks in Table 9.9.

**Table 9.9:** Slosh Frequencies During Ascent and Descent

| Tank | Fill level [−] | 0.2 | 0.4 | 0.6 | 0.8 | 0.909 |
|---|---|---|---|---|---|---|
| $LH_2$ | Frequency, min. acceleration [Hz] | 0.093 | 0.094 | 0.087 | 0.079 | 0.075 |
| | Frequency, max. acceleration [Hz] | 1.200 | 0.669 | 0.466 | 0.357 | 0.317 |
| LOX | Frequency, min. acceleration [Hz] | 0.105 | 0.106 | 0.098 | 0.089 | 0.085 |
| | Frequency, max. acceleration [Hz] | 0.002 | 0.001 | 0.001 | 0.001 | 0.001 |

The slosh frequency varies from a minimum of 0.001 Hz in the LOX tank at a fill level of 0.909 to a maximum of 1.200 Hz in the $LH_2$ tank at a fill level of 0.2. Ideally, none of the frequencies specified in Table 9.9 would be used by the guidance system. However, it is likely that the engines will be gimballed in this frequency range during descent, such as during lateral motion during hazard avoidance. Therefore, it is likely that ring baffles will be required to increase slosh oscillation damping [52]. Detailed design of baffles with the required geometry would include a CFD analysis and would be the next step in future design work.

## 9.6. Risk Assessment

The risks related to the propulsion system are presented in Table 9.10, and their mitigation and contingency strategies are presented in Table 9.11. Most risks are reduced to a moderate or lower level through mitigation measures, however **R-PROP-09** has a high risk level even after mitigation, primarily due to the current low TRL of in-space cryogenic propellant transfer. In-space refuelling is planned to be used extensively in the near future for HLS missions, meaning that the technology will be quickly developed and potential failure modes will be identified and resolved. Therefore, the risk level should decrease in the near future. The definition of the likelihood and consequence levels are discussed in Section 17.1.

**Table 9.10:** Propulsion System Risks

| ID | Risk | Causes | Impact | Req. |
|---|---|---|---|---|
| R-PROP-01 | Inadvertent engine firing | Stuck valves, faulty command to engine | Increased propellant consumption, change in trajectory | HOPE-PROP-040 |
| R-PROP-02 | Engine failure to fire | Stuck valves, debris in plumbing | Potential loss of mission and crew | HOPE-PROP-040 |
| R-PROP-03 | Engine does not produce enough thrust | Non-optimal mass flow ratio | Increased propellant consumption due to increased gravity losses | HOPE-PROP-040 |
| R-PROP-04 | Engine fails to shut down | Stuck valves | Increased propellant consumption, change in trajectory | HOPE-PROP-040 |
| R-PROP-05 | Rupture of propulsion system components | Over-pressurised tanks | Loss of mission and crew | HOPE-PROP-150 & 160 & 340 & 350 & 360 |
| R-PROP-08 | Excessive element propellant boil-off | Cryocooler failure, excessive external temperatures | Increased tank pressure, reduction in available propellant | HOPE-PROP-150 & 160 & 340 & 350 & 360 |
| R-PROP-09 | Propellant transfer failure | Blocked refuelling lines, too small pressure difference | Inability to refuel vehicles and perform missions | HOPE-PROP-130 |
| R-PROP-10 | Failure to vent propellant boil-off | Stuck valves, pressure sensor failure | Tank failure due to over-pressure | HOPE-PROP-350 |

**Table 9.11:** Propulsion System Risk Mitigation and Contingency Plans

| | Pre-mit. | | | | Post-mit. | |
|---|---|---|---|---|---|---|
| ID | L | C | Mitigation | Contingency | L | C |
| R-PROP-01 | U | Ca | Pre-launch valve inspection, redundant valves | Close redundant valves | U | Mo |
| R-PROP-02 | U | Ca | Addition of filters to plumbing to block debris and pre-launch valve inspection | For OTV, return lander on free-return trajectory; for lander, use remaining functional engines for burns | U | Ma |
| R-PROP-03 | P | Ma | Pre-launch valve inspection to ensure precise opening, real-time thrust monitoring, ensuring of proper mass flow ratio | Increase burn time to complete manoeuvre | U | Mo |
| R-PROP-04 | U | Ma | Pre-launch valve inspection, redundant valves | Close redundant valves | U | Mo |
| R-PROP-05 | P | Ca | Design of tanks with safety factors, inclusion of vent valves | Attempt crew rescue mission | U | Ma |
| R-PROP-08 | P | Ma | Add effective tank insulation and thoroughly test cryocooler | Vent excess boil-off gas | U | Mo |
| R-PROP-09 | P | Ca | Addition of filters to block debris, increase design pressure difference | Manual inspection and clearing of refuelling lines | U | Ca |
| R-PROP-10 | P | Ca | Pre-launch valve inspection, redundant valves and sensors | Increase cooling of tank | U | Ma |

## 9.7. Sensitivity Analysis

Finally, a brief sensitivity analysis is presented covering the effect of $I_{sp}$ on the total stack mass. All design calculations were done with a 5 % downwards margin on $I_{sp}$ values to be conservative, and it is useful to see what effect this has on the wet mass of the system. Since most of the stack mass is from the OTV, the lander mass was kept constant and the OTV $I_{sp}$ was changed. The results are shown in Table 9.12. Increasing the $I_{sp}$ significantly decreases the stack mass, so the OTV and lander $I_{sp}$ values should be as high as possible by using the most efficient engines possible, in order to reduce the vehicle mass.

**Table 9.12:** OTV $I_{sp}$ Sensitivity Analysis

| Specific impulse [s] | Total stack mass [tons] |
|---|---|
| 350 | 387 |
| 361 (value used) | 372 |
| 370 | 361 |
| 380 | 349 |

# 10 | Thermal Control System

The vehicle will face a wide range of temperatures throughout the mission, experiencing significant thermal variations between sunlit and shadowed areas, as well as between the interior and exterior. To ensure optimal performance, the Thermal Control Subsystem (TCS) is designed to maintain each part of the vehicle within its specific operational temperature range. The initial task involved identifying the extreme average temperatures the vehicle will encounter. Based on this data, the cooling system for the tanks was appropriately sized, followed by the design of controlled environmental boxes to keep all operational components within their required temperature limits.

**Table 10.1:** Thermal Control System Requirements Verification

| ID | Requirement | Rationale | Verification Method | Check | Value |
|---|---|---|---|---|---|
| HOPE-TCS-010 | The thermal control system shall have a maximum mass of 4900 kg for both vehicles combined. | Needs to comply with an overall mass budget,estimated in baseline report | Inspection | ✓ | 1052 kg |
| HOPE-TCS-040 | The thermal control system shall have a minimum reliability of 0.994 (TBC) over the vehicle's mission lifetime. | Needs to be compatible with HOPE-MISS-070 and the overall reliability budget. | Analysis | ✓ | Compliance expected |
| HOPE-TCS-050 | The lander thermal control system shall not have a single point of failure preventing the safe return of the crew back to Earth. | Needs to ensure the safe return of the crew in case of an emergency. | Analysis | ✓ | |
| HOPE-TCS-060 | The thermal control system shall not diminish the performance of any other subsystem to the extent that it prevents them from meeting their respective requirements. | Ensures minimal interference with other subsystems. | Test, large vacuum chamber | ✓ | |
| HOPE-TCS-080 | The thermal control system shall keep the temperature of all subsystems within their operating temperature ranges. | Need to control temperature for the subsystems to function properly. | Test, large vacuum chamber | | |
| HOPE-TCS-081 | The thermal control system shall keep the temperature of the EPS within a range of 233 K to 293 K. | This follows from recommendations in [51] (5–20 degreeC for batteries). | Analysis | ✓ | |
| HOPE-TCS-084 | The thermal control system shall keep the temperature of the GNC subsystem within a range of 275 K to 315 K. | This follows from recommendations in [51] (0–40 °C). | Analysis | ✓ | |
| HOPE-TCS-085 | The thermal control system shall keep the temperature of the CDH within a range of 291 K to 300 K . | This follows from HOPE-ECLSS-070-4. | Analysis | ✓ | |
| HOPE-TCS-086 | The thermal control system shall keep the temperature of the ADCS within a range of 275 K to 315 K. | This follows from recommendations in [51] (0–40 °C for electronics). | Analysis | ✓ | |
| HOPE-TCS-087 | The thermal control system shall keep the temperature of the LOX tank of the propulsion subsystem within a range of 60 K to 90 K. | This follows from the boil-off considerations from the propulsion subsystem. | Testing | ✓ | |
| HOPE-TCS-088 | The thermal control system shall keep the temperature of the $LH_2$ tank of the propulsion subsystem within a range of 15 K to 20 K . | This follows from the boil-off considerations from the propulsion subsystem. | Testing | ✓ | |
| HOPE-TCS-089 | The thermal control system shall keep the temperature of the $CH_4$ tank of the propulsion subsystem within a range of 130 K to 162 K . | This follows from the boil-off considerations from the propulsion subsystem. | Testing | ✓ | |
| HOPE-TCS-090 | The thermal control system shall determine the temperature of all subsystems. | Needs to know the temperature to properly manage the temperature. | Testing | ✓ | |
| HOPE-TCS-110 | The thermal control system shall use a sustained power of less than 5.4 kW in total for both vehicles. | Need to ensure that power budget is met. | Analysis | ✓ | 1360 W |

## 10.1. Extreme Temperatures

The thermal equilibrium temperatures for both the lander and the Orbital Transfer Vehicle (OTV) were calculated to determine the warmest and coldest conditions they would encounter. Key heat transfer factors considered include the solar intensity of the Sun, the albedo effects from the Moon and Earth, and their infrared radiation emissions. These factors are combined in Equation 10.1 , which illustrates the total heat absorbed by the vehicle's surface. Table 10.2, shows the main parameters required to perform these calculations, these parameters are common for both vehicles. The projected area for the vehicles is 79 $m^2$ and 68 $m^2$ for the lander and OTV respectively these are derived from the vehicle dimensions in Chapter 16.

$$Q_{absorbed} = \alpha_s \cdot J_s \cdot A + \alpha_s \cdot a \cdot \left(\frac{R_{body}}{R}\right)^2 \cdot J_s \cdot A + \varepsilon_{IR} \cdot \sigma \cdot T_{IR_{body}}^4 \cdot A \tag{10.1}$$

**Table 10.2:** Parameters Used in Thermal Calculations, [54]

| Description | Symbol | Value | Unit |
|---|---|---|---|
| Stefan Boltzsman Constant | $\sigma$ | $5.67 \times 10^{-8}$ | $\frac{W}{m^2 \cdot K^4}$ |
| Solar Intensity | $J_s$ | 1361 | $\frac{W}{m^2 \cdot K}$ |
| Earth albedo | $a_E$ | 0.3 | - |
| Moon albedo | $a_M$ | 0.11 | - |
| Distance from Earth | $R_{LEO}$ | 6571000 | m |
| Distance from Moon | $R_{LLO}$ | 1848400 | m |
| Earth effective radiating temperature | $T_{IR_E}$ | 255 | K |
| Moon Effective radiating temperature | $T_{IR_M}$ | 120-380 | K |

Another important consideration is the energy dissipated by components inside the vehicle; the main subsystems considered are ADCS, GNC, CDH and EPS as they have a wide range of electrical components that dissipate heat inside the vehicle. Their heat dissipation was estimated from their electrical power necessities and the given electrical efficiency for its corresponding components, assuming all inefficiencies will be dissipated as heat. This led to an estimated heat dissipation of 306 W for the lander and 255 W for the OTV. By knowing both the heat absorbed from the environment and the heat generated internally, the average equilibrium temperature of the vehicle ($T_{vehicle}$) can be solved from Equation 10.2 and Equation 10.3.

$$Q_{emitted} = \varepsilon_{IR} \cdot \sigma \cdot T_{vehicle}^4 \cdot A_i \tag{10.2}$$

$$Q_{absorbed} + \Sigma P_{dissipated} = Q_{emitted} \tag{10.3}$$

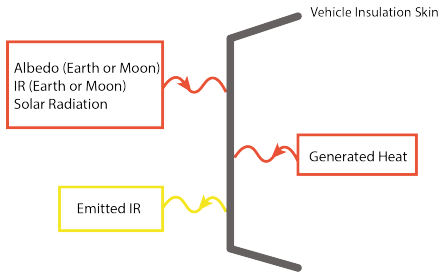


**Figure 10.1:** Vehicle Thermal Equilibrium

This thermal equilibrium, illustrated in Figure 10.1, involves the vehicles absorbing heat from the environment via radiation and subsequently radiating a portion of this heat back into the environment. The absorbed heat is then transferred through conduction through the vehicle's structure to various electronic components and tanks.

**Table 10.3:** Alternative Coatings

| Coating | Absolute Warmest [°C] | Absolute Coldest [°C] | Temperature Range [°C] |
|---|---|---|---|
| Mylar Film (Alumnium Backing) | 21 | −160 | 181 |
| Kapton Film (Aluminium Silicon Oxide Overcoating) | 29 | −157 | 186 |
| Teflon (Gold Backing) | 24 | −169 | 193 |
| Aclar | 11 | −179 | 190 |
| Tefzel | 36 | −166 | 202 |

The aforementioned process, to determine the thermal equilibrium, was carried out for various scenarios, including Earth orbit, lunar orbit, and both shadowed and sunlit conditions to determine both extreme cases. When in earth orbit the environmental heat parameters from the moon were ignored as they become negligible with distance and vice versa [51]. The tool was tuned to find the lowest temperature range possible, this was performed by altering the material chosen by inputting different absorptivity and emissivity values of different materials. Table 10.3 shows the different coatings considered. The best result was shown by a 0.127 mm thin film of mylar foil with aluminised backing as it gave the

lowest temperature range whilst also not affecting significantly the required cooling power of the cryocooler, its respective solar absorptivity and emissivity are 0.19 and 0.77 respectively [55]. After selecting the coating based on these final values, its suitability for this given purpose was verified. This specific coating has a proven track record, having been used successfully in previous space missions, including the Apollo program [56]. Given its historical performance and the results found it is reasonable to expect optimal results with this coating for the current application.

Given the selected coating, the warmest scenario was hence, determined to occur in lunar orbit when exposed to sunlight, with an average internal temperature of 287 K and 294 K for the lander and OTV, respectively, this is mainly due to the high IR reflectance of the moon. Conversely, the coldest scenario was found on the shadow side of the moon, with average internal temperatures of 92 K and 94 K for the lander and OTV, respectively.

## 10.2. Tank Cooling

Cryogenic propellants require low storage temperatures to remain in a liquid state, necessitating a combination of active and passive cooling methods [57]. For passive thermal control, multi-layer insulation is sized to minimise conduction from the vehicle's skin. Active cooling involves the use of a cryocooler to achieve the necessary cold temperatures for storing liquid hydrogen ($LH_2$), methane ($CH_4$), and liquid oxygen (LOX), which are 20 K, 112 K, and 90 K, respectively. The cooling system is designed based on the warmest estimated average temperature the vehicle will experience, as this scenario demands the highest cooling power from the cryocooler. A cryocooler is a device used to cool materials to cryogenic temperatures, by removing heat through a refrigeration cycle, this device will perform the active thermal cooling of the tanks. The temperature differential between the warmest average vehicle temperature and the required tank temperature determines the cooling requirement, for its sizing. However, first, the multi-layer insulation reduces some heat transfer before the cryocooler operation, which is accounted for in Equation 10.4. In this equation, $\lambda$ represents the thermal conductivity of the insulation, t is its thickness, and A is the surface area of the tank, given in Chapter 9.

A multi-layer insulation material was selected which has aluminised mylar as a reflector (outer layer) which therefore is compatible with the coating selected in Section 10.1 and is therefore representable to use for this model. This insulator uses paper as a separator more specifically it uses fibreglass paper [proving to have a final thermal conductivity of 0.135 mW/K [58]. Equation 10.5 shows the calculation to find the required layer thickness the optimal layer density selected is 25 layers/cm [58]. The number of layers was then optimised to try and reduce the cooling power, leading to 100 layers and hence an insulation thickness of 4 cm.

$$Q_{cooling} = \frac{\lambda \cdot \Delta T \cdot A}{t} \tag{10.4}$$

$$t = \frac{Number\ of\ Layers}{Layer\ Density} \tag{10.5}$$

Having the cooling power the cryocooler can be selected or sized from its cooling power, the electrical power can also be estimated using Equation 10.6 where the carnot efficiency is calculated using Equation 10.7 and the cryocooler efficiency is 0.7 [59]. The results are presented in Table 10.4.

$$Electrical\ Power = \frac{Q_{cooling}}{\eta_{carnot} \cdot \eta_{cryocooler}} \tag{10.6}$$

$$\eta_{carnot} = 1 - \frac{T_C}{T_H} \tag{10.7}$$

The radiator area can also be sized using Equation 10.8. Where, $q_{radiator}$ is 180 W/m$^2$ and $\eta_{radiator}$ is 0.7 [59].

$$A_{radiator} = \frac{Cooling\ Power}{q_{radiator} \cdot \eta_{radiator}} \tag{10.8}$$

Table 10.4 shows the final results of the cryocooler sizing, this values serve as the specifications to size the cryocooler for the vehicle. The cooling power includes a 50 % margin as required by the ESA

Margin philosophy when sizing active cooling systems [15].

**Table 10.4:** Cryocooler Sizing Results

| Vehicle | Cooling Power [W] | Electrical Power [W] | Radiator Area [$m^2$] |
|---|---|---|---|
| Lander | 380 | 640 | 3 |
| OTV | 312 | 669 | 2.5 |

Cryocoolers are typically designed to meet the specific requirements of a vehicle, as their size and power vary significantly depending on the application. For this vehicle, a cryocooler will be custom-sized according to the specified requirements, rather than selecting an existing model, as our cooling power needs exceed those of commonly available units. Given the cooling requirements, the most suitable option is to order a turbo-Brayton cryocooler, which can be tailored to sustain from a few mW to kW [60]. The layout of the ordered cryocooler can be visualised in Figure 10.2 and Figure 10.3.

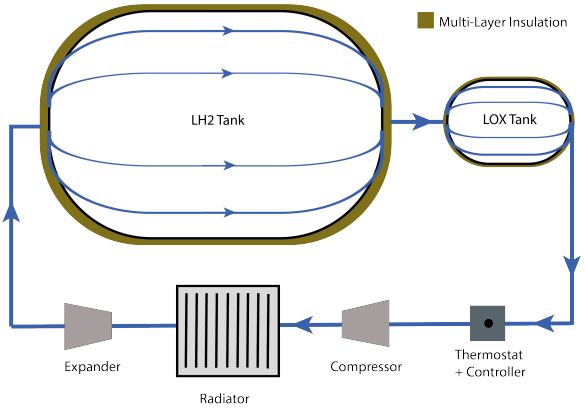


**Figure 10.2:** Lander Cryocooler

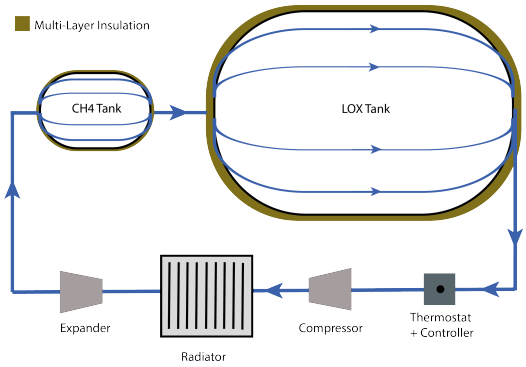


**Figure 10.3:** OTV Cryocooler

The cycle begins with the compressor, which increases the pressure an temperature of the helium gas that operates through the system. This high pressure and high temperature helium flows through the radiator which releases the excess heat while maintaining a high-pressure. The cooled, high-pressure gas subsequently enters the expander, where it undergoes adiabatic expansion, significantly dropping the temperature to reach cryogenic levels. The helium passes through pipes around the tanks, to cool it to the desired level, it is preferred to put the coolest temperature requiring tank first in the loop as done in Figure 10.2 and Figure 10.3 this arrangement is not innovative as it has been proven to be feasible [61]. Finally, the thermostat monitors and regulates the system's temperature, ensuring it remains within the desired range by adjusting the operations of the compressor and expander as needed.

The cryocooler mass was estimated using a cryocooler mass estimation method, which relates the required input power of the cryocooler and its mass [59]. The values derived from this method were compared to another cryocooler mass estimation method which similarly relates the logarithm cryocooler input power required to the logarithm of its mass in kg [62]. From these an average mass of the cryocooler for the lander and OTV of 19 kg and 21 kg respectively was found.

In addition to this the mass of insulation required for the tanks was estimated to be 247 kg and 253 kg given the insulation has a density of 10.7 $g/m^2$ and considering the tanks surface area and the number of layers [58].

## 10.3. Component Thermal Control Box

Maintaining the components at their operational temperature is key for the correct functioning of the vehicle. Therefore, the component thermal control boxes were designed to tackle this challenge. These boxes can be sized in size but also with the correct thermal components, heaters or/and radiators.

Sizing the cooling/heating power requirements was based on the warmest case for radiators and the coldest case for heaters in order to size the limiting power for each device. These thermal control boxes were designed for subsystems that require electrical components with a given operational temperature. The boxes were dimensioned given their electrical component size and they were all assumed to be cubes to simply the model. Therefore, the subsystems requiring boxes were CDH, EPS and ADCS and GNC which were assumed to be together given they share some of their components.

The GNC and ADCS components were distributed in six boxes one at each side of the vehicle with their components evenly distributed. Similarly, the EPS consists of several batteries therefore given their magnitude they will be divided into two boxes. The size and operational temperature of each box are presented in Table 10.5, where the length shows the size of each side of the cube box. These boxes are to be placed around the OTV and lander appropriately.

**Table 10.5:** Characteristics Thermal Control Boxes

| Box | Balance Operational Temperature [°C] | Length [$cm^2$] |
|---|---|---|
| CDH | 20 | 5.5 |
| EPS x2 | 20 | 45 |
| ADCS & GNC x6 | 20 | 35.5 |

The radiated energy is calculated as in Equation 10.9 where the emitted energy is dissipated from the electrical component in the box and the absorbed energy is that entering the box through the vehicle skin. A 50 % margin was taken into account for the radiator power to comply with the ESA design margin philosophy [15]. From Equation 10.10 the area of the radiator can be derived given the emissivity of the radiator is 0.85 [63].

$$Q_{radiator} = Q_{absorbed} + Q_{dissipated} \tag{10.9}$$

$$Q_{radiator} = \sigma \cdot \varepsilon \cdot (T_{Hot}^4 - T_{operations}^4) \cdot A_{radiator} \tag{10.10}$$

For the heaters, a similar method was used the heating power is given in Equation 10.11, which is the thermal equilibrium when a heater is in the system. The emitted power this time is the one radiated through the surfaces of the box, this is calculated as using Equation 10.2. The power is also assumed to be the electrical power for the heater itself as they have really high efficiencies. A 50 % margin was taken into account for the heating power to comply with the ESA design margin philosophy [15]. The selected heater type is a Kapton heater, these are made of a thin adhesive Kapton layer that can be sized appropriately. They have an energy density[1] of 1 W/$cm^2$, therefore using equation Equation 10.12, the required area of the kapton heater can be estimated.

$$Q_{heater} = Q_{emitted} - Q_{dissipated} - Q_{absorbed} \tag{10.11}$$

$$A_{heater} = \frac{Q_{heater}}{q_{heater}} \tag{10.12}$$

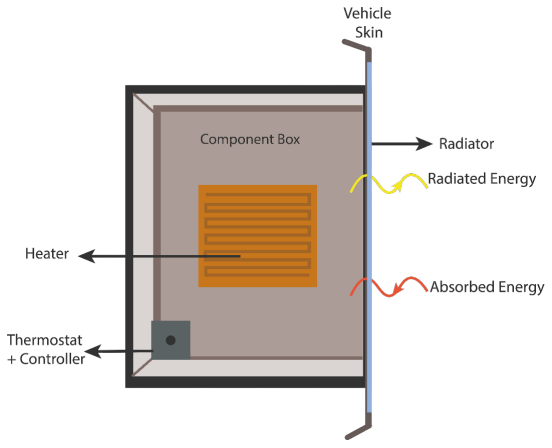


**Figure 10.4:** Component Thermal Control Box

[1] URL https://www.flywarm.com/polyimide-heaters/ [cited 18 June 2024]

The results for the different boxes are presented in Table 10.6, the method and equations presented are based on a NASA one-dimensional thermal model [63].

**Table 10.6:** Thermal Control Boxes

| Box | Area Radiator [$m^2$] | Area of Heater [$cm^2$] | Electrical power [W] |
|---|---|---|---|
| CDH | 0.31 | 0.11 | 0.11 |
| EPS x 2 | 0.89 | 7.4 | 7.4 |
| ADCS & GNC x6 | 0.17 | 0.11 | 0.11 |

Figure 10.4 illustrates an example of the sized control boxes.

Other thermal control considerations extend beyond the spacecraft and into exterior components like antennas and solar arrays. Solar arrays, incorporate anti-reflective coatings made of silicon dioxide ($SiO_2$). These coatings are common and are applied to off-the-shelf solar cells to enhance efficiency by minimising sunlight reflection. Similarly, antennae employ conductive coatings to the disks with transparent layers, made of indium tin oxide, to allow electrical signals to pass whilst regulating the temperature of the antennae itself. However, active control may also be required for these external components. Solar arrays include radiators on the back side to prevent overheating during their operations, they can be sized in a similar way as those for the cryocooler. Antennae may require both heaters and radiators therefore a control box can be sized and placed to protect all antennae components.

## 10.4. Risk Assessment

Table 10.7 shows the risks associated with the thermal control subsystem, the requirements linked to the risks and their respective causes are explained. Table 10.8 shows the risk mitigation and contingency

**Table 10.7:** Thermal Control System Risks

| ID | Risk | Causes | Req. |
|---|---|---|---|
| R-TCS-01 | Thermal Issues Leading to Overheating or Freezing of Critical Components | Insufficient thermal management, extreme environmental conditions | HOPE-TCS-080 |
| R-TCS-02 | Insufficient thermal management, extreme temperature variations | Insufficient thermal management, extreme temperature variations | HOPE-TCS-080 |
| R-TCS-03 | Radiator provides insuficient capacity or fails | Radiator electronic system failure | HOPE-TCS-040 |
| R-TCS-04 | Cryocooler system failure | The cryocooler has a given cooling capacity and lifetime it could fail | HOPE-TCS-040 |
| R-TCS-05 | Heater failure | The heater is an electrical component which can fail | HOPE-TCS-040 |

strategy. It also shows its location in the risk map showing the risk likelihood and consequences before and after the mitigation strategy is applied. The definition of the likelihood and consequence levels are discussed in Section 17.1.

Based on the results of the risk analysis for the thermal control subsystem, redundant components and sufficient margins should be applied throughout the design to ensure that the thermal control subsystem maintains adequate cooling and heating power to meet its required capacity without significant risks. These mitigation strategies have been appropriately incorporated into the design.

The most significant risk identified in this subsystem is R-TCS-04. A failure of the cryocooler could have substantial consequences for the propulsion system, potentially leading to mission failure. Therefore, it is imperative that the cryocooler is designed, tested, and manufactured to achieve high reliability.

**Table 10.8:** Thermal Control Risk Mitigation and Contingency Plan

| ID | Pre-mit. L | Pre-mit. C | Mitigation | Contingency | Post-mit. L | Post-mit. C |
|---|---|---|---|---|---|---|
| R-TCS-01 | P | Ma | Enhanced thermal insulation, active temperature regulation, redundant cooling systems | Emergency shutdown procedures, alternative operational modes | U | Mo |
| R-TCS-02 | P | Ma | Add redundant components where possible and design with margins to have compensate any possible inefficiencies of system | Increase cooling / heating capacity of the active thermal control system | U | Mo |
| R-TCS-03 | Li | Ma | Test radiators for efficiency and operational capacities | Add redundant radiators in case one stops functioning | U | Mo |
| R-TCS-04 | Li | Ca | Test cryocoolers extensively and find its operational limits and reliability | Change spacecraft attitude or operational mode if possible to increase absorbed heat if possible | P | Ma |
| R-TCS-05 | Li | Mo | Select heaters with a high reliability and lifetime | Add redundant heaters | U | Mo |

## 10.5. Sensitivity Analysis

The sizing tools are susceptible to assumptions that may later be proven to be less accurate during the actual design of the thermal control system. Therefore, conducting a sensitivity analysis of these parameters is highly valuable. This analysis serves to show the degree to which variations in these parameters affect the overall system performance and design outcomes. The parameters analysed are the following:

- **Component heat dissipation:** The corresponding values of the dissipated heat of components could vary as the total dissipation values of 306 W and 255 W for the lander and OTV respectively is an estimate based on the preliminary selected components and their estimated efficiency. It was found that increasing or decreasing these values by double will not change the cryocooler cooling power as it is not as significant as the heat absorbed from the environment. However, looking at individual components a 25 % increase in the CDH electronics heat dissipation will cause an increase in the required box radiator area of 20 %. Therefore this parameter is significant when sizing the individual component boxes.
- **Effective radiating temperatures:** This parameter was chosen to be analysed specifically because of the wide range of the radiating temperatures found for the moon, 120 - 380 W [54]. The lowest value specifically drove the coldest average equilibrium temperature significantly. An increase of 25 % in the lowest radiating temperature limit would cause the coldest average temperature to increase by 24 % for the lander and OTV. Moreover decreasing the warmest radiating temperature of the moon by 25 % would cause a decrease of 12 % of the average vehicle warmest temperature this is also significant because this means this condition now occurs in earth orbit instead of lunar orbit as initially calculated. Therefore, inaccurate values can impede the precise prediction of the mission's extreme temperature, complicating the determination of when the coldest and warmest temperatures will occur. Therefore, by developing a more refined model of the body's radiative temperatures, it would be possible to accurately predict the expected temperatures throughout all mission phases.
- **Radiator cooling capacity:** The radiator capacity, 180 $W/m^2$, final value was chosen to analyse given that from literature its value can change significantly depending on its properties. This value can vary from 100 - 300 W [64]. Its increase in 25 % would cause the required area of the equivalent radiator to decrease by 20 %. This changes the sizing of the thermal component significantly. Therefore, being certain of its value for the given radiator is crucial for an accurate model and future design.

These three parameters were identified as the primary drivers for thermal control sizing based on the model's assumptions. Sensitivity analysis suggests one should apply appropriate margins to these parameters if their values are still uncertain or obtain accurate estimates to enhance model reliability.

# 11 | Environmental Control and Life Support System

This chapter concerns the design of the Environmental Control and Life Support System (ECLSS) of the lander. Starting with a discussion of the requirements, assumptions and current state of the technology in Section 11.1, the considered designs are outlined in Section 11.2, along with a description of the required elements for each architecture. Next, the different technologies which can be used for each element are presented in Section 11.3. Calculations performed to determine the final mass of each architecture are developed in Section 11.4, based upon which the final components are then chosen. Finally, in Section 11.5, the configuration of the ECLSS elements is analysed to arrive at a final subsystem design. The system's integration into the spacecraft is determined and the design's main parameters are summarised.

## 11.1. Functional Overview

ECLSS is tasked with accommodating the crew and keeping them alive, healthy and comfortable. These functions are specified by requirements HOPE-ECLSS-010 through HOPE-ECLSS-240 and mostly stem from NASA HLS requirements [9] and the NASA Office of the Chief Health and Medical Officer (OCHMO). Based on these, the scope of the ECLSS subsystem is determined to be the air revitalization, thermal and humidity management of cabin air, monitoring and control of the atmospheric composition/pressure, food, water management, waste disposal and EVA support. The specific requirements defined for ECLSS are presented in Table 11.1

Traditionally, open-loop systems have been used in spacecraft for shorter duration missions, with longer missions, such as the ISS, moving to a closed-loop system to reduce resupply needs. The point where consumable mass for an open-loop system becomes larger than the additional power and mass needed for a closed-loop system is called the crossover point. Determining the crossover point is an important part of ECLSS design. During the preliminary design presented in the ARCH-E Midterm Report [14] the crossover point was determined to be 60 days for a large part of the system. However, the possibility of water reclamation system and a reusable carbon dioxide removal system was examined for the detailed design. Additionally, a modular design which makes use of the reconfigurable design of the spacecraft was examined. An analysis of both these options is presented in Section 11.4.

## 11.2. Architecture Options

### Baseline

The baseline architecture consists of an integrated (non-modular) fully open-loop system, as orginally described in the Mid-Term report. This would include the following:

- Thermal & Humidity Management System (THMS)
- Spacecraft Atmosphere Monitor (SAM)
- Universal Waste Management System (UWMS)
- Trace Contaminant Control System (TCCS)

Water, Oxygen and Nitrogen (for leakage compensation), as well LiOH canisters make up the consumables in this setup. These elements are all fixed into the spacecraft. This architecture can be seen in Figure 11.2.

### Modular

Most of the functions the ECLSS fills are historically designed to accommodate crew. Since the spacecraft will fly in both crew and cargo configurations, some of these functions may be unnecessary

**Table 11.1:** ECLSS Requirements

| ID | Requirement | Rationale | Verification Method | Check | Value |
|---|---|---|---|---|---|
| HOPE-ECLSS-070-1 | The ECLSS shall be able to maintain a cabin pressure between 26.2 kPa and 103 kPa during the entire crewed mission. | Important for the crew's health and safety, structural integrity, and atmospheric control. | Testing (vacuum chamber) | ✓ | Compliance Expected |
| HOPE-ECLSS-070-2 | The ECLSS shall limit the 1-hour average partial pressure of carbon dioxide (ppCO2) in the habitable volume to 3 mmHg. | Ensures that the concentration of $CO_2$ remains within acceptable levels to prevent adverse health effects on the crew. | Testing | ✓ | Compliance Expected |
| HOPE-ECLSS-070-3 | The ECLSS shall limit the levels of lunar dust particles less than 10 µm in size in any habitable atmosphere below a time-weighted average of 1.6 mg/m$^3$ during daily exposure periods that may persist up to 7 days in duration. | Prevents potential adverse health effects, ensuring a safe living and working environment for the crew during lunar missions. | Testing (with dust input) | ✓ | Compliance Expected |
| HOPE-ECLSS-070-4 | The ECLSS shall maintain temperatures between 18 °C-27 °C in the habitable environment. | Provides a comfortable and safe living and working space for the crew. | Testing | ✓ | Compliance Expected |
| HOPE-ECLSS-070-5 | The ECLSS shall maintain humidity between 25%–75% in the habitable environment. | Prevents issues such as dehydration, respiratory discomfort, and skin irritation. | Testing | ✓ | Compliance Expected |
| HOPE-ECLSS-070-7 | The ECLSS shall maintain a ventilation rate with 66.7% of the atmosphere moving with velocities between 4.57 m/min and 36.58 m/min. | Adequate ventilation is crucial for distributing oxygen, removing carbon dioxide and other contaminants, and regulating temperature and humidity. | Testing | ✓ | Compliance Expected |
| HOPE-ECLSS-070-8 | The cabin atmospheric composition shall contain at least 30% diluent gas, assuming a balance with oxygen. | Maintains a safe and breathable environment for the crew. | Analysis | ✓ | 30% |
| HOPE-ECLSS-070-9 | The ECLSS shall limit gaseous pollutant accumulation in the habitable atmosphere below individual chemical concentration limits specified in JSC-20584 [65]. | Safeguards the health and well-being of the crew. | Testing | ✓ | Compliance Expected |
| HOPE-ECLSS-070-10 | The ECLSS shall provide for operation a minimum water quantity of 3.5l/crewday. | To ensure crew survival according to NASA-STD-3001 [66]. | Testing | ✓ | 3.5 l |
| HOPE-ECLSS-070-13 | The water shall be provided at temperatures between 18 °C and 93 °C. | Ensures that water can be used for drinking, washing, and hot food rehydration. | Testing | ✓ | Compliance Expected |
| HOPE-ECLSS-010 | The ECLSS shall have a maximum mass of 4236.5 kg. | Needs to comply with overall mass budget. | Inspection | ✓ | 3616.46 kg |
| HOPE-ECLSS-020 | The ECLSS shall have a maximum total volume of 5 m$^3$. | Needs to comply with overall size constraints. | Inspection | ✓ | Compliance Expected |
| HOPE-ECLSS-030 | The ECLSS shall have a maximum recurring cost of 1 000 000 €. | Needs to comply with the overall cost budget for HOPE-MISS-120. | Analysis | ✓ | Compliance Expected |
| HOPE-ECLSS-040 | The ECLSS shall have a minimum reliability of 0.995 over the vehicle's mission lifetime. | Needs to comply with the overall reliability in HOPE-MISS-070, and the reliability budget. | Analysis | ✓ | Compliance Expected |
| HOPE-ECLSS-060 | The ECLSS shall not alter the performance of any other subsystem to the extent that it prevents them from meeting their respective requirements. | All subsystems need to function together successfully. | Testing | ✓ | Compliance Expected |
| HOPE-ECLSS-080 | The ECLSS shall accommodate for collection, containment, and disposal of body waste. | Maintains a clean and hygienic living environment, and prevents the spread of contaminants and odours. | Inspection | ✓ | Compliance Expected |
| HOPE-ECLSS-100 | The ECLSS shall have an interior configuration that accommodates the crew to perform all mission tasks, and support human performance and behavioral health. | Needs to have a configuration that allows for adequate living and working conditions within the vehicle. | Demonstration | ✓ | Compliance Expected |
| HOPE-ECLSS-110 | The ECLSS shall use less than 1.2 kW for TBD seconds under peak load. | Needs to comply with the overall power budget. | Testing | ✓ | 1087 W |
| HOPE-ECLSS-120 | The ECLSS shall use less than 1 kW under nominal load. | Needs to comply with the overall power budget. | Testing | ✓ | 792 W |
| HOPE-ECLSS-130 | The ECLSS shall accept power from the EPS at 28 V DC. | Electrical interfaces between the two subsystems must be compatible. | Demonstration | ✓ | Compliance Expected |
| HOPE-ECLSS-140 | The ECLSS shall purify water to meet or exceed the contaminant limits outlined in both JSC-63414 and the United States Environmental Protection Agency's maximum contaminant levels [67]. | Maintains a safe and healthy living environment onboard the vehicle. | Testing | ✓ | Compliance Expected |
| HOPE-ECLSS-160 | The ECLSS shall support at least 2 (threshold) and 5 (target) EVAs without corrective repair. | Derived from HLS requirements based on initial operation analysis. | Analysis | ✓ | Compliance Expected |
| HOPE-ECLSS-170 | The ECLSS shall not have a two-point failure preventing the safe return of the crew. | ECLSS needs redundancy so that up to two subsystem failures can be tolerated without endangering the crew see source | Analysis | ✓ | Compliance Expected |
| HOPE-ECLSS-180 | The ECLSS shall provide a quantity of 3035 kcal/day per crew member for the mission duration. | Ensures that each crew member receives sufficient calories and nutrients. | Analysis | ✓ | Compliance Expected |
| HOPE-ECLSS-190 | The ECLSS shall provide a quantity of 2.5 l/day of drinkable water per crew member per day for the mission duration. | Hydration is essential for maintaining the crew's health and well-being. | Analysis | ✓ | 2.5 l |
| HOPE-ECLSS-200 | The ECLSS shall sustain a rate of pressure change of 1551.32 Pa/s during operations. | Essential for maintaining the structural integrity of the vehicle, and for preventing crew injuries or decompression sickness. | Testing | ✓ | Compliance Expected |
| HOPE-ECLSS-210 | The ECLSS shall sustain a pressure change of TBD Pa. | Essential for maintaining the structural integrity of the vehicle over a range of operational pressures. | Testing | ✓ | Compliance Expected |
| HOPE-ECLSS-220 | The ECLSS shall stay within 6894.76 Pa of the commanded pressure. | Reduces discomfort or injuries for the crew members, based on NASA-STD-3001 [66]. | Testing | ✓ | Compliance Expected |
| HOPE-ECLSS-230 | The ECLSS shall accommodate for decompression sickness treatment. | To ensure crew safety. | Testing | ✓ | Compliance Expected |
| HOPE-ECLSS-240 | The ECLSS shall monitor in real-time for toxic atmosphere components. | To ensure crew safety. | Testing | ✓ | Compliance Expected |

without crew present. As such, a modular design where some of these functions are removed from the spacecraft when not in use, could lead to mass savings on cargo missions. This technology has seen a rapid maturation in recent years, with NASA awarding Collins Aerospace (now UTC Aerospace) a contract to develop a modular, palletised ECLSS for Lunar Gateway. [68].

Modularity of the architecture can be achieved by integrating these elements into removable pallets. The mass calculations for the modular design were based on the Collins Aerospace Universal Pallet. This structure, seen in Figure 11.1, aggregates ECLSS functions into functional groups. The pallets can be secured against the wall of the lander by a hinge mechanism for easy stowage and removal, and fit through the NASA Standard Hatch [69]. They are designed to be maintained and fixed in space, with the pallet structure allowing for the use of Maintenance Units in place of the Orbital Replacement Units currently in use on the ISS. [70]. This also gives a high level of flexibility for upgrading/replacing older hardware, maintenance and tailoring of atmospheric control functions to different cargo types. Payloads sensitive to temperature, pressure or humidity could be accommodated simply by not removing certain modules during the reconfiguration of the spacecraft. A drawback is the additional mass of the pallets, which is currently projected to be 35 kg, including a 15 % growth allowance [69]. In a modular architecture, the UWMS, SAM, TCCS would be removed for the cargo configuration, with only the THMS remaining, to retain a suitable atmosphere for the cargo. Fans and ventillation functions would also remain, since these have to be more integrated with the spacecraft.

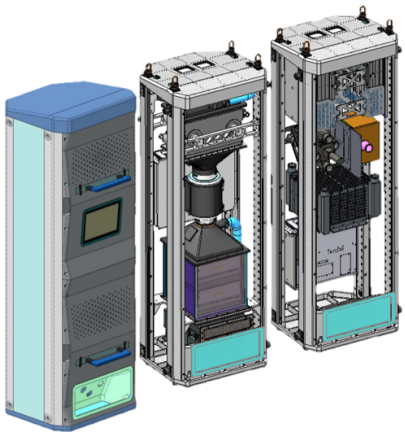

**Figure 11.1:** Universal Pallet

### Partially Regenerative

To reduce the amount of consumables, some of the resource loops can be partially closed. As discussed previously, a fully closed-loop system is not mass-efficient for a mission of this length. However, two regenerative systems will be considered: A Carbon-Dioxide Removal Assembly (CDRA) and a Humidity Reclamation System (HRS).

Considering the high consumable mass of LiOH canisters and water, these could save considerable mass, especially as the humidity emitted by astronauts is the cleanest waste water, and does not require much purification. Combined with the fact that this is a very mature technology, first used on the Mir space station, and humidity accounts for 45 % of the waste water, this could lead to a significant reduction in mass to TLI [71].

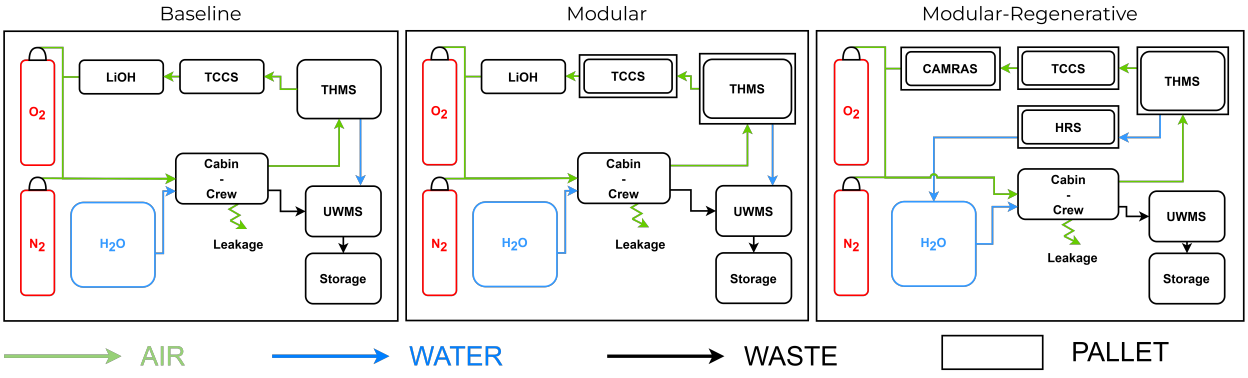


**Figure 11.2:** Proposed ECLSS Architectures

## 11.3. Technologies Considered

A literature study was performed to determine the most suitable technologies to fulfil each of the functions proposed in the previous section. Mass and power figures were also collected for use in the mass analysis presented in the next section.

### THMS

Condensing Heat Exchangers (CHX) have been used in this function for decades. A modern CHX design was obtained from [72], which involves water vapour diffusing from an air stream to a water stream through hollow fibres in a membrane due to a difference in partial pressure. The working mechanism can be seen in Figure 11.3. The membrane is hydrophobic to prevent a backflow of the water stream. This system weighs approximately 20 kg.

### SAM

Utilising the rapid miniaturisation trend in spaceflight, NASA JPL has developed a universal SAM (see Figure 11.4) slated to be used on Orion and Gateway. It measures both air components and contaminants in a 10 kg package, and is already flight-proven on ISS [73].

### HRS

Humidity reclamation and purification will be similar to, and sized based on the SRW-C (System for Water Reclamation - Condensate) used on the Mir space station. The main differences are that this system consists of 3 subsystems, of which the first preforms the separation of water vapour [71]. This is already performed by the THMS, and as such, this subsystem is left out. Subsystems II and III perform water purification and conditioning, as well as distribution and heating. These add up to 70 kg, which is increased to 93.33 kg to account for a crew of 4 instead of 3. This is considered a conservative estimate, as evolution of technology should allow for a lower mass to be achieved.

### UWMS

Improving on the current ISS commode design, the UWMS [74] is currently being certified on board the space station. It weighs only 52.16 kg and will be used in a multitude of spacecraft, making it perfect for this mission. Another option would be the simple fecal collection bags and Urine Collection and Transfer device flown on Apollo, weighing in at 45 kg. [75] However, with the increase in mission length and crew size and the lighter UWMS, the mass savings would be minimal, if any. It does not weigh up to the additional comfort and storage convenience of the UWMS.

### CDRA

For $CO_2$ removal, the simplest option is the use of LiOH scrubbers, similar to those used on the Apollo missions. These canisters get saturated, and as such, a total mass of 207 kg has to be allocated to ensure adequate $CO_2$ capture throughout the mission [14]. Possible regenerative technologies include 4-Bed Molecular Sieves (4BMS), and Solid Amine Water Desorption (SAWD). 4BMS is flight-proven [76], but most current development focuses on SAWD, in particular the Carbon dioxide And Moisture Removal Amine Swingbed (CAMRAS). This assembly weighs 23.5 kg and has enough capacity to accommodate a crew of four [77]. This technology relies on two hinged beds of solid amine material, one actively absorbing $CO_2$ from the cabin atmosphere, the other desorbing while being exposed to a vacuum. The system can be seen in Figure 11.5. Apart from being light, it requires minimal power and maintenance and is currently gathering flight experience on the ISS for future deployment in the Artemis program. A power figure is not available yet, however it only uses a blower and valves [78], and based on this a conservative power estimate of 60 W is used.

### TCCS

For the removal of trace contaminants, a two-stage process is used. The main stage is the oxidisation of the contaminants in a catalytic oxidiser. However, these catalysers are susceptible to poisoning [76]. This necessitates a charcoal bed as a first stage to get rid of these poisoning elements. As a baseline for the mass estimation, a very detailed design by Lockheed Martin for a TCCS of a future US Space Station was used and determined to be in the order of 100 kg [79].

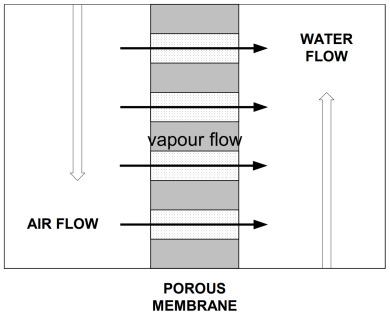


**Figure 11.3:** Membrane CHX [72]

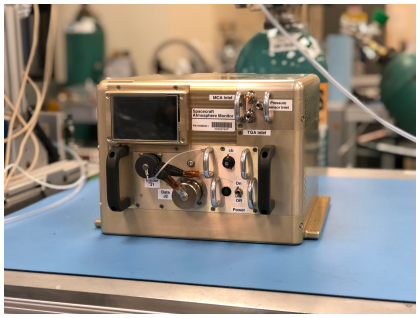

**Figure 11.4:** SAM [80]

**Figure 11.5:** CAMRAS[1]

## 11.4. Trade-Offs

### Assumptions

To get mass estimates for each of the proposed architectures, the following assumptions were made:

- The mass of piping and valves is 50% of the equipment structural mass, except for SAM
- The mass of ventillation and control equipment is equal for all architectures
- Consumable masses are taken from the ARCH-E Baseline Report [81]
- THMS cools the cabin air, cooling of other systems is performed by the TCS, and the cooling fluids (water or otherwise) are not included in the ECLSS
- As a conservative estimate, all subsystems will use their own pallet
- Crew provisions and additional items are sized based on the Mid-Term report [14]

### Power Equivalent Mass

Additionally, a power equivalent mass of 67.2 kg/kW was applied to CDRA and HRS [82]. The higher power consumption of closed-loop systems would lead to a larger EPS subsystem, which this extra calculation accounts for. This is a conservative figure, since the open-loop solutions (e.g. LiOH scrubbers) would also use some power, and this is not accounted for.

### Redundancy

For a mission- and safety-critical system like ECLSS, redundancy is an important design driver. This is also where the modular design shows promise. For the integrated design, multiple copies of critical systems are required on each flight in case of failure. For the modular design, many individual components can be serviced and replaced in-flight, meaning certain redundancies can be swapped for spares instead, saving mass. As a guideline for the amount of redundant components, the Time to Hazard analysis from the UTC Aerospace study on Lunar Gateway ECLSS is used [68]. Critical and low time to hazard systems will have a redundant component, while systems which can be serviced before their failure turns into a hazard will make use of spares.

As a result, two CAMRAS and SAM units will be used for redundancy. In addition, for an integrated architecture a redundant TCCS is carried while the modular option carries 50 kg in spares instead. To arrive a this figure, the philosophy of ”67% of non-structural mass in spares” used by Collins [83] is simplified to 50% of total mass, since the mass breakdown of these components is not available. In a similar way, for the integrated architecture, three CHX modules will be carried on each mission, where two are necessary to accommodate a crew of four, and one is for redundancy. Modular architectures will carry two units and 10 kg of spares.

[1] https://www.americaspace.com/2019/08/09/artemis-updates-2019-08-09/ [accessed 17 June 2024]

### Analysis

This methodology resulted in the masses for each of the architecture options, presented in Table 11.2. Only components which are used to compare the options, are listed, a more complete component listing will be given in the conclusion. For the modular options, the crew configuration is chosen for comparison, since this leads to the highest mass and power, which drives the sizing.

From this table, it can be seen that a modular regenerative architecture gives the lowest mass. Especially the regenerative systems save a lot of mass, but the modular concept also compensates its pallet weight with savings in redundant systems even without taking into account the reconfiguration. When reconfigured, the cargo version loses over 830 kg in mass on account of the architecture.

**Table 11.2:** ECLSS Architecture Mass Calculations ([kg] | [W])

| Element | Integrated system | Modular Open-Loop | Modular Regenerative |
|---|---|---|---|
| THMS | 90 | 70 | 70 |
| TCCS | 300 | 200 | 200 |
| CDRA | | | 70 \| 60 |
| HRS | | | 140 \| 2 [71] |
| LiOH | 207 | 207 | |
| $H_2O$ | 360 | 360 | 198 |
| Pallets | | 70 | 140 |
| Comparative Equivalent Mass | 957 | 907 | 822.67 |

## 11.5. Final Configuration and Integration

Now, the final configuration will be presented. It consists of 4 pallets and the separate UWMS and SAM, storage tanks for consumables and waste, as well as ventillation. The result is Figure 11.6

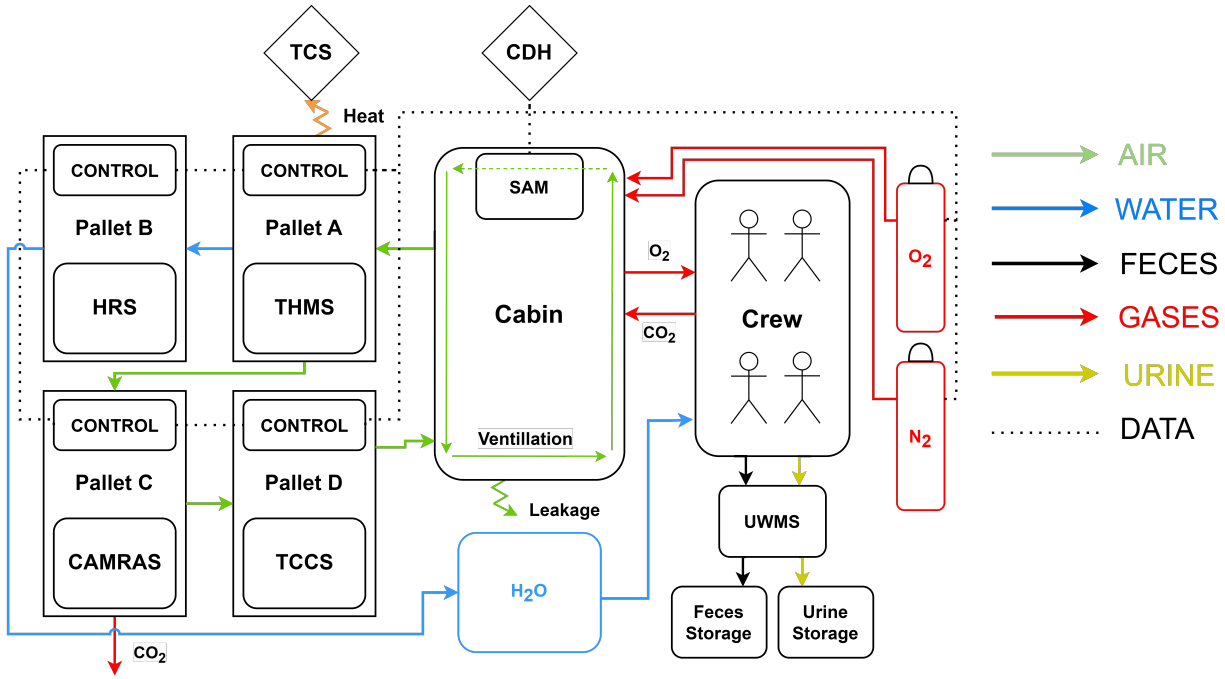


**Figure 11.6:** Final ECLSS Architecture

### Integration

The pallets will be placed against the walls of the spacecraft cabin and fixed in place with a hinged system that allows for easy placement and removal. Since the detailed interior layout of the cabin is outside the scope of this project, the exact position of the pallets is still to be determined. The placement will also allow for a more detailed analysis of the ventillation of the cabin. A decision will have to be made between a ventillation system integrated in the pallets with additional fans placed around the cabin to move the required volume of air as opposed to a distributed system. For this stage of the design, a ventillation system mass of 100 kg is taken based on previous designs. More accurate sizing of the ventillation is a recommendation for future work.

The ECLSS will be controlled by an integrated modular control system [83]. The central functions of interfacing with ground control, monitoring system health and facilitating software updates will be performed with a Command Center contained in the flight computers. The components will be controlled at the pallet level, each containing a small computational unit and monitor. Redundant communications links connect the pallets for coordination between the components. Next to CDH, ECLSS interfaces with TCS, which will carry away the heat extracted by the THMS from the cabin air. A heat exchanger will be connected to the water flow of the THMS which transfer the heat to the TCS before the water is processed by the HRS. A small amount of heat is also generated by the ECLSS components, however as the system is contained in the cabin, this will simply heat the cabin air, which is taken care of by the excess capacity of the THMS.

### Reconfiguration

During reconfiguration from a crew to cargo configuration, the returning crew, transfers the UWMS, SAM and the pallets containing TCCS, CAMRAS and HRS to the Earth-return vehicle. This will be accomplished by disconnecting UWMS from the waste storage tank, HRS from the water loop and potentially a centralised ventillation system from a disaggregated system of fans. Then, along with the removable seats, they are translated through the NASA standard hatch for which they are sized, by using two astronauts, one on either side of the hatch. Here, they continue their functions while the crew reenters and they return back to space with the next crewed mission to be reintegrated. This new mission also carries the consumable gases with it in addition to food and water.

### Final subsystem characteristics

To arrive at final mass figures, the additional crew accommodation items have been added from the mid-term report. The results are presented in Table 11.3

**Table 11.3:** ECLSS Mass Breakdown

| Category | Crewed Mass [kg] | Cargo Mass [kg] | Peak Power [W] |
|---|---|---|---|
| Air Revitalisation | 350.5 | 70 | 240 |
| Water Reclamation & Heating | 140 | | 2 |
| Monitoring & Fire Suppression | 28.3 | 28.3 | 40 |
| Waste Management | 82.16 | 30 | 305 [74] |
| Consumables | 560.25 | 51.75 | 0 |
| Pallets | 140 | 70 | 0 |
| Ventilation | 100 | 100 | 500 [84] |
| Airlock | 455 | 455 | 0 |
| Cabin Air | 61.25 | 61.25 | 0 |
| Crew Provisions | 582 | | 0 |
| Seats & Mobility | 273 | | 0 |
| Crew & Suits | 854 | | 0 |
| Total | 3626.46 | 866.3 | 1087 |

## 11.6. Risk Assessment

This section will cover the risk assessments for ECLSS. The identified risks are presented in Table 11.4 along with their causes and associated requirements. Subsequently, in Table 11.5 the risk likelihood and consequence are presented before and after mitigation and contingency measures. The definition of the likelihood and consequence levels are discussed in Section 17.1.

**Table 11.4:** ECLSS Risks

| ID | Risk | Causes | Associated Req. |
|---|---|---|---|
| R-ECLSS-01 | Loss of habitable pressure environment | Structural Defect, Seal failure | HOPE-STK-HLS-002 |
| R-ECLSS-02 | Loss of breathable atmosphere | Structural defect, Atmospheric contamination/revitalisation failure | HOPE-MISS-180 |
| R-ECLSS-03 | Inadvertent opening of lander EVA hatch | Human error, structural defect | HOPE-STK-ADS-030 |
| R-ECLSS-04 | Crew member exposure to excessive $CO_2$ | Poor ventilation, Life support system malfunction | HOPE-STK-ADS-030 |
| R-ECLSS-05 | Crew member exposure to contamination/toxicity | System Malfunction, Environmental contamination, material off-gassing | HOPE-MISS-180 |
| R-ECLSS-06 | Liquid in habitable environment | Poor Containment, Leakage, Condensation | HOPE-MISS-180 |
| R-ECLSS-07 | EVA crew member experiences decompression sickness | Human Error, Failure of EVA Procedures, Rapid pressure change | HOPE-STK-HLS-002 |
| R-ECLSS-08 | Failure/contamination of potable water system | System Malfunction | HOPE-MISS-180 |
| R-ECLSS-09 | Exhaustion of consumable resources | Poor Planning | HOPE-STK-HLS-002 |
| R-ECLSS-10 | Crew member exposed to lunar dust | Dust carried in on EVA suit | HOPE-ECLSS-070-3 |

**Table 11.5:** ECLSS Risk Mitigation and Contingency Plan

| | Pre-mit. | | | | Post-mit. | |
|---|---|---|---|---|---|---|
| ID | L | C | Mitigation | Contingency | L | C |
| R-ECLSS-01 | R | Ca | Proof-testing of pressurised volumes, MMOD protection | Isolate compromised volume, patch possible leak, mission abort | R | Ma |
| R-ECLSS-02 | R | Ca | Testing of oxygen system, redundancy in oxygen system | Use of oxygen masks, repairs of oxygen generator, mission abort | R | Ma |
| R-ECLSS-03 | R | Ca | Electronic safeguard against hatch opening without depressurised airlock/cabin, redundant lock design | Isolate compromised volume, repair hatch/locking mechanism/software, software override, mission abort | R | Ma |
| R-ECLSS-04 | U | Ma | Proper, adaptable ventilation, active air quality monitoring and warning, redundant CO2 scrubbing capabilities | Medical intervention, mission abort & medevac | R | Mo |
| R-ECLSS-05 | R | Ca | Contamination removal/filters, choice of non-toxic cabin materials, active air quality monitoring | Medical intervention, mission abort & medevac | R | Ma |
| R-ECLSS-06 | U | Mi | Extensive (proof) testing of piping, rehearsal of procedures to avoid crew error in handling water equipment | Proof-testing setup, crew training time | R | I |
| R-ECLSS-07 | R | Ma | Slow decomp/recomp, physical training | Medical intervention, mission abort & medevac | R | Mo |
| R-ECLSS-08 | U | Ma | Redundancy built in, proper operation, ground stress testing | Maintenance, possible mission abort | R | Mo |
| R-ECLSS-09 | P | Ma | Efficient resource management procedures, frequent monitoring of inventory | Activate resupply mission protocols, ration remaining resources, recycle | U | Mo |
| R-ECLSS-10 | Li | Mo | Filter air to remove particulates | Give medical treatment to crew member | P | Mi |

## 11.7. Sensitivity Analysis

The sensitivity analysis for this subsystem is fairly trivial, since the input parameters are crew size and mission length. For both of these, a change would mean a linear change in the consumables needed. Additional jumps in the amount of components needed arise if their capacity is exceeded.

# 12 | Electrical Power System

In this chapter the design of the Electrical Power System (EPS) is described. Firstly in Section 12.1 the function of the EPS is described and the requirements and verification steps are introduced. Following this, the solar array design is carried out in Section 12.2. The battery design follows in Section 12.3, and the power management and distribution in Section 12.4. After the design aspects, the risks associated with this subsystem are discussed in Section 12.5 and finally a sensitivity analysis is done in Section 12.6.

## 12.1. Functional Overview

The EPS must provide sufficient power at the correct voltage to all loads during all phases. To supply this power, the EPS must generate power using solar arrays and distribute this power to each load. It also must store energy using batteries, to provide power when power generation is not available and when the power demand peaks. The EPS requirements are given in Table 12.1. The EPS is either in compliance or expected to comply with each requirement. **HOPE-EPS-040** requires a detailed reliability analysis to ensure it is compliant, and there are clear and definite steps to increase reliability such as increasing redundancy. **HOPE-EPS-061** is currently met as there are not any conflicts between the EPS and other subsystems but a more detailed analysis and a demonstration is needed to prove this. **HOPE-EPS-120** is not met as the battery operating temperature is lower than the requirement. 315 K is too high for a Li-Ion battery for a long cycle life as this will result in high degradation. The presented temperature range is provided by the TCS in Chapter 10. Finally **HOPE-EPS-150** requires battery shielding, which is not yet included explicitly in the design but can be designed during the following phases. Demonstration of this shielding ability is needed to verify the requirement.

There are eight phases considered in the mission, and the vehicle power demands during these phases are given in Table 12.2. A more detailed breakdown per subsystem is provided in Table 6.4 and Table 6.5. 'Burn' refers to any orbital propulsive manoeuvres, while 'Coast' is the trans-lunar coast phase. Table 12.3 shows the duration of each of these phases; only the longest burn is shown, and ascent is not shown for the lander since it has a shorter duration as discussed in Chapter 8. For the lander, the crew and cargo configuration's power demands are different because the cargo version has a reduced ECLSS power requirement. This makes the crew version limiting in every case, so the crew version is used to size the EPS in this chapter.

## 12.2. Solar Array Design

A number of assumptions are made in order to size the solar arrays.

- A1: The 2D eclipse assumption is used, where the solar arrays are either in full sunlight or full shadow. During orbit, this means that there is a short period where full eclipse is assumed although the arrays are in partial sunlight, followed by a short period where full sunlight is assumed although the arrays are partial sunlight. These two cases counteract each other to an extent. Overall in low orbits there is a small effect on eclipse duration due to this assumption, approximately 8 s in LEO (< 1 %) [85]. To account for this, a 5 % margin is applied to all eclipse durations shown in Table 12.3.
- A2: Arrays are stowed and do not generate power during propulsive manoeuvres. This is a conservative assumption as even when folded against the spacecraft body, the arrays will receive some incident sunlight. The arrays are assumed to be stowed to reduce the structural loads.
- A3: The EPS daytime efficiency is 80 % and nighttime efficiency is 60 %. This is based on [51] considering a system using a peak power tracker for the solar arrays. This is later validated in Section 12.4 where a peak power tracker is chosen.

The solar arrays are the sole method of power generation in the EPS. They fulfil the nominal power demands, while also generating excess power to be stored by the batteries and used during eclipse

**Table 12.1:** Electrical Power System Requirements Verification

| ID | Requirement | Rationale | Verification Method | Check | Value |
|---|---|---|---|---|---|
| HOPE-EPS-010 | The electrical power system of the lander shall have a maximum mass of 500 kg. | Needs to comply with mass budget. | Inspection | ✓ | 419.2 kg |
| HOPE-EPS-011 | The electrical power system of the OTV shall have a maximum mass of 500 kg. | Needs to comply with mass budget. | Inspection | ✓ | 245.7 kg |
| HOPE-EPS-020 | The electrical power system shall have a maximum total volume of 0.4 $m^3$. | Needs to fit within launch vehicle fairing, should not be excessively large. | Inspection | ✓ | 0.15 $m^3$ |
| HOPE-EPS-040 | The electrical power system shall have a minimum reliability of 0.994 (TBC) over the vehicle's mission lifetime. | Needs to be compatible with overall reliability requirement and the reliability budget. | Analysis | Compliance Expected | |
| HOPE-EPS-061 | The electrical power system shall not diminish the performance of any other subsystem to the extent that it prevents them from meeting their respective requirements. | Ensures minimal interference with other subsystems. | Analysis/ demonstration | Compliance Expected | |
| HOPE-EPS-070 | The electrical power system shall provide a minimum nominal power of 3500 W (TBC) and a maximum nominal power of 7000 W (TBC) for 2800 s (TBC) at EOL. | Addresses nominal power production throughout the mission lifetime of the vehicle. | Testing | ✓ | 10 992 W |
| HOPE-EPS-071 | The electrical power system shall be able to provide a minimum peak power of 4100 W (TBC) and maximum peak power of 10 000 W (TBC) for 800 s (TBC) at EOL. | Ensures the system can accommodate for temporary increases in power demand. | Testing | ✓ | 10 992 W |
| HOPE-EPS-080 | The electrical power system shall have a power storage capacity of 320 Ah (TBC) at EOL. | Provides for sufficient power reserves during eclipse conditions. | Testing | ✓ | 540 Ah |
| HOPE-EPS-100 | The electrical power distribution system shall be able to distribute power at 28 VDC to 8 subsystems (TBC). | Ensures compatibility with other subsystems' electrical systems. | Demonstration/ testing | ✓ | 28 V |
| HOPE-EPS-110 | The electrical power distribution systems shall provide the correct type of current to 8 subsystems (TBC). | For compatibility with other subsystems' electrical systems. | Inspection | Compliance Expected | |
| HOPE-EPS-120 | The electrical power system shall be able to operate in a temperature range between 275 K (TBC) to 315 K (TBC). | Optimal working environment [51]. | Inspection | X | 233 K-293 K |
| HOPE-EPS-130 | The electrical power system shall be able to generate an average power of 6000 W (TBC) during daylight hours. | Provides for sufficient power generation in daylight conditions. | Analysis, testing | ✓ | 10 992 W |
| HOPE-EPS-131 | The electrical power system shall be able to generate an average power of 3000 W during eclipse conditions. | Provides for sufficient power generation in eclipse conditions. | Analysis, testing | ✓ | 5000 W |
| HOPE-EPS-140 | The electrical power system shall be able to provide venting capabilities in case of battery thermal runaway. | Mitigates risk of damaging other systems. | Demonstration/ Testing | ✓ | Chosen battery has venting capability |
| HOPE-EPS-150 | The electrical power system shall provide battery shielding in case of battery combustion. | Mitigates risk of damaging other systems. | Demonstration/ testing | Compliance Expected | |

**Table 12.2:** Power Demand per Phase [W]

| Vehicle | Burn | Coast | Descent/ Ascent | Orbit | Orbit (Eclipse) | Surface Ops | Slew | Safe |
|---|---|---|---|---|---|---|---|---|
| Lander (crew) | 3713 | 3064 | 4031 | 3359 | 2876 | 2847 | 3971 | 2847 |
| OTV | 2360 | 1617 | 0 | 1912 | 1656 | 0 | 2206 | 1494 |

**Table 12.3:** Duration of Zero Power Generation Phases [s]

| Vehicle | Eclipse LEO | Eclipse LLO | Descent | LOI | TLI |
|---|---|---|---|---|---|
| Lander | 2233 | 2789 | 780 | 1800 | - |
| OTV | 2233 | - | - | - | 339 |

periods or for load levelling during peak power demand. The eclipse period is calculated using the 2D eclipse model by Equation 12.1 and Equation 12.2, where $\lambda$ is the orbited body's half-angle in degrees [85]. The LEO and LLO altitudes are 200 km and 100 km respectively. The resulting eclipse times are given in Table 12.3.

$$\sin \lambda = \frac{R_e}{a} \tag{12.1}$$

$$T_{eclipse} = \frac{2\lambda}{360} T_{orbit} \tag{12.2}$$

### Solar Cell Selection

The type of solar cell used can have a significant effect on the solar array design. Higher efficiency and lower degradation cells are desired to reduce the required array area. Lower cell mass is also desired. Multi-junction cells show higher efficiencies as they can absorb radiation across a wider spectrum [86]. Triple-junction GaAs cells have become the industry standard due to their superior efficiency and radiation resistance [87]. Two of the highest-efficiency cells on the market were considered and are shown in Table 12.4. These are both from Azur Space, a leading European manufacturer. The quadruple junction cell has a slightly higher efficiency, however the triple junction cell was ultimately chosen. This cell has extensive space heritage[1], and reliability over the mission lifetime is a crucial part of the design.

**Table 12.4:** Comparison of Solar Cells

| Cell | Efficiency [%] | Sp. Power [W/m$^2$] | Deg. p%/year] | TRL |
|---|---|---|---|---|
| TJ 3G30-Adv [88] | 30 | 402.7 | 1-2 | 9 |
| QJ 4G32-Adv [89] | 32 | 434.5 | 1-2 | 7 |

### Solar Array Sizing

The solar arrays continuously generate power during daylight. The energy to be used during eclipse is also generated during daylight. The required power generation is then given by Equation 12.3. The daytime and nighttime efficiency are assumed as 80 % and 60 % efficiency, which accounts for the losses in distributing the power to the loads [87]. Nighttime efficiency is lower because the power takes a longer route through the batteries. The power and eclipse times used are given in Table 12.2 and Table 12.3 respectively. For the lander both LEO and LLO were evaluated, and LEO was the more limiting case.

$$P_{SA} = \frac{P_{day}}{\eta_{day}} + \frac{P_{night}}{\eta_{night}} \frac{t_{night}}{t_{day}} \tag{12.3}$$

To determine the area of the arrays, the degradation and efficiency of the solar cells is considered. Equation 12.4 gives the lifetime degradation of the cells, given the yearly degradation factor and number of years in operation. For TJ GaAs cells, a yearly degradation $\delta$ of 2% is used over the 10 year lifetime, based on [87]. This value is on the higher end of the range for LEO, since the spacecraft will spend a small amount of its overall lifetime outside of LEO.

Equation 12.5 is then used to determine the beginning-of-life (BOL) array area required, with the required power generation at end-of-life (EOL). This considers the lifetime degradation factor as well as the inherent degradation factor due to design and assembly losses, as well as shadowing. A value of 0.77 is used for inherent degradation based on [51]. The solar irradiance $Q_{sun}$ is taken as 1361 W/m$^2$ for both LEO and LLO[2]. Since the arrays will not perfectly point to the sun at all times, a conservative value of 23° is taken for the solar incidence angle based on [51]. Although this angle is very large considering the arrays will have a pointing ability, the details of the pointing strategy have not been defined in this report, so the conservative value will be used until a more detailed analysis is done in further design stages. Finally, the cell efficiency of 30% is used from Table 12.4.

$$L_d = (1-\delta)^{x_{years}} \tag{12.4}$$

$$P_{SA} = A_{BOL} \cdot Q_{sun} \cdot \eta_{cell} \cdot I_d \cdot L_d \cdot \cos\theta \tag{12.5}$$

Finally, an additional margin of 20% is applied to the overall required area, as well as a 5% margin on the solar cell power output, according to ESA's margin philosophy [15]. The array sizing results are given in Table 12.5.

[1] URL https://www.azurspace.com/index.php/en/products/products-space/space-solar-cells [cited 10 June 2024]

[2] URL https://nssdc.gsfc.nasa.gov/planetary/factsheet/moonfact.html [cited 10 June 2024]

**Table 12.5:** Solar Array Sizing Results

| Vehicle | No. Cells | Max BOL Power [W] | Max EOL Power [W] | Area [$m^2$] |
|---|---|---|---|---|
| Lander | 16 364 | 13 453 | 10 992 | 42.8 |
| OTV | 9368 | 7702 | 6292 | 24.5 |

### Solar Array Configuration Trade-Off

The configuration of the solar arrays depends on a number of criteria. The need to stow arrays during propulsive manoeuvres, especially during descent and ascent of the lander, limits the maximum length of the arrays. Stowing the arrays reduces the structural loads greatly, as the bending moment is reduced. When the arrays are folded they should not extend beyond the end of the vehicle, as they would be affected by the engine plume (and would impact the lunar surface in the case of the lander). The width of the arrays is limited by the launcher fairing size. Additionally, a smaller number of arrays gives improved redundancy, as the One-Array-Out (OAO) capability, where the EOL power requirements can be fulfilled after one solar array failure, can be achieved with a smaller overall margin. Finally the mass moment of inertia (MMOI) of the arrays is important as this contributes to the overall vehicle MMOI, and a higher MMOI makes attitude adjustments more difficult. Table 12.6 shows a trade of three considered options. Each option uses a Length:Width ratio of three. There is a possibility for two arrays, which is the least complex option but fails to stow fully so it leads to high structural loads. Using four arrays allows full stowing and achieves OAO capability with a lower margin. Finally using two arrays with multiple folding panels allows full stowing, but with much higher complexity due to the extra folding mechanisms. Since detailed sizing of the array thickness is not done here, the MMOI is calculated by approximating each array as a flat plate. Since the thickness is generally on the order of 20 mm [90], this assumption is justified as this is much smaller than the length and width. A density of 3 $kg/m^2$ is also assumed which is comparable to current similarly sized arrays such as in [91], using aluminium or carbon fibre honeycomb sandwich panels.

**Table 12.6:** Solar Array Configurations

| Option | Fully stowable | $I_{zz}$ [$kg\,m^2$] | $I_{yy}$ [$kg\,m^2$] | OAO margin [%] | Complexity |
|---|---|---|---|---|---|
| 2 rigid arrays | No | 1714 | 1790 | 100 | Low |
| 4 rigid arrays | Yes | 1220 | 1258 | 33 | Med |
| 2 Folding arrays | Yes | 1714 | 1790 | 100 | High |

From Table 12.6 it's clear that the four-array option is best, except when low complexity is absolutely essential. However even in this case, the higher complexity can be compensated by redundancy, since a relatively small margin is needed for this. As well as determining the array configuration, the mechanism for stowing and pointing the arrays should be considered. To achieve this, a solar array drive mechanism (SADM) can be used. A biaxial SADM allows the arrays to be folded along the length of the vehicle, and rotated about the axis of the arrays, as described in [92]. This allows the arrays to be pointed independently of the vehicle attitude, and allows power to be transmitted from the arrays. Overall the array sizing results in a total array mass, considering the solar cells and backing structure, of 182.4 kg for the lander and 104.4 kg for the OTV.

## 12.3. Battery Design

The battery design involved a number of assumptions just as with the array design.

- A1: The batteries provide all of the power needed when the arrays are not producing power, and whenever the peak power requirements exceed the arrays' power generation.
- A2: The majority of the vehicle life is in LEO. The mission duration is approximately 22.5 days, and there are ten missions over ten years. This means just 6% of the vehicle life is spent outside of LEO.

The depth of discharge and cycle life can therefore be sized for LEO.

### Battery Selection

There are multiple types of secondary batteries used in space missions. The most popular types which were considered are Ni-Cd, Ni-$H_2$, and Li-Ion batteries. It is desirable for the batteries to have low mass, low volume, and high efficiency. By examining these characteristic properties in Table 12.7 it's clear that Li-Ion batteries are superior in these criteria. This is supported by the fact that they are becoming the industry standard for efficient, high-performance secondary batteries [93]. Thus Li-Ion batteries will be used for energy storage. Most of the 10-year vehicle lifetime will be spent in LEO. With nearly 6000 eclipses per year, the batteries need to last for approximately 60 000 cycles in their lifetime. This will require a low Depth of Discharge (DOD) and high reliability Li-Ion battery, with proven flight heritage. The VES16 8s4p Li-Ion battery from Saft is chosen to fill this need[94]. This is rated for up to 18 years in LEO at 30% DOD and is certified to ECSS standards. The specifications are given in Table 12.8. This battery consists of 32 cells. Selecting a complete battery means the mass of the connections is accounted for and the mass calculation is more accurate. This battery also has a venting capability which is needed to fulfil **HOPE-EPS-140**.

**Table 12.7:** Comparison of Secondary Battery Types [51, 87]

| Battery Type | Energy Density [Wh/kg] | Energy Density [Wh/L] | Energy Efficiency [%] |
|---|---|---|---|
| Ni-Cd | 30 | 90-120 | 72 |
| Ni-$H_2$ | 60 | 90 | 70 |
| Li-Ion | 125 | 600-1000 | 98 |

**Table 12.8:** Chosen Battery Specifications [94]

| Name | Capacity [Ah] | Mass [kg] | Voltage [V] | DOD [%] | Cycle life [−] |
|---|---|---|---|---|---|
| Saft VES16 8s4p | 18 | 5.8 | 28 | 30 | $1 \times 10^5$ |

### Battery Sizing

The batteries are sized to store the energy needed to survive eclipse periods and periods of peak power. The duration of each phase is given in Table 12.3. As with the solar arrays, multiple cases are considered to determine the limiting case. During peak power periods in sunlight, it is assumed that the batteries provide the peak power needs while the arrays continue to provide the nominal power. When the arrays are not producing power (i.e. during eclipse or when the arrays are stowed), the batteries provide all power needed. For each phase, the average power used and duration are important to determine the capacity needed. For the OTV, the longest duration propulsive burn (TLI) and the eclipse period in LEO are considered. For the lander, the longest burn is LOI, and the eclipse in both LLO and LEO must be considered. Additionally for the lander, ascent and descent are considered, since the arrays will be stowed. The average power of each of these phases is given in Table 12.2.

The DOD influences the cycle life of the battery. At a higher DOD, the irreversible loss in capacity at EOL also increases. Since the majority of the battery cycle life is spent in LEO, the DOD in LEO should be at the rated level. However this DOD can be exceeded slightly in edge cases, with minimal impact on the battery life as long as the number of cycles at this higher DOD is limited [95]. This can help avoid oversizing the energy storage for these edge cases, such as LOI of the lander. A detailed analysis of the cycle life of the VES16 cell is provided in [95]. Cycling at a 50 % DOD for a small (<5 %) portion of the lifetime introduces negligible additional capacity loss when compared to cycling just at 30 % DOD [95]. For this reason, 50 % DOD is used outside of LEO, while the rated 30 % DOD is used while in LEO to preserve battery life. This results in an EOL capacity of 84 % BOL. With this in mind, the limiting case for both the OTV and lander is the eclipse in LEO.

The required energy during each phase is the product of the average power and the duration. Equation 12.6 is used to determine the battery capacity required to store this energy, taking into account the battery discharge efficiency (including both the battery discharge and the distribution to the load),the bus voltage, and the DOD. The discharge efficiency is taken as 80 % based on [87]. The bus voltage is 28 V and will be further discussed in Section 12.4. The required BOL capacity is then determined with Equation 12.7 using $\frac{EOL}{BOL} = 84\,\%$.

$$C_{actual} = \frac{P_{load} \cdot t_{load}}{\eta_{discharge} \cdot V_{bus} \cdot DOD} \tag{12.6}$$

$$C_{BOL} = C \cdot \frac{EOL}{BOL}^{-1} \tag{12.7}$$

The resulting capacity has a 5 % margin applied according to ESA's margin philosophy [15] to account for lower hardware performance. The required number of batteries in series and in parallel are given by Equation 12.8 and Equation 12.9 respectively.

$$n_{battery} = \frac{V_{bus}}{V_{battery}} \tag{12.8}$$

$$m_{battery} = \frac{C_{BOL}}{C_{battery}} \tag{12.9}$$

Since the battery voltage is the same as the bus voltage, only one battery needs to be connected in series. The number of batteries in parallel is rounded up and has an additional 10 % margin is added as a contingency to ensure the battery capacity is enough even after some batteries fail. The results are given in Table 12.9.

**Table 12.9:** Battery Sizing Results

| Vehicle | No. Batteries | BOL Capacity [Ah] | Mass [kg] | Volume [$m^3$] |
|---|---|---|---|---|
| Lander | 30 | 540 | 174.0 | 0.149 69 |
| OTV | 18 | 324 | 104.4 | 0.089 81 |

## 12.4. Power Management and Distribution

Power management and distribution (PMAD) is necessary to ensure the correct power and voltage is supplied to each load. The electrical block diagram detailing the PMAD for the lander is shown in Figure 12.1. The bus voltage for both vehicles is set at 28 V. A higher voltage helps to reduce line loss [51, 90], but this voltage must be regulated for each of the individual loads. A very high bus voltage would cause a larger power loss during conversion. For a spacecraft power in the 5–15 kW range, a bus voltage of 20–50 V is appropriate [90]. 28 V is the standard for many legacy spacecraft [90] so many Commercial Off The Shelf (COTS) components are compatible with this voltage.

This has the same layout for the OTV, except that the ECLSS is not present. The EPS will use a distributed, regulated, non-dissipative DC bus. For larger spacecraft a distributed system is generally used, as opposed to the centralised systems found on small satellites [90]. This reduces the power loss which results from long, high-power lines in the vehicle [90]. To regulate the power at each load, DC-DC converters will be placed at the load to convert the bus voltage to the correct level. Switched-mode regulators are the best option here, as the simpler linear regulators have poor efficiency [87, 90]. A non-dissipative system is used by including a peak-power tracker (PPT). It is placed in series with the array and keeps the voltage of the array near the maximum power point, so the full capability of the array is utilised [90]. While this is slightly less efficient than the simpler direct-energy transfer systems, the large and frequent variations in sunlight and temperature experienced in LEO and LLO make the PPT more advantageous [90].

**Table 12.10:** EPS Mass

| Mass [kg] | Lander | OTV |
|---|---|---|
| **Batteries** | 174.0 | 104.4 |
| **Arrays** | 182.4 | 104.4 |
| **Harness** | 62.9 | 36.8 |
| **Total** | 419.2 | 245.7 |

To manage peak power demands, the batteries are used for load levelling. When the power demand increases, power is first diverted from charging the batteries to the load. When the power generation is exceeded by the demand, the batteries are discharged to fill in the gaps. A detailed battery charge/discharge strategy and control loops should be developed in later design phases. The voltage regulation for each component can be done by COTS space-grade DC/DC converters which are readily

available. A central power distribution unit (PDU) distributes power to subsystems as instructed by the central flight computer, and regulation is done at the load by the DC/DC converter. At this stage of the design the electrical harness is not designed in detail, however an estimate can be made of the harness mass. This generally makes up approximately 15 % of the EPS mass, when the harness is considered to include the wiring and the electronic components such as power regulators [87]. This results in a final mass breakdown of the EPS given in Table 12.10.

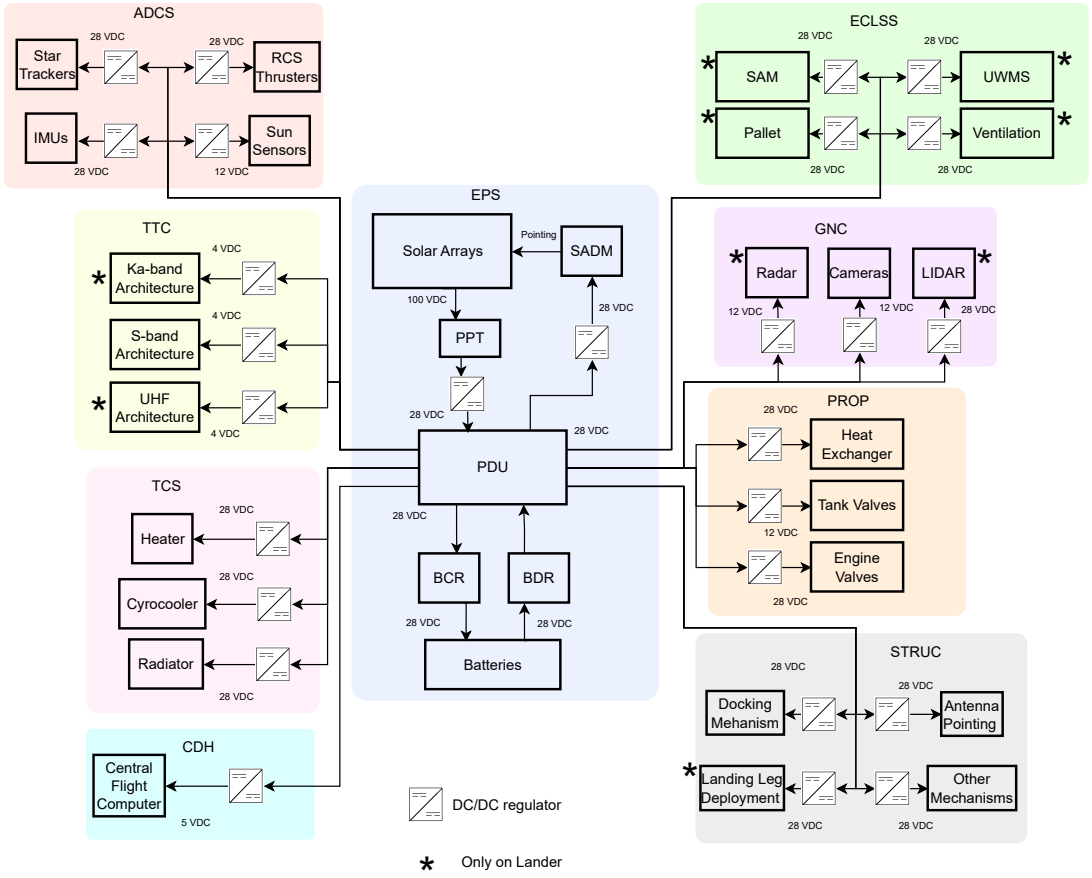


**Figure 12.1:** Electrical Block Diagram

## 12.5. Risk Assessment

The risks related to the EPS are presented in Table 12.11. A common theme among these is component failure due to the harsh environment and long lifetime involved. Radiation, lunar dust and MMOD present significant risks to the EPS. Additionally the high number of cycles of sunlight and eclipse pose a risk to the solar cells and especially to the batteries. The risks in Table 12.11 have associated requirements, some of which were developed for risk mitigation. **HOPE-EPS-040** is associated with many of the risks because it requires a minimum level of reliability for the EPS as a whole. In Table 12.12 the mitigation and contingency plans for each risk is shown, as well as the likelihood and consequence of each risk before and after mitigation. Risks with both a high likelihood and severe consequence are the most critical and require the most attention. Many of the risks presented are mitigated by proper testing and validation of the components used. The risk of circuit failures of the batteries and solar arrays can be effectively mitigated by including diodes in the correct manner to protect against short-circuit damage and allow current to bypass damaged parts. For contingency measures, both contingency margins and redundancy are used to reduce the risk severity. As explained in this chapter, redundancy is built into the design in the batteries, solar arrays and solar cells. The vehicles can operate nominally at EOL if one array stops working due to the contingency margins used. A

conservative value of 2% degradation per year was also used to mitigate **R-EPS-01**. A 10% battery reliability margin was used to mitigate any battery failures, and the large number of individual batteries means that failures can be isolated. Overall all of the identified risks are mitigated to an acceptable level. The EPS risks are included in the complete risk maps in Chapter 17.

**Table 12.11:** EPS Risks

| ID | Risk | Causes | Impact | Req. |
|---|---|---|---|---|
| R-EPS-01 | Higher-than-expected degradation of solar arrays | Extreme environmental conditions | Reduced power generation | HOPE-EPS-040 |
| R-EPS-02 | Failure to deploy solar arrays/wings | Deployment Mechanism Malfunction | Reduced power generation | HOPE-STR-040 |
| R-EPS-03 | Failure to stow solar arrays/wings | Stowing Mechanism Malfunction | Structural damage | HOPE-STR-040 |
| R-EPS-04 | Solar array structural failure | Fatigue, Extreme Operating Conditions, Design flaws | Reduced power generation, destabilisation | HOPE-STR-070 |
| R-EPS-05 | Critical failure of battery | Thermal Stress, Material Defect | Safety issue | HOPE-EPS-040&050 |
| R-EPS-06 | Electrical shock of crew member | Poor insulation | Safety issue | HOPE-EPS-040 |
| R-EPS-07 | Higher-than-expected battery degradation | Extreme environment | Reduced energy storage | HOPE-EPS-040 |
| R-EPS-08 | Electrical circuit failure due to lunar dust | Excessive dust from lading plume | Reduced function of electrical systems | HOPE-EPS-040 |
| R-EPS-09 | Solar array electrical circuit failure | Extreme environment | Reduced power generation | HOPE-EPS-040 |
| R-EPS-10 | MMOD damage to solar arrays | Inadequate shielding | Reduced power generation | HOPE-EPS-040 |
| R-EPS-11 | Failure of solar array drive | Lunar dust, fatigue | Reduced power generation | HOPE-EPS-040 |
| R-EPS-12 | Vehicle loss of electrical power | Electrical system failure | Loss of vehicle function | HOPE-EPS-040&070&071 |
| R-EPS-14 | Solar array string failure due to open-circuit failure of a cell | Solar cell damage | Reduced power generation | HOPE-EPS-040 |
| R-EPS-15 | Reverse current in solar array string due to short-circuit failure of the string | Lower voltage due to shadowing | Heating of array | HOPE-EPS-040 |
| R-EPS-16 | Short-circuit failure of a battery | Excessive current in battery circuit | Battery damage | HOPE-EPS-040 |
| R-EPS-17 | Battery failure due to open-circuit failure of a single cell | Electrical connector failure | Reduced battery capacity | HOPE-EPS-040 |
| R-EPS-18 | Reduced battery performance due to short-circuit failure of a single cell | Electrical connector failure | Reduced battery capacity | HOPE-EPS-080 |
| R-EPS-19 | Overcharging of a battery beyond its electrical capacity | Failure of PDU | Reduced battery life | HOPE-EPS-040&080 |
| R-EPS-20 | Over discharging of a battery beyond its EODV | Failure of PDU | Reduced battery life | HOPE-EPS-080 |
| R-EPS-21 | Battery leakage | Unacceptable temperature range | Damage to electrical system | HOPE-EPS-040&140 |

## 12.6. Sensitivity Analysis

A sensitivity analysis is carried out on the key parameters to check the robustness of the design. Some parameters have a clear linear relation such as the mass of components which will have a direct effect on the overall mass. The parameters analysed are the degradation of solar cells and of the batteries, the magnitude of the power demands and the duration of the eclipse periods.

- **Solar cell degradation**: The 2 % yearly degradation used could increase due to unexpected solar events, improper shielding or manufacturing defects. With an increased yearly degradation of 4 % (the same level as worse-performing solar cell types such as Si-based cells [51]), the BOL array area must increase. This causes an array area increase of 23 % for both the OTV and lander, with a corresponding mass increase. The total EPS mass increases by 11.7 % to 468.4 kg for the lander, and 11.4 % to 273.8 kg for the OTV. The battery mass is unaffected.
- **Battery Degradation**: The 84 % EOL capacity of the batteries is used from a detailed analysis from [95] for a 30 % DOD over 60 000 cycles. A higher loss of 70 % EOL capacity (the worst-case value for 50 % DOD) at the same 30 % DOD is evaluated. The lander battery mass would increase by 20 %, causing an overall EPS mass increase of 9.8% to 460.2 kg. Similarly the OTV battery mass increases by 16.7 %, giving a 8.3 % EPS mass increase to 266.1 kg. The array sizes are unchanged.

**Table 12.12:** Risk Mitigation and Contingency Plan

| ID | Pre-mit. L | C | Mitigation | Contingency | Post-mit. L | C |
|---|---|---|---|---|---|---|
| R-EPS-01 | AC | Ma | Testing of solar cells, close monitoring of performance | Contingency margin on array size | P | Mi |
| R-EPS-02 | U | Mo | Test solar array, regular inspection | Backup up systems in case of primary system failure | R | Mi |
| R-EPS-03 | U | Mo | Test and validate mechanisms, continuous monitoring | Activate back-up stowage systems | R | Mi |
| R-EPS-04 | U | Ma | Robust design, continuous monitoring | Activation of redundant structural elements | R | Mo |
| R-EPS-05 | R | Ca | Testing and qualification of battery systems, monitor battery health | Redundant battery systems, battery cooling systems | R | Ma |
| R-EPS-06 | R | Ca | Electrical safety protocols, training of crew members | Isolation of affected systems | R | Ma |
| R-EPS-07 | R | Ca | Testing of EPS components | Isolation of affected systems | R | Ma |
| R-EPS-08 | P | Mo | Ensure electrical components are shielded from dust | Enter safe mode, direct power from non-essential systems, use redundant systems | U | Mo |
| R-EPS-09 | P | Ma | Testing of electrical circuits, redundant circuits | Enter safe mode, direct power from non-essential systems | U | Ma |
| R-EPS-10 | P | Mo | Use adequate shielding, use redundant circuits in arrays | Analyse damage, redirect power from non-essential systems | U | Mo |
| R-EPS-11 | P | Mo | Test component in failure scenarios | Adjust vehicle attitude to point arrays, multiple arrays for redundancy | U | Mo |
| R-EPS-12 | U | Ca | Testing of electrical system to failure scenarios | Detach lander from OTV | R | Ca |
| R-EPS-13 | U | Ca | Testing of electrical system to failure scenarios | Detach lander from OTV | R | Ca |
| R-EPS-14 | P | Mo | Include one by-pass shunt diode per cell | Reorient arrays to increase incident sunlight | U | Mo |
| R-EPS-15 | Li | Mo | Include one blocking diode per string | Reorient arrays to reduce shadowing | U | Mo |
| R-EPS-16 | P | Ma | Include short-circuit protection in the battery circuit | Use multiple batteries for redundancy | U | Mo |
| R-EPS-17 | P | Ma | Include by-pass shunt diodes for each cell | Use a contingency margin on the battery capacity | U | Mo |
| R-EPS-18 | P | Mo | Testing of batteries, use of highly reliable batteries | Use a contingency margin on the battery capacity | U | Mi |
| R-EPS-19 | P | Mo | Power distribution unit | Discharge battery to the rated level | U | Mo |
| R-EPS-20 | P | Mo | Power distribution unit | Use lower DOD to preserve battery life | U | Mi |
| R-EPS-21 | U | Ma | Battery testing, battery shielding | Isolation of affected battery | R | Mo |

- **Battery DOD**: The 30 % rated DOD is used in LEO as discussed in Section 12.2. As described in [95], a 50 % DOD is expected to be possible for a projected 70 % EOL capacity over 60 000 cycles. If this DOD is used instead with the higher degradation, the battery mass tends to decrease. The lander battery mass decreases by 10 %, causing an overall EPS reduction of 4.9 % to 460.2 kg. The OTV has a larger improvement, showing a 27.8 % decrease in battery mass for an overall EPS mass reduction of 13.9 % to 211.5 kg. The array mass is unchanged.
- **Power Demand**: A 20 % increase of power demand across all phases is considered. This will increase both the array and battery sizes. For the lander, this causes a straightforward 20 % increase in both the array, battery and overall EPS mass, for a new EPS mass of 503.1 kg. The lander experiences a 20 % array mass increase with a 16.7 % battery mass increase, and the EPS mass increases 18.3 % to 290.7 kg.
- **Eclipse Duration**: A 20 % increase to all eclipse periods is considered. The result is practically identical to the power demand increase for the arrays, batteries and overall EPS for both lander and OTV, which was expected.

# 13 | Telemetry, Tracking, and Command

This chapter will discuss the design considerations for the Telemetry, Tracking, and Command (TT&C) subsystem for ARCH-E. Firstly, the decisions for choosing the ground stations to be used throughout various phases of the mission will be discussed. Afterwards, the chosen TT&C architecture specifications will be presented. Then, the calculations into the various link budgets will be presented, as well as the mathematical models and assumptions that have been made. This results in the hardware architecture interaction, as well as the power and mass estimations, and a discussion on the requirements imposed on this subsystem. Finally, a risk assessment and sensitivity analysis of the link budgets are discussed.

## 13.1. Ground Station Network Selection and Operations

In order to start analysing the communications required, a ground station has to be chosen to analyse the link budget. Currently, NASA and ESA's network are able to provide coverage globally. For NASA, this leaves NASA's Deep Space Network (DSN), and Near Space Network (NSN), consisting of the Direct-to-Earth (DTE) ground network, and the Tracking and Data Relay Satellite System (TDRSS), as well as ESA's ESTRACK ground network. The NSN will be expanded by 2030 with 18 m antennas as part of the Lunar Exploration Ground Sites (LEGS) [96]. Moreover, the NSN consists of several commercial ground stations, which could be interesting to use, as institutional networks are more strained by demand [97], and generally have higher operating costs.

A cost analysis was performed on the operating cost for one mission cycle in order to compare. Firstly. to calculate the DSN operating cost, the 34 m BWG class antennas was used, as this class was also used for the preliminary link budget for the midterm [14]. In order to calculate the operating cost of one 34 m BWG station, Equation 13.1 was used [98].

$$\text{OC} = 1420 \cdot (0.9 + F_C/10) \tag{13.1}$$

In Equation 13.1, OC is the operating cost in euros per hour (FY24), and $F_C$ is the number of station contacts per calendar week. The duration of one contact pass is based on a maximum of 12 hours per pass, with integer multiples of 1 hour. ARCH-E will require 10 days for transfer, 1 day day for ascent and descent, 6.5 days days on the lunar surface, and 5 days days for contingencies. For the day of ascent and descent, an LLO revolution time of 2 hours was considered. For this LLO period, 36 contacts are required, based on 3 contacts/day due to Earth's rotation. For the other days (excluding LEO operations), 252 contacts/week for 3 weeks is required for full-time coverage. This means that the total operating cost with DSN sums to a total of 19 277 352 euro (FY24) per mission. For $F_C$, an assumption was made that the mission consists of continuous 12 hour intervals during transfer and on the lunar surface. For the actual mission, $F_C$ would increase, as ARCH-E would go out of view for a particular station, and needs to re-contact.

To calculate the operating cost of the NSN DTE, the estimation rate of 746 euro/pass (FY24) may be used, where the pass is a maximum of 30 minutes [99], which leads to a cost of 2 417 040 euro (FY24) per mission. This is a reduction of 87.5 % compared to full-time communications with the DSN. This reduction could be even greater if the commercial providers are used, but values for these services need to be requested from these providers. As the NSN is currently expanding LEGS, using this network for ARCH-E would still provide the use of high frequency bands (i.e. Ka-band), similar to the DSN, whilst providing a lower operating cost.

As for ESTRACK, a typical mission has a cost range of 419 to 628 euro/hour (FY24) [100]. As ARCH-E is not a typical mission (in terms of number of contacts and contact time), a typical DSN mission has been scaled to ARCH-E's cost per hour. For a typical DSN mission, NASA provides an operating cost of 1792 dollar/hour [99]. ARCH-E has an operating cost of roughly 37 062 euro/hour. Extrapolating these rates, ARCH-E's operating cost for communication is 23 times more expensive. Hence, this

would yield a cost of for 5 199 434 - 7 792 947 euro (FY24) for ESTRACK per mission. Although this analysis is very rough, it does seem to have the same order of magnitude as NASA's NSN network, which is comparible to ESTRACK in terms of performance. However, NSN DTE currently provides more sophisticated modulation and coding techniques than ESTRACK [101, 102]. Hence, the decision was made to use NSN for further analysis.

Finally, for refuelling, the TDRSS will be used. During this period, having full-time communications is essential, not only for rendezvous (OTV, or refuelling vehicle), but generally in operations of resupply an loading and unloading crew or cargo. The cost of a single access is rated at 171 euro/minute (FY24) [99]. Single access was chosen over multiple access, as the data rate for multiple access would not be enough [103]. These data rates will be discussed in Section 13.2. The time in LEO, before returning back to the Moon, is assumed to take 2 days (see Chapter 7). This results in an operating cost of communications during refuelling of 492 480 euro (FY24).

To result the cost analysis, and the selection of the ground station networks, the TDRSS will be used during the Launch and Early Operations Phase (LEOP). Then, after LEO parking orbit, the NSN DTE will take over communications during the remainder of the mission. After ARCH-E comes back to Earth and inserts into a LEO parking orbit for refuelling, TDRSS will take over again. The cost for full-time communications from LEOP to the end of the refuelling phase is estimated at 2 909 520 euro (FY24), which excludes the time during LEOP, assumed to be negligible, at it only last around 2 orbits ($<$ 3 hours) (see Chapter 7).

## 13.2. Intercompatibility, Modulation, and Coding Techniques

In order to start with the design, the required data rates for different signal types needed to be defined. This will drive the used frequency band, as well as the required modulation and coding techniques. However, the viable modulation and coding is also dependent on the ground station and which frequency band being used, limited the maximum spectral efficiency and coding gain that can be achieved.

The data rate requirement for TT&C have been designed with the end-to-end compatibility with future lunar missions in mind, by adhering to the International Communication System Interoperability Standards [104]. This means that a maximum downlink data rate of 84.68 Mbps, and 25.22 Mbps uplink. The combined data rate of other types of data was selected based on the needs of set data (e.g. no audio required for the OTV, as there is no crew), and the maximum capable data rate supported by the link.

From the preliminary design, S-, X-, and Ka-band were considered [14]. The decision was made to have an architecture with the high-gain antennas using S-, and Ka-band. X-band was excluded as it would have not been compatible with future lunar architecture [96]. Furthermore, this band is mostly used for military purposes [105]. The S-band link will be used for low data rates, whereas high data rates are assigned to the Ka-band. Low data rates are defined as data which falls under audio communications, telemetry, commands, file transfers, and software uploads. This data the minimum necessity for operating the vehicle. High data rate is defined as all types of data that could be transmitted or received, which includes all types of data for low data rates, as well as video communications, scientific data and other videos/imagery capabilities. Finally, emergency capabilities are required when the link is lost, and EVA capabilities.

As emergency links do not require high data rates, a low-gain S-band antenna was chosen. This would provide a larger half-power beamwidth (HPBW) than high-gain antennas, which would be easier to detect. For EVAs, omni-directional UHF antennas were chosen. This decision is compliant with ICSIS [104] and the currently in development xEVA suits developed by Axiom[1] [106]. Caution should be exercised when ARCH-E lands on the shielded zone of the Moon (SZM). In this region, many frequencies are banned due to radio astronomy. Therefore, instruments using these frequencies should be placed into quiescent mode or turned off during the EVA [104]. The main S-band will use

[1] URL https://www.axiomspace.com/axiom-suit [cited 19 June 2024]

phased array antennas, due to their high gain and their capability to change the radio-frequency wave without mechanisms. For the Ka-band, a parabolic reflector antenna was chosen, as the high gains (about 40 dB) are hard to be achieved with other antenna types [87].

For S-band, a maximum bandwidth of 5 MHz available per user/band [103]. For Ka-band, this maximum is 1500 MHz [107]. The modulation and coding techniques were chosen based on which one are supported by the ground station, and the required energy per bit and spectral efficiency. Table 13.1 shows each link along with the modulation and coding type, data rate, and data type to be transmitted/received.

**Table 13.1:** Data Rate Allocation

| Link Type | Modulation | Coding Type, Coding Rate | Spectral Efficiency[1] [bps/Hz] [108] | Data Rate [Mbps] |
|---|---|---|---|---|
| **Lander** | | | | |
| Ka-band uplink | QPSK | Uncoded | 2.0 | 25.22 |
| Ka-band downlink | QPSK | LDPC, $r = 7/8$ | 1.67 | 84.68 |
| S-band uplink | QPSK | LDPC, $r = 1/2$ | 1.0 | 3.22 |
| S-band downlink | QPSK | RS (I=1) | 1.67 | 8.33 |
| Emergency S-band uplink | BPSK | LDPC, $r = 7/8$ | 0.83 | 0.220 |
| Emergency S-band downlink | BPSK | LDPC, $r = 1/2$ | 0.5 | 0.470 |
| UHF uplink | - | - | - | 0.016 |
| UHF downlink | - | - | - | 0.256 |
| **OTV** | | | | |
| S-band uplink | BPSK | $1/2$ CC (I=1) with RS | 0.43 | 0.200 |
| S-band downlink | BPSK | $1/2$ CC (I=1) with RS | 0.43 | 0.450 |
| Emergency S-band uplink | BPSK | LDPC, $r = 7/8$ | 0.83 | 0.100 |
| Emergency S-band downlink | BPSK | LDPC, $r = 1/2$ | 0.5 | 0.100 |

[1] Bit error rate of $1 \times 10^{-6}$

Then, for the frequency band chosen for analysis, the lowest frequency of the allocated band was chosen. The center of the band was chosen to be $\frac{1}{2}$ bandwidth $+ f_{lowest}$. Detailed frequency band allocation needs to be discussed and negotiates with the provider.

## 13.3. Link Budget Calculations and Assumptions

Now that the requirements have been set up, a link budget could be made, which drove the design of the antennas on ARCH-E. Only the primary S-band, and Ka-band link will be discussed in the analysis of this report. The other link budgets can be analysed in a similar manner. A real life analysis would include several hundreds of link budgets, at different phases of the mission, and different links. This is out of the scope of this project, and has to be analysed in later phases of the design.

For the receiver side, the transmitted power, losses induced in the system, and the gain of the antenna, as well as pointing loss, were considered. These (except for pointing loss), are usually combined into a combined performance factor, called the equivalent isotropic radiated power (EIRP). For the vehicle, the gain is calculated via Equation 13.2 for parabolic reflector antennas in unitless form, and Equation 13.3 for phased array antennas in dBi.

$$G_{peak,parabolic} = \frac{\pi^2 D^2}{\lambda^2}\eta \qquad (13.2) \qquad G_{peak,array} = 10log_{10}\left(\frac{A}{\lambda^2}\right) + 8 \qquad (13.3)$$

In Equation 13.2 and Equation 13.3, $D$ is the diameter of the reflector in m, $\lambda$ is the wavelength of the frequency in m, and $\eta$ is the efficiency of the antenna, unitless. $A$ is the surface area of the array in $m^2$.

The pointing loss for a parabolic antenna can be calculated with Equation 13.4 in dB. Where the HPBW for the same type of antenna is shown in Equation 13.5 in °. For the array antenna, this pointing loss was assumed to be zero, as the HPBW is usually much higher than for parabolic antennas [109]. Hence, the pointing offset angle was assumed zero. Moreover, due to this antenna operating in

S-band, these losses (if assumed a parabolic antenna), are usually in the order of $1 \times 10^{-3}$ for offset angles of 0.1°, justifying this decision. Then, the free space loss is calculated with Equation 13.6, unitless. This "loss" is due to the the inverse square law, which spreads the energy, hence reducing the information capable to be captured by the receiver.

$$L_{pr} = -12 \left( \frac{e_t}{\alpha_{1/2}} \right)^2 \quad (13.4) \qquad \alpha_{1/2} = \frac{21}{fD} \quad (13.5) \qquad L_s = \left( \frac{\lambda}{4\pi S} \right)^2 \quad (13.6)$$

In Equation 13.4 and Equation 13.5, $e_t$ is the pointing offset angle in °. $\alpha_{1/2}$ is the HPBW in °, $f$ is the frequency in MHz, and $D$ is the antenna diameter in m. In Equation 13.6, $\lambda$ is the wavelength in m, $S$ is the distance between transmitter and receiver in m.

Then, on the receiver side, the pointing loss, gain, system loss due to implementation of modulation/coding, cables and noise temperature, are summed up. These are calculated in the same manner as just discussed, but in reversed order. However, instead of EIRP, a gain-to-system noise temperature parameter is introduced, which is the gain of the receiver, minus the system noise temperature (in dB).

### Weather attenuation

There is still one parameter to be discussed, which are the weather attenuation. This can be split up into two types, losses due to the gasses/particles in the atmosphere, and losses due to rain. For these losses, recommendations from the radio-communication sector of International Telecommunication Union (ITU) were used. For gas attenuation, ITU-R P.676-10[2] was used to obtain the attenuation for different frequencies. For rain attenuation, ITU-R P.838-3[2] was used for calculating the specific attenuation in dB/km, as shown in Equation 13.7. The rain height is calculated with Equation 13.9 in km.

$$\gamma_R = kR^{\alpha} \quad (13.7) \qquad \alpha = [k_H \alpha_H + k_V \alpha_V + (k_H \alpha_H - k_V \alpha_V) \cos^2(\theta) \cos(2\tau)]/2k \quad (13.8)$$

$$h_R = h_0 + 0.36 \quad (13.9) \qquad k = [k_H + k_V + (k_H - k_V) \cos^2(\theta) \cos(2\tau)]/2 \quad (13.10)$$

As seen in Equation 13.7, $k$ and $\alpha$ are nameless coefficients, calculated in Equation 13.10 and Equation 13.8 respectively. And $R$ is the rain rate in mm/h, obtained from the ITU rain zone from ITU-R PN.837-1[2]. In Equation 13.9, $h_0$ is obtained from ITU-R P.839-3[2]. $\tau$, is the polarisation tilt angle relative to the horizontal. For this link budget, a circular polarisation was used ($\tau = 45°$), as this it the operating polarisation used by the DSN and NSN.

Finally, it is important to factor in the elevation angle of the vehicle with respect to the ground station. The aforementioned attenuations are for Zenith. However, ARCH-E will be at a non-optimal elevation angle. To factor this in, a flat Earth assumption was made, which results in $A(\theta) = A_{zen}/sin(\theta)$. This is a conservative estimate [107]. Here, $A_{zen}$ is the attenuation at Zenith in dB. $\theta$ is the elevation angle in °. For this analysis, ground sites seen in Table 13.2 have been analysed, which are considered worst case scenario, which was a balance between elevation and performance (EIRP, G/T) factors. The results have been tabulated in Table 13.2.

As can be seen in Table 13.2, Ka-band rain attenuation cannot be ignored. For S-band, the main attenuation comes from gas attenuation.

Now that all the parameters for the link budget have been discussed, the actual link budget can be presented. For the S-band study case, the primary S-band link will operate in all phases of the mission. From the analysis, it was concluded that the loss due to smaller elevation angles is negligible compared to the losses encountered due to free space. This is the result of the small losses in S-band as concluded from Table 13.2. Hence this link was analysed between the Earth to the Moon, with the previously chosen phased array antenna. Same holds for the Ka-band parabolic antenna, as its purpose is mainly to send/receive non-critical data, designed to only operate during lunar operations.

[2]URL https://www.itu.int/pub/R-REC [cited 19 June 2024]

**Table 13.2:** Location Properties based on Chosen Ground Station and Center Frequency

| Ground Station | Latitude [°] | ITU Rain Zone | Rain Height [km] | Rain[1] Attenuation [dB] | Gas Attenuation [dB] |
|---|---|---|---|---|---|
| **LEGS, Ka-band ($f_{up}$ = 23 GHz \| $f_{down}$ = 26 GHz)** | | | | | |
| White Sands, USA | 32.54 | E | 3.36 | -0.2687 \| -0.3595 | -0.4131 \| -0.3100 |
| Matjiesfontein, S-Africa | -33.23 | E | 3.36 | -0.5631 \| -0.7536 | -0.8660 \| -0.6495 |
| TBD, Australia[2] | -30 | M | 3.36 | -3.341 \| -4.251 | -0.7821 \| -0.5866 |
| **DTE, S-band ($f_{up} = f_{down}$ = 2 GHz)** | | | | | |
| Alaska Satellite Facility, USA (AS2) | 64.86 | C | 1.36 | -0.0001 | -0.040 |
| Svalbard, Norway (SG2) | 78.23 | C | 1.36 | -0.0002 | -0.065 |
| Hartebeesthoek, S-Africa (HBK-02) | -25.89 | E | 3.36 | -0.0003 | -0.056 |

[1] Assumed availability over 99.0%. [2] Worst case rain zone

**Table 13.3:** Ka-band Architecture Link Budget

| Parameter | Uplink | Downlink | Unit | Comments Uplink | Comments Downlink |
|---|---|---|---|---|---|
| (1) Transmitter Power | - | 13.61 | dBW | - | 23 W TWTA |
| (2) Transmitter Loss | - | −0.969 | dB | - | 0.8 loss [110] |
| (3) Transmitting Antenna Gain | - | 40.77 | dBi | - | 0.55 m diameter, Equation 13.2 |
| (4) Equivalent Isotropic Radiated Power | 89 | 53.41 | dBW | [111] | (1)+(2)+(3) |
| (5) Transmitting Antenna Pointing Loss | −0.332 | −0.001 | dB | [111], incl. autotrack loss | $e_t = 0.01°$, Equation 13.4 |
| (6) Forward Distortion Loss | −1 | 0.0 | dB | [111] | - |
| (7) Atmospheric Gas Attenuation | −0.782 | −0.587 | dB | Table 13.2 | |
| (8) Rain Attenuation | −3.341 | −4.251 | dB | Table 13.2 | |
| (9) Transmission Path Loss | −4.123 | −4.837 | dB | (7)+(8) | |
| Distance | 408 788 | 408 788 | km | Maximum distance Earth to Moon | |
| Center Frequency | 22 600 | 25 550 | MHz | Center (22.55-22.65 GHz) | Center (25.50-25.60 GHz) |
| (10) Free Space Loss | −231.8 | −232.8 | dB | Equation 13.6 | |
| (11) Receiving Antenna Pointing Loss | 0.000 | −0.332 | dB | $e_t = 0.01°$, Equation 13.4 | [111], incl. autotrack loss |
| (12) Receiving Antenna Gain | 39.70 | - | dBi | 0.55 m diameter, Equation 13.2 | - |
| (13) Receiver Loss | −1.549 | - | dB | 0.7 loss [110] | - |
| (14) System Noise Temperature | 24.62 | - | dBK | 290 K conservative, [112, 113] | - |
| (15) Receiver Gain-to-Noise-Temperature | 13.53 | 47.5 | dB/K | (12)+(13)+(14) | [111] |
| (16) Required Data Rate | 74.02 | 79.28 | dBHz | See Table 13.5 | |
| (17) Implementation Loss | 0.0 | −2.0 | dB | - | [111] |
| (18) Boltzmann Constant | −228.6 | −228.6 | dBW/K/Hz | $10log_{10}K$ | |
| (19) Obtained SNR | 19.38 | 10.24 | dB | (4)+(5)+(6)+(9)+(10)+(11)+(15)-(16)+(17)-(18) | |
| (20) Required SNR | 10.5 | 3.8 | dB | See Table 13.5 | |
| (22) Margin | 8.876 | 6.441 | dB | (19)-(20) | |

**Table 13.4:** Primary S-band Architecture Link Budget

| Parameter | Uplink | Downlink | Unit | Comments Uplink | Comments Downlink |
|---|---|---|---|---|---|
| (1) Transmitter Power | - | 18.33 | dBW | - | 68 W TWTA |
| (2) Transmitter Loss | - | −0.969 | dB | - | 0.8 loss [110] |
| (3) Transmitting Antenna Gain | - | 27.17 | dBi | - | 1.53 $m^2$ area, Equation 13.3 |
| (4) Equivalent Isotropic Radiated Power | 51 | 44.52 | dBW | [103] | (1)+(2)+(3) |
| (5) Transmitting Antenna Pointing Loss | −0.003 | 0.0 | dB | Equation 13.4, [103] | - |
| (6) Forward Distortion Loss | - | - | dB | - | - |
| (7) Atmospheric Gas Attenuation | −0.065 | −0.065 | dB | Table 13.2 | |
| (8) Rain Attenuation | 0.000 | 0.000 | dB | Table 13.2 | |
| (9) Transmission Path Loss | −0.065 | −0.065 | dB | (7)+(8) | |
| Distance | 408 788 | 408 788 | km | Maximum distance Earth to Moon | |
| Center Frequency | 2027.5 | 2202.5 | MHz | Center (2025-2030 MHz) | Center (2200-2205 MHz) |
| (10) Free Space Loss | −210.8 | −211.5 | dB | Equation 13.6 | |
| (11) Receiving Antenna Pointing Loss | 0.0 | 0.0 | dB | - | [103], Equation 13.4 |
| (12) Receiving Antenna Gain | 26.45 | - | dBi | 1.53 $m^2$ area, Equation 13.3 | - |
| (13) Receiver Loss | −1.549 | - | dB | 0.7 loss [110] | - |
| (14) System Noise Temperature | 24.62 | - | dBK | 290 K conservative, [112, 113] | - |
| (15) Receiver Gain-to-Noise-Temperature | 49.52 | 19.1 | dB/K | (12)+(13)+(14) | [103] |
| (16) Required Data Rate | 65.08 | 69.21 | dBHz | See Table 13.5 | |
| (17) Implementation Loss | 0.0 | −2.0 | dB | - | Assumption, [111] |
| (18) Boltzmann Constant | −228.6 | −228.6 | dBW/K/Hz | $10log_{10}K$ | |
| (19) Obtained SNR | 3.914 | 9.415 | dB | (4)+(5)+(6)+(9)+(10)+(11)+(15)-(16)+(17)-(18) | |
| (20) Required SNR | 0.9 | 6.4 | dB | See Table 13.5 | |
| (21) Margin | 3.014 | 3.015 | dB | (19)-(20) | |

Table 13.3 and Table 13.4 show the results from the analysis to close the links. A margin of 3 dB was maintained as minimum. For the downlink for Ka-band, a 6 dB margin was used. This is due to the fact that due to higher uncertainly in the antenna pointing pattern and ground station performance in near-Earth, a higher margin is needed to be accounted for [51]. In order to close the Ka-band link, a 0.55 m diameter parabolic antenna was used, with a minimum transmit power of 23 W, which is in line with typical values seen in literature[3] [87]. For the S-band link, a surface area of 1.53 $m^2$ was required, along with a transmit power of 68 W.

## 13.4. TT&C Architecture

Based on the the previous discussions in this chapter, as well as literature performed on several TT&C system designs on previous mission[3], a block diagram for the lander TT&C was made, as seen in Figure 13.1.

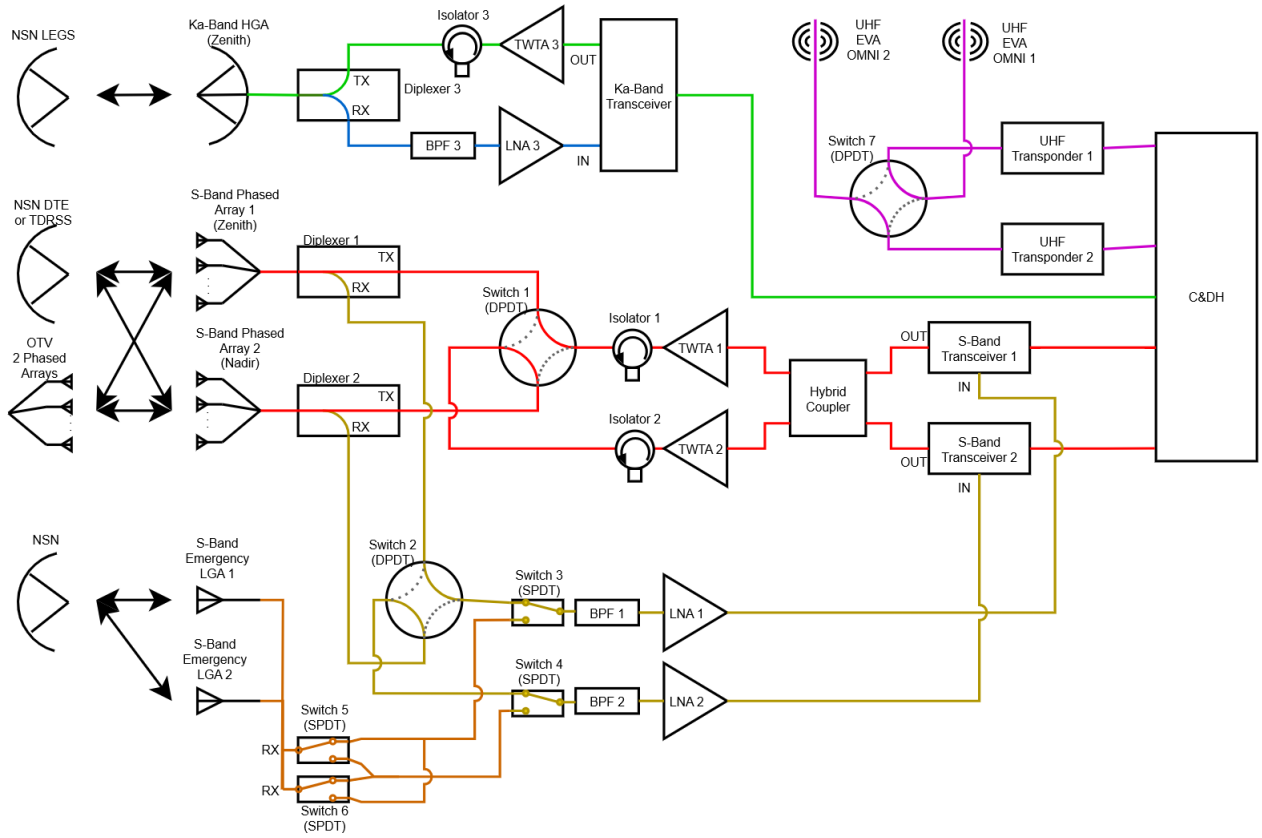


**Figure 13.1:** Lander Telemetry, Tracking, and Command System Block Diagram

Figure 13.1 For the OTV, the block diagram is similar, but it only has the S-band architecture. Based on Figure 13.1, as well as the results obtained from Table 13.3 and Table 13.4, the estimated mass and power budgets were obtained, based on similar components used in flight proven missions[3]. The power requirements have been scaled based on the difference in transmit power between literature and the required transmit powers calculated. The results are shown in Table 13.5. Finally, during the design of the TT&C architecture, all requirements as seen in Table 13.6 were considered.

[3]URL https://descanso.jpl.nasa.gov/propagation/propagation.html [cited 19 June 2024]

**Table 13.5:** TT&C Architecture Power and Mass

| | Unit Power [W] | Unit Mass [kg] | | Unit Power [W] | Unit Mass [kg] |
|---|---|---|---|---|---|
| **S-Band Architecture** | | | **Ka-Band Architecture** | | |
| Low gain antenna (2) | 0 | 0.1 | High gain antenna (1) | 0 | 0.61 |
| High gain antenna (2) | 0 | 13.1 | Gimbals & motors | 0.26 | 1.25 |
| Diplexer (2) | 0 | 1.4 | Diplexer (1) | 0 | 0.9 |
| TWTA (2) | 68 | 5.1 | TWTA (1) | 23 | 1 |
| Transceiver (2) | 27.4 | 6.9 | Transceiver (1) | 5.3 | 3.2 |
| Switches | 0 | 2.1 | Other components | 0 | 1.4 |
| Cables | 0 | 2.3 | Total Ka-band | 28.5 | 8.4 |
| Other components | 0 | 3.5 | | | |
| Total S-band | 190.8 | 61.1 | **UHF Architecture** | 17.4 | 13 |
| **Total Lander (=S+Ka+UHF)** | **236.7** | **82.5** | **Total OTV (=S)** | **190.8** | **61.1** |

**Table 13.6:** TT&C Requirements

| ID | Requirement | Rationale | Verification Method | Check | Value |
|---|---|---|---|---|---|
| HOPE-TTC-010 | The TTC subsystem shall have a maximum mass of 4400 kg (TBC). | Needs to comply with the mass budget | Inspection | ✓ | 144 kg |
| HOPE-TTC-030 | The TTC subsystem shall have a maximum recurring cost of €20 × $10^6$. | Based on worst case cost estimation | Analysis | ✓ | €2.9 × $10^6$ |
| HOPE-TTC-040 | The TTC subsystem shall have a minimum reliability of 0.994 (TBC) over the vehicle's mission lifetime. | HOPE-MISS-070. Derived by assuming that each subsystem has the same probability of failure ($0.95^8$) during its entire lifetime | Analysis | ✓ | Compliance Expected |
| HOPE-TTC-070a | The TTC subsystem shall use less than 284 W for 1838 s (TBC) under peak load. | Time to downlink non-critical data back to Earth within line of sight with Earth. | Testing | ✓ | 236.7 W |
| HOPE-TTC-080 | The TTC subsystem shall use less than 229 W under nominal load. | For compliance with power budget | Testing | ✓ | 190.8 W |
| HOPE-TTC-COMMS-070a | The OTV TTC subsystem shall be able to provide a minimum downlink to allow for telemetry data. | For compliance with ICSIS targets | Testing | ✓ | 0.450 Mbps |
| HOPE-TTC-COMMS-080a | The OTV TTC subsystem shall be able to receive a minimum uplink to allow for commands and software uploads. | For compliance with ICSIS targets | Testing | ✓ | 0.200 Mbps |
| HOPE-TTC-COMMS-090 | The OTV TTC subsystem shall operate using radio waves in the S, and Ka frequency bands. | Ensures compatibility with all Artemis systems (space and ground segments) | Inspection | ✓ | |
| HOPE-TTC-COMMS-100 | The TTC subsystem shall maintain a link budget margin of at least 3 dB during all mission phases. | Ensures the link is closed whilst accounting for unexpected link losses | Analysis | ✓ | |
| HOPE-TTC-090 | The TTC subsystem shall not have any single point failures for components critical for crew survival. | Ensures crew survival | Testing | ✓ | |
| HOPE-TTC-100 | The TTC subsystem shall be able to provide an emergency radio system in case of loss of a communications link. | Ensures redundancy in case of loss of communications | Testing | ✓ | |
| HOPE-TTC-110 | The TTC subsystem shall have a bit error rate not greater than 10 × $10^{-6}$. | Limits errors in information sent and received | Analysis | ✓ | |
| HOPE-TTC-120a | The lander TTC subsystem shall be able to provide a minimum return link of 10 Mbps. | For compliance with ICSIS targets | Testing | ✓ | 84.68 Mbps |
| HOPE-TTC-130a | The lander TTC subsystem shall be able to receive a minimum forward link of 2 Mbps. | For compliance with ICSIS targets | Testing | ✓ | 25.22 Mbps |
| HOPE-TTC-140a | The lander TTC subsystem shall operate using radio waves allowing communications between the OTV and EVA. | Provides communication with the OTV and with the lander during EVA | Testing | ✓ | |
| HOPE-TTC-150 | The TTC subsystem shall comply with the allocated frequency turn around ratio. | For compliance with DSN guidelines/rules | Analysis | ✓ | Compliance Expected |
| HOPE-TTC-160a | The TTC subsystem shall use a bandwidth no bigger than 5 MHz for S-band frequency and 1500 MHz for Ka-band frequency. | For compliance with regulations and allocated bandwidth of the ground station | Analysis | ✓ | |
| HOPE-TTC-190 | The TTC subsystem shall provide undisturbed line of sight of the antenna to ground station | Communications link should not be obstructed | Inspection | ✓ | |
| HOPE-TTC-230 | The TTC subsystem shall support a period of non-direct link with Earth of TBD hrs. | There may be points during the mission where vehicle does not have a direct link | Analysis | ✓ | |
| HOPE-TTC-240 | The TTC subsystem shall support an united frequency band supporting tracking and ranging by the ground segment | Ground segment should know the location and direction of the vehicle | Testing | ✓ | |

## 13.5. Risk Assessment

The risks formulated during the project, seen in Table 13.7, were assessed, and mitigated (see Table 13.8) during the design of the TT&C system. The mitigation for R-TTC-01 can primarily be seen in Figure 13.1, where two redundant emergency LGA were introduced, and a second primary S-band was added. Furthermore, the option of phased arrays over parabolic reflectors for the S-band architecture stemmed from the risk of having a higher pointing offset than required. This decision was primarily driven due to phased arrays having a much higher HPBW than parabolic reflectors.

R-TTC-02 was also taken into account, with the compatibility to multiple ground stations, by keeping in mind the lowest performing ground stations (having low EIRP and G/T, as well as unfavourable latitude angles), as well as the best performing modulation and coding techniques that could be used which would be compatible with most ground stations. This is the reason why the data rate had to be limited, as higher modulation, such as 8-PSK or higher, was not supported by most ground stations. Turbo coding was also deemed infeasible, as the difficulty in decoding means the supported data rates are highly restricted.

**Table 13.7:** TT&C Risks

| ID | Risk | Causes | Req. |
|---|---|---|---|
| R-TTC-01 | Loss of communication and/or tracking capabilities | Communication system failure, signal interference | HOPE-TTC-050 |
| R-TTC-02 | Ground station inaccessible due to over capacity | Over use of ground station by other missions. multiple spacecraft simultaneously wanting link | HOPE-TTC-100 |

**Table 13.8:** Risk Mitigation and Contingency Plan

| | Pre-mit. | | | | Post-mit. | |
|---|---|---|---|---|---|---|
| ID | L | C | Mitigation | Contingency | L | C |
| R-TTC-01 | U | Ma | Use redundant communication systems/install emergency radio system, filter signals | Implement emergency communication protocols | U | Mo |
| R-TTC-02 | P | Ma | Design for other or multiple GS / add multiple antennas for different frequency bands | Attempt connection to different ground station, reduce data rate | U | Mo |

## 13.6. Sensitivity Analysis

Finally, a sensitivity analysis was performed on the link budget calculations. The main assumptions which the results are sensitive to are briefly discussed. The first assumption concerns the 99 % availability of the ground station due to rain attenuation. If this requirement is increased, then for the S-band frequency, even for 99.999 % availability, the attenuation stays at the order of $1 \times 10^{-2}$ dB. However, for the K-band frequency, for 99.9 %, the attenuation goes to 3.32 - 22.0 dB (For White Sands, and Australia, respectively). It can be seen that full-time availability can only be realistically achieved for 99.0 % of time for Ka-band, and 99.999 % for S-band.

Then, the second sensitivity is the pointing offset angle, especially for Ka-band. If the offset is 0.1°, the loss goes to the order of $1 \times 10^{-2}$ dB. For 1°, this jumps to the order of 1 dB. After 1°, the link can practically not be closed anymore, achieving losses of over $1 \times 10^{2}$ dB for 5° or more. For S-band, if the assumption of perfect alignment by the phased arrays is invalid, for 1°, losses of order $1 \times 10^{-1}$ dB can be expected. For 5°, these reach order of 1 dB. It is found out that these losses are encountered, the data rate needs to be reduced by 78 %, or the ground station needs to switch from the NSN DTE to LEGS. For the downlink, the data rate needs to reduce by 83 %, or the power needs to increase by 492 % from 68 W to 402 W. For the S-band, this may severely limit mission data being send to-and-fro. Recommendations may be to increase the transmit power required. The total S-band architecture would require a similar power percentage increase, jumping to 1128 W. Hence, such alignment deviations should be mitigated, as otherwise TT&C would increase unacceptably.

# 14 | Guidance, Navigation, and Control & Command and Data Handling

This chapter will cover the design of the GNC and CDH systems, first covering their general functions and the associated requirements. This is followed by the design architecture of the GNC system, which in turn is followed by the detailed design of the CDH system. Then, the risks will be discussed, and finally, the sensitivity analysis.

## Function and Requirements

The Guidance, Navigation, and Control system, or GNC, is the onboard system responsible for the safe navigation of the spacecraft throughout the entire mission. To do this, the GNC system must determine the vehicle state with the necessary accuracy and the desired spacecraft trajectory for all phases of flight. This is then translated into the necessary control inputs for the vehicle.

Command and Data Handling (CDH) is responsible for the executive and computational functions of the spacecraft. It is closely related with GNC as it calculates the guidance solutions. Apart from this, it interfaces and controls nearly every other subsystem. It consists of a main flight computer, redundant/complementary computers and a data storage device.

**Table 14.1:** GNC & CDH Requirements

| ID | Requirement | Rationale | Verification Method | Check | Value |
|---|---|---|---|---|---|
| HOPE-GNC-010 | The GNC subsystem devices shall have a maximum mass of 120 kg. | Needs to comply with the mass budget. | Inspection | ✓ | 98.9 kg |
| HOPE-GNC-020 | The GNC subsystem devices shall occupy a maximum total volume of 1.1 $m^3$. | Needs to fit within the launch vehicle and should not be excessively large. | Inspection | ✓ | 1.04 $m^3$ |
| HOPE-GNC-040 | The GNC subsystem shall have a minimum reliability of 0.994 (TBC) over the vehicle's mission lifetime. | Needs to be compatible with HOPE-MISS-070. Derived by assuming that each subsystem has the same probability of failure ($0.95^8$) during its entire lifetime. | Analysis | ✓ | Compliance Expected |
| HOPE-GNC-100 | The GNC subsystem shall autonomously perform orbital manoeuvres. | Derived from HOPE-STK-HLS-008. | Inspection | ✓ | Compliance Expected |
| HOPE-GNC-110 | The GNC subsystem shall facilitate the autonomous landing within 100 m (3σ) of target landing site on the Moon. | Derived from HOPE-STK-HLS-008 and HLS required level of accuracy. | Inspection | ✓ | Compliance Expected |
| HOPE-GNC-130 | The GNC subsystem shall use less than 600 W for 1000 s under peak load. | Needs to comply with power budget. | Demonstration | ✓ | 559.4 W and 936 s |
| HOPE-GNC-140 | The GNC subsystem shall use less than 300 W under nominal load. | Needs to comply with power budget. | Demonstration | ✓ | 241.4 W |
| HOPE-GNC-150 | The GNC subsystem shall not diminish the performance of any other subsystem to the extent that it prevents them from meeting their respective requirements | Ensure minimal interference with other subsystems. | Analysis/ Demonstration | ✓ | Compliance Expected |
| HOPE-GNC-160 | The GNC subsystem shall prevent collision with known debris or meteoroids that could comprise the mission | If any collision is expected, the spacecraft should be capable of preventing that collision, potentially by changing to a different orbit. | Analysis | ✓ | Compliance Expected |
| HOPE-GNC-170 | The GNC subsystem shall comply with the International Docking System Standard requirements | The lander will have to be able to dock with the OTV and gateway | Testing | ✓ | Compliance Expected |
| HOPE-GNC-180 | The GNC subsystem shall be able to determine the vehicle position within 250 m (3σ) between powered descent initiation and the approach gate | Ensures safe operations and supports precise maneuvering. | Analysis/Testing | ✓ | ±100 m |
| HOPE-GNC-181 | The GNC subsystem shall be able to determine the vehicle position within 150 m (3σ) between the approach gate and the terminal gate | Ensures safe operations and supports precise maneuvering. | Analysis/Testing | ✓ | ±50 m |
| HOPE-GNC-182 | The GNC subsystem shall be able to determine the vehicle position within 3 m (3σ) between the terminal gate and touchdown on the lunar surface | Ensures safe operations and supports precise maneuvering. | Analysis/Testing | ✓ | ±1.25 m |
| HOPE-GNC-190 | The GNC subsystem shall be able to determine the vehicle position within 50 m (3σ) in low earth orbit | Ensures safe operations and supports precise maneuvering. | Analysis/Testing | ✓ | Compliance Expected |
| HOPE-GNC-191 | The GNC subsystem shall be able to determine the vehicle position within 400 m (3σ) in the transfer orbit | Ensures safe operations and supports precise maneuvering. | Analysis/Testing | ✓ | ±125 m |
| HOPE-GNC-CDH-100 | The CDH subsystem shall use less than 200 W for 1000 s under peak load. | Needs to comply with power budget. | Demonstration | ✓ | 160.5 W and 936 s |
| HOPE-GNC-CDH-110 | The CDH subsystem shall use less than 125 W under nominal load. | Needs to comply with power budget. | Demonstration | ✓ | 112.5 W |
| HOPE-GNC-CDH-120 | The CDH subsystem shall be able to provide a minimum of 251.925 GB of data storage. | The system has to store this data while in a communications blackout. | Demonstration | ✓ | 4 TB |
| HOPE-GNC-CDH-140 | The CDH subsystem shall be able to handle a data rate of 100 Mbps (TBC) from the TT&C subsystem. | To be able to handle the data rate of the communication subsystem. The value is derived from the ICSIS standards and is used by NASA for Artemis. | Demonstration | ✓ | 40 GB/s |

## 14.1. GNC Design Architecture

The GNC system is built around four Inertial Measurement Units (IMUs), two of which are part of the ADCS system. Each of these IMUs will provide the spacecraft's position, velocity, and attitude information at all times. However, IMUs are susceptible to drift, and errors in state estimation will grow with time. They must be regularly corrected with more accurate information from other sensors to ensure that the uncertainty in the vehicle's state remains acceptable [114].

Six operational phases can be identified: low earth orbit, transfer orbit to and from the Moon, low lunar orbit, lunar descent and ascent, docking, and finally, lunar surface operations. Each of these phases has different requirements for the precision with which the state of the vehicle must be determined, and as such, different sets of sensors will be used throughout every phase. These sensors will then be used to correct the IMUs.

The TT&C system will get an accurate state estimation through communication with the Near Earth Network in low Earth orbit, transfer orbit, and low Lunar orbit. Ground stations on Earth will determine the position and velocity of the spacecraft with great accuracy, which can be used to correct the drift in the IMUs.

During lunar descent, the required precision of the GNC system will be much greater than during other phases. The descent phase starts at the Powered Descent Initiation (PDI) point with a height of 10 km. Before the descent is initiated, all four IMUs must be re-calibrated to ensure sufficient accuracy during the descent. At PDI, the descent radar will be turned to provide altimetry, velocimetry, and attitude information with increasing accuracy as the altitude decreases. Once the vehicle passes the approach gate, the Optical Navigation System (ONS) will be turned on to provide increasingly detailed information on the expected landing site for hazard detection and avoidance. The ONS consists of a Wide Angle Camera (WAC) for low-altitude operations and a Narrow Angle Camera (NAC) for high-altitude. Furthermore, the ONS will also function as a separate source for altimetry, velocimetry, and attitude information. Since the ONS is optical in nature, the system must at all times maintain line of sight to the expected landing site. This introduces an attitude constraint during the descent phase, as was discussed in Section 8.2. Finally, during the final phase of the lunar descent, the descent LIDAR will provide detailed topology information on the exact landing site for precise hazard avoidance and detection [115]. For the docking phase, the guidance consists of a docking camera and LIDAR. The docking LIDAR will function as the primary source of information, while the camera serves as a backup.

Finally, the GNC system also includes a set of scientific instruments. DEBIE-I is a small scientific instrument that measures the concentration of micrometeorites hitting the spacecraft. Four DEBIE-Is have been included in the GNC system to take measurements during the mission. The sensors were included in the GNC system because it was deemed superfluous to create a separate payload system for just a single sensor. The reason for including the DEBIE-I sensors in the design can be found in Chapter 2 [8].

The reliability of the GNC system is absolutely paramount, and thus, the system has been designed so that no one failure will compromise the safety of the mission. Figure 14.1 shows the design architecture of the GNC system. The sensors are distributed so that the mission can still be completed successfully if either bus A or B is lost. However, it should be noted that this will lead to a reduction of performance, especially the loss of the descent LIDAR, which will have a strong effect on the efficacy of the hazard of avoidance capability. Nonetheless, the ONS and other sensors provide sufficient information that the landing can be continued safely or aborted.

## 14.2. CDH Design Architecture

The architecture of the CDH system has been designed with redundancy in mind at all times. At the core of the system is the Central Flight Computer (CFC), which consists of five identical independent flight computers. Two computers will run at all times (nominally A and B), and their computation will be

**Table 14.2:** Estimated GNC State Determination Accuracy ($3\sigma$) for Critical Mission Phases (a) and Specifications (b) [8, 114, 115]

| Phase | Position [m] | Velocity [m/s] |
|---|---|---|
| Low Lunar Orbit | ±125 | ±1.0 |
| PDI to AG | ±100 | ±0.8 |
| AG to TG | ±50 | ±0.05 |
| TG to Touchdown | ±1.25 | ±0.02 |

(a)

| Parameter | OTV | Lander |
|---|---|---|
| Nominal Power | 147.84 W | 241.44 W |
| Peak Power | 241.44 W | 559.44 W |
| Mass | 54.74 kg | 98.94 kg |
| Volume | 0.444 $m^3$ | 1.044 $m^3$ |

(b)

compared with the results of a third computer (nominally C). In the case of a discrepancy between any two computers, the disagreeing computer can be identified and isolated, ensuring that the flight computers still function as intended. However, this also means that at any one time, at least three flight computers must be available to identify a faulty computer. Nonetheless, it should be noted that the system will still be fail-safe with only two computers operating, but in the case of a disagreement between the two computers, the faulty computer can not be identified. The system will be able to handle a computer failure in the fail-safe mode but will not be able to identify a faulty computer, which makes the system too unreliable to continue the mission. However, it does serve as a final backup mode that can be used to return the vehicle to Earth orbit in the case of computer failures. In short, the CFC can lose two out of five flight computers without losing any functionality and up to three while operating in the backup fail-safe only mode.

Like the CFC architecture, the data connections between the subsystems have been designed such that a single failure will not compromise the success of the mission. All subsystems are connected with the CFC through two independent data connections, data bus A and data bus B. Figure 14.2 shows a data handling diagram of the complete CDH system, including the connections between the subsystems, major internal subsystem connections, connections with the CFC, and the CFC itself. The diagram differentiates three types of connections: internal connections, which are connections contained entirely within a subsystem; data connections, which are connections for two-way data flow; and command connections, which indicate the path taken by commands sent by the CFC. Finally, it should be noted that the landing gear control unit is exclusive to the lander and is not present on the OTV; all other diagram elements are identical between both vehicles.

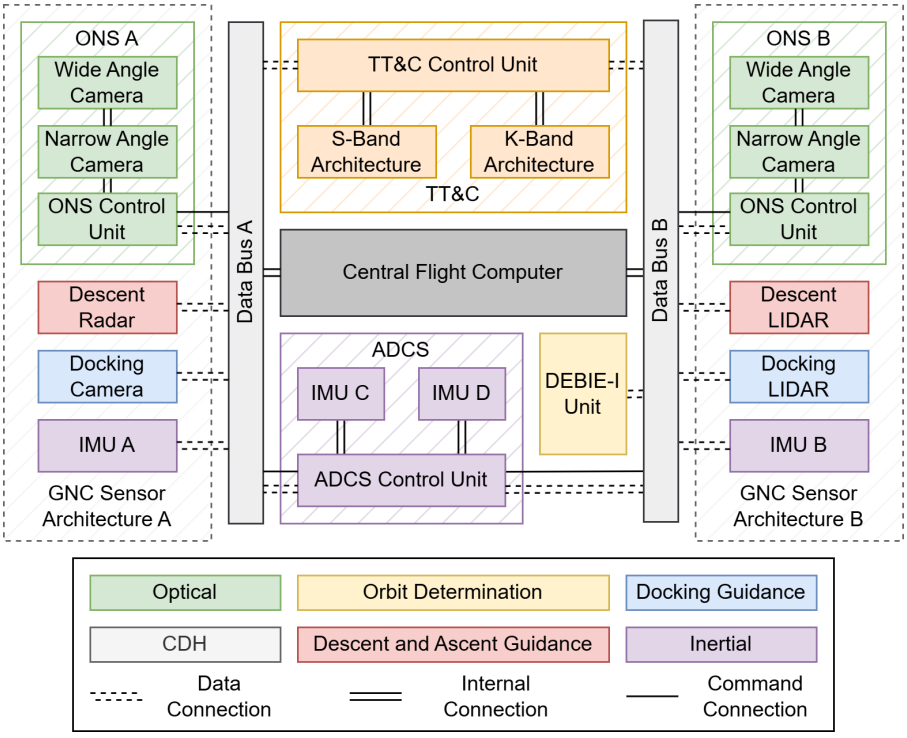


**Figure 14.1:** GNC Hardware Diagram

## Processor

For Command & Data Handling (CDH), the main focus is on selecting on on-board processing unit and sizing the RAM and storage requirements. In the past, the CPU was sized based on the throughput, expressed in million instructions per second (MIPS). However, the exponential increase in computing power available for space-based applications has made the MIPS obsolete as a limiting factor. Naturally, the MIPS of modern spacecraft has also increased, but has not kept pace with the advances in computing [87]. BAE Systems' RAD5545 runs upwards of 5600 MIPS, which is already 15 times faster than the computers aboard the ISS[1]. As a result, reliability is the key requirement to ensure system is failure-resistant for 10 years. The Mean Time Between Failures is not available yet, as it is a relatively new system. However, calculating with a value of 500 000 hours (a factor of 10 lower than the previous-generation RAD750 to account for the increased complexity)[2] gives a reliability of 81.7% over 10 years. This will be increased by having 3 redundant flight computers, increasing the reliability to 99.4%. This figure accounts for 3 flight computers running at the same time, comparing computations. The RAD5545 also supports 4 GB of radiation-hardened DRAM[1], which is more than enough to run the software required.

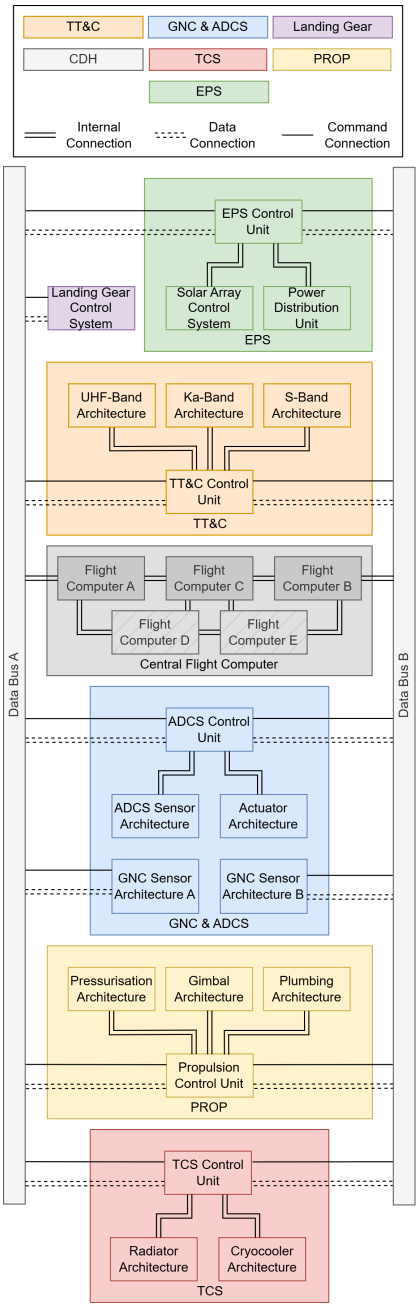


**Figure 14.2:** Data Handling Diagram

## Program development & memory

Both the amount of program memory needed and its associated development costs are sized based on the number of source lines of code (SLOC) [87]. The method for estimating SLOC described by Wertz and Larson results in a figure in the order of 10-20k SLOC, however, this is based on estimates from over three decades ago for a mission much smaller in scope. A more accurate estimate can be obtained from contemporary spacecraft such as Orion. A bottom-up estimate obtained from a study by Prokop [116] arrives at a figure over 1 million SLOC. To account for the 15 years between the development of Orion and ARCH-E and the additional updates it may receive over its 10 years of operation, the program memory is sized for double this figure, which together with a 50% margin results in 3 million SLOC. Using the conversion for code written in C, this would result in 128 bits per line of code, or 48 GB total. The cost for this amount of code can be estimated from the software development cost estimate in SMAD, giving 800 USD FY10 per SLOC, leading to a cost of 3.21 billion euro for software development and testing. This is a conservative estimate, as part of the guidance code can be reused from earlier missions.

## Data Storage

While out of communication range, the gathered data needs to be stored until it can be transmitted. The data rate and blackout lengths are used to size the data storage capability needed. At a maximum blackout time of 5361.8 seconds and a downlink data rate of 82 Mb/s, the system has to be able to store 55.95 GB of data. Note that not all of this can be sent back in the remaining orbit time. As such, an additional 112 GB buffer will be used. This ensures that. in case of a communications failure, the

[1] URL https://www.baesystems.com/en-media/uploadFile/20210404061759/1434594567983.pdf [cited 14 June 2024]
[2] URL https://www.cs.unc.edu/~anderson/teach/comp790/powerpoints/hardware.pdf [cited 12 June 2024]

spacecraft can complete three orbits before having to overwrite non-essential data. Under normal operations, this means between four and five orbits worth of data can be stored. As per the margin philosophy, a 50% margin will be added [15] to arrive at a final minimum storage capacity of 251.925 GB. This will be achieved with the CORECI 2, with a storage capacity of 4 TB. It has a measured reliability of 99% over 10 years in orbit[3]. A redundant unit will improve this to 99.99%.

## 14.3. Risk Assessment

This section will cover the risk assessments for the GNC and CDH systems. The definition of the likelihood and consequence levels are discussed in Section 17.1.

**Table 14.3:** GNC & CDH Risks

| ID | Risk | Causes | Impact | Req. |
|---|---|---|---|---|
| R-GNC-01 | Corruption/loss of avionics command | Software bugs, Hardware failure | Loss of spacecraft control | HOPE-GNC-040 |
| R-GNC-02 | Loss of navigation and landing sensor data | Sensor malfunction, interference | Loss of spacecraft control | HOPE-GNC-040 |
| R-GNC-03 | Software-based control errors | Coding errors, algorithm faults | Loss of spacecraft control | HOPE-GNC-040 |
| R-GNC-05 | Automated terrain sensing for landing errors | Sensor inaccuracies, terrain complexity | Loss of spacecraft control | HOPE-GNC-100 |
| R-CDH-01 | Faulty data from one flight computer in the CFC | Single event upset due to exposure to cosmic radiation | Loss of spacecraft control | HOPE-GNC-040 |
| R-CDH-02 | Faulty data from multiple flight computers in the CFC | Single event upset due to exposure to cosmic radiation | Loss of spacecraft control | HOPE-GNC-040 |
| R-CDH-03 | Loss of a flight computer in the CFC | Excessive exposure to solar and cosmic radiation | Loss of spacecraft control | HOPE-GNC-040 |
| R-CDH-04 | Loss of multiple flight computers in the CFC | Excessive exposure to solar and cosmic radiation | Loss of spacecraft control | HOPE-GNC-040 |
| R-CDH-05 | Failure of data bus | Excessive exposure to solar and cosmic radiation | Loss of communication between subsystems | HOPE-GNC-040 |
| R-CDH-06 | Corruption of Data Storage | Single event upset | Loss of saved data | HOPE-GNC-040 |

**Table 14.4:** Risk Mitigation and Contingency Plan

| | Pre-mit. | | | | Post-mit. | |
|---|---|---|---|---|---|---|
| ID | L | C | Mitigation | Contingency | L | C |
| R-GNC-01 | P | Ma | Software testing, redundancy in critical systems, fail-safe mechanisms | Manual override procedures, backup control systems | U | Mo |
| R-GNC-02 | U | Mo | Redundant sensors systems, sensor health monitoring, real-time data validation | Manual navigation procedures, alternative landing sites | R | Mi |
| R-GNC-03 | Li | Ma | Code review processes, testing, redundancy in critical control algorithms | Manual override procedures, alternative control modes | P | Mo |
| R-GNC-05 | R | Ca | Redundant terrain sensors, terrain database validation, real-time terrain analysis | Manual landing procedures, alternative landing sites | R | Ma |
| R-CDH-01 | U | Ca | Use multiple flight computers in the CFC to identify faulty computers | Identify/turn off the faulty computer and turn on back-ups | U | Mi |
| R-CDH-02 | R | Ca | Use multiple flight computers in the CFC to identify the faulty computers | Identify/turn off the faulty computers and turn on back-ups | R | Mo |
| R-CDH-03 | U | Ca | Use multiple flight computers in the CFC to replace the lost flight computer | Turn on back up flight computer | U | Mi |
| R-CDH-04 | R | Ca | Use multiple back-up flight computers to take over from the failed computers | Turn on back-up flight computer | R | Mo |
| R-CDH-05 | U | Ca | Include two independent data busses in the design | Use both data busses independently to support switching | U | Mo |
| R-CDH-06 | Li | Ca | Include multiple independent flight computers with radiation shielding | Identify/turn off faulty computers and turn on back-ups | R | Ca |

## 14.4. Sensitivity Analysis

The dependence on input parameters for this subsystem is fairly trivial. Only the number of flight computers or sensors can change in case the mission duration is increased for satisfactory reliability. As future design activities progress, it is possible that the design changes slightly in these regards, but the general principles and overall architecture remain the same.

[3]URL https://www.airbus.com/sites/g/files/jlcbta136/files/2023-02/CORECi-2.pdf [cited 13 June 2024]

# 15 | Attitude Determination and Control System

Attitude determination and control are crucial for managing a spacecraft's orientation, ensuring proper alignment and reorientation. This system stabiles the spacecraft, maintains desired orientations, and minimes disturbance torques [54]. This chapter will detail the conceptual design process for the subsystem of the ARCH-E vehicle. First, the mission was broken down into the necessary control modes for the ADCS, identifying the control modes used in different maneuvers to understand the system's requirements in Section 15.2. Second, considerations, requirements, and verification methods for the ADCS system are detailed in Section 15.3, along with the reference frame used for attitude determination in Section 15.1. Next, the attitude determination method is evaluated and described in Section 15.4. The disturbance torques, both external and internal, that the ADCS must counteract are quantified and discussed in Section 15.5. Based on the values determined in this section, as well as sizing calculations, the attitude control method is outlined in Section 15.6, including the manual control mechanism for the crew in case of emergency. The chapter concludes with a functional diagram of the system in Section 15.7, the potential risks affecting the ADCS in Section 15.8.

## 15.1. Axis Definitions

The ADCS design uses a body-fixed reference frame. For both the lander and the orbital transfer vehicle, the x-axis is aligned with the nose or longitudinal side and positive in the direction of the flight velocity (roll axis), and the y-axis aligns with the lateral side (pitch axis) going through the docking port and parallel to the corresponding solar array beam, and the z-axis is perpendicular to create a right-handed coordinate system (yaw axis). These axes apply similarly when both vehicles are docked and undocked as visualed in Figure 15.1 for the lander, and Figure 15.2.

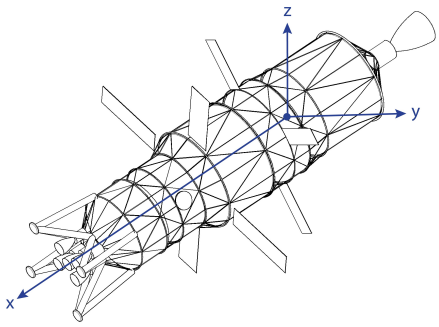


**Figure 15.1:** Docked Lander with OTV Body-Reference Frame

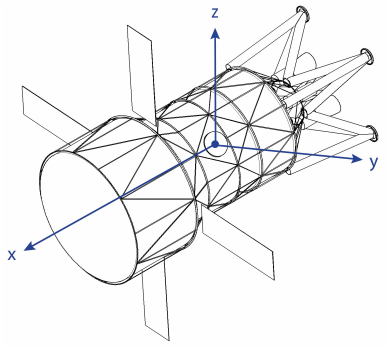


**Figure 15.2:** Axis for Vehicles Separated

## 15.2. Control Modes

To understand the various requirements that the ADCS must fulfill, different modes of operation during the mission were identified for the attitude determination and control system, each with its specific requirements [54, 87]. They were determined based on available literature and insights from past missions and then customised to suit the specific requirements of the ARCH-E vehicle throughout its missions [87, 117, 118]. To better visualise the operation of the ADCS, a preliminary map of the maneuvers conducted during the mission was created, correlating each maneuver with the corresponding control modes to be utilised. **De-tumble mode:** This mode is a rate regulation mode, used when the spacecraft experiences unwanted rotation rates that need to be reduced to near zero to regain control, particularly after separation. For the insertion to LEO, it is assumed that the launcher will handle it and orient the vehicle for orbital flight (A-LAU-01). Typically, the customer specifies the desired orientation at the time of separation relative to orbit insertion, which simplifies

the spacecraft design. Following separation from the launcher, the De-tumble mode will be utilised to mitigate the spin induced by the separation. It is necessary to perform an initial acquisition and design for a maximum induced unstable rotation to stabilise the system [54, 117]. **Attitude acquisition mode:** This mode is used when reference points need to be found for attitude determination and to stabilise the spacecraft for communication with the ground and power generation. During orbiting in LEO and chasing or phasing maneuvers, an initial determination to stabilise the vehicle is made that would require higher accuracy and can last a few seconds using sophisticated algorithms [117]. Docking is a crucial maneuver that requires absolute attitude determination using the Attitude acquisition mode and relative attitude determination using a docking system composed of cameras. During trans-lunar coast, orbit maintenance, and orbiting in LLO, it is used for obtaining onboard attitude references. While orbiting in LLO, the vehicle will require an initial attitude acquisition after insertion, orientation corrections, and operation in the nominal mode. **Orbit insertion/injection mode:** This mode is used when adjusting the acceleration of the spacecraft to reach an orbit, during and after boost while it is brought to the final orbit. During trans-lunar injection, insertion in LLO, and de-orbit burns, it will re-establish the 3-axis stability of the spacecraft and orient it in the desired direction after the maneuver, which requires a large impulse and may be a driving factor. An inertial measurement unit (IMU) may be necessary for accurate reference and velocity measurement. During de-orbit maneuvers, it is especially important to maintain the firing direction. During the Earth orbit insertion of the OTV, it is employed to withstand the critical disturbances caused by Earth's influence, being a driving factor for the system. **Normal mode:** This mode represents the majority of the mission when the ADCS counteracts external and internal disturbance, providing stability and pointing accuracy. During orbiting in LEO and phasing or chasing maneuvers, the Normal mode will maintain 3-axis stabilisation and control, which is a driving factor due to its predominant use. Furthermore, during trans-lunar coast, orbit maintenance, and orbiting in LLO, the Normal Mode will be employed for the majority of the mission for approximately 3-day duration. **Slew mode:** It corrects significant attitude deviations, reorienting the vehicle when required. For orbiting in LEO and phasing or chasing maneuvers, the Slew mode will be employed for significant reorientations of the spacecraft and will last around a few minutes. For low rates, reaction wheels may be fully capable; for high rates, thrusters may be needed [87]. During docking, it will be employed to orient the vehicle for precise docking to the correct orientation, necessitating good pointing accuracy and stability around the 3 axes without the need for final relative attitude determination [119]. During trans-lunar coast, orbit maintenance, and orbiting in LLO, the Slew Mode is employed for correcting and adjusting orientation. During the Lunar Flyby of the OTV, the subsystem must ensure robust attitude control to maintain the flyby and counteract lunar disturbances during this maneuver, utilising the Attitude acquisition mode and Slew mode. Gyros will be necessary to detect the rapidly changing body rates [120]. **Lunar descend mode:** It provides the stability and accuracy required during descent to the lunar surface, enabling the spacecraft to reorient if the landing site changes. It enables the lander to autonomously descend during the braking, approach, and terminal phases. In preparation for landing, the lander will change its attitude for the deceleration maneuver, requiring vehicle stabilisation. The actual direction must align with the commanded direction from the guidance algorithm, and pointing control will be managed by a PID controller and special sensors. The relative angular velocity with the surface will reach zero, and alignment with the landing attitude must be achieved and maintained. The sensors will analyse the terrain and adjust the landing site if necessary [121]. This will last approximately 10 minutes and will be a crucial and driving maneuver for the subsystem design. **Lunar ascent mode:** It provides the stability and accuracy required during descending on the lunar surface. Through it, the lander orientation must be kept sufficiently close to the thrust alignment condition, and the thrust vector control must be maintained to keep the lander sufficiently close to the reference trajectory [114]. **Safe mode:** It is employed in emergencies when the normal mode fails or is disabled, utilising fewer components and less power to meet minimal power and thermal requirements [87].

## 15.3. Requirements and Constraints for ADCS

The ADCS must maintain or provide the necessary orientation and angular rate for various maneuvers, and meet requirements from other subsystems, such as accurately pointing antennas for crucial

communications, maintaining stability during solar panel rotation, ensuring accuracy for scientific instruments, supporting the landing phase, and minimising jitter, particularly during stable states [54]. Additionally, it must comply with slew rate requirements, especially in the crewed version, where stricter values are imposed. Furthermore, it must adhere to the power budget, maintain control during $\Delta V$ burns, offer vehicle autonomy, and endure the mission's lifetime.

## 15.4. Attitude Determination

The attitude determination function measures and computes the orientation of the spacecraft relative to specific references [54]. This is accomplished using attitude sensors. To obtain comprehensive information about the spacecraft's state, a strategy employing complementary sensors that provide data on the angular position, rotational velocity, and acceleration of the spacecraft must be implemented.

This strategy also involves calculating attitude errors. Various sensors are available for determining the attitude of a spacecraft, and the potential options are illustrated in a design options tree in Figure 15.3. It also states the number of measurable vectors or the minimum required number of a certain type of sensor, which is relevant for the theory that two non-parallel unit vectors must be measured in the body-fixed system to determine the transformation matrix, which is then used to find the rotation angles and, consequently, the attitude. However, in this deterministic process, any errors in the measured or computed vectors significantly impact the computed attitude. To mitigate this problem, more than two vectors will be measured redundantly, and an extended Kalman filter (EKF) will be used to estimate the attitude error of the non-linear systems in real-life dynamics which is beneficial for sequential and real-time processes and can account for process noise representing the amount of deviation of the true motion of the object from the chosen motion model [122, 123]. However, this is not an optimal estimator and may yield poor performance; therefore, tuning and optimation are necessary.

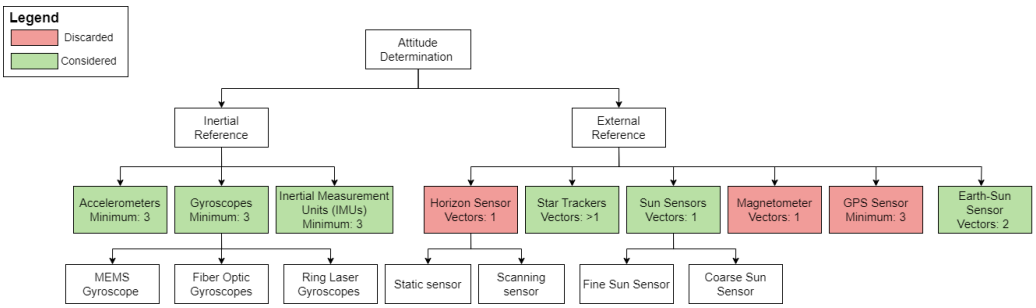


**Figure 15.3:** Design Options Tree for Attitude Determination Sensors

Horizon sensors were discarded due to their low accuracy, unsuitable for this mission, of approximately 1° for static sensors which are mostly used in GEO missions, and 0.1° for scanning sensors which are used both in LEO and GEO [122]. Similarly, magnetometers were discarded due to their reliance on a magnetic field and low accuracy resulting from shifts in the Earth's magnetic field over time. GPS receivers were not considered for orientation purposes due to their typical use in LEO, limited study in GEO, and the structural complexity they would add by requiring three GPS antennas. Sun sensors are promising due to their high accuracy and the mission's proximity to the Sun, while star trackers can identify bright star patterns with extremely high precision. Both are widely used in attitude determination for space exploration. Additionally, the coarse Earth-Sun sensors will be explored for use in the Earth's proximity, inspired by the GRACE spacecraft [124]. Gyroscopes are promising because they can measure the speed or angle of rotation from an initial reference. They are widely used in precise attitude determination when combined with external references such as Sun or star sensors. Considering their integration into an inertial measurement unit for all three axes, along with accelerometers for position and velocity sensing, would be beneficial [54, 87, 122].

**Table 15.1:** Attitude Determination and Control System Requirements

| ID | Requirement | Rationale | Verification Method | Check | Value |
|---|---|---|---|---|---|
| HOPE-ADCS-070 | The reaction control thrusters shall be able to provide a minimum slew rate of 0.5°/s over all three axes. | Ensures that the spacecraft can re-orient itself with sufficient speed to switch between pointing modes (TBC). | Analysis: assess dynamic performance, integrating with ADCS control systems, and conducting environmental and operational tests to ensure consistent and reliable performance. | ✓ | Expected compliance |
| HOPE-ADCS-090 | The ADCS shall be able to counteract a disturbance torque up to 100 N m for the lander. | Prevents disturbances from re-orienting the spacecraft [54]. | Testing: subjecting the system to controlled torque disturbances and measuring its ability to stabile and maintain desired attitudes under varying operational conditions. | ✓ | Expected compliance |
| HOPE-ADCS-091 | The ADCS shall be able to counteract a disturbance torque up to 300 N m for the OTV. | Prevents disturbances from re-orienting the spacecraft [54]. | Testing: validate the used mathematical and statistical models | ✓ | Expected compliance |
| HOPE-ADCS-100 | The ADCS shall provide a pointing accuracy of at least 0.01°. | Ensures sufficient pointing accuracy for docking, orienting, and communications. | Testing: simulations to ensure consistent and precise spacecraft orientation relative to specified targets or reference points. | ✓ | <0.01° |
| HOPE-ADCS-140 | The ADCS shall provide pointing knowledge better than 300 nrad within $3\sigma$ during nominal conditions and high vibration phases including engine burns around all three axes. | Ensures sufficient pointing accuracy for manoeuvres, docking, orienting, and communications. | Analysis: conduct vibration and engine burn simulations to assess the system's ability to maintain precise attitude determination within specified tolerances across all operational phases. | ✓ | <300 nrad |
| HOPE-ADCS-160 | The ADCS shall not allow a jitter of more than 0.01° over 60 s (TBC). | Ensures that the pointing deviation stays minimal, preventing excessive blurring of sensor data [87]. | Analysis or testing: assess and ensure the system maintains stable spacecraft orientation within specified tolerances under various operational conditions. | ✓ | Expected compliance |
| HOPE-ADCS-170 | The ADCS shall not allow a drift of more than 0.01° over 20 min (TBC). | For the vehicle to remain stable and correctly oriented when it does not receive frequent command inputs [87]. | Analysis: conduct end-to-end tests including the entire ADCS loop (sensing, computing, and actuating) | ✓ | Expected compliance |
| HOPE-ADCS-180 | The ADCS shall not have a single point of failure preventing the safe return of the crew back to Earth. | Ensures crew survival. | Analysis | ✓ | Compliant |
| HOPE-ADCS-190 | The ADCS shall move propellants such that only the correct phase of propellant is provided to the engines. | Prevents ullage and engine starvation in the propulsion subsystem. | Analysis | ✓ | Expected compliance |
| HOPE-ADCS-200 | The ADCS shall have a maximum dry mass of 3500 kg for OTV. | Needs to comply with the mass budget. | Inspection | ✓ | Expected compliance |
| HOPE-ADCS-201 | The ADCS shall have a maximum dry mass of 700 kg for the lander. | Needs to comply with the mass budget. | Inspection | ✓ | Expected compliance |
| HOPE-ADCS-220 | The ADCS propellant shall have a maximum cost of €900 M for the OTV. | Needs to comply with the cost budget. | Analysis | ✓ | Expected compliance |
| HOPE-ADCS-221 | The ADCS propellant shall have a maximum cost of €200 M for the lander. | Needs to comply with the cost budget. | Analysis | ✓ | Expected compliance |
| HOPE-ADCS-230 | The ADCS shall have a minimum reliability of 0.994 over the vehicle's mission lifetime (TBC). | Needs to comply with the total vehicle reliability. This value was found assuming a uniform normal distribution of the total required reliability of the system. | Analysis: software model result validated by signal simulator that can initially operate in a computer-based simulation environment and later incorporate the actual sensors | ✓ | Expected compliance |
| HOPE-ADCS-240 | The ADCS shall not diminish the performance of any other subsystem to the extent that it prevents them from meeting their respective requirements. | Ensures minimal interference with other subsystems. | Analysis or demonstration | ✓ | Expected compliance |
| HOPE-ADCS-250 | The ADCS shall use a maximum power of 65 W under nominal load (TBC). | Needs to comply with power budget. | Testing or demonstration: electrical tests on sensors and actuators | ✓ | Expected compliance |
| HOPE-ADCS-251 | The ADCS shall use a maximum power of 655 W under peak load (TBC). | Needs to comply with power budget. | Testing or demonstration: electrical tests on sensors and actuators | ✓ | Expected compliance |
| HOPE-ADCS-252 | The ADCS shall use a maximum standby power of 0 W (TBC). | Needs to comply with the power budget. | Testing or demonstration | ✓ | Expected compliance |
| HOPE-ADCS-270 | The ADCS shall have the capability to be refuelled during the mission. | Needs to be reusable. | Testing or demonstration | ✓ | Expected compliance |
| HOPE-ADCS-280 | The ADCS shall accept power supplied at 28 V DC. | Needs to be compatible with the electrical bus. | Testing: electrical tests on sensors and actuators | ✓ | 28 V DC |
| HOPE-ADCS-290 | The ADCS shall be able to provide a pointing accuracy of 0.02° (TBC) around all three axes. | Provides (static) stability based on values from literature [125]. | Testing or comparison: verify and validate the utilised software model to ensure it accurately processes inputs and outputs the necessary commands | ✓ | Expected compliance |
| HOPE-ADCS-310 | The ADCS shall allow for a maximum of 10% overshoot, decaying less than 0.1° (TBC) in 1 min (TBC). | Provides (dynamic) stability. These are preliminary values and will be revised [51]. | Testing: validate used mathematical and statistical models | ✓ | Expected compliance |
| HOPE-ADCS-320 | The crew shall not be exposed to a peak rotational acceleration greater than 3800 rad/s$^2$. | Derived from HLS-HMTA-0415 Transient Rotational Acceleration [9] | Demonstration or testing | ✓ | <3800 rad/s$^2$ |
| HOPE-ADCS-321 | The crew shall not be exposed to a rotational rate greater than 0.5 rad/s for 700 s. | Derived from HLS-HMTA-0061 Sustained Rotational Acceleration Due to Cross-Coupled Rotation [9]. | Demonstration or testing | ✓ | <0.5 rad/s for 700 s |
| HOPE-ADCS-322 | The crew shall not be exposed to a peak rotational rate greater than 5 rad/s. | Derived from HLS-HMTA-0061 Sustained Rotational Acceleration Due to Cross-Coupled Rotation [9]. | Demonstration or testing | ✓ | <5 rad/s |
| HOPE-ADCS-323 | The crew shall not be exposed to rotational accelerations greater than 2200 rad/s$^2$ during nominal conditions. | Derived from HLS-HMTA-0415 Transient Rotational Acceleration [9]. | Demonstration or testing | ✓ | <2200 rad/s$^2$ |

Utilising these viable sensors, various configurations can be designed to ensure 3-axis stability, high accuracy, and reliability over a mission lifetime of 10 years. Redundancy is also implemented to mitigate single-point failures. The following configurations are proposed for the trade-off: **6 star trackers, 6 gyros (2 three-axis IMUs):** The gyroscopes give the spacecraft's rotation rate w.r.t. a given reference system compared to an earlier point in time. The star tracker data can be used to update the initial orientation [122]. Two of the star trackers will determine the orientation with respect to different star patterns, while another two are designated for the latter half of the mission, given their average lifespan of five years. Additionally, two star trackers are included as redundancies in case of failures. The gyroscope is integrated into an IMU to enhance measurement and processing efficiency, reduce volume, and utilise accelerometers for GNC purposes. A second IMU is provided for redundancy. **6 sun sensors, 3 star trackers, 6 gyros (2 three-axis IMUs):** The Sun sensors are arranged with one primary and one redundant sensor on each axis, accommodating the possibility of the Sun being on different sides of the spacecraft. These Sun sensors capture the orientation relative to the Sun. The star trackers provide a complementary vector; however, one star tracker serves as a redundancy and the other is reserved for use in the latter part of the mission. **3 star trackers, 6 coarse Earth-Sun sensors, 6 gyros (2 three-axis IMUs):** The orientation is determined by one star tracker, with another one as a redundant backup and a third reserved for the second half of the mission. The complementary vector is provided by the Earth-Sun sensor, which offers attitude measurements relative to the Earth and Sun. These measurements are particularly useful during docking, orbiting Earth, and Earth orbit insertion [124]. **3 star trackers, 6 sun sensors, 6 coarse Earth-Sun sensors, 6 gyros (2 three-axis IMUs):** The orientation is provided by one star tracker, with another reserved for the second half of the mission and a third for redundancy. This is complemented by sun sensors, with one on each axis to account for the different positions of the Sun and additional redundant sensors on each axis. An Earth-Sun sensor is used for increased accuracy during docking, orbiting Earth, and Earth orbit insertion, with one on each axis and redundant sensors on each axis.

The trade-off criteria are motivated as follows: **Accuracy (30%)**: Accuracy is crucial for precise vehicle orientation and proper alignment of scientific instruments or communication antennas. It directly influences mission success, reliability, and efficiency. Even minor deviations can significantly impact outcomes, making accuracy the highest priority. **Lifetime (20%)**: Reliable operation throughout the mission duration in harsh space environments is essential, influencing cost and complexity. Lifetime reliability is prioritised due to its direct impact on mission success, as even the most advanced system is ineffective if it fails to meet the required 10-year mission duration. **Mass (10%)**: Spacecraft adhere to strict size and weight constraints due to launch vehicle capacity and mission needs. A lightweight ADCS design maximises payload capacity and reduces launch costs, impacting overall design and structural integrity. However, its priority is lower due to minimal sensor mass differences compared to other subsystems. **Cost (10%)**: Cost is significant in mission planning, covering development, manufacturing, integration, and operational expenses. Balancing cost is crucial for achieving cost-effective solutions that meet customer requirements. However, cost is less critical than criteria directly related to mission success and performance, especially when sensor prices are similar across configurations. **Power Consumption (10%)**: Spacecraft must conserve power to extend mission duration and operational capabilities. Minimising power consumption influences design for power budgeting and thermal management. While crucial for optimising resources, it is prioritised lower than accuracy and reliability, which are more critical for mission success and performance. **Reliability (20%)**: Ensuring reliable operation in harsh space environments is vital. This includes robust fault tolerance mechanisms, impacting cost and complexity. High priority is placed on reliability due to the potential for ADCS failures to jeopardise mission success.

Therefore, the trade-off was conducted based on quantitative reasoning where values were available such: as the average specifications describing a Sun sensor (for coarse sensors: accuracy of 1°/s, lifetime up to 15 years; and for fine sensors: accuracy of 0.01°, lifetime of around 13 years; average mass of 0.5 to 2 kg, price of around $15,000 and power consumption between 0.1 to 3 W), a star tracker (high accuracy of less than 0.001° at a rotation of less than 0.1°/s, lifetime of around 5 years, heavy mass around 2 to 7 kg, expensive at around $30,000, average power consumption between 5

to 20 W), a coarse Earth-Sun vector (Earth vector: accuracy of 5-10°, Sun vector: accuracy of 3-6°, lifetime around 15 years, mass of 0.8 kg, price is expected to be similar with a coarse Sun sensor's, the power consumption is zero), a gyro (drift of 0.03°/hr to 1°/hr, lifetime of 15-20 years, a mass between 0.5 to 5 kg, price varying to several thousands of dollars, average power consumption of around 10 W). Qualitative analysis evaluated reliability and accuracy trade-offs among configurations, considering sensor capabilities and deficiencies, and estimating overall configuration accuracy based on component accuracies [54, 122, 124, 126–130]. The trade-off is described in Table 15.2.

**Table 15.2:** Attitude Determination Configuration Trade-Off Table

| Criteria / Design Option | **Accuracy (30%)** | **Lifetime (20%)** | **Mass (10%)** | **Cost (10%)** | **Power Consumption (10%)** | **Reliability (20%)** |
|---|---|---|---|---|---|---|
| 6 star trackers, 6 gyros (2 three-axis IMUs) | High accuracy due to star trackers | 2 additional star trackers needed because of their short lifetime | Estimated at 72 kg | Estimated at $210,000 | Estimated at 180 W | Star trackers are sensitive, can be confused by sunlight from thruster exhaust gases [122] |
| 6 Sun sensors, 3 star trackers, 6 gyros (2 three-axis IMUs) | Star trackers contribute high accuracy, while sun sensors mitigate their limitations | 1 additional star tracker needed due to their short lifetime | Estimated at 63 kg | Estimated at $255,000 | Estimated at 189 W | Sun sensors' accuracy is limited by Sun's diameter and eclipses, but complemented by their strategic positioning and the use of star trackers [122] |
| 3 star trackers, 6 coarse Earth-Sun sensors, 6 gyros (2 three-axis IMUs) | High accuracy of star trackers, but low accuracy of coarse Earth-Sun sensors | 1 additional star tracker needed due to their short lifetime | Estimated at 55.8 kg | Estimated at $210,000 | Estimated at 120 W | Earth-Sun sensors have reliable acquisition, crucial for safe mode near Earth [124] |
| 3 star trackers, 6 Sun sensors, 6 coarse Earth-Sun sensors, 6 gyros (2 three-axis IMUs) | High due to the complex configuration | 1 additional star tracker needed due to their short lifetime | Estimated 67.8 kg | Estimated $300,000 | Estimated 138 W | High due to the complex configuration, Distance limitations of Earth-Sun sensors |

| Legend | Unacceptable | Barely acceptable | Good | Excellent |
|---|---|---|---|---|

The identified winning configuration includes 6 Sun sensors, 3 star trackers, and 6 gyroscopes integrated into 2 three-axis IMUs. This setup ensures high accuracy, accommodating varying Sun positions with strategically placed sensors and addressing eclipse periods with efficient star tracker

technology. Gyroscopes are widely adopted in the industry for measuring rotational rates across the body frame's axes. While this configuration scored lower in cost and power consumption compared to top performers (21.42% and 57.5% relative difference, respectively), the inclusion of redundant sensors for the second half of the mission resolves potential issues with star tracker lifetime limitations. The second-ranked configuration includes 3 star trackers, 6 Sun sensors, and 6 coarse Earth-Sun sensors. However, the system's efficiency does not justify its high price and increased complexity. To verify the decision resulting from the trade-off, a sensitivity analysis is conducted.

**Sensitivity analysis:** Further verification and validation procedures for each component and the overall configuration system will demonstrate that the setup meets the necessary data requirements and accuracy standards. Additionally, it must be proven that the assembly integrates seamlessly and is compatible with the overall system. Increasing the required precision of the attitude determination sensors could potentially result in larger and more costly sensors that use more power; however, the overall effect on the vehicle is not expected to be significant.

**Components:** Since the orbital transfer vehicle and lunar lander will be docked and traveling at similar distances from celestial bodies during the vast majority of the mission, they are assumed to share identical main systems for attitude determination. While separated, these systems individually meet the requirements. However, while docked, an additional advantage arises: by utilising a system of short-distance transceivers (one placed on each vehicle), they can exchange measurements through an inter-vehicle link, ensuring verification and resulting in enhanced accuracy. Commercially available sensors were chosen after conducting research to identify components that meet the mission's requirements, selecting those with the highest performance. The AA-STR autonomous star tracker from Leonardo that provides a radiation-hardened design and accurate three-axis attitude determination was chosen (mass of 2.6 kg, power consumption of 5.6 W at 20°C, accuracy lower than 0.000917° (pitch & yaw) and lower than 0.00433° (roll)) [131]. The ISS-T5 Sun sensor from SolarMems was chosen, providing measurements for two axes at an accuracy lower than 0.005° (mass of 0.1 kg and average power consumption of 0.2805 W) [132]. Finally, the MIMU from Honeywell is a widely favored choice for space exploration programs, providing 3-axis angular momentum measurements using GG1320 Ring Laser Gyroscopes. It features a bias of less than 0.02°/hr nominal per year, weighs 4.6 kg, and consumes an average of 25 W [133].

## 15.5. Disturbance Torques

In the frictionless space environment, a rotating spacecraft will continue its motion indefinitely unless acted upon. The spacecraft's rotation must be actively started and stopped. Furthermore, any disturbance will cause the spacecraft to rotate, and because there is no damping, even minor disturbances can result in significant orientation errors. Most disturbances are time-varying and depend on factors such as the spacecraft's position, attitude, solar intensity, and the strength of its residual magnetic field. To ensure a conservative design approach, creating a robust system capable of withstanding the extreme conditions of space, the critical values were analysed in regions where each torque is dominant. The disturbances that are external to the spacecraft were analysed. The four main disturbances experienced by the vehicles were quantified below, and the results of these calculations are presented in Table 15.7. These torques are evaluated across all three axes independently for both the OTV and lander, as well as when they are docked together. These disturbances dictate the specific amount and type of attitude control necessary for the vehicles, determining the thrust, torque, and momentum that must be designed accordingly [54].

**Gravity gradient torque:** This torque arises when the spacecraft's center of gravity is not aligned with its center of mass relative to the local vertical. It varies with the spacecraft's attitude relative to the orbiting body, increasing as the angle between the local vertical and the spacecraft's principal axis increases, always trying to align the spacecraft with the local vertical [87]. It is described by the following equation, Equation 15.1 [87], around the x principal-axis [54].

$$T_g = \frac{3\mu}{2R^3} \mid I_{zz} - I_{yy} \mid \sin(2\theta) \tag{15.1}$$

Where $I_{yy}$, $I_{zz}$ are the mass moments of inertia about the y- and z-axis, $\theta$ is the angle local vertical and the z principal-axis, $\mu$ is the gravitational parameter of the body about which the motion takes place (Earth: 398 600 km$^3$/s$^2$, Moon: 4902.8695 km$^3$/s$^2$), and $R$ is the distance from the center of this body. The angles were assumed to be $90^\circ$ to account for the largest orientation case (A-GRAV-01). For the mission's vehicles, the most extreme conditions are considered to occur when they are in closest proximity to the bodies they orbit, particularly in Low Earth Orbit (LEO) at 8413 km from the center of Earth, and Low Lunar Orbit (LLO) at 1837.4 km from the center of the Moon. The mass moments of inertia around the y- and z-axes were estimated for three vehicle states: the lander, the OTV, and the two vehicles docked together. The gravity gradient becomes weak at the GEO altitude of 35,786 km and fades to almost nothing far from the gravitational fields of the planets [87]. These calculations accounted for the worst-case scenario, including the solar panels. As these mass moments of inertia are based on preliminary vehicle dimensions, which are very similar to the final ones, represented in Figure 15.4, they provide a foundation for initiating a preliminary design of this subsystem. The mass moments of inertia for the space vehicles were determined by calculating the moments of inertia of their components and applying the parallel-axis theorem (A-GRAV-02) [134]. The components' moments of inertia were estimated by modeling them as cylinders (A-GRAV-03), and the mass of the tanks was assumed to be equivalent to the mass of the propellant they carry (A-GRAV-04). The results are presented in Table 15.3.

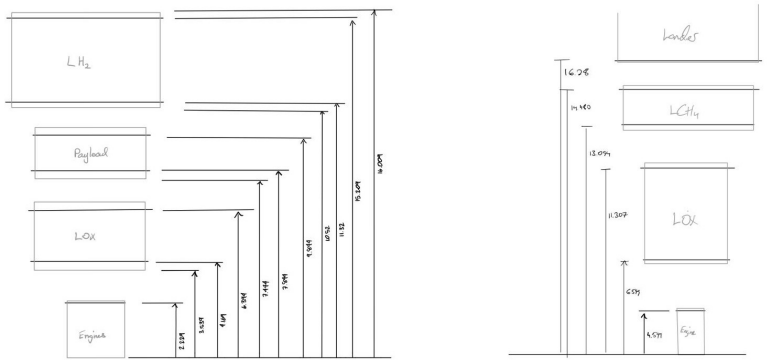


**Figure 15.4:** Preliminary Dimensions Used for the Mass Moments of Inertia Calculations

**Table 15.3:** Gravity Gradient Torques

| **Vehicle** | $I_{yy}$ **[kg m$^2$]** | $I_{zz}$ **[kg m$^2$]** | $T_g$ **in LEO [N m]** | $T_g$ **in LLO [N m]** |
|---|---|---|---|---|
| Lander (cargo) | 1,024,892.974 | 1,024,839.327 | 0.0629 | 7.427E-14 |
| OTV | 2,265,026.085 | 2,244,929.858 | 20.187 | 2.3836E-11 |
| Lander + OTV | 11,233,122.56 | 11,212,954.69 | 20.25 | 2.391E-11 |

From Table 15.3, it is evident that the torque affecting the OTV is substantially higher: over 300 times greater than the torque affecting the lander. This seems to be due to the large difference between the mass moments of inertia along the vehicle's axes. This significant difference arises from the OTV's shape, which causes the disparity between its mass moments of inertia around the z-axis and y-axis to be more than 300 times greater than that of the lander. Increased symmetry or structural optimisation, or a refinement of the calculations, would be required to address this issue. However, this is expected due to the vehicles' long length and their proximity to Earth's gravitational influence.

During descent on the Moon, other torques are much more influential, such as thrust from descent engines, aerodynamic effects (though minimal on the Moon due to the lack of atmosphere), and interactions with the lunar surface. These factors generally overshadow the minor effects of gravity gradient torque.

**Magnetic torque:** The magnetic fields of celestial bodies exert significant influence on the surrounding

space. The spacecraft's residual magnetic moment, a weak magnetic field it generates itself, depends on its size or onboard compensation. This torque occurs when the spacecraft's magnetic moment is not aligned with the local magnetic field, causing it to attempt alignment with the local field. The worst-case scenario is considered to be in LEO when the vehicles are closest to Earth and latitude orbiting at magnetic poles [87]. The influence of the Moon is not considered for this torque, as it is now understood to lack a significant magnetic field[1]. The Earth is modelled as a dipole in the following formula:

$$T_m = D \cdot B = D \cdot \left(\frac{M}{R^3}\right) \cdot \lambda \qquad (15.2) \qquad D = 0.0035 \cdot m_{vehicle} \qquad (15.3)$$

Where $D$, in $A \cdot m^2$, represents the residual dipole moment of the spacecraft, quantified according to Equation 15.2 [87], using the vehicle's mass classification as Class II, when magnetic torques are comparable to other torques [135]. The magnetic field strength of the Earth, $B$, in Tesla, is quantified by multiplying $M$, the magnetic constant, $7.8 \times 10^{15}$ Tesla $\cdot$ m$^3$, and $\lambda$ is a unitless function, from 1 at the magnetic equator to 2 at the magnetic poles. Its value was assumed 2 to design for the worst-case scenario (A-MAG-01) [87]. Finally, $R$ is the distance from the center of the Earth at LEO, in m. The magnetic field is considered influential up to the GEO altitude of 35,786 km, beyond which it is deemed too weak to be significant. The calculations for this torque are summarised in Table 15.4. The masses used in the calculations were provided by a preliminary sizing assessment from the Structures department.

**Table 15.4:** Magnetic Torques

| **Vehicle** | **Mass [kg]** | **Dipole moment [A $\cdot$ m$^2$]** | **Magnetic torque [N $\cdot$ m]** |
|---|---|---|---|
| Lander (with cargo) | 108125.84 | 378 | 0.00991 |
| OTV | 281441.47 | 985 | 0.0258 |
| Lander docked with OTV | 389567.31 | 1360 | 0.0357 |

**Solar radiation pressure torque:** Sunlight exerts pressure on objects it strikes, generating torque when the center of pressure of the absorbing or reflecting area is offset from the center of mass. This value can be calculated assuming uniform reflectance in the following equation (A-SRP-01) and constant solar intensity (A-SRP-02) [87]:

$$T_s = \frac{\Phi}{c} A_s (1+q)(c_{p_s} - c_m) cos(\phi) \qquad (15.4)$$

Where $\phi$ is the solar constant, 1366 W/m$^2$ at 1 AU and $c$ is the speed of light ($3 \times 10^8$ m/s). $A_s$ is the sunlit area in m$^2$ this value varies for different vehicle configurations, and it is assumed the highest cross-sectional area while the solar arrays are deployed for the three cases of vehicle configurations to account for the worst-case scenario (A-SRP-03), considered a flat plate, such as $\phi$ is assumed to be $90°$ for the same reasoning (A-SRP-04). Additionally, $q$ is the assumed uniform reflectance of the Mylar aluminum foil, chosen in Chapter 10, covering the majority of the lander and OTV's surfaces, including the propellant tanks and cabin (A-SRP-05) [55]. This reflectance value of 0.81 is chosen because the solar cells on the panels, chosen in Chapter 12, are covered by an anti-reflective coating, which has a near-zero reflectance factor [88]. $c_{p_s}$ is the center of solar pressure which is assumed to be the centroid of the cross-sectional area (A-SRP-06) and $c_m$ is the center of mass. Additionally, the center of mass is assumed to coincide with the center of gravity (A-SRP-07). To calculate the magnitudes of this torque, the solar pressure force is assumed to act perpendicular to the largest sunlit area it can face, considering the solar panels to be deployed and perpendicular to the direction of the force. The sunlit area was calculated using the dimensions of the OTV and lander components from Figure 15.4. Therefore, the centers of pressure were determined by calculating the centroid of the vehicles in Figure 15.4 using the formula for a system of discrete bodies [134]. The centers of mass,

[1] URL https://www.nasa.gov/solar-system/earth-and-moon-once-shared-a-magnetic-shield-protecting-their-atmospheres/ [cited 10 June 2024]

provided by the Structures department, are based on the case of full tanks. This results in a distance between the center of pressure and the centroid ($c_{p_s}$ and $c_m$) along the x-axis, and a 1.5-meter distance along the z-axis, which may vary as propellant shifts within the tanks. Consequently, this torque is calculated about the x- and z-axes, in Table 15.5.

**Table 15.5:** Solar Radiation Pressure Torques

| **Vehicle** | $A_s$ [m$^2$] | $cp_s$-$c_m$ **distance on z-axis [m]** | $cp_s$-$c_m$ **distance on x-axis [m]** | $T_s$ **about x-axis [Nm]** | $T_s$ **z-axis [Nm]** |
|---|---|---|---|---|---|
| Lander | 99.9705 | 1.5 | 3.534 | 0.001236 | 0.00291 |
| OTV | 73.29056 | 1.5 | 2.08 | 0.000906 | 0.001257 |
| Lander + OTV | 173.26106 | 1.5 | 1.96731 | 0.002143 | 0.002811 |

**Aerodynamic torque:** The rarified atmosphere can apply pressure forces on a spacecraft. However, because atmospheric density exponentially decreases with altitude, the worst-case scenario is considered in Low Earth Orbit (LEO), assuming an altitude of 200 km. Torque occurs when the center of atmospheric pressure, determined by the spacecraft's exposed area in the direction of orbital velocity, is not aligned with the center of mass. The aerodynamic torque can be estimated with the following formula [87]:

$$T_a = \frac{1}{2}\rho C_d A_r V^2 (c_{p_a} - c_m) \tag{15.5}$$

Where $\rho$ is the atmospheric density which is assumed constant at $10 \times 10^{-9}$ kg $\cdot$ m$^3$ based on NASA's Earth's atmosphere model [136] (A-AER-01), $C_d$ was assumed 2.2, the same value used in the orbital trajectory analysis, in Chapter 7 (A-AER-02), and $V$, the orbital velocity, is considered to be 7790 m/s for the given altitude in LEO. The ram area, $A_r$, is the surface facing the spacecraft's direction of motion. As the vehicles will change orientation during flight, a similar assumption to A-SRP-03 is made: it is considered to be the frontal area of the vehicle while orbiting in LEO (A-AER-03). To estimate the magnitude of this torque, the vehicles are assumed to fly with the x-axis aligned with the orbital flight direction. A cannonball model is used for the spacecraft, estimating the ram area as the sum of the highest frontal areas, including that of the largest component tank and solar panels [137]. Finally, the values of the center of mass and center of pressure (assumed to be the centroid of the area) were calculated in the same way as for the solar radiation pressure calculations. Since the aerodynamic force acts in the direction of the orbital velocity, and the center of mass and the center of pressure are aligned along the nose axis of the vehicles, moving along this axis while using propellant but not deviating from it, no torque is generated. To get a general estimate of the possible magnitude of this torque, a potential shift in the center of mass from the axis along the nose was considered. As a result of an ullage analysis that considered how much the center of mass would shift if all the propellant mass moved to the transversal side of the tank, a value of 1.5 meters is used.

**Table 15.6:** Aerodynamic Torques

| **Vehicle** | $A_r$ [m$^2$] | $c_{p_s}$-$c_m$ | $T_a$ **(LEO) [N m]** |
|---|---|---|---|
| Lander (cargo) | 75.6907 | 1.5 | 7.58 |
| OTV | 57.8355 | 1.5 | 5.79 |
| Lander + OTV | 75.6907 | 1.5 | 7.58 |

**Table 15.7:** Total Torques

| **Vehicle** | **Torque [Nm]** |
|---|---|
| **Lander** | 7.65 |
| **OTV** | 26 |
| **Lander+OTV** | 27.8 |

The aerodynamic drag is notably high at 200 km altitude for large vehicles like these. As altitude increases by 100 km, atmospheric density decreases by $10^{-3}$ following the NASA atmospheric model, resulting in a corresponding decrease in the torque value [136].

In the worst-case scenario of orbiting in LEO, the ADCS system must counteract the strongest torques

within their influence. The total torque affecting each vehicle state is summarised as follows, Table 15.7:

There are also internal disturbances within the spacecraft, such as misalignments in the center of gravity and thrusters during thrusting, which are corrected through a closed-loop control system and on-orbit thruster calibration. Additionally, reaction wheels may require friction compensation in their control modes. The disturbance effects of the propellant tanks should be examined during design and mitigated through propellant management devices. Another aspect to consider is the uncertainty in the center of gravity, which can create unwanted torques during the firing of coupled thrusters [87].

## 15.6. Attitude Control

Given the estimated disturbances the actuators required for attitude control can be sized and selected. Given the characteristics of the vehicle, the vehicle shall be able to fly autonomously but also allow for manual control, at any time if in the crew configuration. The methods considered for attitude control are presented below in a design options tree, in Figure 15.5. The options marked in red were deemed unsuitable for this mission, while those marked in green are under further consideration for attitude control configurations.

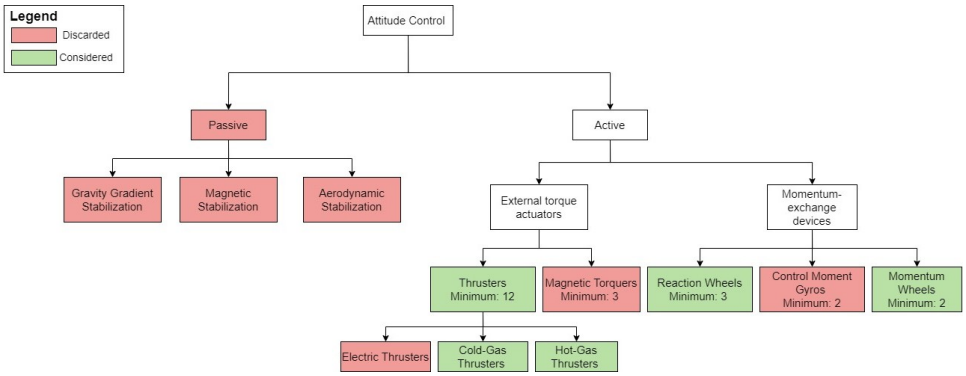


**Figure 15.5:** Design Options Tree for Attitude Control Actuators

Passive stabilisation methods have been dismissed because they provide limited control over only two axes, which is inadequate for the mission's needs. Furthermore, once the vehicles depart from Earth's influence, they will no longer be able to rely on its effects for stabilisation. Magnetic torquers were ruled out because the spacecraft will travel out of the region influenced by Earth's magnetic field after orbiting in LEO. Similarly, electric thrusters were also ruled out due to their lack of amount of thrust required for fast slew maneuvers [138]. In terms of momentum-exchange devices, control-moment gyros were not considered due to their susceptibility to wheel saturation, known shorter lifetime compared to other actuators, susceptibility to wear and tear, as well as their higher weight, cost, and power consumption [87]. The remaining options for the attitude control configuration of the vehicles include thrusters using cold-gas or hot-gas, as well as momentum-exchange devices such as momentum wheels or reaction wheels. For thrusters, a minimum of 12 are needed for pure 3-axis control, with 2 couple thrusters creating moments around each of the 3 axes in both directions. Additionally, 3 more couples of thrusters should be employed for redundancy. In terms of reaction or momentum wheels, a minimum of 3 are needed to control about the all 3-axis, but a skewed configuration would be more beneficial, adding a back-up wheel for any of the other three wheels. In terms of reaction or momentum wheels, a minimum of 3 are needed to control all 3 axes. However, a skewed configuration would be more beneficial, including a backup wheel to ensure redundancy in case any of the other three wheels fail [54]. The final attitude control configuration and its capabilities will be chosen based on the calculations presented in Section 15.6.1.

### 15.6.1. Momentum, Torque, and Thrust Sizing

The torque for which the actuators are sized includes a margin factor of 20% for unforeseen events, as required by ESA standards [15]. It is given by Table 15.7, where $T_D$ is the total most critical external

disturbance torque value found in Section 15.5 in Nm. In the case of attitude control thrusters, the required thruster torque is given by Equation 15.7, where $L$ is the moment arm in meters assumed to be the longest possible arm for a couple of thrusters (for lander: 16 m, and for OTV: 16.28 m).

$$T_{dist} = T_D(1 + MF) \quad (15.6) \qquad F_{T_{dist}} = \frac{T_D(1 + MF)}{L} \quad (15.7) \qquad T_{slew} = \frac{4I \cdot \theta}{t^2} \quad (15.8)$$

The thrust required for this case is 0.574 N for the lander and 1.92 N for the OTV. The torque to provide a slew angle, $\theta$, in radians, to the vehicle in $t$ seconds is given by Equation 15.8, where $I$ is the moment of inertia about a given axis, in kg m$^2$. The vehicle is assumed to rotate 90° in 180 seconds if the parabolic antenna for communications fails, allowing the opposite antenna to take over. In the case of attitude control thrusters, the thrust force for a slew rate $\omega$ in $t$ seconds is given by Equation 15.9.

$$F_{T_{slew\,rate}} = \frac{I \cdot \omega}{L \cdot t} \quad (15.9) \qquad h_{dist} = \frac{\sqrt{2}}{2} \cdot T_P \cdot \frac{P}{4} \quad (15.10) \qquad h_{slew} = \frac{T_D}{\theta_a} \cdot \frac{P}{4} \quad (15.11)$$

To account for the worst-case scenario regarding torque, the attitude control method should be sized for the total torque due to external disturbances and slew angle: $T = T_{dist} + T_{slew}$. When using wheels to counteract sinusoidal disturbance torques with period $P/2$, the maximum angular momentum $h$ stored in the wheel is given by Equation 15.10. The momentum storage in a wheel required for a maximum allowed rotation $\theta_a$ around an axis perpendicular to the wheel axis is given by Equation 15.11.

In the case of wheels, they are sized for the worst-case scenario, when summing the momentum to store for counteracting a sinusoidal disturbance torque and allow for a slew angle, $h = h_{dist} + h_{slew}$. Applying Equation 15.10, the momentum or reaction wheels of the lander would need to momentum store 7183.85 N m s for a period of 5309 seconds while orbiting in LEO and counteracting disturbance torques, but to allow for a rotation around an axis perpendicular to the wheel axis, it would be needed an angular momentum of 3233.87 N m s. Most commercially available reaction wheels, typically designed for small satellites weighing a few hundred kilograms, provide only a few tens of N m. To give a sense of scale, a control moment gyroscope (CMG) operates on a similar principle but uses gimbals to tilt a spinning rotor. One such CMG, found in literature, offers 7000 N m s of angular momentum, weighs approximately 250 kg, requires a peak power of 500 W, and costs around $1 million. Given these specifications, and knowing that four wheels would be needed to achieve control around all three axes with redundancy, the costs would be exorbitant, and the design would be extremely challenging [139]. These numbers are very high due to the significant disturbance torques that need to be counteracted in LEO. This would result in a very large and heavy reaction wheel system. Therefore, using reaction wheels as an attitude control method is not feasible, and the investigation focuses solely on the use of reaction control thrusters.

The sum of the values resulting from Equation 15.7 and Equation 15.9 is the worst-case required thrust. This value is used in Equation 15.13 to find the mass of propellant needed. To find the total operational time during the entire mission, Equation 15.12 can be used, where $t$ is the pulse duration in seconds, and $N_{max}$ is the maximum number of pulses during the mission. A more detailed outline and requirements of the use of reaction control thrusters during the mission's maneuvers is needed to determine the following values.

$$T_{tot} = N_{max} \cdot t \quad (15.12) \qquad m_{propellant} = \frac{F_T \cdot t_{burn}}{g \cdot I_{sp}} \quad (15.13)$$

**Components:** To select feasible thrusters for the lander and OTV, the burn time and generated thrust must be balanced as described in Equation 15.9. Additionally, the chosen thrusters must be capable of counteracting the disturbance torques. The OTV thrusters will use $CH_4$/OX propellants stored in the tanks. A commercially available thruster, the RCS 20 lbf, was deemed suitable, assuming a burn time[2] of 20 seconds. In the worst-case scenario, the OTV thruster must provide 62.6 N of thrust, and the RCS 20 lbf from Astrobotic offers a margin factor and optimisation of the placement. The thrusters are well-suited for future in-space operations, though limited information is available about them. The burn time would generally need to be reduced, but this would require even higher thrust. In the case

[2]URL https://masten.aero/rocket-engines/ [cited 19 June 2024]

of $CH_4$/OX thrusters, development is still ongoing to address this need. NASA is currently developing $CH_4$/OX reaction control thrusters with thrust capacities ranging from 100 to 220 N [140]. Regarding the lander, the reaction control thrusters are powered by $H_2$/OX propellants stored in the tanks. The desired thruster for this configuration is a 110 N gaseous $H_2$/OX thruster, as demonstrated by the Rocketdyne Division of Rockwell International on the Space Tug [141, 142]. When docked, thrusters on both vehicles are synchronised to provide balanced and precise attitude control. This coordination helps manage fuel consumption and optimise control actions.

**Mass and power:** The dry mass of the ADCS, including the mass of the sensors and thrusters, is estimated in Table 6.1. However, to estimate the mass of the propellant needed for the RCS thrusters, additional specifications about the thrusters are required, along with a detailed explanation of the frequency and duration of the thruster firings throughout the mission. An estimation of the power consumed by the system is provided in Table 6.4 and Table 6.5, which accounts for the power consumption of the sensors and the engine valves of the RCS thrusters.

**Sensitivity analysis:** There are concerns about the high values of the disturbance torques and the mass moments of inertia, which may be due to the spacecraft's elongated shape and its close orbit to Earth. Developing more detailed models of these disturbances, along with a clear outline of the spacecraft's spatial displacement and maneuvers, would provide more accurate values. The general sizing method does not vary with the uncertainty in disturbance torques. It is possible that larger than expected disturbances require more propellant or thrusters, however, the same thruster hardware and general system architecture can be used.

### 15.6.2. Manual Control

Manual control is crucial for specific maneuvers and operations when a crew is onboard, ensuring mission success and safety if automated systems fail, particularly in precise navigation and hazard avoidance. To enable manual control, the crew must have sufficient situational awareness. This is obtained through the windows installed in the crew compartment as well as displays as shown in Figure 15.6. Previous space flights have demonstrated that the benefits of human intervention outweigh the risks of potential human error [143]. The crew should be able to access manual control during maneuvers requiring precision requirements; docking, refilling operations, lunar descent, touchdown, and hazard avoidance. An attitude controller, main thrust controller, and docking controller are needed. These are shown in Figure 15.6.

Crew members use the controllers for manual attitude control of the spacecraft through a PID (Proportional-Integral-Derivative) controller. This system achieves precise orientation adjustments by continuously calculating the error between the desired and current attitudes and applying corrections based on proportional, integral, and derivative terms. To ensure optimal performance and stability of the spacecraft's attitude control system, proper tuning of the gain parameters within this closed-loop system should be performed through optimisation simulations. This tuning process adjusts the gains in the system to achieve the best possible response of the actuators to the controller inputs, minimising error and preventing instability. Crew training is essential for them to be familiar with the controller sensitivity. ARCH-E's display panel will also feature an important characteristic which is modularity. Similar to the ECLSS system during the reconfiguration of the spacecraft this device needs to allow for easy removal or installation. This will be done by dividing the display panel into three main modular sections that can be removed and placed even when using an EVA unit. This type of technology is developed in other industries however it will have to be adapted for this purpose in a space.

## 15.7. Functional Diagram of ADCS

Figure 15.7 shows the functional diagram of the ADCS which operates continuously by comparing the vehicle's actual attitude, measured by the attitude determination sensors, with a reference signal representing the desired target attitude. The difference between these signals is represented by the estimated attitude which is the primary input for the controller, which processes the error between target and estimated. The controller uses pre-defined algorithms to process the error signal to determine the

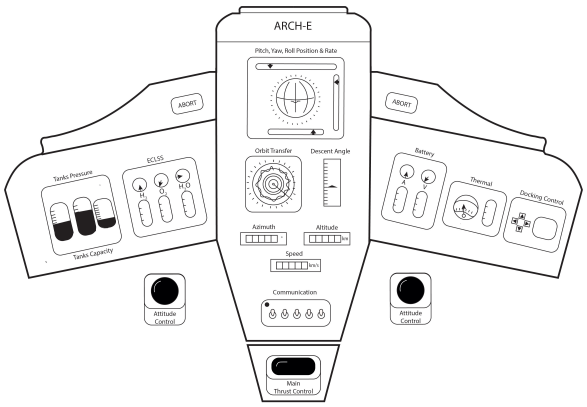


**Figure 15.6:** Display Panel & Controllers

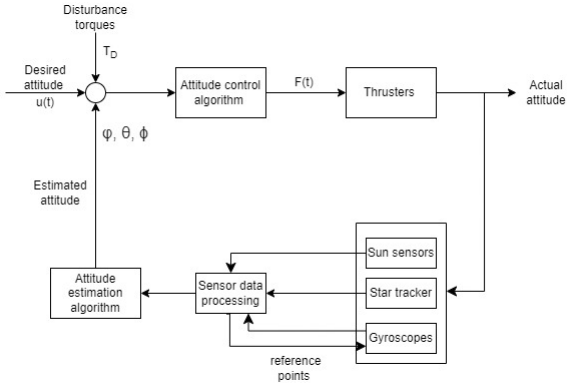


**Figure 15.7:** ADCS Functional Diagram

corrective action needed. The controller output translates into an actuator command signal, which directs the vehicle's thruster to generate the torque to reorient. The external disturbances, $T_D$, can introduce deviations from the intended trajectory. The system factors in these disturbances by adapting the actuator commands to compensate for their effects and maintain stability. This continuous feedback loop ensures the ARCH-E remains precisely oriented throughout the mission.

## 15.8. Risk Assessment

Table 15.8 describes the risks associated with ADCS, the requirements linked to the risks, and their respective causes. Table 15.9 shows the risk mitigation and contingency.

**Table 15.8:** Attitude Determination and Control System: Risks

| ID | Risk | Causes | Req. |
|---|---|---|---|
| R-ADCS-01 | Sensor failure | Hardware malfunction or damage | HOPE-ADCS-100, HOPE-ADCS-140 |
| R-ADCS-02 | Thruster Failure | Hardware malfunction or propellant leakage | HOPE-ADCS-070&090&091&160&170 |
| R-ADCS-03 | Communication failure between components | Faulty wiring, connectors, or interference | HOPE-ADCS-230 |
| R-ADCS-04 | Data Corruption | Software errors or radiation effects | HOPE-ADCS-230 |
| R-ADCS-05 | Environmental interference | Solar flares, debris impact, or radiation | HOPE-ADCS-090, HOPE-ADCS-189 |
| R-ADCS-06 | Gyroscope drift | Inherent sensor bias and errors over time | HOPE-ADCS-100, HOPE-ADCS-170 |
| R-ADCS-07 | Control law bug | Inadequate testing or coding errors | HOPE-ADCS-230 |
| R-ADCS-08 | Sensor alignment drift | Gradual misalignment affecting accuracy | HOPE-ADCS-070, HOPE-ADCS-140 |

**Table 15.9:** Attitude Determination and Control System: Risk Mitigation and Contingency Plan

| | Pre-mit. | | | | Post-mit. | |
|---|---|---|---|---|---|---|
| **ID** | **L** | **C** | **Mitigation** | **Contingency** | **L** | **C** |
| R-ADCS-01 | P | Ma | Redundancy: Use multiple redundant sun sensors, star trackers, and gyroscopes | Switch to redundant sensors and recalibrate | U | Mo |
| R-ADCS-02 | U | Ma | Redundancy: Utilise redundant thrusters and monitor performance | Switch to redundant thrusters; reconfigure mission priorities if necessary | R | Mo |
| R-ADCS-03 | P | Mo | Implement robust communication protocols and shielding techniques | Diagnose and repair comm. lines; switch to alt. data transmission | U | Mi |
| R-ADCS-04 | U | Ma | Implement data validation and error-correction algorithms | Revert to last known good state or use backup data sources | R | Mo |
| R-ADCS-05 | P | Ca | Use shielding for sensors and thrusters; apply noise reduction and filtering to sensor data | Activate shielding protocols and switch to filtered sensor data | U | Ma |
| R-ADCS-06 | P | Mo | Regular calibration and use of complementary sensors (star trackers) to correct drift | Recalibrate gyroscopes using star tracker data; increase use of other sensors for attitude determination | U | Mi |
| R-ADCS-07 | U | Ma | Rigorous testing, code reviews, and the use of real-time monitoring and diagnostics | Roll back to previous stable software version; deploy software patch | R | Mo |
| R-ADCS-08 | P | Mi | Implement periodic recalibration routines and use alignment correction algorithms | Perform in-situ recalibration using known reference points | U | I |

# 16 | Structures System

The structure of a spacecraft contributes significantly to the empty mass of the vehicle. Especially for a lander as the legs are required to support the entire vehicle on impact.

Starting with masses of other subsystems a democratised mass system is created for the structural sizing of both vehicles. Based on the structure sized a modal analysis will be performed to ensure both vehicles can survive launch vibrations. The structural sizing will end with the landing leg sizing, ensuring that the legs can sustain the impact as well as prevent the lander from tipping over.

Prior to any design, it is vital to consider the requirements of the structural subsystem. The compliance with the requirements is shown in Table 16.1. The requirement compliance discussion raises risks associated with the Structures system. These are shown in Table 16.2 and their mitigation and contingency plans are in Table 16.3.

**Table 16.1:** Structures Requirements Verification

| ID | Requirement | Rationale | Verification Method | Check | Value |
|---|---|---|---|---|---|
| HOPE-STR-010 | The structures subsystem shall have a maximum mass of 3480 kg and 17 760 kg for the lander and OTV respectively. | Needs to comply with mass budget | Inspection | ✓ | Lander 2280 kg, OTV 2281 kg |
| HOPE-STR-020 | The structures subsystem shall fit in the launch vehicle. | Needs to fit within the launch vehicle fairing. | Inspection | ✓ | |
| HOPE-STR-040 | The structures subsystem shall have a minimum reliability of 0.994 (TBC) over the vehicle's mission lifetime | Needs to be compatible with HOPE-MISS-070. The initial minimum reliability of 0.994 which is to be confirmed and was derived by assuming that each subsystem has the same probability of failure ($0.95^8$) during its entire lifetime | Analysis | Partial Compliance Expected | |
| HOPE-STR-061 | The structures subsystem shall not diminish the performance of any other subsystem to the extent that it prevents them from meeting their respective requirements | Ensures minimal interference with other subsystems | Analysis/ Demonstration | Compliance Expected | |
| HOPE-STR-070 | The structures subsystem shall survive all nominal loads applied throughout all mission phases | Needs structural integrity to perform mission | Analysis/ Testing | ✓ | |
| HOPE-STR-090 | The structures subsystem shall survive all nominal vibrations applied throughout all mission phases | Needs structural integrity to perform mission | Testing | ✓ | |
| HOPE-STR-110 | The structures subsystem shall provide the capability to touch down on the lunar surface 10 times | Needs to be compatible with a reusable design | Testing | Partial Compliance Expected | |
| HOPE-STR-120 | The structures subsystem shall provide the vehicle with the capability to reconfigure the payload between crew and cargo | Needs to be compatible with a reconfigurable design | Demonstration | ✓ | |
| HOPE-STR-130 | The structures subsystem shall provide attachment points for the crew to perform their mission(s) | Ensures safe EVAs without requiring manoeuvrability equipment | Inspection | Compliance Expected | |
| HOPE-STR-140 | The structures subsystem shall provide the capability for the crew to access the lunar surface | Ensures crew can perform their mission | Inspection/ Demonstration | Compliance Expected | |
| HOPE-STR-150 | The structures subsystem shall provide the crew with non-electronic visibility capabilities | Provides redundancy for navigation | Inspection | Compliance Expected | |
| HOPE-STR-160 | The structures subsystem shall provide access to the cargo on the lunar surface | Needs to allow for loading and unloading of cargo. | Inspection/ Demonstration | Compliance Expected | |
| HOPE-STR-190 | The vehicle shall be capable of returning scientific payload of at least 100 kg in mass and 0.16 $m^3$ in volume. | Provides for lunar sample return capabilities | Inspection | ✓ | |
| HOPE-STR-200 | The structure shall have a yield stress safety factor of 1.25 and an ultimate strength safety factor of 1.4 | To ensure structural integrity | Analysis | ✓ | |

Both structures fit within the launch vehicle, evident in Figure 18.8, complying with **HOPE-STR-020**, verified with inspection. There is a risk that the fairing dimensions of Starship will change due to it still experiencing heavy development, this is further explored in Chapter 17, with R-LAU-07. **HOPE-STR-040** and **HOPE-STR-110** have partial expected compliance as further analysis is required to assess the feasibility of ten landings on the same legs. Not only will impact on the surface heavily stress the spring damping system, but the regolith blown due to the engine exhaust will act as an abrasive likey damaging the legs. It is expected that this will require maintenance at some point during the 10 mission. This created risk R-STR-12. Compliance is expected with **HOPE-STR-061** due to the landing legs currently constraining the gimbal limit of the engines to 10°, this does not hinder the descent or ascent stage at the current design fidelity. This limit was determined geometrically. **HOPE-STR-070**

and **HOPE-STR-090** have been complied with, and the structure has been sized to comply with both in Section 16.1 and Section 16.2. **HOPE-STR-120, 130, 140** and **160** relate to the capabilities of the crew with respect to the vehicle. Compliance is expected, however, will require testing once built. To ensure that the selected EVA suits and removable parts of the vehicle are compatible with the structure. **HOPE-STR-160** compliance is also expected but will need to be proven. There is expected compliance with **HOPE-STR-150** with the current design of the cabin. The exact sizing of a window would follow the detailed design of the cabin interior. **HOPE-STR-160** can either be achieved with existing infrastructure on the lunar surface or systems discussed in [144] such as a block and tackle. This is deemed possible with the current configuration as large static payload on the order of 5 tons are likely designed for lunar bases, which should be capable of assisting unloading. Whereas smaller mobile payloads will be unloadable using a system such as a block and tackle [144]. Finally, the cabin has a current volume of 60 $m^3$ where the scientific payload can fit the volume and mass required for **HOPE-STR-190**. The definition of the likelihood and consequence levels are discussed in Section 17.1.

**Table 16.2:** Structure Risks

| ID | Risk | Causes | Req. |
|---|---|---|---|
| R-STR-01 | Primary structure failure | Extreme Operating Conditions, Design flaws, Defects, Fatigue | HOPE-STR-050 |
| R-STR-02 | Landing leg structural failure | Design Flaw, Material Defect | HOPE-STR-050 |
| R-STR-03 | Disruption between stage integration | Lack of collaboration between the engineering departments, Structural flaws | HOPE-STR-060 |
| R-STR-04 | Failed/incomplete docking of lander to OTV | Mechanical failure, software errors | HOPE-STR-060 |
| R-STR-05 | Failure to separate lander from OTV | Structural issues, propulsion malfunction | HOPE-STR-050 |
| R-STR-06 | Damage to vehicle during reconfiguration procedures | Procedural errors, structural failure | HOPE-STK-ADS-040 |
| R-STR-07 | Error made during reconfiguration procedure | Human error, Procedural error | HOPE-STK-ADS-040 |
| R-STR-08 | MMOD Impact to Vehicle / Integrated Lander | Inadequate shielding | HOPE-MISS-040 |
| R-STR-09 | MMOD impact to lander | Inadequate shielding | HOPE-MISS-040 |
| R-STR-10 | MMOD impact to OTV | Inadequate shielding | HOPE-MISS-040 |
| R-STR-11 | Failed development of reusable landing legs | Hard impact on landing, complicated mechanism hasn't seen this amount of use | HOPE-STR-140 |
| R-STR-12 | Excessive damage due to lunar dust | Lunar dust acting as an abrasive when being blown in by the engine exhaust | HOPE-STR-110 |
| R-STR-13 | Landing leg constraining gimbal limits of engines | Leg position preventing required gimbal limits | HOPE-STR-61 |

**Table 16.3:** Structure Risk Mitigation and Contingency Plan

| ID | Pre-mit. L | C | Mitigation | Contingency | Post-mit. L | C |
|---|---|---|---|---|---|---|
| R-STR-01 | R | Ca | Robust material selection, environmental testing | Emergency repair procedures, alternative materials | R | Ma |
| R-STR-02 | U | Mo | Rigorous design reviews, quality control measures | Correction protocols, alternative components | R | Mi |
| R-STR-03 | P | Ma | Integrated testing protocols, clear communication channels | Contingency integration procedures, alternative integration methods | U | Mo |
| R-STR-04 | P | Ma | Redundant docking mechanisms, thorough testing | Alternative docking methods | P | Mo |
| R-STR-05 | P | Ma | Redundant staging mechanisms, rigorous testing | Emergency separation procedures | P | Mo |
| R-STR-06 | U | Ma | Careful handling procedures, structural reinforcement | Repair protocols, alternative reconfiguration methods | R | Mo |
| R-STR-07 | Li | Ma | Procedure checklists | Correction protocols, alternative reconfiguration methods | P | Mo |
| R-STR-08 | P | Ma | Improved shielding design, real-time monitoring | Repair procedures, alternative shielding methods | U | Mo |
| R-STR-09 | P | Ma | Improved shielding design, real-time monitoring | Repair procedures, alternative shielding methods | U | Ma |
| R-STR-10 | P | Ma | Improved shielding design, real-time monitoring | Repair procedures, alternative shielding methods | U | Ma |
| R-STR-11 | Li | Ca | Repeated testing of landing leg impact (needs lunar loads), Additional R&D of new technologies, More focus on soft landing | Replacement of legs during in-orbit maintenance | P | Ma |
| R-STR-12 | Li | Ca | Repeated testing of lunar dust abrasion | Replacement of legs during in-orbit maintenance | P | Ma |
| R-STR-13 | P | Ma | Set clear dimension requirements, use design margins | Redesign/repositioning of legs and engines | R | Ma |

**R-STR-11, R-STR-12** are still deemed as high risk after mitigation and contingency strategies. Both risks have a consequence of major due to having to replace the legs in orbit violating **HOPE-MISS-090**, if the leg design is inadequate. Testing of the leg design can be done prior to the maiden launch, however, it remains complex to accurately predict the degradation of legs in the lunar environment. This part of the design will need special attention during further development of the project to reduce the risk level.

## 16.1. Main Structure

The main structure of both vehicles will be designed in a similar fashion. There will be rings connecting to the top and bottom of each of the tanks, the payload hold, as well as the engines. These rings will be connected with a number of both vertical and diagonal beams that connect corner joints together. This structural layout, as seen in Figure 16.1, was chosen as it will be able to efficiently carry both lateral and axial loads that the vehicle will experience. As well as allowing freedom to change individual cross-sectional areas to accommodate various load paths resulting in a lighter structure.

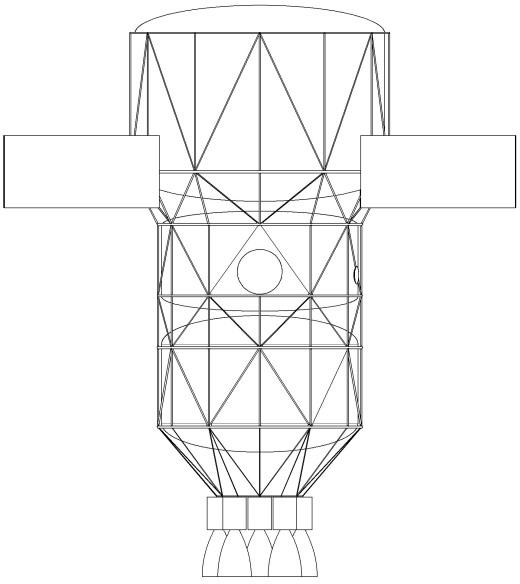

**Figure 16.1:** Lander Main Structure

For the sizing of these structures, the radius of each ring and the connection height between rings were determined by both the payload envelope of the launch vehicle and the volume requirement of

the tanks and other components of the spacecraft. The cross-sectional areas of the rings and the connecting beams were sized for all load cases the vehicle will be exposed to. This sizing was done using ANSYS Static Structural tool. A three-dimensional model and mesh were created of the structure and loads were applied to it ensuring that the stress does not exceed the yield stress of the material chosen for the structure. As done in Section 9.4.2, a safety factor of 1.25 and 1.4 was taken on the yield and ultimate strength.

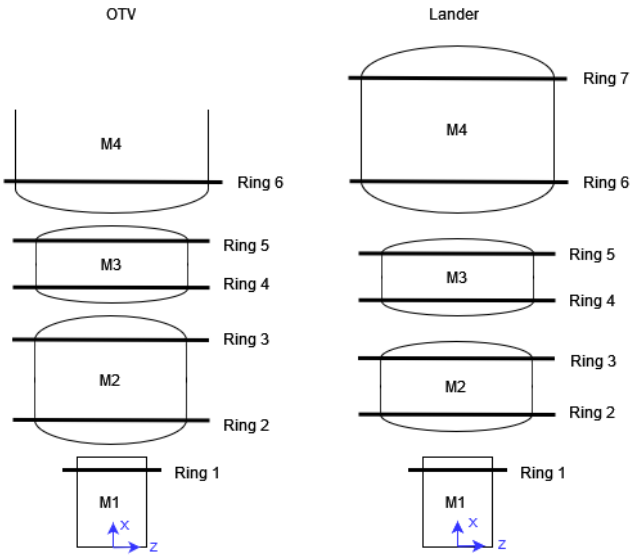


**Figure 16.2:** Discrete Mass System Vehicle

To accurately model the loads that the vehicle will experience in the simulation the structures of both vehicles were modeled with 4 discrete masses, A fixed boundary condition was applied to the surface of the ring that was connected to the engine or launch vehicle.

The four discrete masses were positioned according to where the engines, propellant tanks, and where the payload were. The masses of other subsystems were added to the masses where they were closest to. Both vehicles had their structural mass added to the mass element closest to their centre of mass.

For the lander, this means that M4 included the mass of the EPS and TCS as well as the fuel tank and the $LH_2$ onboard during that loading case. The TCS was added here as $LH_2$ requires the most thermal control. EPS was placed high on the vehicle to minimise the damage of lunar dust on the solar panels during landing, take-off, and lunar operations. M3 includes the payload if any, the cabin, the ECLSS in cargo configuration, and TTC. The heaviest the vehicle will become is in the cargo configuration so the sizing of the vehicle will reflect that mass. M2 consists of the LOX and its tank, as well as, CDH, GNC, and ADCS. ADCS is put here as it is closest to the center of mass of the lander and will have mass element spanning the entire vehicle. M1 for the lander consists of its legs and engines.

The OTV was split into three discrete masses shown in Figure 16.2, M1 consisting of the engine. M2 consists of the LOX tank, TCS, as the LOX is more cryogenic than $LCH_4$, EPS, GNC, ADCS, and CDH. M3 includes the $LCH_4$, its tank, and TTC. M4 represents the wet lander as well as the docking interface between the two vehicles.

For the masses held by one ring, M4 on the OTV, and M1 for both vehicles the end ring force equivalency is applied seen in Figure 16.3a. $F_{longitudinal}$ and $F_{lateral}$, shown in red, act through the centre of mass of the mass element at a height $h$ above the ring. To transport these loads onto the green forces, $F'_{longitudinal}$ and $F'_{lateral}$, a moment $M_Y$ needs to be applied to the ring. From force equivalency, the relationship between the two load cases can be derived shown in Equation 16.1, Equation 16.2, and Equation 16.3.

$$F'_{longitudinal} = F_{longiduinal} \quad (16.1) \qquad F'_{lateral} = F_{lateral} \quad (16.2) \qquad M_Y = -F_{lateral} \cdot h \quad (16.3)$$

For masses connected to two rings, separated by $h_1$, Figure 16.3b shows the equivalent force applied to each ring. The red loads, $F_{longitudinal}$ and $F_{lateral}$, act on the centre of mass, positioned from the bottom ring by $h_2$. $h_2$ are not necessarily half of $h_1$, due to a majority of the masses in the tanks being the propellant mass, which are susceptible to ullage and slosh during manoeuvres as well as being depleted over the course of the mission. To account for these liquids it is assumed that the ratio of $h_1$ and $h_2$, $\alpha$, varies between 0 and 1 as it is analogous to the fraction of the load carried by the upper

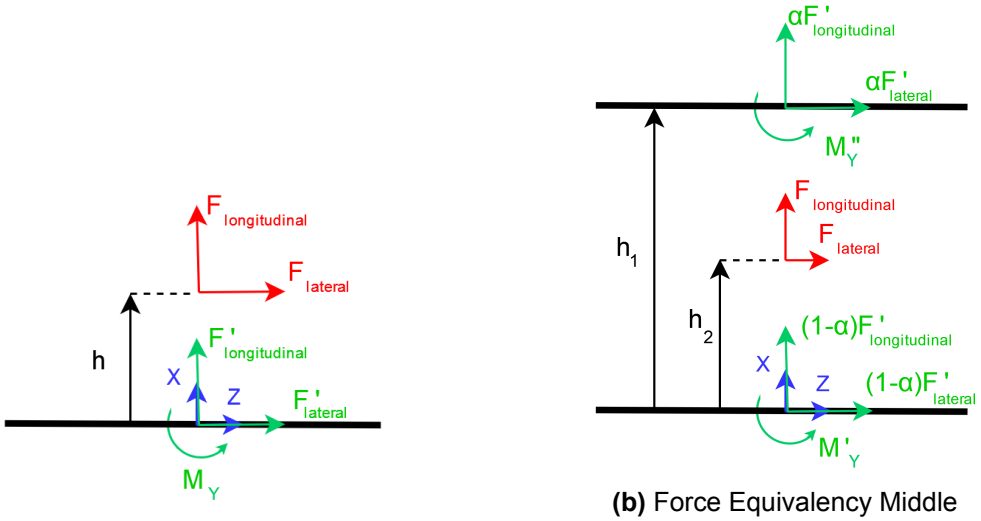


**(a)** Force Equivalency End Ring

**(b)** Force Equivalency Middle Rings

**Figure 16.3:** Force Equivalency Free Body Diagrams

ring, which can take values only between 0 and 1. The difference in heights will cause a moment to be created by the resulting forces which is counteracted by $M'_Y$ and $M"_Y$, which is assumed to be carried by both rings equally. The relationship between the forces applied to the mass and the forces applied to the ring are shown in Equation 16.4, Equation 16.5, and Equation 16.6.

$$F'_{longiduninal} = F_{longitudinal} \quad (16.4) \qquad F'_{lateral} = F_{lateral} \quad (16.5) \qquad M'_Y = M"_Y = -\alpha \cdot F_{lateral} \cdot h_1 \quad (16.6)$$

The $\alpha$ values used in the analysis range from 0.4 to 0.6, where the corresponding sensitivity analysis with the maximum stress each combination causes in the structure can be found in 16.1. In order to reduce the number of combinations, the same value for $\alpha$ will be used for all the ring pairs. The values used originally for $\alpha$ are given in Table 16.4 for the TLI load case, where the lander is upside down since it is docked to the OTV from the top of M4 and OTV is firing its engine. For manoeuvres where the lander is firing its own engines, the values for $\alpha$ should be switched by $1 - \alpha$ as the direction of the load changes, and the same also applies to the OTV.

**Table 16.4:** Values Originally Used for the $\alpha$ Parameter in TLI Load Case

| Vehicle | Rings 2-3 | Rings 4-5 | Rings 6-7 |
|---|---|---|---|
| Lander | 0.6 | 0.55 | 0.6 |
| OTV | 0.45 | 0.4 | - |

There is no value in rings 6-7 since there is no ring 7 in OTV. The centre of gravity does not lie exactly in the middle of the rings along the x-axis, which causes a little imbalance in the load carried by each ring. The values are estimated using the approximate location of the centre of gravity for each mass element utilizing the 3D models. In addition to the loads, boundary conditions had to be applied to the models. For the OTV this meant a fixed boundary condition on ring 1 for all load cases except launch which had the boundary condition on ring 6. The lander had ring 7 fixed for launch and TLI. The lander's ring 1 was fixed for all other load conditions.

### Load Analysis

The main structure of the spacecraft will have to sustain heavy loads in multiple phases of the mission. Launch, TLI, LOI, and EOI are the main ones, as well as landing. An overview of the load cases that both vehicles experience are given in Table 16.5 and Table 16.6. They show the mass of each of the discrete masses during the various phases as well as the maximum lateral and longitudinal

acceleration, in their respective body frames shown in Figure 15.1 and Figure 15.2. It is important to consider various mission phases as both the mass and the accelerations vary, this will cause the load path to vary throughout the structure. However, the limits of highest mass and lowest acceleration and lowest mass and highest acceleration will cause the most variation in the loads through the structure. That is why TEI is omitted from Table 16.5, as LOI loads have more mass, and EOI has more acceleration, so TEI will not be a limiting case on the structural sizing. The ascent and descent load cases are omitted for the same reason.

Both the OTV and lander will launch upside down, with their engines facing upwards. This is due to the volume constraints of the fairing. Resulting in negative 6 $g_0$ which is the peak axial load from the LV [145]. This means that the launch loads will be acting in the other direction than when the vehicle's own engines are firing, which will need to be designed for. The lander will also experience upside-down loads during TLI as it will be docked nose to nose with the OTV, as seen in Figure 6.1 also resulting in negative accelerations.

The landing acceleration was assumed to be the gravitational acceleration on the lunar surface of 1.624 m/s$^2$, this was determined in Section 16.2. All the other accelerations were found from the force applied by the engines during that mission phase. For OTV manoeuvres the thrust is 2.53 MN from the Raptor vacuum[1] and 222.4 kN for the Lander based on five BE-7 engines[2]. These thrusts were divided by the total vehicle mass at that moment in the manoeuvres to get the acceleration that each mass element experiences.

The lateral accelerations were conservatively approximated based on the launch vehicle's peak axial loading condition of 6g and 0.5g lateral acceleration. This same ratio is assumed for all other manoeuvres. The lateral accelerations are all considered positive as the truss structure is rotationally symmetric, so having loads in both positive and negative lateral axes only changes the location of the stress not the magnitude of them. Sizing will also be done with axial symmetry resulting in the same structure regardless of the sign of the lateral accelerations.

**Table 16.5:** Load Cases of Lander During Mission Phases

| Mission Phase | LANDER [kg] M1 | M2 | M3 | M4 | Lateral Acceleration [$g_0$] | Longitudinal Acceleration [$g_0$] |
|---|---|---|---|---|---|---|
| Launch | 1417 | 3608 | 6225 | 1630 | +2 | -6 to +2 |
| Start of TLI | 1417 | 80 895 | 6225 | 14 511 | +0.06 | -0.694 |
| End of TLI | 1417 | 80 895 | 6225 | 14 511 | +0.147 | -1.769 |
| Start of LOI | 1417 | 80 895 | 6225 | 14 511 | +0.018 | +0.220 |
| End of LOI | 1417 | 64 700 | 6225 | 11 811 | +0.023 | +0.270 |
| Landing | 1417 | 35 964 | 6225 | 7022 | -0.028 | -0.340 |
| Start of EOI | 1417 | 16 215 | 3975 | 3730 | 0.075 | +0.895 |
| End of EOI | 1417 | 5126 | 3975 | 1882 | +0.152 | +1.829 |

Table 16.5 M3 mass includes the payload mass which varies once in the cargo configuration when the down payload of 5000 kg gets replaced with the up payload of 2750 kg, as explained in Section 6.2. The vehicle is sized to be able to carry the cargo payload during launch. The start and end of TLI have the fully loaded lander as the OTV is performing the manoeuvre. The start of LOI is the first time that the BE-7 engines will fire, resulting in a positive acceleration. The end of TLI only sees masses change in M2 and M4 due to the propellant being used up for the manoeuvre. The same logic follows for the other mass changes. The end of EOI still has residual propellants, explaining why the masses in M2 and M4 are higher than during the empty launch condition.

[1] URL https://www.spacex.com/vehicles/starship/ [cited 18 June 2024]

[2] URL https://www.blueorigin.com/engines/be-7 [cited 18 June 2024]

**Table 16.6:** Load Cases of OTV During Mission Phases

| Mission Phase | OTV [kg] M1 | M2 | M3 | M4 | Lateral Acceleration [$g_0$] | Longitudinal Acceleration [$g_0$] |
|---|---|---|---|---|---|---|
| Launch | 1600 | 8169 | 4433 | 0 | +2 | -6 to +2 |
| Start of TLI | 1600 | 207 586 | 59 631 | 103 048 | +0.058 | 0.694 |
| End of TLI | 1600 | 29 580 | 11 584 | 103 048 | +0.147 | +1.769 |
| Start of EOI | 1600 | 33 911 | 11 584 | 0 | +0.457 | +5.478 |
| End of EOI | 1600 | 12 076 | 5518 | 0 | +1.120 | +13.440 |

Both the OTV and lander will be launched empty to reduce the maximum loads that their structures have to carry. This will significantly decrease the mass of both structures resulting in less propellant mass and less cost and launches over the entire 10 missions, but does increase the initial launch costs of getting the fully loaded vehicle into orbit. The quantification of this choice is explored in Section 18.1.

In Table 16.6, M1 doesn't vary as the engine remains the same during all mission phases. M2 and M3 represent dry mass elements of the vehicles as well as the LOX and $LCH_4$ load respectively. As the OTV burns during TLI and EOI these masses decrease resulting in higher accelerations while the thrust level remains the same. This results in a high acceleration for the EOI case of 13.4 $g_0$, due to the engine being sized for pushing the entire stack mass. This high acceleration was not the limiting case for the structure. M4 is the wet lander mass during TLI and 0 when the lander is not attached to the OTV.

Now that the loads and model have been selected structural sizing can be done to ensure that it will not collapse under the various load cases. The results will follow modal analysis in Table 16.1

### Modal Analysis

In the design of any mechanical structure, modal analysis plays a vital role as it is a method of understanding the structure's dynamic behaviour. There are various types of external loads that the structure experiences during its operational lifetime with varying properties. One of the important properties of the external loads is their frequency, which should not be at or even close to the eigenfrequencies of the structure. Otherwise, the amplitude of the vibrations in the structure would be amplified by the external loads until the structure fails, having catastrophic consequences on the mission and the payload. Therefore, it is of utmost importance to perform a modal analysis to check the eigenfrequencies of the structure and compare them with the frequency range of the external loads obtained by Starship User's Guide [145] to ensure the structure won't suffer from resonance. The frequency range of the external loads, which applies for both the lander and OTV, is given to be between 100-10000 Hz [145].

Modal analysis has also been performed on ANSYS using the 3D model of both the lander and OTV. Distributed masses are added to the truss structure to model the payload module and propellant tanks, where they are connected to the relevant rings. It is recommended for further work to model them using their actual 3D models and integrate them into the truss structure with representative connections, which can increase the accuracy of the results significantly. A fixed support is applied at the top end of the structure, where it will be supported by the launcher during launch as both the lander and OTV will be launched upside down. This was done because the location and strength of other supports are not known to the extent that they can be implemented into the modal analysis, affecting the accuracy of the results negatively. Further work is recommended on the interfaces that the launcher can provide to have a more accurate representation of the supports. No external forces are applied to the structure, meaning that the eigenfrequencies of the structure are its natural frequencies, which is commonly done in modal analysis to analyse the free vibrational behaviour of the structure. The first 500 eigenfrequencies of both structures are calculated, which is a small portion of the total number of them, and some of them are presented in Table 16.7.

**Table 16.7:** Eigenfrequencies of the Structure of Both Vehicles

| Vehicle | $f_{e_1}$ | $f_{e_{100}}$ | $f_{e_{200}}$ | $f_{e_{300}}$ | $f_{e_{400}}$ | $f_{e_{500}}$ |
|---|---|---|---|---|---|---|
| Lander [Hz] | 1.412 | 12.485 | 22.552 | 29.089 | 35.917 | 43.258 |
| OTV [Hz] | 0.724 | 6.245 | 7.864 | 11.581 | 13.526 | 16.154 |

In the lander structure, 2720508 eigenfrequencies can be computed whereas it is 3080562 for the OTV because of the number of nodes in the structures, where each node has 6 DOFs with an eigenfrequency per DOF. As can be seen in Table 16.7, the eigenfrequencies show a significant increase, getting closer to the range of 100-10000 Hz even in the first 500 of them, which indicates that for higher modes, there will be eigenfrequencies entering the given range, implying resonance might occur in the structures of both vehicles. In order to overcome this, dampers and dynamic absorbers can be used to limit the vibrations according to [146], requiring further analysis in the later design phases.

### Structural Results

After the model and loads were analysed the FEM simulation could be run. Giving the stress throughout the vehicle's structures, after selecting a material to base the simulation on. The material selected was Al7075-T6, and its properties are shown in Table 16.8[3]. It was selected mainly because of its high specific strength, cost, and its usage in the aerospace industry. Other alternatives considered were stainless steel and titanium. The chosen aluminium alloy outperformed stainless steel due to its higher specific strength according to [50] whereas titanium was eliminated due to its much higher cost [4,5]. The high mass of the lander and OTV imposes significant stresses, requiring a material with high yield strength to ensure elastic deformation and low density to minimize mass. Thus, the material is required to have high specific strength. From this requirement, aluminium alloys were chosen to be the general material type. By looking into the past usage of aluminium alloys, the options were narrowed down to alloy 7075 as it was used before in the Apollo Lunar Module structure. [147] Then, the heat treatment has been chosen by looking into the highest yield strength among the available options, which leads Al7075-T6 to be the material of the structures in the lander and OTV.

**Table 16.8:** Al7075-T6 Properties

| Property | Value | Units |
|---|---|---|
| Density | 2810 | kg/m$^3$ |
| Modulus of Elasticity | 71.7 | GPa |
| Yield Stress | 503 | MPa |
| Ultimate Strength | 572 | MPa |

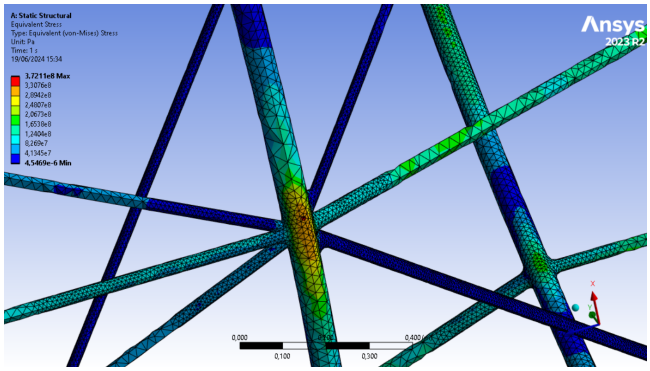


**Figure 16.4:** Simulation Results of a Connection Point in the Lander Structure

In structural sizing, applying safety factors to the design values is crucial to ensure the structure is strong enough to carry all the loads experienced during the mission, including the increases due to unexpected external loads. Therefore, a 25 % safety factor has been applied to the yield strength of the material to be the maximum allowable stress the structure will be designed according to. This value is mentioned to be enough for the yield strength in [49], making the maximum allowable stress 402 MPa for both structures.

After adding the 3D model of the truss structures in the lander and OTV, relevant load cases have been added as distributed loads on the corresponding rings. For the launch load case of both

[3]URL https://www.matweb.com/search/DataSheet.aspx?MatGUID=4f19a42be94546b686bbf43f79c51b7d&ckck=1 [cited 19 June 2024]
[4]URL https://www.matweb.com/search/DataSheet.aspx?MatGUID=b350a789eda946c6b86a3e4d3c577b39 [cited 25 June 2024]
[5]URL https://www.matweb.com/search/DataSheet.aspx?MatGUID=4f19a42be94546b686bbf43f79c51b7d [cited 25 June 2024]

vehicles, only one fixed support has been added for the same reason mentioned in 16.1. In the other manoeuvres, again only one fixed support has been applied at the ring rigidly connected to the engines since it will be the only part that stays fixed relative to the engines while they are firing. A zoomed-in view of the stress behaviour of the lander truss structure is given in Figure 16.4 as an example.

The limiting load case for the lander structure was the end of TLI, which was expected from Table 16.5, as that is when the maximum mass of the lander as well as high acceleration, resulting in a lander main structural mass of 1499 kg. The maximum stress encountered during this load case is 372 MPa, which is lower than the maximum allowable stress by 7 %. The OTV structure was driven by the start of the TLI load case, mainly due to the large mass of both vehicles together. This resulted in a main OTV structural mass of 2074 kg with a maximum stress of 399 MPa, less than the maximum allowable stress by 0.7 %. A margin of 10 % is added for fasteners and connections as per [15], resulting in the masses shown in Table 16.9. The maximum stress values encountered by the structure for different values of the $\alpha$ parameter can be found in Table 16.10. Due to load uncertainty on each ring, all maximum stresses must be below the maximum allowable stress for all cases in Table 16.10.

**Table 16.9:** Structural Mass

| Vehicle | Structural Mass [kg] |
|---|---|
| OTV | 2281.4 |
| Lander | 1649.1 |

**Table 16.10:** Maximum Stress for Various $\alpha$ Values in TLI Load Case

| Vehicle | $\alpha$ = 0.6 | $\alpha$ = 0.5 | $\alpha$ = 0.4 |
|---|---|---|---|
| Lander [MPa] | 371 | 378 | 392 |
| OTV [MPa] | 342 | 368 | 400 |

## 16.2. Landing Legs

Now, the landing leg design will be discussed. Firstly, the structural analysis is presented, where failure modes are presented and designed against. This is followed by the vibrational analysis, which discusses the impact of deceleration and damping of the vehicle.

Selecting the configuration of the struts was the first consideration. Due to the main structure having an even number of connections around its circumference, a four-legged configuration was favoured over three or five legs. Inverted tripod and cantilevered designs were considered for the strut configuration, both consisting of a primary strut and secondary struts. This configuration is typical in landing gear design [148]. The inverted tripod design was favoured over a cantilever design due to the slight increase in stability and lower loads acting on each of the strut elements. Some general assumptions also have to be discussed. Lunar soil mechanics are not considered, and the ground is assumed to be a rigid body. For the structural analysis, elasticity and energy absorption are not considered. This yields conservative conclusions as these assumptions yield the most severe results [149].

### Structural Analysis

The landing legs first must be sized to ensure that the vehicle does not tip over before a certain angle. The lander will land on slopes of up to 14°, excluding a 20 % margin. The relationship between the tip-over angle $\phi$ and the base $b$ of the landing legs is found as follows. The minimum horizontal distance between the centre of gravity and the stability square for four legs is given by $b\cos 45° = b/\sqrt{2}$ as seen in Figure 16.5. This is the distance that the centre of gravity can move horizontally before tipping over, by rotating around the footpads of two adjacent legs as seen in Figure 16.6 such that the height of the centre of gravity $h_{cg}$ is vertically above the edge of the stability square. Hence the sum of the tip-over angle $\phi$ and the angle $\theta = \arctan\left(h_{cg}/\left(b/\sqrt{2}\right)\right)$ equals 90°, and so the relation between $\phi$ and $b$ is:

$$\phi = 90° - \arctan\left(\frac{h_{cg}}{b/\sqrt{2}}\right) \tag{16.7}$$

$$b = \frac{b\sqrt{2}}{\tan\left(90° - \phi\right)} \tag{16.8}$$

Using $h_{cg} = 7.879$ m above the ground, assuming a 1 m ground clearance, the base length $b$ is calculated to be 3.364 m. The lengths of each strut can now be found as defined in Figure 16.7.

$$L_{AB} = \sqrt{(b - r_2)^2 + h_2^2} \quad (16.9) \qquad L_{AC} = \sqrt{(b - r_1 \cos\delta)^2 + (r_1 \sin\delta)^2 + h_1^2} \quad (16.10)$$

The landing force $F$ creates compression and bending in the primary strut, and tension in the secondary struts. Assuming an upwards force $F$ acting on the bottom of each leg, the structure was solved analytically to obtain the internal forces in each member as well as their reaction forces, as can be seen in Figure 16.7. The structure was assumed to be a truss with pinned connections and was solved with the method of joints, leading to the following force equations:

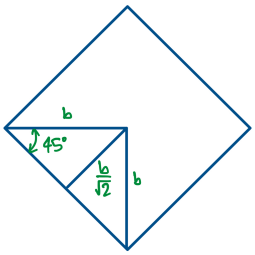


**Figure 16.5:** Stability Square

$$F_{AC} = \frac{F L_{AC}}{2\left(h_2 \frac{b - r_1\cos\delta}{b - r_2} - h_1\right)} \quad (16.11) \qquad F_{AB} = -2\frac{L_{AB}}{b - r_2}\frac{b - r_1\cos\delta}{L_{AC}} F_{AC} \quad (16.12)$$

$$B_x = -\frac{b - r_2}{L_{AB}} F_{AB} \quad (16.13) \qquad B_z = \frac{h_2}{L_{AB}} F_{AB} \quad (16.14)$$

$$R_x = -\frac{b - r_1\cos\delta}{L_{AC}} F_{AC} \quad (16.15) \qquad R_y = \frac{r_1 \sin\delta}{L_{AC}} F_{AC} \quad (16.16) \qquad R_z = \frac{h_1}{L_{AC}} F_{AC} \quad (16.17)$$

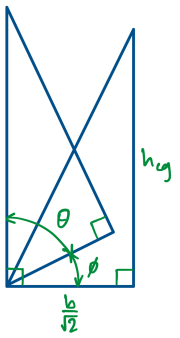


**Figure 16.6:** Tip-over Angle

The force experienced by the four legs on landing is the weight of the lander upon landing [150], which is 82 269 N. Therefore, the force on each leg is 20 567 N. Using the equations above, the landing leg dimensions and forces were calculated assuming a ground clearance of 1 m. Additionally, the inner and outer radii of the members were chosen. A larger radius is beneficial to reduce mass as it decreases the slenderness ratio for a given length and thus increases buckling stress [151], but the legs must fit inside Starship's fairing during launch. With this in mind, an outer radius of $r_o = 0.22$ m was chosen for both the primary and secondary struts.

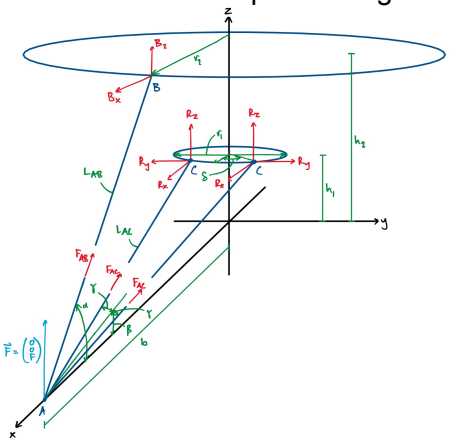


**Figure 16.7:** Lengths and Forces

Once the forces were found, the stresses due to tension, compression, and bending could be analysed in order to find the inner radii of the struts and their thicknesses. The axial stresses for members AB and AC are given by:

$$\sigma_{ax_{AB}} = \frac{F\sin\alpha}{\pi\left(r_{o_{AB}}^2 - r_{i_{AB}}^2\right)} \quad (16.18) \qquad \sigma_{ax_{AC}} = \frac{F\sin\beta}{\pi\left(r_{o_{AC}}^2 - r_{i_{AC}}^2\right)} \quad (16.19)$$

Where $F$ is the vertical force on each leg and $r_o$ and $r_i$ are the outer and inner radii of members AB and AC. The bending stresses are given by (see Figure 16.8) [152]:

$$\sigma_{b_{AB}} = x' F\cos\alpha \frac{4r_{o_{AB}}}{\pi\left(r_{o_{AB}}^2 - r_{i_{AB}}^2\right)} \qquad \sigma_{b_{max_{AB}}} = F(b - r_2)\frac{4r_{o_{AB}}}{\pi\left(r_{o_{AB}}^2 - r_{i_{AB}}^2\right)} \quad (16.20)$$

$$\sigma_{b_{AC}} = x'' F\cos\beta \frac{4r_{o_{AC}}}{\pi\left(r_{o_{AC}}^2 - r_{i_{AC}}^2\right)} \qquad \sigma_{b_{max_{AC}}} = F(b - r_1)\frac{4r_{o_{AC}}}{\pi\left(r_{o_{AC}}^2 - r_{i_{AC}}^2\right)} \quad (16.21)$$

Buckling must also be taken into account for member AB as it is in compression. Firstly, the critical effective slenderness ratio was found to determine whether Johnson or Euler buckling formulas should be used [151]. This is compared with the member AB's effective slenderness ratio $\rho_s = KL_{AB}\sqrt{A/I}$,

where $K = 2.1$ is a design factor taking into account the beam end pinned condition [153]. It was found that AB is slender enough to use Euler buckling equations, where the critical buckling stress is given by Equation 16.22.

$$\sigma_{cr} = \frac{\pi^2 EI}{(KL_{AB})^2 A} \tag{16.22}$$

$$MS = \frac{\sigma_{cr_{AB}}}{\sigma_{ax_{AB}} + \sigma_{b_{AB}}} - 1 \tag{16.23}$$

With the relevant stress equations defined, the process for sizing the inner radii of members AB and AC can be described. The maximum axial and bending stresses allowable are the yield strength of the material divided by a safety factor of 1.25 [49]. For combined compression and bending loading, which is the case for member AB, there must be a safety margin of 0.25 above the expected loading. This is given by Equation 16.23 [154].

For member AB, the inner radius $r_{i_{AB}}$ is sized such that the maximum compressive and bending stress is less than the material yield strength divided by 1.25, and the margin of safety for combined loading is greater than 0.25. For member AC, the inner radius $r_{i_{AC}}$ is sized such that the maximum compressive and bending stress is less than the material yield strength divided by 1.25. At this point, the landing leg material was chosen using a trade-off. Three materials were considered: aluminium 7075-T6, titanium Ti-6Al-4V grade 5, and stainless steel 301 full hard. These were traded off using the following criteria, and the trade-off table is shown in Table 16.11:

- Compressive yield strength to density ratio (50%): This should be as high as possible to minimise the mass required to take a given load.
- Ease of manufacturing (30%): This is an important consideration to ensure the legs can be produced, but as the shapes are relatively simple (thin-walled tubes), this criterion is given a smaller weight than the first one.
- Cost per unit mass (20%): It is beneficial to minimise the landing leg cost to comply with the overall cost budget, but if an expensive material is the only feasible option, then it must be used.

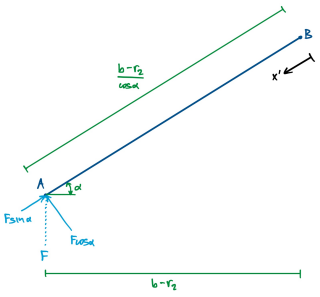

**(a)** Force on Member AB

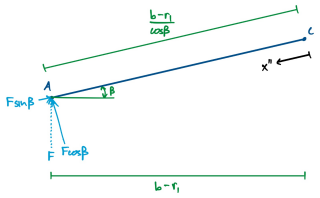

**(b)** Force on Member AC

**Figure 16.8:** Forces on the Struts

**Table 16.11:** Landing Leg Material Trade-off Table[6,7] [50]

| Criteria / Design Option | Compressive yield strength to density ratio (MPa/(kg/m$^3$)) (50%) | Ease of manufacturing (30%) | Cost per unit mass (USD/kg) (20%) |
|---|---|---|---|
| Aluminium 7075-T6 | 0.18 | Very poor weldability, good machinability | 2.20 |
| Titanium Ti-6Al-4V grade 5 | 0.24 | More difficult to weld than steel, difficult to machine | 7.04 |
| Stainless steel 301 full hard | 0.16 | Good weldability, good machinability | 0.81 |

| Legend | Unacceptable | Barely acceptable | Correctable deficiencies | Good, meets requirements | Excellent, exceeds requirements |
|---|---|---|---|---|---|

Based on this trade-off, titanium Ti-6Al-4V grade 5 was chosen for the landing leg material, primarily due to its high compressive yield strength to density ratio allowing for light legs. The relatively simple leg geometry means that despite titanium's relative difficulty to manufacture, the legs can still be produced. Titanium TI-6Al-4V grade 5 has a compressive yield strength of 1070 MPa, an elastic

[6] URL https://www.matweb.com/search/DataSheet.aspx?MatGUID=b350a789eda946c6b86a3e4d3c577b39 [cited 17 June 2024]
[7] URL https://www.matweb.com/search/DataSheet.aspx?MatGUID=4f19a42be94546b686bbf43f79c51b7d [cited 17 June 2024]

modulus of 114 GPa, and a density[8] of 4430 kg/m$^3$. With these values, the inner radii of members AB and AC were calculated such that the maximum compressive and bending stresses were less than $1070/1.25 = 856$ MPa and the margin of safety $MS$ was greater than 0.25. This led to an inner radius of 0.2174 m for the primary strut and 0.2196 m for the secondary struts. From the inner and outer radii, the strut lengths, and the material density, the strut mass was calculated, assuming a uniform mass distribution. The geometric parameters and mass of each strut are shown in Table 16.12.

**Table 16.12:** Landing Leg Geometric Parameters and Mass

| Landing leg component | Length (m) | Inner radius (m) | Outer radius (m) | Mass (kg) |
|---|---|---|---|---|
| **Primary strut** | 5.1919 | 0.2174 | 0.2200 | 83.237 |
| **Secondary strut** | 4.1803 | 0.2196 | 0.2200 | 10.964 |

This preliminary sizing method only estimates the mass of the struts. In future more detailed design stages, the hinges, locks, and other mechanisms required for deployment should be designed and analysed in detail. Additionally, the legs would require some shielding against lunar regolith kicked up by the engines upon landing, which would also require a detailed analysis. For now, a 50 % margin is applied to account for additional attachments, leading to a total landing leg mass of 631 kg.

### Vibrational Analysis

Finally, an analysis was performed on the damping and deceleration imposed on the system and crew by the impact. A mass-spring-damper system was used to model the vehicle, where the mass of the landing legs was assumed to be negligible and the spring and damper are in parallel. Furthermore, the same assumptions during impact as previously described are applicable to this model. The aim of this analysis was to examine the compression of the energy absorbing elements (i.e. dampers and springs), and the resulting deceleration, which may not exceed the maximum deceleration for crew safety.

The system is assumed to be underdamped, and the Moon is assumed to be stationary. Furthermore, the assumption was made that the impact is a non-elastic collision, where a coefficient of restitution of 0.03 was used [155]. The vehicle is reusable, so no structures can be used which plastically absorb the impact energy. Hence, a damping ratio of 0.07 was chosen[9], which corresponds to a metal structure with joints, which models the landing legs. A step function was used to model the force, which activates on impact. This force was equated with the weight [156]. The equation of motion is given by Equation 16.24.

$$m\ddot{x}(t) + F = -kx(t) - c\dot{x}(t) \quad x(0) = 0\,\text{m}, \quad \dot{x}(t) = 0.5\,\text{m/s} \tag{16.24}$$

The final solution of Equation 16.24 is shown in Equation 16.25. This is the displacement of the center of gravity with respect to before impact.

$$x(t) = -\frac{e}{1+e}\frac{F_0}{k}\left[1 - e^{-\zeta\omega_n(t-t^*)}\left\{\frac{\zeta\omega_n}{\omega_d}\sin(\omega_d(t-t^*)) + \cos(\omega_d(t-t^*))\right\}\right] \tag{16.25}$$

In Equation 16.25, $e$ is the coefficient of restitution, unitless. $F_0$ is the impact force, in N. $\zeta$ is the damping ratio, unitless. $\omega_n$ is the natural frequency in rad/s, $\omega_d$ the damped natural frequency in rad/s, $k$ the spring coefficient in N/m. Assuming each strut has a spring in series, with a spring constant of 10 kN/m, and the dimensions and materials presented in the structural analysis, a maximum deflection during landing was calculated as −37.77 mm. With the initial conditions, this leads to a deceleration of 0.34 G, which is below the maximum acceptable value stipulated by HLS requirements [9]. The damping time reducing the amplitude to 5% of the equilibrium value was determined to be 23 s.

[8] URL https://www.matweb.com/search/DataSheet.aspx?MatGUID=b350a789eda946c6b86a3e4d3c577b39 [cited 17 June 2024]

[9] URL https://www.jpe-innovations.com/precision-point/structural-damping-properties-mechanical-systems/ [cited 19 June 2024]

# 17 | Risks

In this chapter the mission risks are presented. The subsystem risks are presented in the respective preceding chapters, while this chapter is concerned with the system risks. First, the risks are presented and assessed in Section 17.1. Following this, the risk mitigation and contingency is described in Section 17.2. Proper assessment and mitigation of risks is critical to fulfilling mission requirements, particularly **HOPE-MISS-070**, which states that the vehicle shall have a reliability of 95% or higher.

## 17.1. Technical Risk Assessment

This section presents the identified risks, their causes, impacts on performance and associated requirements. Table 17.1 shows the mission risks related to operations not covered in subsystems and non-technical logistical risks related to project management and markets. The technical risks relate to Extra-Vehicular Activities (EVA), landing, radiation, launch and fire. Assessing these system risks is essential, and many of them directly relate to subsystem requirements as shown in Table 17.1. As well as the technical risks, there are risks relating to project cost, project time, legal risks, available resources (other than financial and time) and market risks. These can be just as critical as the technical risks as they can cause failure of the project even if there are no significant technical issues.

## 17.2. Mitigation and Contingency

The mitigation and contingency strategies are presented in this section in Table 17.4. The pre-mitigation and post-mitigation likelihood (L) and consequence (C) are given. The likelihoods, shown in Table 17.2, are given as five categories: rare (improbable but could still occur), unlikely (remotely possible but not probable), possible (could occur), likely (expected to occur), and almost certain (almost guaranteed). The consequences, shown in Table 17.3, also have five categories: insignificant (inconvenience or non-operational impact), minor (short-term inconvenience), moderate (degradation of secondary mission or small reduction in technical performance), major (reduction in technical performance and questionable mission success), and catastrophic (severe effects and mission failure). The effects of the mitigation and contingency strategies are shown in the pre-mitigation and post-mitigation risk maps shown in Table 17.5 and Table 17.6 respectively. These risk maps also include all of the risks from the subsystems.

There are seven risks which remain at a high level after mitigation and contingency is applied. These are shown in Table 17.6. Further risk mitigation efforts should focus on these risks as they are deemed most critical to the project. **R-COST-01** is a fundamental risk of any engineering project, as exceeding the project budget can severely impact the design and budget issues are common among complex space engineering projects. **R-COST-03** is closely related to this, where the budget is cut rather than exceeded. For these two risks, detailed contingency plans should be made and a surplus should be kept for such a scenario. **R-RES-03** is another critical risk; launch vehicles can become unavailable for a number of reasons. Currently available vehicles can be decommissioned, future vehicles can be delayed and any vehicle can experience issues which make it temporarily unavailable. In ARCH-E's case, SpaceX's Starship is expected to be available in time for the first launches, but delays in its development and testing would pose a major risk. To mitigate this risk, contact should be made with the launch provider to get more information on the future plans and timeline for the vehicle. The subsystem risks **R-TCS-04**, **R-STR-11&12** and **R-PROP-09** are also deemed as high risk post-mitigation. These are discussed in Section 10.4, Chapter 16 and Section 9.6 respectively.

**Table 17.1:** Risk Mitigation and Contingency

| Risk ID | Risk Description | Causes | Impact | Req. |
|---|---|---|---|---|
| R-EVA-02 | Crew member Loss of Restraint | Human error, Poor training, Equipment failure | Safety concern | HOPE-SYS-150 |
| R-EVA-03 | EVA Suit Contamination | Seal breach | Health risk | HOPE-STK-ADS-030 |
| R-EVA-04 | Airlock Malfunction | Mechanical failure, door seal failure | Health risk | HOPE-MISS-070 |
| R-LAND-01 | Failure to Land at the Landing Site | Navigation errors, sensor inaccuracies | Off-target landing, Increased expense for recovery efforts | HOPE-MISS-250 |
| R-LAND-02 | Inappropriate Lighting Conditions | Extreme environmental factors, equipment limitations | Impaired visibility, potential aborted landing, Delayed landing | HOPE-GNC-ADCS-120 |
| R-LAND-04 | Failure to Properly Land due to Local Surface Hazards | Small-sized terrain irregularities | Structural damage, potential mission failure, Delayed landing | HOPE-GNC-050 |
| R-LAND-05 | Blown dust degrades landing site determination | Extreme environmental conditions, sensors interference | Reduced sensors accuracy, potential aborted landing, Increased expenses for recalibration | HOPE-GNC-050 |
| R-LAND-06 | Automatic Guidance Fails the Precision Landing | Software errors, hardware failures | Off-target landing, potential mission abort, Delayed landing | HOPE-GNC-050 |
| R-LAND-07 | Insufficient Propellant for Hovering Flight | Fuel miscalculation, propulsion inefficiency | Inability to maintain hover, potential crash landing | HOPE-EPS-040 |
| R-LAND-08 | Braking Manoeuvres Fail | Brake system malfunction, insufficient braking force | Inability to stop, potential runway overrun | HOPE-SYS-180 |
| R-RAD-01 | Cosmic Radiation-Induced Electronics Failure | Poor Shielding, Electronic vulnerability | Electronics malfunction | HOPE-STR-090 |
| R-RAD-02 | Crew Exposure to Unsafe Levels of Cosmic Radiation | Insufficient shielding | Health risk | HOPE-PROP-050 |
| R-LAU-01 | Resonant Launch-Induced Vibration | Launch dynamics, Choice of launch vehicle | Structural damage, Delayed launch | HOPE-STR-090 |
| R-LAU-02 | Rocket Engine Fails | Engine malfunction, propulsion system failure | Incomplete launch | HOPE-MISS-160 |
| R-LAU-03 | Vehicle Component Fractures due to Dynamic Loads | Structural weaknesses, Dynamic loads | Structural failure | HOPE-SYS-010 |
| R-LAU-04 | Inclement Weather Conditions such as Winds or Lightning | Environmental factors, Poor planning | Launch delay, Increased costs for rescheduling | HOPE-SYS-020 |
| R-LAU-07 | Vehicle does not fit in launcher payload bay | Poor communication, inaccurate launcher data | Launch delay, Increased costs for rescheduling | HOPE-STR-050 |

| Risk ID | Risk Description | Causes | Impact | Req. |
|---|---|---|---|---|
| R-LAU-08 | Disintegration of launch vehicle | Improper design or operations of launch vehicle | Cost of redesign, cost of delayed launch | HOPE-STR-050 |
| R-FIRE-01 | Fire or explosion event on vehicle | Electrical faults, combustible components | Potential loss of vehicle | Non-specific |
| R-COST-01 | Program cost budget is exceeded | Budget of the project | Delays, search for additional funding | Non-specific |
| R-COST-02 | Insufficient or late funding | Economic market and stakeholder(s) | Delays, search for additional funding | Non-specific |
| R-COST-03 | Cut in cost budget or funding | Economic market and stakeholder(s) | Delays, search for additional funding | HOPE-STK |
| R-TIME-01 | Delays caused by changes in stakeholder(s) requirements | Insufficient communications and/or changes in the market leading to a change in mind of the stakeholder(s) | Cost increase, delay of launch, revenue loss | Non-specific |
| R-TIME-02 | Delays caused by major (sub)system redesign | Changes in requirements or spending too much time on non-optimal designs/re-iterations | Cost increase, delay of launch, revenue loss | HOPE-MISS-LEG |
| R-LEG-01 | Changes in political regulations | Political situation | Cost of mission redesign, delay of launch | HOPE-MISS-LEG |
| R-LEG-02 | Changes in legal regulations | Legal situations | Cost of mission redesign, delay of launch | Non-specific |
| R-RES-01 | Unavailability of specific materials | Economic Market and resource value | Increased design cost, delay of launch | Non-specific |
| R-RES-02 | Unavailability of specific machinery or (testing) facilities | Machinery decommission or out of service | Additional transport costs | HOPE-STK-ADS-020 |
| R-RES-03 | Unavailability of selected launch vehicle | Launcher decommission or out of service | Cost of delayed launch, alternate launcher needed, redesign costs | HOPE-SYS-010 |
| R-RES-04 | Launch facilities become unavailable | Launch accident at launch facilities | Cost of delayed launch, alternate launcher needed, redesign costs | Non-specific |
| R-MAR-01 | Increased market competition | Emerging similar projects, or faster progress in HLS/SpaceX program than expected | Obsolescence of vehicle | Non-specific |
| R-MAR-02 | Advent of new technology or invention | Technological advances | Obsolescence of vehicle | Non-specific |
| R-MAR-03 | Reputational damage due to technical mistake or decisions | Unpredicted mistakes, insufficient verification | Loss of future revenue | Non-specific |

**Table 17.2:** Likelihood Categories

| Rating | Symbol |
|---|---|
| Almost Certain | AC |
| Likely | Li |
| Possible | P |
| Unlikely | U |
| Rare | R |

**Table 17.3:** Consequences Legend

| Rating | Symbol |
|---|---|
| Catastrophic | Ca |
| Major | Ma |
| Moderate | Mo |
| Minor | Mi |
| Insignificant | I |

**Table 17.4:** Technical Risks During the Mission

| | Pre-mit. | | | | Post-mit. | |
|---|---|---|---|---|---|---|
| **ID** | **L** | **C** | **Mitigation** | **Contingency** | **L** | **C** |
| R-EVA-02 | U | Mo | Training in restraint usage and safety protocols, robust design | Emergency retrieval procedures, safety tether systems | R | Mi |
| R-EVA-03 | R | Ma | Frequent suit inspection and maintenance, training on decontamination procedures | Emergency return to the airlock, decontamination procedures | R | Ma |
| R-LAND-01 | P | Ma | Redundant navigation systems, real-time position correction algorithms | Emergency landing procedures, alternative landing sites | U | Mo |
| R-LAND-02 | U | Mo | Advanced lighting systems, real-time visibility assessment | Manual landing procedures, alternative lighting sources | R | Mi |
| R-LAND-04 | Li | Ma | Real-time hazard detection, terrain analysis | Manual hazard avoidance procedures, alternative landing sites | P | Mo |
| R-LAND-05 | Li | Ma | Dust-resistant sensors, real-time sensor calibration | Dust-resistant equipment, sensor calibration tools | P | Mo |
| R-LAND-06 | P | Ma | Redundant guidance algorithms, fail-safe mechanisms | Emergency landing procedures, manual override capabilities | U | Mo |
| R-LAND-07 | U | Ma | Fuel margin assessment, real-time fuel consumption monitoring | Emergency refuelling procedures, alternative landing sites | R | Mo |
| R-LAND-08 | P | Ma | Brake system redundancy, real-time braking force monitoring | Emergency braking procedures, alternative landing sites | U | Mo |
| R-RAD-01 | P | Ma | Use radiation-hardened electronics, implement shielding | Implement redundant systems, manual override capabilities | U | Mo |
| R-RAD-02 | U | Ma | Shielding materials, monitoring radiation levels | Immediate return to spacecraft, administer medical treatment | R | Mo |
| R-LAU-01 | P | Mo | Install vibration damping systems, conduct structural analysis | Reinforce structure, alternative launch methods | U | Mi |
| R-LAU-02 | P | Ma | Use redundant propulsion systems, conduct rigorous pre-flight testing | Emergency abort procedures, use alternative launch vehicles | U | Mo |
| R-LAU-03 | U | Ca | Strengthen structure, conduct thorough testing | Emergency repair procedures, use alternative launch vehicles | R | Ma |
| R-LAU-04 | U | Ma | Monitor weather conditions, establish launch criteria | Implement weather contingency procedures, select alternative launch windows | R | Mo |
| R-LAU-07 | P | Ma | Set clear dimension requirements, use design margins | Redesign vehicle body to fit within dimensions | R | Ma |

| ID | Pre-mit. L | Pre-mit. C | Mitigation | Contingency | Post-mit. L | Post-mit. C |
|---|---|---|---|---|---|---|
| R-LAU-08 | U | Ca | Choose a reliable launch vehicle | *No contingency strategy* | R | Ca |
| R-FIRE-01 | U | Ca | Install fire suppression systems, implement electrical safety measures | Evacuate personnel, conduct salvage operations | R | Ma |
| R-COST-01 | AC | Ma | Ensure at all times of the mission there is a margin or spare budget for any unforeseen events | Find new funding | Li | Mo |
| R-COST-02 | P | Ma | Make agreements and contracts before starting the production and mission | Have alternative funding strategies or possible loan strategies | U | Mo |
| R-COST-03 | P | Ca | Always keep a contingency margin for unforeseen events and keep make regular meetings with stakeholder(s) for updates | Find new funding | P | Ma |
| R-TIME-01 | Li | Mo | Ensure sufficient communications is held with the stakeholders about made (design) decisions | Requests for changes in deadlines and/or funding | U | Mo |
| R-TIME-02 | Li | Mo | Ensure all requirements are properly checked and agreed by all parties before further designing. Limit amount of re-iteration | Put more manpower in specific parts of design that require changes | P | Mi |
| R-LEG-01 | P | Mi | Reduce the amount of international dependence | Adapt to new regulations | P | I |
| R-LEG-02 | P | Mo | Make binding and stable contracts that to ensure legal changes won’t affect this specific mission | Adapt to new regulations | P | Mi |
| R-RES-01 | P | Ma | Monitor the material resources continuously | When the material resources fall under a determined value, order new batch of material supply | U | Mi |
| R-RES-02 | Li | Mo | Create a list of available machinery to take into account in the design phase, or make reservation of (testing) facility in time | Create a list of machinery that might be needed in the manufacturing phase but unavailable in current facilities. Find facilities that have that machinery and are close to current facilities. | P | Mo |
| R-RES-03 | Li | Ma | Monitor the schedule of the launch vehicle on a regular basis | Find other feasible launch vehicles. Or, adapt the mission to be executed on other dates | P | Ma |
| R-RES-04 | R | Ma | Select reliable launch location | Select alternative location requiring minimum redesign | R | Ma |
| R-MAR-01 | Li | Mi | Keep up-to-date with competitors progress | Ensure product has unique value | Li | I |
| R-MAR-02 | P | Mi | Keep up-to-date with latest technological innovation in research | Implement new technology in design or ensure product has other unique value(s) | P | I |
| R-MAR-03 | U | Mo | Consult consultancy advisors and/or inform stakeholder(s) before releasing information to public | Prepare apology statement and/or withdraw decision | R | Mo |

**Table 17.5:** Pre-mitigation Risk Map

| | Severity of Consequences | | | | |
|---|---|---|---|---|---|
| L ↓ | I | Mi | Mo | Ma | Ca |
| AC | | | | R-COST-01, R-EPS-01 | |
| Li | | R-MAR-01 | R-TIME-01, R-TIME-02, R-RES-02, R-EPS-15, R-ECLSS-10, R-TCS-05 | R-LAND-04, R-LAND-05, R-RES-03, R-GNC-03, R-TCS-03, R-STR-07 | R-CDH-06, R-TCS-04, R-STR-11, R-STR-12 |
| P | | R-LEG-01, R-MAR-02, R-ADCS-08 | R-LAU-01, R-LEG-02, R-EPS-08, R-EPS-10, R-EPS-11, R-EPS-14, R-EPS-18, R-EPS-19, R-EPS-20, R-ADCS-03, R-ADCS-06 | R-LAND-01, R-LAND-06, R-LAND-08, R-RAD-01, R-LAU-02, R-LAU-07, R-COST-02, R-RES-01, R-TTC-02, R-EPS-09, R-EPS-16, R-EPS-17, R-ECLSS-09, R-GNC-01, R-TCS-01, R-TCS-02, R-STR-03, R-STR-04, R-STR-05, R-STR-08, R-STR-09, R-STR-10, R-ADCS-01, R-PROP-03, R-PROP-08, R-STR-13 | R-COST-03, R-ADCS-05, R-PROP-05, R-PROP-09, R-PROP-10 |
| U | | R-ECLSS-06 | R-EVA-02, R-LAND-02, R-MAR-03, R-TTC-02, R-EPS-02, R-EPS-03, R-GNC-02, R-STR-02 | R-LAND-07, R-RAD-02, R-LAU-04, R-TTC-01, R-EPS-21, R-ECLSS-04, R-ECLSS-08, R-STR-06, R-ADCS-02,R-ADCS-04, R-ADCS-07, R-PROP-04 | R-LAU-03, R-LAU-08, R-FIRE-01, R-EPS-12, R-EPS-13, R-CDH-01, R-CDH-03, R-CDH-05, R-PROP-01, R-PROP-02 |
| R | | | R-EPS-04 | R-EVA-03, R-RES-04, R-ECLSS-07 | R-EPS-05, R-EPS-06, R-EPS-07, R-ECLSS-01, R-ECLSS-02, R-ECLSS-03, R-ECLSS-05, R-GNC-05, R-CDH-02, R-CDH-04, R-STR-01 |

**Table 17.6:** Post-Mitigation Risk Map

| | Severity of Consequences | | | | |
|---|---|---|---|---|---|
| L ↓ | I | Mi | Mo | Ma | Ca |
| AC | | | | | |
| Li | R-MAR-01 | | R-COST-01 | | |
| P | R-LEG-01, R-MAR-02 | R-TIME-02, R-LEG-02, R-EPS-01, R-ECLSS-10 | R-LAND-04, R-LAND-05, R-RES-02, R-GNC-03, R-STR-04, R-STR-05, R-STR-07 | R-COST-03, R-RES-03, R-TCS-04, R-STR-11, R-STR-12 | |
| U | R-ADCS-08 | R-LAU-01, R-RES-01, R-EPS-18, R-EPS-20, R-CDH-01, R-CDH-03, R-ADCS-03, R-ADCS-06 | R-LAND-01, R-LAND-06, R-LAND-08, R-RAD-01, R-LAU-02, R-COST-02, R-TIME-01, R-TTC-01, R-EPS-08, R-EPS-10, R-EPS-11, R-EPS-14, R-EPS-15, R-EPS-16, R-EPS-17, R-EPS-19, R-ECLSS-09, R-GNC-01, R-CDH-05, R-TCS-01, R-TCS-02, R-TCS-03, R-TCS-05, R-STR-03, R-STR-08, R-ADCS-01, R-PROP-01, R-PROP-03, R-PROP-04, R-PROP-08 | R-EPS-09, R-STR-09, R-STR-10, R-ADCS-05, R-PROP-02, R-PROP-05, R-PROP-10 | R-PROP-09 |
| R | R-ECLSS-06 | R-EVA-02, R-LAND-02, R-EPS-02, R-EPS-03, R-GNC-02, R-STR-02 | R-LAND-07, R-RAD-02, R-LAU-04, R-MAR-03, R-EPS-04, R-EPS-21, R-ECLSS-04, R-ECLSS-07, R-ECLSS-08, R-CDH-02, R-CDH-04, R-STR-06, R-ADCS-02, R-ADCS-04, R-ADCS-07 | R-EVA-03, R-LAU-03, R-LAU-07, R-FIRE-01, R-RES-04, R-EPS-05, R-EPS-06, R-EPS-07, R-ECLSS-01, R-ECLSS-02, R-ECLSS-03, R-ECLSS-05, R-GNC-05, R-STR-01, R-STR-13 | R-LAU-08, R-EPS-12, R-EPS-13, R-CDH-06 |

**Table 17.7:** Risk Map Legend

| Risk | Low | Moderate | High | Extremely High |
|---|---|---|---|---|

# 18 | Operations

In this chapter, the operational procedures that will be carried out during the mission will be discussed, as well as their logistics. The operations receiving focus in Section 18.1 are refuelling, reconfiguration, re-usability, lunar ascent & descent, extra-vehicular activities (EVA) and end-of-life (EOL) operations. The characteristics of these operations regarding reliability, availability, maintainability, and safety will be discussed in Section 18.2.

## 18.1. Operations and Logistics

The design phase of the mission is only one part of the bigger picture, whereas another important part is the operational procedures and logistics to bring the design to life, which should be planned and carried out with utmost care. For ARCH-E, each mission may look slightly different as there may be discrepancies in the wishes of customers over the ten missions. Nevertheless, a mission sequence of operations is shown in Figure 18.1, to represent what one of these missions would approximately look like.

### Launch

Both vehicles with within the normal Starship fairing volume as specified in the user guide as seen in Figure 18.8 [145]. If any of the two vehicles increase in size during further design stages there is a possibility to use the extended fairing volume going from 17.24m to 22m. Additionally, the expected payload capability of Starship is uncertain, ranging from 100 tons to 200 tons. The most conservative value was taken and a margin of 20% was taken as per ESA's margin philosophy [15]. With two launches required for the dry mass of the vehicles with the cargo payload, five launches are required to bring up the propellants. This accounts for the additional mass required to hold to propellant in the launch vehicle.

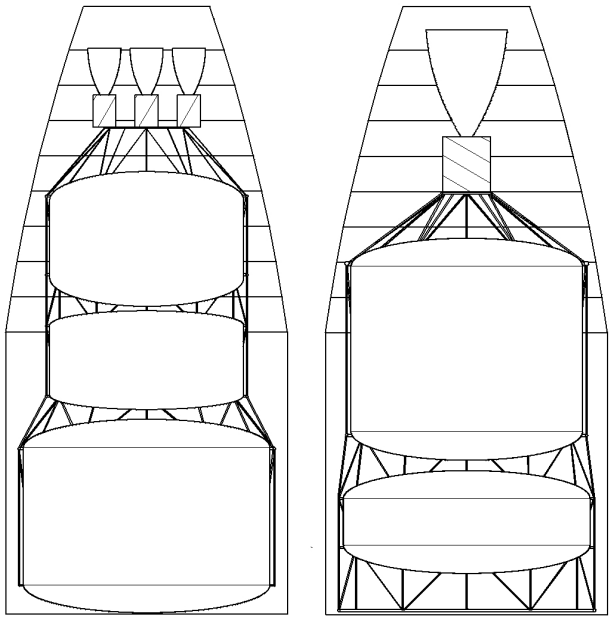

**Figure 18.8:** Lander (L) and OTV (R) in Starship Fairing

For safety and operation reasons crew will have to be launched separately on a vehicle such as SpaceX's Dragon[1]. This would mean for crew refueling one additional launch would be required. This results in a range of launches of 62 for all crewed missions down to 51 launches for all cargo missions. The risks concerning launch are discussed in Chapter 17.

Both vehicles are launching empty, such that dry mass can go down. If we were to launch both vehicles fueled to the capacity of the launch vehicle it is estimated that the structural mass will increase 2 fold. This increases the stack mass by 61 tons, increasing the total amount of launches by 1 for cargo and crew refuelling, leading to 10 more launches over the entire mission duration, increasing costs. Additionally, the increased volume of the propellant tanks will require the extended fairing increasing the risk of not fitting within the launch vehicle.

[1] URL https://www.spacex.com/vehicles/dragon/ [cited 18 June 2024]

### In-Orbit Refuelling

Following the selected general mission architecture, the decision was made to refuel in LEO upon return to Earth instead of refuelling on Earth's surface. This involves complex operations, including phasing manoeuvres and docking manoeuvres. An operational flow block diagram of refuelling in Earth orbit is presented below in Figure 18.2.

Block 4.0 is kept as two different options to consider. Being able to launch a refuelling vehicle into Earth orbit when the OTV returns to Earth means a phasing manoeuvre could possibly be avoided. However, this would be expensive as there would be high recurring costs. Thus it may be more plausible to use an existing refuelling vehicle that is already in Earth orbit. The architecture for the refuelling mission is shown in Figure 7.8, in the case it needs a phasing procedure.

In the most ideal case, the timing of the EOI manoeuvre should be designed such that the spacecraft will rendezvous with the refuelling vehicle at the EOI point. This would require another burn to decelerate the OTV to be able to dock to the refuelling vehicle without a collision. If meeting with the refuelling vehicle at the intersection point fails or is not possible because of its relative position to the OTV, a phasing orbit can be utilised to meet with the refuelling vehicle later at the intersection point. In the case of having a phasing orbit before the rendezvous, a deceleration is still required to get the velocity of the OTV relative to the refuelling vehicle to a sufficiently low level for successful docking.

A major risk pertaining to the refuelling procedure involves the orbital lifetime of the system. The period over which the OTV can stay in LEO is limited by the design lifetime of the vehicle, orbital propellant boil-off rates, and risks associated with micrometeoroids and orbital debris (MMOD). As a consequence, there should be a restriction on the time window for the lander's return to Earth. The restriction placed here is that the lander may remain on the lunar surface for a maximum of 6.5 days before heading back to Earth.

If instead of a large tanker already in orbit, multiple smaller tanker launches are used to refuel the OTV and lander, there will be more risks pertaining to a large number of opportunities for mission failure. Many launches, rendezvous, and docking events may be required to fully refuel the OTV and lander which all have the potential to disrupt the overall mission. In spite of the individual events having high reliability, performing many of these tasks in series will decrease the overall mission reliability.

Refuelling in Earth orbit offers several advantages. It decreases the need for maintenance because there will be no re-entry upon arrival to Earth so, the spacecraft would not experience high amounts of loads and temperatures during the re-entry. This would enable optimising the design more based on the objectives of the mission to increase the spacecraft's performance as Earth re-entry imposes driving constraints on the structural strength and temperature endurance of the spacecraft.

### In-Orbit Reconfiguration

Reconfigurability is one of the most important characteristics of the mission as it forms a large part of the market case, meaning it will be one of the main reasons why a customer would choose to transfer their payload to the Moon using this lander. It refers to switching the internal structure of the lander to a version that can have a better performance for its corresponding configuration, either crew or cargo. The process will follow directly after the OTV and lander are docked to each other (step 13.0 of the refuelling procedure), which can also be seen in the operational block flow diagram of the reconfiguration process in Figure 18.4. The spacecraft that the lander will dock to during the reconfiguration procedure will be referred to as the in-orbit vehicle (IOV).

Having two different configurations creates four possible combinations that can happen during the operation of the mission, which are stated in boxes 17.1, 17.2, 17.3, and 17.4 with their unique operations merging into one universal flow later to finalise the procedure. The differences between the combinations originate from the idea that there must be a crew present in the process, either the crew that performed the previous mission, the crew launched with the ascent spacecraft, or the crew that was already on the ISS, as having crew present was concluded to be a better option in the midterm

report [14]. Another reason is the fact that the seats, displays, controls, and parts of the ECLSS will have to be removed or integrated back while changing the configuration between crew and cargo.

### Lunar Descent & Ascent

Lunar descent & ascent operations are essential to the mission as they should ensure safe and reliable landing and departure from the lunar surface. These operations must be carefully planned and executed, using advanced technologies such as descent RADAR for altitude, Optical Navigation Systems (ONS) for visual terrain recognition and descent LIDAR for high-resolution terrain mapping.

Figure 18.4 shows the high-level operational flow of the procedure. The descent begins from the 10 km LLO with a systems check before re-calibrating the IMUs to ensure accurate navigation. Powered Descent Initiation follows from this, whereafter RADAR, ONS and LIDAR are activated. Upon activation of these systems, the lander has better reconnaissance of the surface, and thus small trajectory adjustments are possible. The descent is completed by a controlled touchdown, subsequently shutting down the engines and deactivating the sensors.

The ascent procedure then starts at block 16.0, where it is necessary to switch the RADAR and ONS sensors back on to ensure an accurate trajectory. The ascent burn is followed by more trajectory verifications and small adjustments to reach the desired orbit. Once the ascent procedure is complete, the lander performs LOI and a systems check to confirm readiness for the next mission phase.

### Extra-Vehicular Activities

In any crewed mission destined for a lunar touch-down, extra-vehicular activities (EVAs) are inevitable events. These can include scientific activities, construction, exploration, and maintenance if applicable. It should be noted that the activities depend greatly on the nature and the objectives of the mission. If the objective is to colonise the Moon, then it is expected to have EVAs mainly for the construction of the lunar base. If the objective is to understand and explore the lunar environment, then scientific activities and exploratory voyages can be expected. In any case, the design of specific EVA activities is not part of the ARCH-E mission objectives. Thus it will be left to future missions to design these activities. The ARCH-E mission does provide a comprehensive overview of how EVA activities should be approached, including preparations, system checks, operations, and close-out procedures. The operational procedures concerning the success of EVAs and the safety of astronauts that are universal across missions can be seen in the operational block flow diagram in Figure 18.5.

As can be seen in Figure 18.5, the procedures mainly follow from crew safety concerns listed in Section 18.2, but also the vehicle and equipment being used. Since the duration and frequency of EVAs are limited, these activities should be planned and executed carefully. Thus, briefing both before and after the EVA is critical, as is managing gathered data and reporting all the findings. Adhering to all other safety procedures and recommendations is necessary to ensure the success of the EVAs.

### End-Of-Life Procedures

End-of-life (EOL) procedures considered for ARCH-E are twofold. Depending on whether the ultimate mission is for cargo or crew, different EOL procedures may be implemented. These will focus on the continued use or safe disposal of the spacecraft, respectively. The lander and OTV may thus have different fates depending on the last mission, as will be explained below.

**1. Crew case: Controlled Re-Entry** This will ensure ARCH-E's safe disposal by re-entering Earth's atmosphere and burning up, minimising space debris or other potential hazards. The start of the ultimate mission will look the same as any other. The OTV performs a free-return trajectory and arrives back at Earth, while the lander spends some time on the lunar surface after which it also returns to Earth. However, before the OTV returns back to Earth it must perform an MCC such that it will perform direct-controlled re-entry, whereby it targets a specific remote area over the Pacific Ocean to prevent falling debris hazards. The lander on the other hand must first enter LEO, as it is still carrying the crew. The lander then docks to a station where the crew is able to transfer, and all other desired equipment

will be removed from the lander. It then performs a series of de-orbit burns to lower the spacecraft's perigee into Earth's atmosphere, after which it follows a controlled re-entry trajectory. The target point for both vehicles will be point Nemo, which is the point farthest away from land and is frequently used as a spacecraft graveyard. During the trajectory through Earth's atmosphere, the spacecraft burns up due to aerodynamic heating, safely disintegrating. Note that this means the spacecraft will not be recovered. A diagram of this procedure is shown below in Figure 18.6.

**2. Cargo case: Lunar Surface Support Station (LSSS)** This is not done for the crew configuration, as the lander would need to complete an extra trip to the Moon after deploying the crew back in LEO, resulting in a large unnecessary $\Delta V$ expenditure and thus extra costs. This will ensure the continued utility of ARCH-E by bringing the lander onto the lunar surface where it can act as an interface between lunar-bound spacecraft and the lunar surface, providing critical support for future missions. This procedure should minimise space debris or other potential hazards while still retaining the functional aspects of the lander. To mention some specific functions, ARCH-E will be able to act as a relay station for communications between Earth and the lunar surface. It will also serve as a cargo hold for other lunar missions. Furthermore, ARCH-E may serve as a platform to host scientific instruments for observations and lunar surface experiments. Lastly, the spacecraft could be used as a power supply or act as a navigation reference point for other nearby landers. While the OTV is designated with the same fate as in option 1, the lander will simply remain on the lunar surface. Subsequently, its systems will be adjusted to limit energy consumption, the solar panels should be adjusted to maximise energy absorption and communication links should be set up with Earth. When other missions wish to access the lander, similar procedures apply to the EVA in terms of the hatch opening. A diagram of this procedure is shown below in Figure 18.7.

### Ground Support

Ground support provided by mission control centres ensures that mission objectives are met while maintaining the safety and functionality of the spacecraft and crew. The role of ground support is to communicate with the crew or other spacecraft, track the spacecraft and detect any failures or anomalies that occur during the vehicle's lifetime, which can then be fixed remotely by mission control. The operational block flow diagram of the ground support operations can be found in Figure 18.8.

## 18.2. Operational RAMS

There are universal operational aspects that should be taken into account in any mission, namely the reliability, availability, maintainability, and safety of the mission, as they affect the decisions made in the design phase and set additional constraints that should be complied with by the design. These aspects will be discussed based on the operational procedures mentioned in Section 18.1.

### Reliability

The reliability of the refuelling system is critical, as it must perform multiple procedures without failure in harsh space conditions. Expected reliability metrics are based on past missions that have used similar in-orbit refuelling procedures, such as docking operations used by the SpaceX Dragon, and on refuelling simulations run by NASA. NASA demonstrated high reliability of these procedures, with a success rate above 95% [157]. To ensure high reliability, the design of a robust fuel transfer mechanism and reliable docking systems that can withstand orbital perturbations and mechanical stresses is necessary.

The reconfiguration procedure similarly must perform multiple operations without failure in harsh conditions. The main difference is that whereas for refuelling there may be one standard procedure, for reconfiguration there are four. This means that several more possible failure points exist for the reconfiguration procedure. Furthermore, estimating values for the reliability of this procedure is an unconventional task, as these procedures have not been implemented in previous space missions and ARCH-E will be pioneering in this field. There is a general consensus that modularity provides a level of redundancy and robustness to failures, although each subsystem may become less reliable (e.g.

failures at connections) [158]. Nevertheless, a component-based reliability estimation approach may be employed to obtain a high-level reliability figure for the reconfiguration process. A tool should be used that can simulate the reconfiguration procedure and estimate its reliability this way. In any case, the procedure should be designed such that it at least matches with the mission reliability of 95 %.

Concerning the lunar ascent and descent procedure, reliability may be estimated by its components. According to [159], when using RADAR, LIDAR and trajectory control sensors, the lunar landing procedure has a reliability of 99 % which is feasibly high considering the mission standards. This may be attributed to the presence of multiple sensors which build redundancy when they run in parallel. They also estimate the reliability of automated proximity operations (such as docking and rendezvous) to be 98.97 %.

### Availability

A high availability means that the refuelling system is ready for operation whenever needed. Referring to Figure 18.2, specifically block 4.0, it becomes clear that the option of using a refuelling vehicle that is already in LEO would be beneficial in terms of availability. Launching the refuelling vehicle into orbit every time is operationally and logistically much more complex than just focusing on phasing manoeuvres. Furthermore, the refuelling system should have minimal downtime to ensure that it may be used whenever needed. Additionally, the system should have a fail-safe design, so that it can remain partly operational in case of a failure. This would also contribute to reliability.

An inherent property of the reconfiguration philosophy is that it has a high availability. In [158] is reported that modularity ensures that the overall system has a higher availability and improved ability to recover from failures. A procedure has been defined to reconfigure the lander for each possible changeover. The design thus facilitates quick swaps and repairs of components such as ECLSS modules or control interfaces, which are designed with standardised interfaces allowing for fast replacement. This is similar to how payloads may be handled on the ISS using the Common Berthing Mechanism (CBM) [160]. Nevertheless, a robust and fault-tolerant design should be employed to ensure that the availability of the mission remains high. Hence, whatever mission is needed next, the crew may simply adjust the vehicle for this specific mission, making it readily available for further use.

### Maintainability

An important consideration concerning the maintenance is the requirement **HOPE-MISS-090**. This requirement implies that scheduled in-space maintenance should not be an option. Nevertheless, in the event of a part being in critical condition and requiring maintenance, it should be performed to avoid catastrophic failures. Maintenance may consist of pre-refuelling checks and fuel system maintenance. Diagnostics of the fuel transfer mechanism and docking mechanism should be conducted prior to these activities. This could include checks on alignment sensors and seals. Furthermore, it could include possible calibration of fuel flow meters or fuel pumps which should be conducted to ensure accurate fuel transfer. EVA activities such as replacing seals may be necessary to preserve the integrity of the fuel transfer mechanism (**R-PROP-09**). Maintenance may also include emergency leak containment or anomaly response procedures. The system should thus be equipped with leak detection sensors, and there should be contingency measures in place in the event that a leak occurs. The maintenance for this involves replacing/repairing parts of the fuel line. In case of a failed docking manoeuvre, there should be diagnostics in place that can detect and rectify the fault. Consequently, it may be required to replace damaged components like fuel nozzles or docking clamps.

The lander's level of maintainability is strengthened by its modular design, which allows for components to be removed individually. This eliminates the need for extensive disassembly while undergoing replacement procedures. Again, this approach has similarities to the ISS which also allows individual sections to be replaced or removed. To ensure that this theoretical high maintainability is materialised, there should be detailed training programs in place, which should be enhanced by the use of specialised tools. Regular diagnostic checks such as those presented in Figure 18.3 also guide the maintenance process, enabling both astronauts and possibly automated systems to perform their tasks.

### Safety

Safety measures for refuelling in LEO consist of maintaining safety-critical functions and applying a redundancy philosophy. Safety-critical functions include for example leak detection in fuel transfer systems, emergency disengagement mechanisms for docking, and automatic shutdown systems. Active redundancy measures can be used to back up these functions, such as duplicating critical components like pumps, clamps, or valves that can take over instantly after failure. Passive redundancy systems may also be employed, and involve fail-safe designs that can bring the system to a safe state after a failure.

As mentioned previously, Figure 18.3 shows that there are diagnostic checks in place during the reconfiguration procedure. Aside from contributing to the maintainability of the procedure, these also enhance the safety aspect. For example, if an anomaly is detected in pressure, humidity, or during ECLSS configurations, the system can stop the procedures and indicate that maintenance should be performed. Furthermore, redundant ECLSS is employed, and backup power systems will be activated in the event that the primary system fails. In terms of crew safety procedures, there are emergency procedures in place designed to safeguard the crew. These should be practised regularly, as would occur on the ISS.

For EVAs, an additional safety analysis is required due to the hostile space environment which demands a high degree of risk management to ensure astronaut safety. There are several safety considerations and safety-critical functions for this part of the mission. Pressure integrity of the space suit is necessary to prevent decompression sickness. Functional oxygen supply and $CO_2$ scrubbing systems are needed to provide breathable air and prevent hypoxia. Temperature regulation is necessary to prevent hypothermia and to protect astronauts from extreme space temperatures. Another vital aspect is a functioning communication system to guide astronauts in case of an emergency. Restraints like tethers are crucial to prevent astronauts from drifting into space. The crew's health should also be monitored to ensure that they remain in safe operating conditions. In the event of an emergency, there should be safety protocols in place for astronaut rescue. Redundant ECLSS should be available in case of primary system failure. Lastly, astronauts should be able to manage small tears in their suits through access to suit repair kits. These functions are reflected in Figure 18.5.

Concerning the lunar descent and ascent procedure, safety is extremely important when the lander is in crew configuration. Humans are not robust compared to the spacecraft itself and hence appropriate measures must be realised to ensure the safety of the crew. In general, safety-critical functions include the ability to perform trajectory adjustments, precise engine thrust control, and accurate altitude measurement using RADAR and LIDAR. Hazard detection and reliable communication with ground control are also necessary. These functions must also limit the acceleration experienced by the crew to prevent injuries or fatalities.

### Reusability

Reusability can be derived from the lifetime requirement of the OTV and lander. They must not malfunction, so it should not be necessary to replace them with a new OTV or lander. This aspect increases the frequency of missions/TLIs and decreases the operational costs significantly. In order to have both a reusable OTV and lander, the durability of the subsystems plays a vital role in avoiding malfunctions and allowing for reusing both the OTV and the lander. Therefore, the reliability of both vehicles should be sufficient to reduce the risk of failure scenarios.

The reusability performance of the lander is set by the customer requirement **HOPE-MISS-080**, which requires at least 10 Earth-Moon return trips in both configurations. One of the subsystems that need special attention to meet this requirement is the propulsion subsystem. Engine failure is a high-risk event (**R-PROP-01** through **R-PROP-04**) due to the relatively low reliability characteristics of the propulsion subsystem compared to other subsystems. The number of burn cycles should also be analysed in detail to allow for the required Earth-Moon return trips as it is an important parameter constraining the lifetime of the engine and hence the propulsion system.

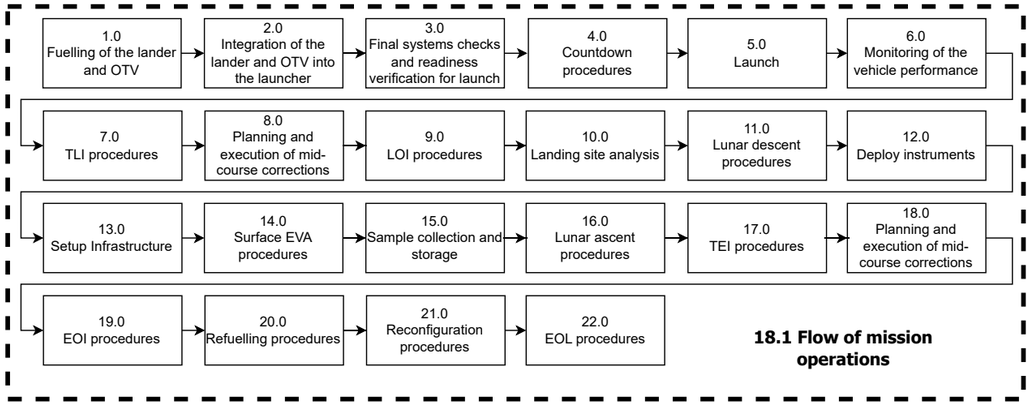


**18.1 Flow of mission operations**

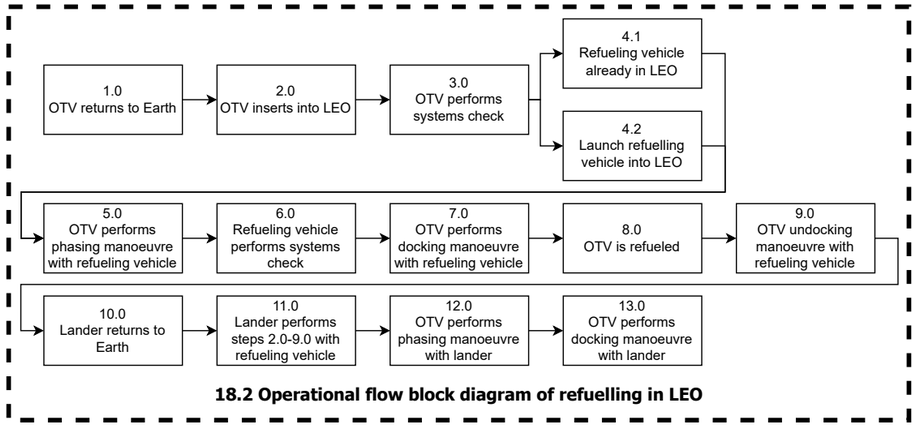


**18.2 Operational flow block diagram of refuelling in LEO**

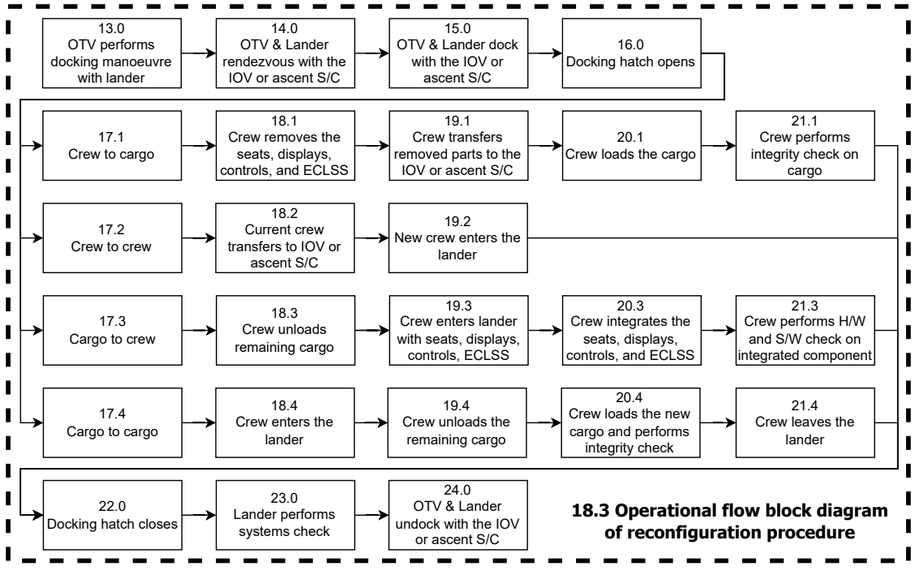


**18.3 Operational flow block diagram of reconfiguration procedure**

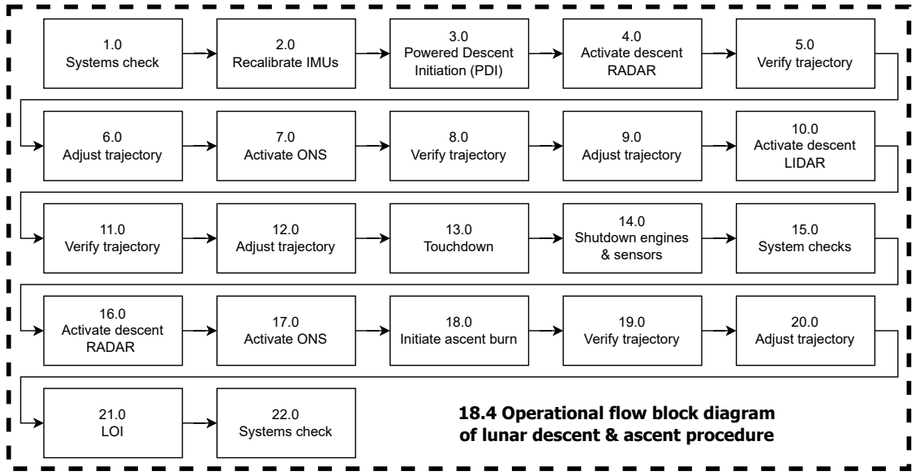


**18.4 Operational flow block diagram of lunar descent & ascent procedure**

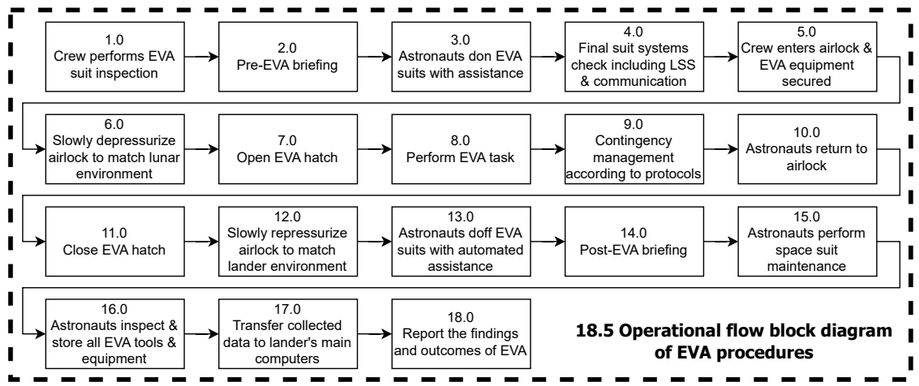


**18.5 Operational flow block diagram of EVA procedures**

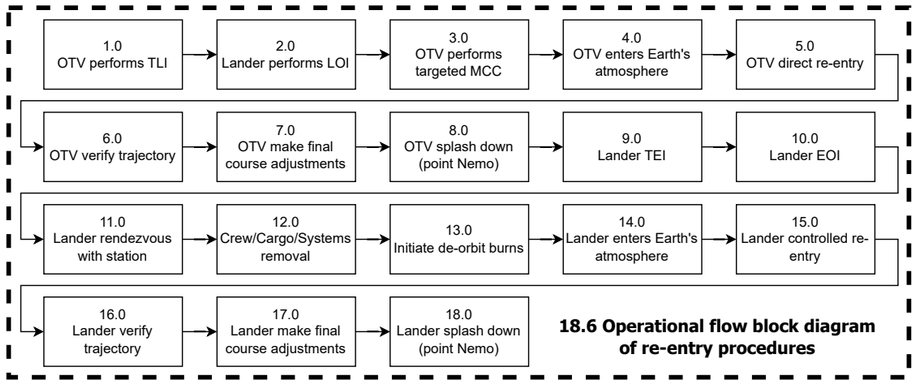


**18.6 Operational flow block diagram of re-entry procedures**

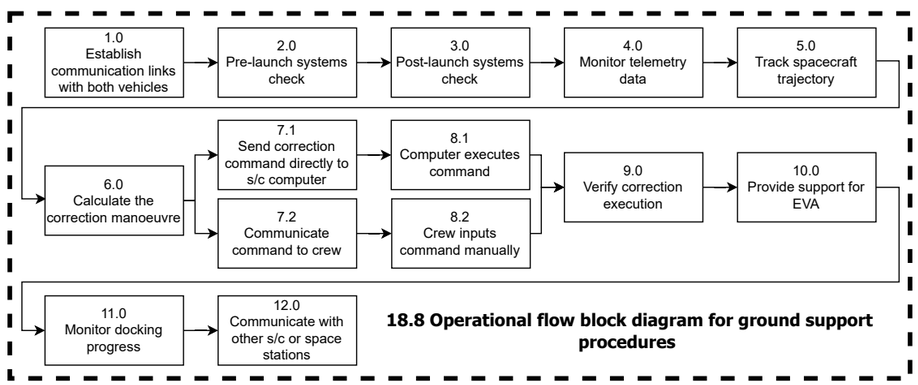


**18.8 Operational flow block diagram for ground support procedures**

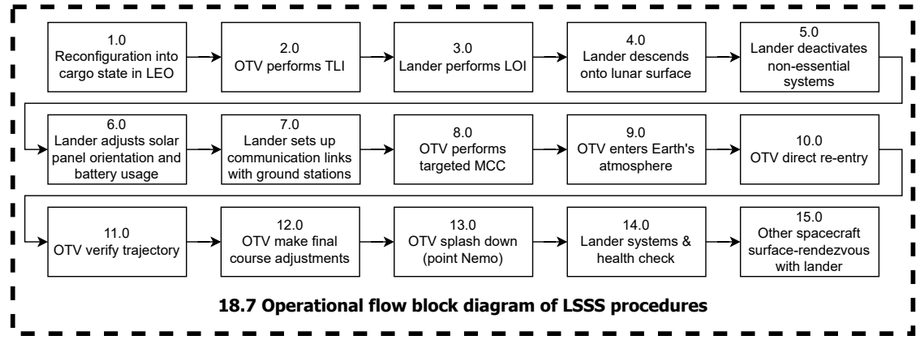


**18.7 Operational flow block diagram of LSSS procedures**

# 19 | Sustainable Development Strategy

A comprehensive life cycle assessment of a vehicle is crucial for ensuring its sustainable production and utilisation throughout its entire life span [161]. This assessment evaluates emissions and environmental impacts during each phase: design, production, nominal operations, and disposal. The ARCH-E mission prioritises sustainable practices by incorporating reusability and reconfigurability as key features. These attributes enhance the vehicle's versatility and value, significantly reducing its environmental footprint by enabling up to 10 missions to the moon, unlike single-use vehicles like Apollo.

Previous research indicates that integrating environmental performance considerations early in the design phase and including them as a main component of the concurrent design organisation leads to substantial improvements in sustainability [161]. In line with this, the design process of ARCH-E incorporated sustainability into all relevant trade-offs. This approach ensures that every aspect of ARCH-E's development aligns with the mission's sustainability goals and requirements from initial design decisions to the final phases of its lifecycle. These requirements are listed in Table 19.1.

**Table 19.1:** Sustainability Requirement Verification

| ID | Requirement | Rationale | Verification | Check |
|---|---|---|---|---|
| HOPE-SUST-010 | A spacecraft or launch vehicle orbital stage operating in Earth orbit shall include passivation capabilities. | Hazard avoidance, [162] | Demonstration | ✓ |
| HOPE-SUST-020 | The orbital element injected into Earth orbit shall guarantee that it can be tracked by a space surveillance segment supporting collision avoidance processes. | Traking of vehicle, [162] | Testing | ✓ |
| HOPE-SUST-040 | In Lunar orbit, intentional break-up of a spacecraft or launch vehicle orbital stage shall not be performed. | Contamination, [162] | Demonstration | ✓ |
| HOPE-SUST-050 | The space and ground segments associated with a spacecraft or launch vehicle orbital element shall be designed to have ephemerides available for space traffic coordination. | Continuous tracking of vehicle, [162] | Testing | ✓ |
| HOPE-SUST-060 | The vehicle shall be cleared from LEO or GEO protected area deliminated by ESA after mission is terminated | Derived from ESA Space Debris Mitigation Requirements, [162] | Inspection | ✓ |

## 19.1. Design and Production

The selection of propellants is crucial for the lander's sustainable design. For propulsion, LH2 and LOX were chosen, producing non-toxic hydrogen and water vapour as exhaust, which have negligible impact on the lunar atmosphere. The OTV uses Methane and LOX, resulting in carbon dioxide and water vapour. Since the OTV operates solely in space, these gases disperse harmlessly in the vacuum, minimising environmental impact [163]. This strategic choice ensures minimal environmental consequences while maintaining necessary performance.

Material selection for ARCH-E is another area where sustainability has been rigorously applied. The choice of materials considers not only their performance and durability but also their environmental footprint. During the trade-off to quantify the sustainability criteria of the materials two main aspects were analysed their embodied energy, which quantifies the total amount of energy associated with the extraction, processing, production, and delivery of a material and secondly its recyclability. These aspects were quantified by Matmatch, on their complete guide to sustainable material selection [164].

Space debris is the main challenge regarding the sustainable development of the space industry [165]. Therefore, the vehicle's design includes specific features to address this challenge. The first is the ADCS and GNC systems, which include hazard avoidance capabilities integrated into control modes and maneuver capacities, as required by **HOPE-SUST-010**. Another capability, mandated by **HOPE-SUST-060**, is the provision of ephemerides values for space traffic control. This is achieved

through attitude determination sensors and an improved communication system, allowing precise tracking and reporting for collision avoidance and traffic coordination. To prevent the spacecraft from contributing to space debris through in-orbit breakups, it is designed with robustness in mind, minimising the number of separate components and reducing potential failure points. By using as many integral parts of the structure as possible, the design minimises the risk of parts breaking off and creating additional debris, as required by **HOPE-SUST-050**.

The production of the ARCH-E lunar lander follows a lean manufacturing strategy to reduce waste and maximise value. This approach improves production efficiency by cutting down unnecessary transportation, using just-in-time production, and continuously improving logistics. Sustainable materials are prioritised, using recycled and locally sourced where possible and with eco-friendly extraction methods. Energy-efficient practices, like using renewable energy and advanced machinery, further reduce environmental impact. This integrated strategy makes ARCH-E's production both environmentally responsible and highly efficient.

## 19.2. Nominal Operation and End-of-Life

During the missions, its operations also aims to minimise environmental impact. According to requirement **HOPE-SUST-030**, the vehicles will be tracked by the ground segment, with real-time comparisons to the Space Surveillance Tracking (SST) segment and the Meteoroid and Space Debris Terrestrial Environment Reference (MASTER) model by ESA [166] to be able to predict any severe collisions. ARCH-E will also carry a sensor known as DEBIE-1[1], a standard in-situ impact detector, which will help detect and track debris in its orbit while assisting ESA in refining its model by reducing major uncertainties.

To ensure ARCH-E operates in compliance with the United Nations Moon Agreement[2], the mission must be designed for peaceful purposes, focusing on scientific research or technological demonstration. The mission operations must minimise environmental impact, prevent contamination, and follow protocols for safe disposal of the lander. Transparent communication international community about the mission's objectives and plans is essential. Following, these sustainable operational procedures will also make ARCH-E align with stakeholder requirement, **HOPE-STK-ADS-031**, where ARCH-E is required not to contaminate the lunar surface with any significant debris.

The end-of-life consideration for ARCH-E is highly sustainable due to its design for reutilisation and adaptability. By repurposing the payload bay to store various payloads on the lunar surface and enabling it to be used as a future lunar habitat or storage bay. The spacecraft infrastructure is valuable as it has already been designed to support crew and payload therefore only minor changes would be required in the lunar surface for it to serve as a lunar storage place. Secondly, the OTV will be safely disposed, via reentry into Earth's atmosphere, ensuring it does not contribute to space debris accumulation in ESA's LEO protected area. This operation aligns with sustainability requirement, **HOPE-SUST-070**.

Finally, a recommendation for ARCH-E to ensure sustainable practices in its future phases is to seek a ranking by the Space Sustainability Rating[3], a new initiative designed to promote sustainability in the space industry. This rating will help monitor and enhance ARCH-E's sustainability performance, ensuring that it minimises its environmental impact while also promoting responsible space operations across other missions or companies.

[1] URL https://space-env.esa.int/r-and-d/instrumentation/standard-in-situ-impact-detector-debie/ [cited 15 June 2024]

[2] URL https://www.unoosa.org/oosa/en/ourwork/spacelaw/treaties/moon-agreement.html [cited 15 June 2024]

[3] URL https://spacesustainabilityrating.org/ [cited 12 June 2024]

# 20 | Verification and Validation

This chapter outlines the verification and validation procedures that will certify the functionality of the overall system, as detailed in Section 20.1. According to NASA definitions, verification provides proof of compliance with design specifications and descriptive documents, while validation demonstrates that the product meets its intended purpose based on stakeholder expectations. Next, the level of mission compliance with the system requirements is detailed in Section 20.2.

## 20.1. Verification and Validation Procedures

This section outlines the methods of verification and validation, and elaborates on specific procedures that could be implemented for this mission's system.

**Testing:** Testing involves the use of a final product to gather data needed to verify a requirement, or to gather sufficient information to verify the requirement through further analysis. It produces data at discrete points under controlled conditions for each requirement. It is also the most resource intensive method of verification[1]. A list of possible tests that may be performed on the spacecraft is presented below[2]. **Flatbed Test** The spacecraft's components will be laid out on a flat platform to test their functionality. The required materials for this test may be a flat platform, simulation equipment and monitoring tools. **Vibration Test** The spacecraft or its components will be subjected to vibrational forces to simulate conditions during launch. The required materials for this test may be a vibration table, accelerometers, and data acquisition systems [167]. **Thermal Vacuum Test** The spacecraft or its components will be exposed to a vacuum environment and extreme temperatures to test thermal systems. The required materials for this test may be a thermal vacuum chamber, temperature control systems and vacuum pumps. **Electromagnetic Compatibility Test** The spacecrafts electronic systems will be run to test whether they interfere with each other. The required materials for this test may be an EMC chamber, spectrum analysers and signal generators. **Acoustic Test** The spacecraft or its components will be exposed to high-intensity sound waves to simulate conditions during launch. The required materials for this test may be an acoustic chamber, high-power speakers and microphones. **Shock Test** The spacecraft or its components will be subjected to sudden high loads to simulate conditions during events such as separation. The required materials for this test may be a blunt force machine, accelerometers and data acquisition systems. **Radiation Test** The spacecraft or its components will be exposed to radiation levels expected in space to test whether it can function under these conditions. **Deployment Test** Mechanisms such as the solar arrays, antenna or scientific instruments will be deployed to test their functionality. **Burn-in Test** The spacecrafts systems will be run for an extended period of time to test for early failures. **Software Verification Test** The spacecraft's software will be tested under scenarios to test their functionality and reliability. **System Integration Test** The spacecraft's subsystems will be tested for their functionality once integrated into the complete spacecraft.

**Testing Locations:** NASA's diverse simulation and testing facilities are critical for developing and validating next-generation landers. At NASA Langley Research Center, the Flight Simulation Facilities (FSF) provide high-fidelity simulations for refining control systems, while the Vertical Motion Simulator (VMS) at Ames Research Center offers realistic piloted simulations for evaluating lander handling. The Space Environments Complex (SEC) at Glenn Research Center simulates launch and flight stresses, and the Space Environment Simulator at Goddard Space Flight Center tests lander materials under extreme thermal and vacuum conditions. Additionally, Goddard's Spacecraft Magnetic Test Facility ensures proper functioning of magnetic-sensitive instruments, and the Sunspot Thermal Vacuum Testing Facility at Marshall Space Flight Center exposes landers to the harsh environments of space. These facilities collectively ensure that landers meet all performance and safety standards for their missions[3]. Through the NSTF, RAL Space provides facilities for the final integration and testing of

[1] URL https://www.nasa.gov/reference/5-3-product-verification/#hds-sidebar-nav-6 [cited 19 June 2024]
[2] URL https://www.esa.int/Science_Exploration/Space_Science/Building_and_testing_spacecraft [cited 19 June 2024]
[3] URL https://www.nasa.gov/setmo/facilities/ [cited 19 June 2024]

large space payloads and satellites. The NSTF offers two spacious test preparation clean rooms along with a comprehensive suite of test facilities, all within a clean environment. These resources can be utilised for the integration and testing of the ARCH-E lander[4].

**Analysis:** Analysis is the use of mathematical models to verify that a product complies with a specified requirement. This can be done through either analytical methods or simulations. Analysis is typically used when testing is to verify a requirement is not possible. Usually, because it is too expensive, technically infeasible, poses an unacceptable risk, or is incompatible with the project timeline. Examples include the thermal analysis of a subsystem to ensure the appropriate operating temperature is maintained or the shift in the center of mass throughout the mission[1] [168, 169].

**Inspection**: Inspection consists of the visual examination of the final product, which is used to verify physical design features. This could include inspection of drawings and documents. The prime example would be to verify the total spacecraft mass requirement by simply placing it on a scale and reading the measurement[1]. **Visual Inspection** The spacecraft or its components will be examined for visible defects and irregularities. **Weighing** The spacecraft or its components will be placed on a scale to determine their mass and check whether they comply with design specifications. **Measuring** The spacecraft's or its component's dimensions will be assessed to check whether they comply with design specifications.

**Demonstration:** Demonstration consists of showing that the use of the final product complies with a specified requirement. It can be seen as a confirmation of performance capability which differs from testing because of the lack of detailed data gathering. This may involve either the use of either physical models or mock-ups to verify the requirement. For instance, ensuring that all controls are reachable by the astronaut can be verified by having an astronaut perform mission tasks in a spacecraft mock-up or simulator. Demonstration may also involve the operation of final products by the astronaut. Astronauts could also demonstrate the capability to operate the spacecraft at extreme performance limits, such as complex EVAs or testing the spacecraft's ability to withstand harsh conditions[1]. **Functional Demonstration** Demonstrating basic operation of the spacecraft or its components to verify performance. **Operational Demonstration** Performing tasks with the spacecraft under realistic operational conditions to verify performance. **Pilot-in-the-Loop Demonstration** An astronaut will perform tasks in or on the spacecraft, or possibly a simulator to verify human factors and compatibility. **Deployment Demonstration** Mechanisms such as the solar arrays, antenna or scientific instruments will be deployed to demonstrate their reliability. **End-to-End System Demonstration** Testing the entire spacecraft from beginning to end of mission to ensure all components function. **Emergency Procedure Demonstration** Simulating emergency procedures to test the crew's and spacecraft's response. **Autonomous Operations Demonstration** Demonstrating the spacecraft's ability to autonomously perform operations.

## 20.2. Mission Requirement Compliance

This section outlines the expected mission compliance with the requirements. It discusses the rationale behind partially and non-compliant requirements in Section 20.2. Additionally, Table 20.1 provides details on the compliance status and verification methods for the remaining requirements.

### Partial and Non-Compliant Requirements

The non-compliant requirements have been assembled and are listed below. These are followed by a brief explanation regarding their non-compliance. **HOPE-MISS-090** The lander vehicle shall require no in-space maintenance for a minimum design lifetime of $10$ years: At this stage, the design is expected to be partially compliant with HOPE-MISS-090 because this requirement would drive the design to an unacceptable extend. Nonetheless, the vehicle has been designed to minimise in-space maintenance as much as possible. **HOPE-MISS-120** The launch cost shall be lower than 25 k€/kg of payload delivered to the Moon (calculated taking into account only recurring costs, not including

[4]URL https://www.ralspace.stfc.ac.uk/Pages/Large-scale-test-facilities.aspx [cited 19 June 2024]

any development or qualification costs): The design will only be partially compliant with requirement HOPE-MISS-120 due to the complicated nature of the design. The recurring cost is driven primarily by the need to refuel the vehicle every mission. Nonetheless, the design is still partially compliant because recurring costs have been minimised as much as is reasonably possible. **HOPE-SYS-330** The vehicle shall be capable of $156$ hours of uninterrupted surface operations in continuous darkness: The lander will not be compliant with **HOPE-SYS-330** because it would drive the design to an unacceptable extent that would lead to the mission becoming unfeasible.

**Table 20.1:** Mission Requirements

| ID | Verification Method | Value | Check |
|---|---|---|---|
| HOPE-MISS-010 | Testing: Simulate the payload integration, launch, and delivery, ensuring the total mass meets or exceeds the specified threshold. | 5000 kg | ✓ |
| HOPE-MISS-020 | Inspection: Measuring dimensions of the cargo compartment will give the usable volume, which is a straightforward way to check compliance. | 50 $m^3$ | ✓ |
| HOPE-MISS-030 | Analysis: Assess its capacity, conduct simulations or mock-ups, review life support systems, evaluate human factors, and ensure compliance with safety standards and operational scenarios. | 4 | ✓ |
| HOPE-MISS-040 | Demonstration: An end-to-end system demonstration will simulate the complete mission profile, which can verify the vehicle's capability to autonomously execute the aforementioned mission phases. | Compliance Expected | ✓ |
| HOPE-MISS-060a | Inspection: Since the materials and propellants used exist already, a simple safety inspection may verify that all materials and propellant comply with the non-toxicity standard and health and safety regulations. | Compliance Expected | ✓ |
| HOPE-MISS-070 | Analysis: A reliability analysis may be conducted using statistical methods to determine failure rates based on historical data and/or simulations. | Compliance Expected | ✓ |
| HOPE-MISS-080 | Analysis and demonstration: Assess structural integrity, component reliability, thermal protection, propellant efficiency, flight software capability, and ground handling procedures, and conduct simulated mission tests to validate performance under varied operational conditions, the final confirmation will follow from performing the mission. | 10 | ✓ |
| HOPE-MISS-090 | Analysis: A reliability or durability analysis based on historical data or simulations will output failure rates and degradation rates which will indicate whether maintenance must be performed. | Partial Compliance Expected | × |
| HOPE-MISS-120 | Analysis: detailed analysis of all recurring costs, including launch vehicle procurement, launch operations, mission operations, and propellant expenses. | Partial Compliance Expected: 45.73 k$/kg | × |
| HOPE-MISS-150 | Testing: Functional assessments of life support systems, safety drills for emergency scenarios, environmental stress testing, integration with other spacecraft systems, human factors evaluations, and compliance with regulatory standards. | Compliance Expected | ✓ |
| HOPE-MISS-161 | Testing: Simulating engine failures, inducing sensor degradations, and assessing the vehicle's ability to maintain trajectory and stability using redundant systems and controlled simulations. | Compliance Expected | ✓ |
| HOPE-MISS-180 | Testing: An ECLSS test should be conducted to evaluate systems that create a habitable environment. This includes air quality/temperature control, waste management, and water supply in simulated mission conditions. | Compliance Expected | ✓ |
| HOPE-MISS-190 | Analysis: An analysis on habitat sustainability is performed to determine the required ECLSS and power requirements which is used to verify whether the spacecraft meets this specification. | $6.5$ days | ✓ |
| HOPE-MISS-200 | Demonstration: A docking interface demonstration may be executed during a test mission which will verify whether the crew is able to transfer. | Compliance Expected | ✓ |

| ID | Verification Method | Value | Check |
|---|---|---|---|
| HOPE-MISS-210 | Demonstration: A global landing demonstration may be performed on various locations such as the lunar poles, equator, and highlands to verify whether the lander is capable of reaching and landing on any designated site. | Compliance Expected | ✓ |
| HOPE-MISS-220 | Demonstration: prototype functionality, conducting simulation exercises, and validating operational scenarios. | Compliance Expected | ✓ |
| HOPE-MISS-230 | Testing: A propellant transfer test can be performed using a controlled transfer of propellant between the staging vehicle and the mission vehicle in a simulated environment. | Compliance Expected | ✓ |
| HOPE-MISS-241 | Test: Load the vehicle with 100 kg of cargo and perform simulated transport operations from the lunar surface to LEO. | 2760.16 kg | ✓ |
| HOPE-MISS-270 | Demonstration: A test mission shall be performed to demonstrate the capability of the vehicle to return lunar samples. | Compliance Expected | ✓ |
| HOPE-MISS-271 | Demonstration: A test mission shall be performed to demonstrate the capability of the vehicle to return the human crew. | Compliance Expected | ✓ |
| HOPE-MISS-272 | Demonstration: A test mission shall be performed to demonstrate the capability of the vehicle to be refuelled in orbit. | Compliance Expected | ✓ |
| HOPE-MISS-272 | Demonstration: A test mission shall be performed to demonstrate the capability of the vehicle to be reconfigured in orbit. | Compliance Expected | ✓ |
| HOPE-MISS-274 | Demonstration: A test mission shall be performed to demonstrate the capability of the vehicle to be reloaded in orbit. | Compliance Expected | ✓ |
| HOPE-MISS-275 | Analysis: Run a numerical transfer simulation to determine the transfer time from LEO to the Moon and back (time of flight). | 2.888 days | ✓ |
| HOPE-MISS-276 | Analysis: Run a numerical transfer simulation to determine the transfer time from LEO to the Moon and back (time of flight). | 2.888 days | ✓ |
| HOPE-MISS-277 | Demonstration: A test mission shall be performed whereby the spacecraft in crew configuration will land on the lunar surface. | Compliance Expected | ✓ |
| HOPE-MISS-278 | Demonstration: A test mission will be performed to verify the capability of the spacecraft to collect and return lunar samples. | Compliance Expected | ✓ |
| HOPE-MISS-279 | Analysis, testing, and demonstration: perform analysis and sizing of the operations on the lunar surface, conduct tests in a similar mock environment, and monitor key parameters during the mission to demonstrate that the selected lunar parking orbit enables successful cargo landings on the lunar surface. | Compliance Expected | ✓ |
| HOPE-MISS-290 | Analysis: Perform numerical launch simulations to verify whether the launch azimuth is compliant for every mission. | Compliance Expected | ✓ |
| HOPE-MISS-LEG-010 | Inspection: mission documentation and compliance certificates, and consult with space law experts to verify adherence to the Outer Space Treaty of 1967. | Compliance Expected | ✓ |
| HOPE-MISS-LEG-020 | Inspection: reviewing the mission documentation and obtaining certification from Airbus Defence and Space UK. | Compliance Expected | ✓ |
| HOPE-MISS-LEG-030 | Inspection: conduct a thorough review of mission plans and procedures, ensuring adherence to all relevant mitigation measures outlined in the guidelines. | Compliance Expected | ✓ |
| HOPE-MISS-LEG-040 | Inspection: review mission documentation and obtain confirmation of compliance from relevant UN COPUOS authorities or member states. | Compliance Expected | ✓ |
| HOPE-MISS-LEG-050 | Inspection: review the company's legal requirements and obtain confirmation of compliance from legal counsel or regulatory authorities overseeing the launch operations. | Compliance Expected | ✓ |
| HOPE-MISS-LEG-060 | Inspection: legal documentation, permits, and regulatory approvals obtained for the mission, ensuring adherence to national laws governing space activities at the launch site. | Compliance Expected | ✓ |
| HOPE-MISS-LEG-070 | Inspection: mission documentation, procedures, expert consultation, and certification from regulatory authorities. | Compliance Expected | ✓ |

**Table 20.2:** System Requirements

| ID | Verification Method | Value | Check |
|---|---|---|---|
| HOPE-SYS-010 | Demonstration: A test launch to LEO will be performed to verify successful deployment of the spacecraft by the launcher. | Compliance Expected | ✓ |
| HOPE-SYS-020 | Testing: Vibration tests and shock tests will subject the system to expected launch loads to verify whether it can handle launch conditions. | Compliance Expected | ✓ |
| HOPE-SYS-060 | Demonstration: A passivation demonstration will safely neutralise the stored chemical energy sources in the vehicle, such as propellants and batteries. | Compliance Expected | ✓ |
| HOPE-SYS-070 | Demonstration: A containment demonstration involves monitoring the spacecraft during a test mission to verify whether all components stay in place. | Compliance Expected | ✓ |
| HOPE-SYS-081 | Analysis: A mathematical simulation of the trajectory is used to determine the accelerations experienced by the spacecraft. | Compliance Expected | ✓ |
| HOPE-SYS-082 | Analysis: A mathematical simulation of the trajectory is used to determine the accelerations experienced by the spacecraft. | Compliance Expected | ✓ |
| HOPE-SYS-083 | Analysis: A mathematical simulation of the trajectory is used to determine the accelerations experienced by the spacecraft. | Compliance Expected | ✓ |
| HOPE-SYS-084 | Analysis: A mathematical simulation of the trajectory is used to determine the accelerations experienced by the spacecraft. | Compliance Expected | ✓ |
| HOPE-SYS-085 | Analysis: A mathematical simulation of the trajectory is used to determine the accelerations experienced by the spacecraft. | Compliance Expected | ✓ |
| HOPE-SYS-086 | Analysis: A mathematical simulation of the trajectory is used to determine the accelerations experienced by the spacecraft. | Compliance Expected | ✓ |
| HOPE-SYS-100 | Analysis: A risk and impact analysis using probabilistic models may be used to evaluate the likelihood of collision and consequently penetration. | Compliance Expected | ✓ |
| HOPE-SYS-110 | Demonstration: An autonomous abort procedure can be performed during a test flight to demonstrate that the spacecraft is capable of this task. | Compliance Expected | ✓ |
| HOPE-SYS-120 | Demonstration: The vehicle may perform 10 test flights representing actual mission conditions to verify whether it can sustain this requirement. | Compliance Expected | ✓ |
| HOPE-SYS-130 | Demonstration: An end-to-end communication demonstration includes setting up and testing the spacecraft's communication capabilities during a test flight to the lunar surface. | Compliance Expected | ✓ |
| HOPE-SYS-140 | Testing: Docking compatibility test means testing docking interfaces between the system and HLS crew staging vehicles to ensure proper integration. | Compliance Expected | ✓ |
| HOPE-SYS-200 | Demonstration: A cargo test flight may be performed to the lunar surface to verify whether the cargo remains undamaged. | Compliance Expected | ✓ |
| HOPE-SYS-260 | Demonstration: A full test mission may be performed to verify whether the spacecraft leaves no components behind on the lunar surface. | Compliance Expected | ✓ |
| HOPE-SYS-280 | Demonstration: A docking interface demonstration may be executed during a test mission which will verify whether the crew is able to transfer without EVA. | Compliance Expected | ✓ |
| HOPE-SYS-300 | Demonstration: A docking interface demonstration may be executed during a test mission which will verify whether the cargo is able to transfer without EVA. | Compliance Expected | ✓ |
| HOPE-SYS-310 | Demonstration: An in-orbit refuelling demonstration should be performed during a test flight to demonstrate that the procedure is feasible. | Compliance Expected | ✓ |
| HOPE-SYS-330 | Testing and demonstration: Simulated tests, operational simulations, thermal analysis, power system validation, and endurance testing | 5.4 hrs | × |
| HOPE-SYS-360 | Analysis: A failure mode analysis may be performed to evaluate potential failure points which ensures that redundancy measures will be in place. | Compliance Expected | ✓ |
| HOPE-SYS-370 | Inspection: Lunar eclipse are known dates, hence future missions must simply be scheduled when they do not occur. | Compliance Expected | ✓ |

# 21 | Post-Design Study Activities

This chapter will start by providing an overview of all the activities to be performed after the completion of the phase 0 design study. This is supported by a Gantt chart showing the expected timeline from phase 0 up to and including phase F.

## 21.1. Project Design and Development Logic

The design activities to date correspond to pre-Phase A (or Phase 0) from ESA's project phasing standards [170]. Most of the work to complete the project has yet to come, during phases A-F. The development activities during these following phases up to EOL are shown in Figure 21.1. The Mission Definition Review (MDR) marks the end of phase 0, where the contents of this report are presented. This review outcome is used to judge whether the project is ready to move to phase A.

In phases A and B, the mission function and requirements are defined in further detail. The Preliminary Requirements Review (PRR) marks the end of phase A. The requirements definition continues beyond this and concludes in the Preliminary Design Review (PDR) in which phase B is concluded, and the decision is made on whether the design should continue to phase C. The main objective of the PDR is the verification of the preliminary design and solutions against project and system requirements [170].

Phase C includes the detailed design definition of all system elements, as well as the development of critical components and complete planning of assembly, integration, and testing [170]. This culminates in the Critical Design Review (CDR), which determines whether the project can move forward to phase D. The final design is released at this stage, as well as the complete planning for phase D.

In phase D, the production and qualification takes place. Production includes the manufacturing and acquisition of parts, assembly of components and subsystems, and vehicle integration. Acquisition includes procurement of parts and components from suppliers. In case custom parts are being acquired, this should be done as soon as possible after the CDR. When sufficient components have been acquired, the assembly will begin, which will run alongside the acquisition and manufacturing of parts. Finally, the vehicle integration continues until the end of the production phase. Alongside production, verification and validation takes place. All elements, from parts to integrated vehicles, undergo verification and validation against the design specifications and requirements. Software verification can begin immediately, while part verification can begin after parts start to arrive. Verification and validation of the integrated vehicle is the last step in this phase. The Qualification and Acceptance Review (QAR) is held at the end of phase D to determine whether the product is ready for delivery. This ensures that the verification process has demonstrated that the design meets the requirements and that the product is ready for use.

Phase D will differ from most traditional space projects because ARCH-E consists of two independent vehicles that will be produced and verified in parallel. This means that if delays are incurred during either production or verification with either of the two vehicles the project will be delayed as a whole. Thus particular care must be taken to ensure that both vehicle will be ready for the QAR at the same time.

Operations take place in phase E. Firstly, the space and ground segments need to be prepared for launch. This includes loading the vehicle into the launch vehicle and carrying out pre-flight checks. After the necessary launch preparations, the Flight Readiness Review (FRR) takes place. This verifies that the flight and ground segments are ready for launch [170]. Similar to phase D, special care must be taken to ensure that both vehicles will be ready for the FRR at the same time. The initial launches to place the vehicles in orbit can take place once the FRR is passed. First, both vehicles are launched and will be dock in LEO, the will then be followed by the pre-mission activities which includes the refuelling of the vehicle in LEO and verifying that all systems are operating nominally. At this point, the missions can begin. The mission operations phase is the longest part of the project, lasting ten years from 2030-2040. During this time, at least ten missions can be carried out. After the last mission,

phase E concludes with the End of Life Review (ELR). This confirms that the mission is completed and the EOL disposal plan is in place.

Finally, phase F covers the mission EOL, which is the safe disposal of all mission elements. Two options for end-of-life were discussed in Chapter 18, for either option, the OTV will be safely disposed of by reentry over Point Nemo, while the lander can either be disposed of similarly to the OTV, or used as cargo storage on the lunar surface. This will be followed by the Mission Close-out Review (MCR), to ensures that the vehicles have been disposed of as intended.

## 21.2. Project Outline

Figure 21.1 shows a gantt chart of the post-design study activities discussed in the previous section. The gantt chart begins at the start of the DSE (phase 0) and goes up to the end of life of the mission (phase F). The activities to be performed are shown in green, which are separated by the relevant design reviews. Margins have been included in the timeline to ensure that the project can progress as expected even if small delays are incurred. Finally, the expected start and end dates are given for each phase.

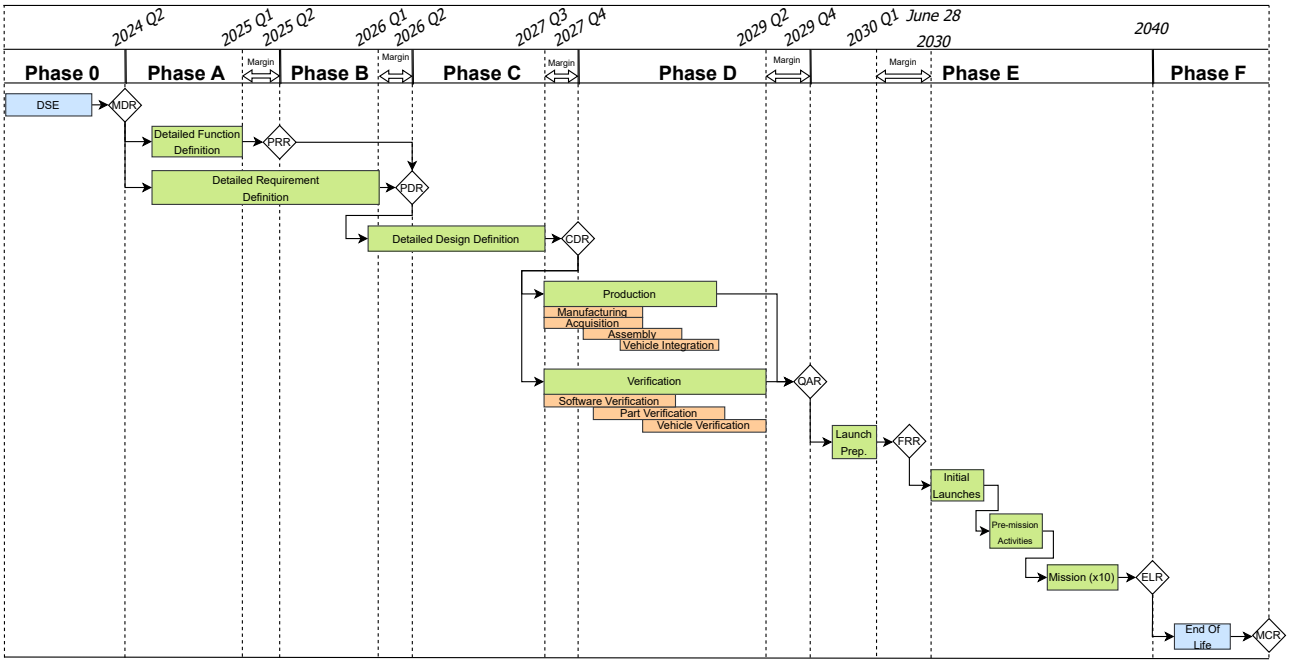


**Figure 21.1:** Further Development Activities

# 22 | Conclusion and Recommendations

The ARCH-E (Autonomous Reconfigurable Crew/Cargo Hauler for Exploration) mission represents a pioneering concept in lunar exploration, with a targeted launch by 2030. Fuelled by NASA's significant investment in lunar technology development and the increasing interest in lunar exploration within the space market, ARCH-E is determined to compete against established competitors like SpaceX and Blue Origin, as well as emerging cargo transportation landers. This innovative vehicle is designed to be reconfigurable and reusable, providing a versatile solution for crewed and cargo missions to the lunar surface.

The trade-off of the mission architecture considered various concepts for the number and types of mission elements involved, as well as refuelling strategies. This included options involving Orbital Transfer Vehicles (OTV), In-Situ Resource Utilisation (ISRU) propellants, and refuelling in Earth orbit, lunar orbit, or on the Earth's surface. The initial concepts were narrowed down using a qualitative trade-off, which was followed by a more detailed, quantitative trade-off of the remaining options. A sensitivity analysis confirmed that the resulting decision was robust. The chosen option consists of one OTV, which transports the single-stage lander from Low Earth Orbit (LEO) to a free-return trajectory around the Moon. From this point, the lander inserts itself into lunar orbit, performs lunar descent and ascent, and returns to LEO alone. The OTV returns to LEO alone, and both vehicles can refuel in LEO.

Since mission analysis is a key part of the project, an analysis and trade-off were carried out for the possible trajectories. A free-return trajectory from LEO to LLO was deemed the best option, which supports the mission architecture decision. The details of this trajectory simulation outsourced reliable $\Delta V$ values of 8.5264 km/s for the lander and 8.1191 km/s for the OTV, which were then imperative to size the propellant mass and, eventually, the structure of the vehicle. Additionally, the strategic planning for launch windows from Kennedy Space Center allowed for a planned launch window on the 28th of June 2030. A lunar ascent and descent simulation was also developed from which precise $\Delta V$ requirements were derived, resulting in a total $\Delta V$ of 4 km/s for this mission phase. Future work should focus on developing comprehensive simulations that integrate landing sensor data models and vehicle attitude dynamics to enhance simulation result confidence. In the detailed propulsion system, the main features are the propellants and its engines. Originally, the propellant was planned to be $LH_2$/LOX for both the OTV and lander, but the OTV was switched to $LCH_4$/LOX due to the volume constraints of SpaceX's Starship fairing. Slosh was preliminarily analysed however a more in-depth analysis could be performed to show its specific impacts on the vehicle's control. Given the tight development timelines existing engines were chosen. The engine choices are Blue Origin's BE-7 for the lander, which allows for precise control during descent and ascent phases, crucial for a soft and controlled lunar touchdown, and SpaceX's Raptor 2 Vacuum engines for the OTV. Both vehicles utilise autogenous pressurisation for propellant tanks, minimising mass and complexity by using the propellant's own gases for tank pressurisation instead of separate high-pressure systems. Future phases should detail the position of the plumbing mass and the routing of the propellants.

The vehicles structure features rings that connect the tanks, payload and engines. These rings are supported with vertical and diagonal beams to carry both lateral and axial loads. The dimensions of these components are determined from the trans lunar orbit of the launch vehicle, as it was found to be the limiting case given that the vehicle is launched empty, therefore discarding the launch itself as limiting. A structural analysis tool, ANSYS, served as a useful tool to aid during the sizing ensuring that the yield stress of the material selected, Aluminum Alloy 7075-T6, was not exceeded. The landing legs are designed to prevent tipping over when landing on a slope at the lunar surface. The sizing led to a four-legged configuration ensuring the stability of the vehicle. Future recommendations, for the structural sizing involve considering the thermal loads, to take into account the expansion of the structure and of the various materials to consider any induced stress as well as detailed sizing of the mechanism for example the solar array hinge and the landing leg deployment. Attention should be paid in future investigations to the sandblasting-like effects from engine exhaust and lunar dust.

The environmental control and life support system considered many technologies in order to design a modular system whilst saving as much mass as possible. It was found that a modular regenerative design saved the most mass, especially when in cargo configuration compared to the other configurations. The system features four pallets placed against the wall with hinges for easy removal during the reconfiguration operations. For future development of the ECLSS, it is recommended to finalise the cabin layout and determine optimal pallet placement, as well as refine ventilation sizing and specify the connector types between pallets.

The thermal control system is composed of a turbo-brayton cryocooler sized specifically for the vehicle to cool the propellant to cryogenic levels. It also consists of nine thermal control boxes that ensure that all electronic components operate at their operational temperature. Finally, the whole vehicle is wrapped with a mylar foil with an aluminium backing insulation layer, which was found optimal to protect the vehicle's systems from experiencing extreme temperatures. It is recommended to explore finer thermal models maybe a three dimensional model in order to more accurately estimate the temperature variations through the vehicle.

The attitude control and guidance of the vehicles is provided by the ADCS and GNC systems. These are composed of several sensors, including sun sensors, star trackers, and IMUs, that work together with the reaction control thrusters to determine and control the attitude. The GNC is composed of a radar, cameras, and LIDAR sensors that determine more accurate attitude and proximity detection, allowing the vehicle to have hazard avoidance capabilities. The decisions were taken considering detailed calculations of the torques, however, more detailed models could be used to get more accurate values of the torques and hence a more optimal design of the vehicles required maneouvres.

The vehicles will be powered by Saft VES16 8s4p Li-Ion batteries which were chosen given its capacities and depth of discharge. 30 are required for the lander and 18 for the OTV to meet all power requirements. These batteries provide power during eclipses and peak demands. During other phases solar arrays will provide power, their power was sized based on eclipse durations, array efficiency, and degradation, leading to select Triple-junction GaAs cells. The final configuration of the arrays was to carry four arrays for better redundancy and stowability. For future advancements in this system, it is beneficial to integrate a detailed structural sizing and degradation analysis of solar arrays and batteries. Additionally, emphasis should be placed on future optimisation of the harness design, selecting suitable DC converters, and designing robust battery shielding with effective venting capabilities to ensure reliable performance.

The mission was finally concluded to contain four main phases; refuelling, extra-vehicular operations, reconfiguration and its final end-of-life operations. After through analysis of missions risk, mitigation efforts should still be prioritised to mitigate the most critical risks identified: budget overruns, budget cuts, and launch vehicle availability. Detailed contingency plans and maintaining a budget surplus are essential for managing financial risks. For launch vehicle availability, engagement with SpaceX to understand Starship's timeline is crucial.

Initial research highlighted the importance of sustainability in the industry. Sustainable materials were selected based on energy efficiency and recyclability. The vehicles also incorporate ADCS and GNC systems for space debris management and lean manufacturing to minimise waste. Real-time tracking and debris detection systems are employed during operations to reduce environmental impact. At end-of-life, the payload bay is repurposable for lunar missions, and the OTV will be safely deorbited. In future phases the project will explore participation in the Space Sustainability Rating to enhance sustainability efforts further.

The cost estimation for ARCH-E missions is $45.73k/kg (FY24), indicating profitability for any price above this threshold. In comparison, a main competitor, Astrobotics, charges $300k/kg (FY24), highlighting ARCH-E's significant margin for providing value and generating revenue. This optimistic outlook underscores ARCH-E's market feasibility and potential competitiveness in the sector.

# Bibliography


[1] Euroconsult, “Prospects for Space Exploration,” Tech. rep., 2023.
[2] Data Bridge, “Helium-3 Market | Global Industry Report, 2031,” Tech. rep., Transparency Market Research Inc., Wilmington, Delaware, November 2021.
[3] Jones, H.W., “The Recent Large Reduction in Space Launch Cost,” Tech. Rep. ARC-E-DAA-TN56851, NASA, July 2018.
[4] Scatteia, L. and Perrot, Y., “Lunar market assessment: market trends and challenges in the development of a lunar economy,” Tech. rep., PwC Space Practice, 2021.
[5] Prachi Kawade, A. M., “”Moon-as-a-service” business models: the next leap for commercial space players,” *Lunar market, 4th edition*, May 2024.
[6] Hurlbert, E. A., Whitley, R., Klem, M. D., Johnson, W., Alexander, L., D’Aversa, E., Ruault, J.-M., Manfletti, C., Sippel, M., Caruana, J.-N., Ueno, H., and Asakawa, H., “International Space Exploration Coordination Group Assessment of Technology Gaps for LOx/Methane Propulsion Systems for the Global Exploration Roadmap,” Tech. rep., American Institute of Aeronautics and Astronautics, 2016.
[7] Safety Office, John F. Kennedy Space Center, “Liquid propellants safety book,” Tech. rep., NASA, 1965.
[8] Kuitunen, J., Drolshagen, G., McDonnell, J. A. M., Svedhem, H., Leese, M., Mannermaa, H., Kaipiainen, M., and Sipinen, V., “DEBIE - first standard in-situ debris monitoring instrument,” Tech. rep., ESA, 2001.
[9] NASA, “Human Landing System (HLS) Requirements Document,” Tech. rep., NASA Marshall Spaceflight Center, 2019, HLS-RQMT-001.
[10] Lueders, K. L., “Source Selection Statement - Appendix H: Human Landing System, Option A Next Space Technologies for Exploration Partnerships-2 (NextSTEP-2) NNH19ZCQ001K APPENDIX-H-HLS,” Tech. rep., NASA, 2021.
[11] Free, J. M., “Source Selection Statement - Next Space Technologies for Exploration Partnerships-2 (NextSTEP-2) Appendix P: Human Landing system (HLS) Sustaining Lunar Development (SLD),” Tech. rep., NASA, 2023.
[12] Singh, M., Korniichuk, T., and Gay-Fulconis, B., “Space: The $1.8 Trillion Opportunity for Global Economic Growth,” Tech. rep., World Economic Forum, 2024.
[13] Bank of America, “Transforming Space, The New Space Era: Expansion of the Space Economy,” Tech. rep., Bank of America Institute, January 2023.
[14] DSE Group 21, “Midterm Report Moon 2030 - A New Hope ARCHE,” Tech. rep., TU Delft, 2024.
[15] SRE-PA & D-TEC staff, “Margin Philosophy for Science Assessment Studies,” Tech. rep., ESA ESTEC, Noordwijk, The Netherlands, 2012.
[16] ECSS-E-ST-10-02C Rev.1 Working Group, “Space Engineering Verification,” Tech. Rep. ECSS-E-ST-10-02C, ESA-ESTEC, 2018.
[17] Executive Cost Analysis Steering Group, *NASA Cost Estimating Handbook*, 4th ed., NASA, 2015.
[18] Defense Logistics Agency, “Standard Prices for Aerospace Energy Category Items,” Tech. rep., United States Department of Defense, 2023.
[19] Bitten, R., Emmons, D., and Freaner, C., “Using Historical NASA Cost and Schedule Growth to Set Future Program and Project Reserve Guidelines,” NASA, IEEE Aerospace Conference, 2007.
[20] Schoenmaekers, J., Jehn, R., Landgraf, M., and Khan, M., “Mission analysis - Towards a European harmonisation,” *ESA bulletin. Bulletin ASE. European Space Agency*, Vol. 2008, 05 2008, pp. 10–19.
[21] Sathyan, S., Bhatt, M., Chowdhury, M., Gläser, P., Misra, D., Srivastava, N., Narendranath, S., Sajinkumar, K., and Bhardwaj, A., “Potential landing sites characterization on lunar south pole: De-Gerlache to Shackleton ridge region,” *Icarus*, Vol. 412, 2024, pp. 115988.
[22] Curtis, H. D., *Orbital Mechanics for Engineering Students: Revised Fourth Edition*, 4th ed., Elsevier, 2021.
[23] Schaub, H. and Junkins, J. L., *Analytical Mechanics of Space Systems*, American Institute of Aeronautics and Astronautics, Inc, 2018.
[24] Wheeler, R., “Launch windows essay,” Tech. rep., NASA, 2009.
[25] Mohamed Khalil Ben Larbi, E. S., “Spacecraft Formation Control Using Analytical Integration Of Gauss’ Variational Equations,” 2016.
[26] Espenak, F., “Lunar eclipses: 2021 - 2030,” .
[27] Liu, X., Li, S., and Xin, M., “Comparison of Powered Descent Guidance Laws for Planetary Pin-point Landing,” *Acta Astronautica*, Vol. 187, 2021, pp. 101–114.
[28] Açıkmeşe, B. and Ploen, S. R., “Convex Programming Approach to Powered Descent Guidance for Mars Landing,” *Journal of Guidance, Control, and Dynamics*, Vol. 30, No. 5, 2007.
[29] Gerth, I., *Convex Optimization for Constrained and Unified Landing Guidance*, Master’s thesis, Delft University of Technology, Delft, The Netherlands, 2014.
[30] de Ridder, K. M., *Convex Guidance, Navigation, and Control for Pin-Point Lunar Landing*, Master’s thesis, Delft University of Technology, Delft, The Netherlands, 2016.
[31] Ito, T. and Sakai, S., “Throttled Explicit Guidance for Pinpoint Landing Under Bounded Thrust Acceleration,” *Acta Astronautica*, Vol. 176, 2020, pp. 438–454.
[32] Blackmore, L., “Autonomous Precision Landing of Space Rockets,” Tech. rep., The Bridge, 2016.
[33] Lee, A. Y., Ely, T., Sostaric, R., Strahan, A., Riedel, J. E., Ingham, M., Wicentsen, J., and Sarani, S., “Preliminary Design of the Guidance, Navigation, and Control System of The Altair Lunar Lander,” Tech. rep., Jet Propulsion Laboratory, 2010.
[34] Chandler, D. C. and Smith, I. E., “Development of the Iterative Guidance Mode with its Application to Various Vehicles and Missions,” *Journal of Spacecraft and Rockets*, Vol. 4, No. 7, 1967, pp. 898–903.
[35] Brand, T. J., Brown, D. W., and Higgins, J. P., “Space Shuttle GN&C Equation Document,” Tech. Rep. NASA-CR-134148 Vol. 24, NASA, June 1973.
[36] Ahmad, N., Hawkins, M., Von der Porten, P., Pinson, R., Dukeman, G., and Fill, T., “Closed Loop Guidance Trade Study for Space Launch System Block-1B Vehicle,” Tech. Rep. AAS 18-270, NASA, Huntsville, AL, 2018.
[37] Brown, K. R., Harrold, E. F., and Johnson, G. W., “Rapid Optimization of Multiple-Burn Rocket Flights,” Tech. Rep. NASA CR-1430, International Business Machines Corporation, Cambridge, MA, 1969.
[38] Cox, K. J., “Space Shuttle Guidance, Navigation and Control Design Equations,” Tech. Rep. NASA-TM-X-67218 Vol. 2, NASA, April 1971.
[39] Cox, K. J., “Space Shuttle Guidance, Navigation and Control Design Equations,” Tech. Rep. NASA-TM-X-68368 Vol. 3, NASA, December 1971.
[40] Sostaric, R. and Merriam, R., “Lunar Ascent and Rendezvous Trajectory Design,” NASA Johnson Space Center, 31st Annual AAS Guidance and Control Conference, 2 2008.
[41] Talebzadeh, S. and Beik, O., “Spacecraft Medium Voltage Direct-Current (MVDC) Power and Propulsion System,” *Electronics*, Vol. 13, No. 10, May 2024, pp. 1810.
[42] Hedayat, A., Steadman, T., Knight, K., Brown, T., Champion, Jr., R., and White, Jr., C., “Pressurization, Pneumatic, and

Vent Subsystems of the X-34 Main Propulsion System," *34th AIAA/ASME/SAE/ASEE Joint Propulsion Conference and Exhibit*, Jul 1998.
[43] Dresar, N. T. V., "Pressurization of Cryogens: A Review of Current Technology and its Applicability to Low-Gravity Conditions," Tech. rep., NASA Lewis Research Center, 1992.
[44] Stuart, B. and McEnulty, J., "Overview of the SLS Core Stage Thrust Vector Control System Design," Tech. rep., NASA Marshall Spaceflight Center, 2023.
[45] Gordan, A. L., "Centaur D1-A Systems in a Nutshell," Tech. rep., NASA Lewis Research Center, 1987.
[46] Zegler, F., "An Integrated Vehicle Propulsion and Power System for Long Duration Cryogenic Spaceflight," Tech. rep., United Launch Alliance, Centennial, Colorado, 2011.
[47] Giuliano, V. J., Leonard, T. G., Lyda, R. T., and Kim, T. S., "CECE: Expanding the Envelope of Deep Throttling Technology in Liquid Oxygen/Liquid Hydrogen Rocket Engines for NASA Exploration Missions," Tech. rep., NASA Marshall Space Flight Center, Nashville, TN, 2010.
[48] NASA, "Atlas-Centaur AC-12 Flight Performance for Surveyor III," Tech. rep., NASA Lewis Research Center, Cleveland, Ohio, November 1968.
[49] Modlin, C. T. and Zipay, J. J., "The 1.5 & 1.4 Ultimate Factors of Safety for Aircraft & Spacecraft – History, Definition and Applications," Tech. rep., NASA, February 2014.
[50] INCO, "Austenitic Chromium-Nickel Stainless Steels at Subzero Temperatures – Mechanical and Physical Properties," Tech. rep., Nickel Institute, 2021.
[51] Larson, W. J. and Wertz, J. R., *Space Mission Analysis and Design*, Space Technology Library, 3rd ed., Microcosm Press, El Segundo, CA, 1999.
[52] Lee, A. Y., Strahan, A., Tanimoto, R., and Casillas, A., "Preliminary Characterization of the Altair Lunar Lander Slosh Dynamics and Some Implications for the Thrust Vector Control Design," Tech. Rep. AIAA 2010-7721, Jet Propulsion Laboratory, Pasadena, CA, August 2010.
[53] Dodge, F. T., *The New Dynamic Behavior of Liquids in Moving Containers*, Southwest Research Institute, San Antonio, TX, 2000.
[54] AE1222-II Teaching Staff, *AE1222-II: Aerospace Design & Systems Engineering Elements I. Part I: Spacecraft (Bus/Platform) Design and Sizing Reader*, TU Delft, 2021-2022.
[55] Henninger, J. H., "Solar and Thermal Emittance of some common spacecraft thermal-control coatings," Tech. Rep. NASA-RP-1121, NASA, Washington D.C., April 1984.
[56] "Radiation Insulation," Tech. Rep. 20020078360, NASA, 1995.
[57] Borst, M., "Mass optimisation of cryogenic fluid systems for long-duration space missions," Tech. rep., TU Delft Aerospace Engineering, Delft, Netherlands.
[58] Bicai, D., Shaoqi, Y., Xiujuan, X., Yunlong, W., Xing, B., Linghui, G., and Li, Q., "Study of the thermal performance of multilayer insulation used in cryogenic transfer lines," Tech. rep., Chinese Academy of Sciences, Beijing 100190, China.
[59] Kittel, P., "Cryocooler Performance Estimator," Tech. rep., University Affiliated Research Center, Palo Alto, CA, 94303, 2007.
[60] tanchon, J., "Turbo Brayton for Space," Tech. rep., Absolute System, Seyssinet Pariset, France.
[61] Guzik, M. C. and Tomsik, T. M., "An Active Broad Area Cooling Model of a Cryogenic Propellant Tank With a Single Stage Reverse Turbobrayton Cycle Cryocooler," Tech. rep., NASA Glenn Research Center, 2011.
[62] Ladner, D. R., "Performance and Mass vs. Operating Temperature for Pulse Tube and Stirling Cryocoolers," Tech. rep., N-Science Corporation Golden, 2011.
[63] Peabody, H., "Thermal Design for Spaceflight," Tech. Rep. 20230003714, NASA Goddard Space Flight Center, Greenbelt, MD, March 2022.
[64] Jianyin, M., Qi, Z., Qiwei, Z., and Xin, Z., *Spacecraft Thermal Control Technologies*, Springer, 2021.
[65] Ryder, V., "Spacecraft Maximum Allowable Concentrations for Airborne Contaminants Human Health and Performance Directorate," Tech. Rep. JSC 20584 Rev A, NASA, Houston, TX, 2020.
[66] "NASA Spaceflight Human-System Standard Volume 1, Crew Health," Tech. Rep. NASA-STD-3001, Volume 1, Revision C, NASA Office of the Chief Health and Medical Officer, September 2023.
[67] Ryder, V., "Spacecraft Water Exposure Guidelines," Tech. Rep. JSC-63414, NASA, Houston, TX, 2017.
[68] Stapleton, T., Heldmann, M., Torres, M., O'Neill, J., Scott-Parry, T., Corallo, R., White, K., and Schneider, S., "Environmental Control and Life Support System Developed for Deep Space Travel," *47th International Conference on Environmental Systems*, UTC Aerospace Systems, Charleston, SC, July 2017.
[69] Clawson, J., Barta, D., Schneider, W., Howard, D., and Cox, M., "NextSTEP Appendix A Modular ECLSS Effort Lessons Learned," *52nd International Conference on Environmental Systems*, Stellar Solutions, Inc., Calgary, Canada, July 2023.
[70] Rohrig, J. A., O'Neill, J., and Stapleton, T. J., "In-Flight Maintenance Design Philosophy for Gateway and Deep-Space Life Support Systems," *49th International Conference on Environmental Systems*, Collins Aerospace, Boston, MA, July 2019.
[71] Samsonov, N. M., Bobe, L. S., Novikov, V. M., Farafonov, N. S., Abramov, G. K., Pinsky, B. J., Zaitsev, E. N., Protasov, N. N., Komolov, V. V., Grioriev, A. I., and Sinjak, J. E., "The MIR space station regenerative water supply," *Sixth European Symposium on Space Environmental Control Systems*, Vol. 400 of *ESA Special Publication*, Aug. 1997, p. 793.
[72] Brodt, K., "Membrane Gas-Water Separation: Membrane Condensing Heat Exchanger (MCHX) Technology Demonstrator," Tech. Rep. MGWS-DO-RP-007, Astrium for ESTEC Contract No. 12333/97/NL/GD, Noordwijk, NL, 2021.
[73] Schowalter, S., Madzunkov, S., Darrach, M., Diaz, E., Moore, B., Simcic, J., Nikolic, D., and Bae, B., "The Technology Demonstration of the Spacecraft Atmosphere Monitor," *49th International Conference on Environmental Systems*, Jet Propulsion Laboratory, Boston, MA, July 2019.
[74] Autrey, D. E., Kaufman, C. A., Kocher, J. G., and Fuller, J., "Development of the Universal Waste Management System," Tech. Rep. ICES-2020-278, Collins Aerospace, Houston, TX, 2020.
[75] James L. Broyan, J., "Waste Collector System Technology Comparisons for Constellation Applications," Tech. Rep. 07ICES-273, NASA Lyndon B. Johnson Space Center, Houston, TX, 2007.
[76] Eckart, P., *Spaceflight Life Support and Biospherics*, Space Technology Library, 1st ed., Microcosm Press & Springer-Science+Business Media, B.V., Hawthorne, CA, 1996.
[77] Nalette, T., Papale, W., and Smith, F., "Development Status of the Carbon Dioxide and Moisture Removal Amine Swing-bed (CAMRAS)," Tech. Rep. 2007-01-3157, 37th International Conference on Environmental Systems (ICES), Chicago, IL, 2007.
[78] Lin, A., Smith, F., Sweterlitsch, J., Nalette, T. A., and Papale, W., "Further Testing of an Amine-Based Pressure-Swing System for Carbon Dioxide and Humidity Control," Tech. Rep. 08ICES-0184, NASA Glenn Research Center, 2008.
[79] Olcott, T., Lamparter, R., Maine, B., Weitzmann, A., Luce, R., Olivier, G., Kawasaki, E., Masi, ., Richardi, C., and Selle, J., "Design, Fabrication, and Test of a Trace Contaminant Control System," Tech. Rep. LMSC-D462467, Lockheed Missiles and Space Co., Sunnyvale, CA, 1975.
[80] Maiwald, F., Simcic, J., Nikolic, D., Belousov, A., , and Madzunkov, S., "Compact High Resolution QITMass Spectrometers for Lunar and Planetary Applications," NASA JPL, European Geosciences Union, May 2020, Presentation slides.

[81] DSE Group 21, “Baseline Report Moon 2030 - A New Hope ARCHE,” Tech. rep., TU Delft, 2024.
[82] Ewert, M. K., , Chen, T. T., and Powell, C. D., “Life Support Baseline Values and Assumptions Document,” Tech. Rep. NASA/TP-2015–218570/REV2, NASA Johnson Space Center, February 2022.
[83] Stapleton, T., Torres, M. A., O’Neill, J., Corallo, R., and Bowers, J., “Environmental Control and Life Support Module Architecture for Deployment across Deep Space Platforms,” *49th International Conference on Environmental Systems*, UTC Aerospace Systems, Boston, MA, July 2019.
[84] Stecklein, J. M. and Petro, A., “Lunar Lander Conceptual Design,” Tech. rep., NASA, 1988.
[85] Encarnação, J., “AE2230-I: Flight and Orbital Mechanics Lecture Slides,” Tech. rep., Delft University of Technology, March 2023.
[86] Ebrahami, M., *Power Generation Technologies: Foundations, Design and Advances*, 1st ed., Academic Press, 2023, pp. 419–461.
[87] Wertz, J. R., Everett, D. P., and Puschell, J. J., *Space Mission Engineering: The New SMAD*, Space Technology Library, 2nd ed., Microcosm Press, Hawthorne, CA, July 2011.
[88] “TJ Solar Cell 3G30C - Advanced,” Tech. Rep. OHSAS 18001, Azur Space, Theresienstr. 2 74072 Heilbronn, May 2019.
[89] “QJ Solar Cell 4G32C - Advanced,” Tech. Rep. OHSAS 18001, Azur Space, Theresienstr. 2 74072 Heilbronn, May 2019.
[90] Hyder, A. K., Wiley, R. L., Halpert, G., Flood, D. J., and Sabripour, S., *Spacecraft Power Technologies*, Vol. 1 of *Space Technology Library*, 2nd ed., Imperial College Press, London, January 2000.
[91] Ferrando, E., “SpaceTech Solar Arrays,” Tech. rep., SpaceTech GMBH, Seelbachstraße 13, Immenstaad, 2019.
[92] Phillips, N., Ferris, M., and Scheidegger, N., “Bi-Axial Solar Array Drive Mechanism: Design, Build and Environmental Testing,” *ESA Special Publication*, Vol. 737, Sept. 2015, p. 15.
[93] Bugga, R., Smart, M., Whitacre, J., and West, W., “Lithium Ion Batteries for Space Applications,” *2007 IEEE Aerospace Conference*, 2007, pp. 1–7.
[94] “Saft solution for LEO and small GEO applications,” Tech. rep., Saft, Poitiers Cedex 9, France, June 2020.
[95] Prevot, D., Borthomieu, Y., Ligneel, E., Hague, R., Peres, J.-P., and Cenac-Morthe, C., “Performances of Saft Lithium-Ion Cells in LEO Cycling,” *E3S Web of Conferences*, Vol. 16, 01 2017, pp. 06005.
[96] Baldwin, P., Heckler, G., Petro, A., Schier, J., Berner, J., Evans, W., and Weir, E., “Space Communications in Support of the Artemis Program,” NASA, SPACEOPS 2021: The 16th International Conference on Space Operations, 2021.
[97] Hayes, J., “SCaN: Deep Space Network Updates,” Tech. rep., NASA, 2024.
[98] SCaN Integrated Network Configuration Control Board, “Space Communications and Navigation (SCaN): Mission Operations and Communications Services (MOCS),” Tech. rep., NASA, 2014.
[99] SCaN Integrated Network Configuration Control Board, “Space Communications and Navigation (SCaN): Mission Operations and Communications Services (MOCS),” Tech. rep., NASA, 2021.
[100] Maldari, P. and Bobrinsky, N., “Cost Efficient Evolution of the ESA Network in the Space Era,” *Journal of Space Operations & Communicator*, Vol. 5, No. 1, Jan 2008.
[101] ESA, “ESA Tracking Stations (ESTRACK) Facilities Manual (EFM),” Tech. rep., European Space Operations Centre, 2008.
[102] NASA, “Near Earth Network (NEN) Users’ Guide,” Tech. rep., NASA Goddard Space Flight Center, 2019, Rev. 4.
[103] NASA, “Near Space Network Services Brochure,” Tech. rep., NASA, n.d., Rev. 1.2.
[104] Board, M. C., “International Communication SYstem Interoperability Standards (ICSIS),” Tech. rep., International Space Station Partner Agencies, 2020, Rev. A.
[105] Weerackody, V. and Cuevas, E., “Technical Challenges and Performance of Satellite Communications on-the-Move Systems,” *Johns Hopkins APL Technical Digest*, Vol. 30, No. 2, 2011.
[106] EVA Exploration Working Group, “Exploration EVA System Concept of Operations,” Tech. rep., NASA, 2020, EVA-EXP-0042.
[107] Jet Propulsion Laboratory, “DSN Telecommunications Link Design Handbook,” Tech. rep., CA Institute of Technology, 2020.
[108] The Consultative Committee for Space Data Systems, “TM Synchronization and Channel Coding - Summary of Concept and Rationale,” Tech. Rep. CCSDS 130.1-G-3, NASA, 2020.
[109] Xia, L., Liu, N., Zhu, L., and Fu, G., “Dual-CP Antenna with Wide-HPBW and Wide-ARBW Performance for Wide-Angle Scanning Phased Array,” *IEEE Transactions on Antennas and Propagation*, Vol. 72, No. 5, May 2024.
[110] Cervone, A. and Speretta, S., “AE2111-II: Aerospace Design and System Engineering Elements II,” Tech. rep., Delft University of Technology, 2022.
[111] NASA, “Lunar Exploration Ground Sites Brochure,” Tech. rep., NASA, 2023.
[112] Koudelka, O., “Link Budget Calculations,” Tech. rep., Institute of Communication Networks and Satellite Communications.
[113] Maral, G., Bousquet, M., and Sun, Z., *Satellite Communications Systems: Systems, Techniques and Technology*, 6th ed., John Wiley & Sons Ltd, 2017.
[114] Ely, T., Sostaric, R. R., and Riedel, J., “Preliminary Design of the Guidance, Navigation, and Control System of The Altair Lunar Lander,” Tech. rep., NASA and California Institute of Technology, Pasadena CA and Houston TX, August 2010.
[115] “Robotics and Space Operations: LEIA,” Tech. rep., MDA Space, United Kingdom, Didcot, 2022.
[116] Prokop, L., “A requirements-based, bottom-up SLOC estimate and analysis of NASA’s Orion crew exploration vehicle spacecraft flight software,” *Innovations in Systems and Software Engineering*, Vol. 10, 2014, pp. 93–101.
[117] Carrara, V., Kuga, H., Massad, P., and Carvalho, M., “Attitude Determination, Control and Operating Modes for Conasat Cubesats,” *24th International Symposium on Space Flight Dynamics (ISSFD)*, Laurel MD, May 2014.
[118] Fritz, M., Shoer, J., Singh, L., Henderson, T., McGee, J., Rose, R., and Ruf, C., “Attitude Determination and Control System Design for the CYGNSS MicroSatellite,” *IEEE Aerospace Conference Proceedings*, Vol. 2015, March 2015.
[119] Chowdhary, A., Jain, N., and Subramanian, M., “Design of Attitude Determination and Control System for Autonomous Docking of Small Satellites,” *70th International Astronautical Congress (IAC)*, Washington D.C., October 2019.
[120] Chiang, R., Lisman, S., Wong, E., Enright, P., Breckenridge, W., and Jahanshani, M., “Robust Attitude Control for Cassini Spacecraft Flying by Titan,” Tech. Rep. 19930067353, NASA Jet Propulsion Laboratory, California Institute of Technology, Pasadena, CA, Jan 1993.
[121] Eiden, M. J., “Chapter 8 - Collision Avoidance Systems,” *Safety Design for Space Systems*, Butterworth-Heinemann, Waltham, MA, 2009, pp. 267–300.
[122] Cervone, A., “AE2111-II - Aerospace Design and Systems Engineering Elements II, Lecture S1: Spacecraft Attitude Determination & Control System,” Tech. rep., Delft University of Technology, 2022/2023.
[123] Markley, F. L., “Attitude Error Representations for Kalman Filtering,” Tech. Rep. 20020060647, NASA, Jan 2002.
[124] “Coarse Earth Sun sensor: CESS,” Tech. rep., SpaceTech GMBH, Seelbachstraße 13, Immenstaad, 2019.
[125] Matra Marconi Space, “Lunar Landing Systems Study,” Tech. Rep. TIDC-CR-6118, ESA, Noordwijk, NL, 1997.
[126] Hall, J. M. and Harris, M., “Spacecraft Sun Sensors,” Tech. Rep. NASA SP-8047, NASA Electronics Research Center and Exotech, Inc, June 1970.
[127] Bonde, H. H., “T3 Star Tracker Datasheet,” Tech. rep., TERMA, 2024.

[128] Rogers, G. D., Schwinger, M. R., Kaidy, J. T., Strikwerda, T. E., Casini, R., Landi, A., Bettarini, R., and Lorenzini, S., "Autonomous star tracker performance," *Acta Astronautica*, Vol. 65, No. 1, 2009, pp. 61–74.
[129] Li, H., Wang, S., Huang, C., and Mu, X., "Summary of Evaluating Inertial Gyro Storage Life Based on Accelerated Life Test," *Proceedings of the 2018 International Conference on Mechanical, Electronic, Control and Automation Engineering (MECAE 2018)*, Atlantis Press, 2018/03.
[130] Gurrisi, C., Seidel, R., Dickerson, S., Didziulis, S., Frantz, P., and Ferguson, K., "Space Station Control Moment Gyroscope Lessons Learned," Tech. Rep. 20100021932, USA, May 2010.
[131] "Autonomous Star trackers: A-STR and AA-STR," Tech. Rep. MM07786 1-17, Leonardo: Airborne & Space Systems, Italy, 2017.
[132] "Sun Sensor ISS-TX Technical Specifications," Tech. rep., SolarMems Technologies S.L., Seville, Spain, 2009.
[133] "Miniature Inertial Measurement Unit datasheet," Tech. Rep. N61-1613-000-000, Honeywell Aerospace, Phoenix, USA, March 2021.
[134] Hibbeler, R., *Engineering Mechanics:Statics*, Engineering mechanics, 14th ed., Pearson, Hoboken, NJ, 2016.
[135] Schalkowsky, S. and Harris, M., "Spacecraft Magnetic Torques," Tech. Rep. NASA-SP-8018, NASA Electronic Research Center and Exotech, Inc, March 1969.
[136] Weidner, D. K., Hasseltine, C. L., and Smith, R. E., "Models of Earth's atmosphere (120 to 1000 km)," Tech. Rep. NASA-SP-8021, NASA Marshall Space Flight Center, Huntsville AL, May 1969.
[137] Ariadna Farres, Cassandra Webster, D. F., "High fidelity modeling of SRP and its effect on the relative motion of Starshade and WFIRST," Tech. Rep. GSFC-E-DAA-TN49849, NASA Goddard Space Flight Center, Jan 2018.
[138] Espen Oland and Raymond Kristiansen and Per Johan Nicklasson, "Combined Chemical and Electric Thruster Solution for AttitudeControl," Tech. rep., Department of Scientific Computing, Electrical Engineering and Space TechnologyNarvik University College, 2009.
[139] Bong Wie and Carlos Roithmayr, "Integrated orbit, attitude, and structural control system design for space solar power satellites," Tech. rep., Arizona State University and NASA Langley Research Center, 2001.
[140] Hurlbert, E. A., Whitley, R., Klem, M. D., Johnson, W., Alexander, L., D'Aversa, E., Ruault, J.-M., Manfletti, C., Sippel, M., Caruana, J.-N., Ueno, H., and Asakawa, H., "International Space Exploration Coordination Group Assessment of Technology Gaps for LOx/Methane Propulsion Systems for the Global Exploration Roadmap," Tech. Rep. JSC-CN-35694, NASA, Sept 2016.
[141] Eberle, E. and L.Kusak, "Liquid oxygen/liquid hydrogen auxiliary power system thruster investigation," Tech. Rep. NASA-CR-159674, NASA, Dec 1979.
[142] Reed, B. D. and Schneider, S. J., "Hydrogen/Oxygen Auxiliary Propulsion Technology," Tech. Rep. NASA-TM-105249, NASA, Sept 1991.
[143] Koerner, S. A., "Human Landing Systems (HLS) White Paper for Manual Control and Windows," August 2019.
[144] Gill, T. R., Jr., J. D. J. G., Pittman, D., Lewis, M., Deaton, K., Chappell, S., and Kessler, P., "Lunar Surface Cargo Offloading Concepts," Tech. rep., Internation Conference on Environmental Systems, MN, 2022.
[145] SpaceX, "Starship Users' Guide," Tech. Rep. Rev. 1, SpaceX, Hawthorne, CA, 2020.
[146] Bonsel, J. H., *Application of a dynamic vibration absorber to a piecewise linear beam system*, Master's thesis, Eindhoven University of Technology, Eindhoven, Netherlands, September 2003.
[147] El-Hameed, A. and Abdel-Aziz, Y., "Aluminium Alloys in Space Applications: A Short Report," *Journal of Advanced Research in Applied Sciences and Engineering Technology*, Vol. 22, No. 1, January 2021, pp. 1–7.
[148] Zupp, G. and Doiron, H., "A Mathematical Procedure for Predicting the Touchdown Dynamics of a Soft-Landing Vehicle," Tech. rep., NASA Manned Spacecraft Center, 1971.
[149] Zupp, G., "An Analysis and a Historical Review of the Apollo Program Lunar Module Touchdown Dynamics," Tech. rep., NASA Johnson Space Center, 2013.
[150] Flügge, W., "Landing-Gear Impact," Tech. Rep. 20000508 215, Stanford University, 1952.
[151] Melkert, J. and Rans, C., "Buckling AE2135-I Structural Analysis and Design," Delft University of Technology, 2022.
[152] Rans, C., "Theory of Elasticity and Generalized Bending AE2135-I Structural Analysis and Design," Delft University of Technology, 2022.
[153] Gere, J. M. and Goodno, B. R., *Mechanics of Materials*, 8th ed., Cengage Learning, July 2012.
[154] Coburn, T. D., *Aerospace Strength Handbook*, Vol. 2, Todd Coburn, 2021.
[155] Colwell, J. and Taylor, M., "Low-Velocity Microgravity Impact Experiments into Simulated Regolith," Tech. rep., University of Colorado, 1998.
[156] Flügge, W., "Landing-Gear Impact," Tech. rep., NACA, 1952, Technical Note 2743.
[157] Cirillo, W., Stromgren, C., and Cates, G., "Risk Analysis of On-Orbit Spacecraft Refueling Concepts," *AIAA SPACE 2010 Conference and Exposition*, Aug 2010.
[158] Jefferies, S. A., Arney, D. C., Jones, C. A., Reeves, D., Moses, R. W., and Bowman, L., "Impacts of in-space assembly as applied to Human Exploration Architectures," *2018 AIAA SPACE and Astronautics Forum and Exposition*, Sep 2018.
[159] "NASA exploration systems architecture study," Aug 2008.
[160] Mclaughlin, R. J. and Warr, W. H., "The Common Berthing Mechanism (CBM) for International Space Station," *SAE Technical Paper Series*, July 2001.
[161] Austin, J., "Developing a standardised methodology for spacespecific Life Cycle Assessment," Tech. rep., European Space Agency, 2015.
[162] Space Debris Mitigation Working Group, *ESA Space Debris Mitigation Requirements*, ESA, 1st ed., Oct 2023.
[163] Fernini, I., Burns, J. O., Taylor, G. J., Sulkanen, M., Duric, N., and Johnson, S., "Dispersal of gases generated near a lunar outpost," Tech. Rep. 19910029622, NASA, 1990.
[164] "The Complete Guide to Sustainable Materials Selection," Tech. rep., MatMatch, 2024.
[165] ESA Space Debris Office, "ESA'S Annual Space Environment Report," Tech. rep., European Space Agency, 2023.
[166] Braun, V., Horstmann, A., Lemmens, S., Wiedemann, C., and Ottcher, L. B., "Recent Developments In Space Debris Environment Modelling, Verification And Validation With Master," Tech. rep., European Space Agency, 2021.
[167] Associate Director of JSC Engineering Directorate, "Vibration Testing," Tech. Rep. FS-2011-07-043-JSC, NASA, 2011.
[168] Oliviero, F., Gill, E. K., Jyoti, B., and Cervone, A., "AE2230-I: Flight and Orbital Mechanics," Tech. rep., Delft University of Technology, March 2024.
[169] "NASA Procedural Requirements," Tech. Rep. NPR 1400, NASA, March 2019.
[170] ECSS-M-ST-10 Working Group, "Space Project Management: Project Planning and Implementation," Tech. Rep. ECSS-M-ST-10C, ESA, Noordwijk, NL, 2009.